INSIGHTS IN HEART VALVE DISEASE: 2021

EDITED BY: Elena Aikawa, Adrian Chester, Laura Iop and Roney Orismar Sampaio

PUBLISHED IN: Frontiers in Cardiovascular Medicine

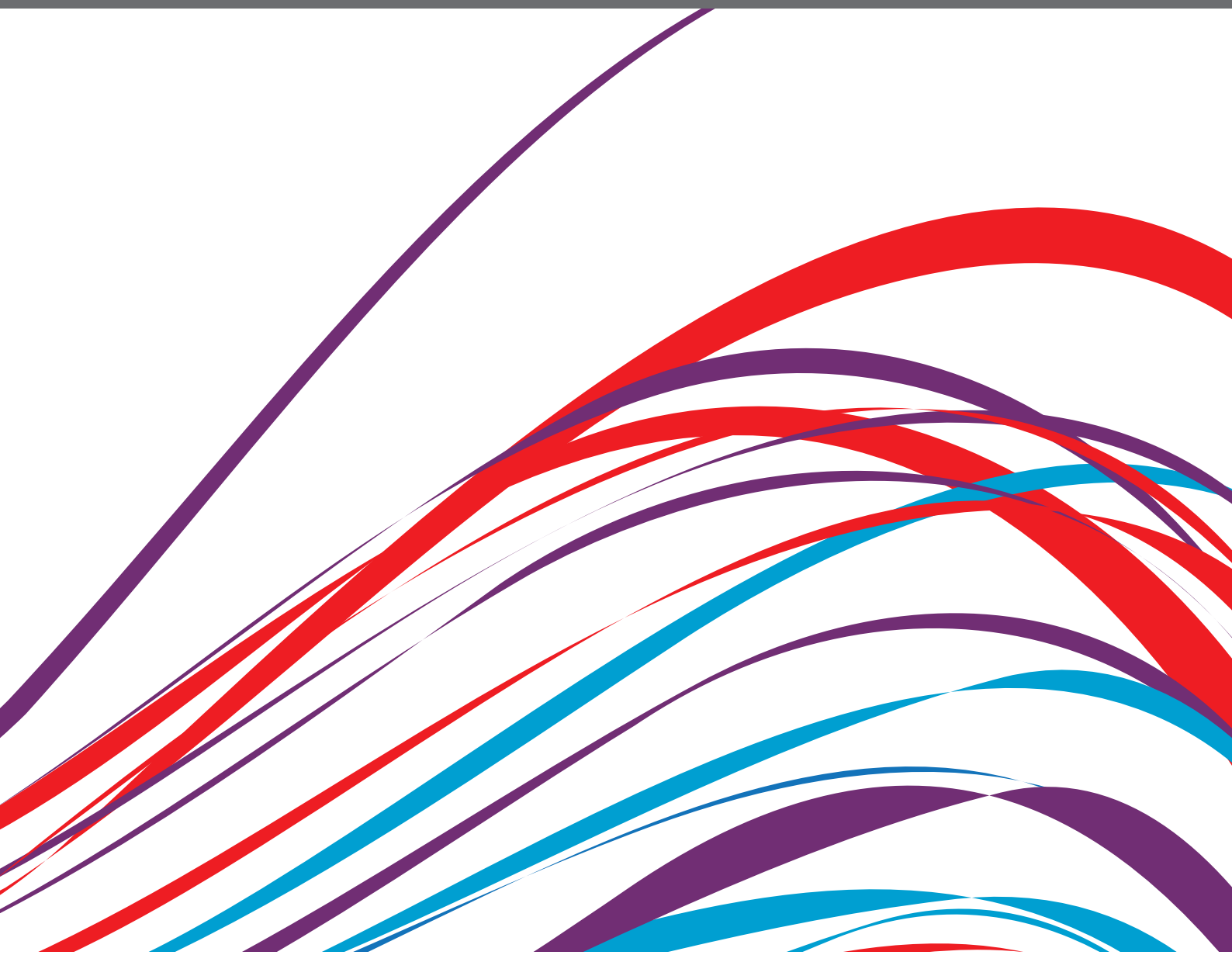

frontiers Research Topics

ISSN 1664-8714
ISBN 978-2-88976-658-1
DOI 10.3389/978-2-88976-658-1

About Frontiers

Frontiers is more than just an open-access publisher of scholarly articles: it is a pioneering approach to the world of academia, radically improving the way scholarly research is managed. The grand vision of Frontiers is a world where all people have an equal opportunity to seek, share and generate knowledge. Frontiers provides immediate and permanent online open access to all its publications, but this alone is not enough to realize our grand goals.

Frontiers Journal Series

The Frontiers Journal Series is a multi-tier and interdisciplinary set of open-access, online journals, promising a paradigm shift from the current review, selection and dissemination processes in academic publishing. All Frontiers journals are driven by researchers for researchers; therefore, they constitute a service to the scholarly community. At the same time, the Frontiers Journal Series operates on a revolutionary invention, the tiered publishing system, initially addressing specific communities of scholars, and gradually climbing up to broader public understanding, thus serving the interests of the lay society, too.

Dedication to Quality

Each Frontiers article is a landmark of the highest quality, thanks to genuinely collaborative interactions between authors and review editors, who include some of the world's best academicians. Research must be certified by peers before entering a stream of knowledge that may eventually reach the public - and shape society; therefore, Frontiers only applies the most rigorous and unbiased reviews.
Frontiers revolutionizes research publishing by freely delivering the most outstanding research, evaluated with no bias from both the academic and social point of view. By applying the most advanced information technologies, Frontiers is catapulting scholarly publishing into a new generation.

What are Frontiers Research Topics?

Frontiers Research Topics are very popular trademarks of the Frontiers Journals Series: they are collections of at least ten articles, all centered on a particular subject. With their unique mix of varied contributions from Original Research to Review Articles, Frontiers Research Topics unify the most influential researchers, the latest key findings and historical advances in a hot research area! Find out more on how to host your own Frontiers Research Topic or contribute to one as an author by contacting the Frontiers Editorial Office: frontiersin.org/about/contact

INSIGHTS IN HEART VALVE DISEASE: 2021

Topic Editors:
Elena Aikawa, Brigham and Women's Hospital, Harvard Medical School, United States
Adrian Chester, The Magdi Yacoub Institute, United Kingdom
Laura Iop, University of Padua, Italy
Roney Orismar Sampaio, University of São Paulo, Brazil

Citation: Aikawa, E., Chester, A., Iop, L., Sampaio, R. O., eds. (2022). Insights in Heart Valve Disease: 2021. Lausanne: Frontiers Media SA.
doi: 10.3389/978-2-88976-658-1

Table of Contents

frontiers | Frontiers in Cardiovascular Medicine

TYPE Editorial
PUBLISHED 26 August 2022
DOI 10.3389/fcvm.2022.998862

OPEN ACCESS

EDITED AND REVIEWED BY
Hendrik Tevaearai Stahel,
Bern University Hospital, Switzerland

*CORRESPONDENCE
Laura Iop
laura.iop@unipd.it

SPECIALTY SECTION
This article was submitted to Heart Valve Disease, a section of the journal Frontiers in Cardiovascular Medicine

RECEIVED 20 July 2022
ACCEPTED 12 August 2022
PUBLISHED 26 August 2022

CITATION
Iop L, Chester AH, Sampaio RO and Aikawa E (2022) Editorial: Insight in heart valve disease: 2021. *Front. Cardiovasc. Med.* 9:998862. doi: 10.3389/fcvm.2022.998862

Editorial: Insight in heart valve disease: 2021

Laura Iop[1]*, Adrian H. Chester[2,3], Roney Orismar Sampaio[4] and Elena Aikawa[5]

[1]Department of Cardiac Thoracic Vascular Sciences and Public Health, Padua Medical School, University of Padua, Padua, Italy, [2]Magdi Yacoub Institute, London, United Kingdom, [3]National Heart & Lung Institute, Imperial College London, London, United Kingdom, [4]Department of Cardiopneumology, São Paulo Medical School, University of São Paulo, São Paulo, Brazil, [5]Cardiovascular Medicine, Brigham and Women's Hospital, Harvard Medical School, Boston, MA, United States

KEYWORDS

heart valve disease, heart valve physiology, heart valve disease management, heart valve disease mechanisms, heart valve bioprostheses

Editorial on the Research Topic
Insight in heart valve disease: 2021

As with many fields of medicine, the last decade of this century has witnessed tremendous progress in the understanding of the physiology, disease mechanism, and the treatment of heart valve disease. The Research Topic entitled "Insights in Heart Valve Disease: 2021" is dedicated to these recent advancements through the original research and perspectives of editorial board members, who seminally contributed to the field.

Heart valve pathology: Which is its clinical impact in 2021?

Cardiovascular disease is the main cause of mortality worldwide, with several forms of heart valve pathology having a significant contributory role. The article by Hartley et al. proposed an epidemiology study on aortic valve stenosis and demonstrated trends in mortality from aortic stenosis in Europe in 2000–2017 (Hartley et al.). The authors offered an updated overview of the related mortality trends in 23 countries by also considering the impact of transcatheter aortic valve insertion (TAVI) in the last 10 years. Except for Germany and the Netherlands, these trends do not appear declining despite the adopted prevention and care measures. Indeed, they dramatically upraised in some countries of the Eastern European area (e.g., Croatia, Poland, and Slovakia), mostly due to disparities in the clinical practice. Gender still plays a fundamental role: although a greater number of cardiovascular risk factors is generally reported for male patients, females develop more severe aortic stenosis, often difficult to treat even with TAVI due to anatomic-interventional peculiarities. Thus, it emerges a substantial need to revise international guidelines of aortic stenosis care management for an effective, conjoint confrontation of this life-threatening disease.

The article by Perl et al. put the accent on the yet underestimated, long-term impact of ischemic mitral regurgitation through a prospective registry involving more than 3,000 patients in Israel (Perl et al.). This study evidenced the decline of ischemic mitral regurgitation over 20 years but its strong impact on prognosis for diagnosed heart disease patients, who undergo a duplicate one-year mortality risk with respect to the non-diagnosed sub-court.

Heart valve physiology and pathophysiology: Is our knowledge complete?

Many relevant pieces of the puzzle are still missing in the understanding of the pathophysiology of native valve disease. Original research published in this special issue helps to gain more insights into the mechanism leading to the degeneration of native heart valves. The DNA methylation study performed by Halawa et al. increased the knowledge of both valve biology and disease by the analysis of the left semilunar and atrioventricular valves (Halawa et al.). Almost 600 gene promoters were found differentially methylated in the comparison between aortic and mitral valves and among these, epigenetic modifications were observed in those associated with the WNT-, Cadherin-, Endothelin-, PDGF- and VEGF-pathways, but also the so far less associated TGFB-, NOTCH-, and Integrin-signaling. Consequently, any epigenetic changes occurring in these pathways with relevance for the developmental and pathophysiological events of endothelial-mesenchymal transition (EndMT) and extracellular matrix (ECM) remodeling should also be carefully evaluated during the process leading to the generation of effective, natural heart valve substitutes by tissue engineering. De facto, EndMT reactivation is a potent contributor to valve degeneration even when different pathologies are considered, as shown by Latif et al.. Through TGFB- pathway activation, valve endothelial cells especially acquire a smooth muscle phenotype involving the upregulation of the SM-genes α-SMA, calponin, SM22, SM-myosin, and their co-activators MRTF-A and myocardin in both bicuspid and rheumatic valves, with a phenomenon likely more pronounced in the latter. TGFB- signaling involvement in myxomatous mitral valve degeneration is well renowned, as systematically reviewed in the article by Tang et al.. Mitral valve prolapse manifests in both dogs and humans after myxomatous degeneration with secondary or syndromic forms and is among the major causes of heart failure due to high morbidity and mortality. Although several mechanistic studies have been proposed *in vitro* and *in vivo*, there is still much molecular work to carry out to tackle the disease at its onset by adequate pharmacological targeting instead of surgical interventions.

Another striking original study was advanced by Nasim et al. relating together pigment valve distribution and valve biomechanical functionality (Nasim et al.). By the analysis of aortic valves of transgenic mice with differentially expressed pigments, a proportional increase in elastin content was observed in hyperpigmented animals leading to a surge in stiffness with respect to wild-type animals. On the opposite, hypopigmentation was found to be associated with decreased elastin content and reduced stiffness. Surprisingly, no echocardiographic modifications were found in these different mouse models, as well as no melanocyte cell content could be related to the differential pigment expression. Future experiments will be necessary to investigate more in-depth the possible pathologic link between altered pigmentation levels and valve micromechanical dysfunction.

Biomechanical impairment is widely recognized as a causal event in atrioventricular valve degeneration, too, although only secondary again to an upregulation of TGFB-signaling. Vinciguerra et al. focused on this molecular valve dysfunction culprit in their two review articles (Vinciguerra et al.; Vinciguerra et al.). The mechanical stress generated by mitral plasticity can be counteracted by the surgical approach of subvalvular correction reassuring an appropriate leaflet coaptation. Pharmacological treatments, such as renin-angiotensin-aldosterone system (RAAS) inhibitors, demonstrated to be equally effective, by contrasting valve remodeling consequent to acute myocardial infarction. Among these drugs, losartan showed to be promising, also proving a strong ability in blocking EndMT in valve endothelial cells and valve fibrosis. A minor medical interest has been relieved over time by tricuspid regurgitation, which, however, is increasingly documented as strongly relevant for its impact on cardiovascular disease prognosis. This novel awareness has rendered possible a greater characterization of the tricuspid regurgitation subtypes, due to right ventricle overload and tricuspid annular dilatation resulting from left heart valve disease. The application of three-dimensional echocardiography imaging through a transthoracic window was demonstrated to be efficacious in the diagnostic course and severity stratification, while cardiac magnetic resonance rendered finally feasible quantitative studies on right heart remodeling, and particularly associated valve regurgitation.

Heart valve disease: Are current therapies successful in the long-term?

Surgical and mini-invasive treatments are becoming more targeted and effective, also with reference to the management of electrical conduction abnormalities. Valve correction, as well as substitution with bioprosthetic

TABLE 1 Take-home messages from the Research Topic 'Insight in heart valve disease: 2021'.

Heart valve disease management	Article title	Key points	Possible implications	Reference
Heart valve disease epidemiology	Trends in Mortality From Aortic Stenosis in Europe: 2000–2017	• Increasing mortality rates from aortic stenosis in Europe • Women develop more severe aortic stenosis than men • European countries have different standards of care	• Need to substantially revise international guidelines of aortic stenosis care management	Hartley et al.
	Trends in Ischemic Mitral Regurgitation Following ST-Elevation Myocardial Infarction Over a 20-Year Period.	• Ischemic mitral regurgitation has declined over 20 years. • However, diagnosed patients have a double mortality risk than non-diagnosed ones.	• Strong impact on prognosis	Perl et al.
Heart valve (patho)physiology	Profiling Genome-Wide DNA Methylation Patterns in Human Aortic and Mitral Valves.	• 600 gene promoters were found differentially methylated between aortic and mitral valves • Epigenetic modifications were observed in those associated with the WNT-, Cadherin-, Endothelin-, PDGF-, VEGF-, TGFB, NOTCH, and Integrin signaling.	• Epigenetic changes in these pathways, relevant for EndMT and ECM remodeling, should be carefully evaluated during heart valve tissue engineering.	Halawa et al.
	Atypical Expression of Smooth Muscle Markers and Co-activators and Their Regulation in Rheumatic Aortic and Calcified Bicuspid Valves.	• Upon TGFB- pathway activation, valve endothelial cells acquire a smooth muscle phenotype with upregulation of the SM-genes and their co-activators in both bicuspid and rheumatic valves	• EndMT reactivation contributes to valve degeneration in both bicuspid and rheumatic valves	Latif et al.
	The Role of Transforming Growth Factor-β Signaling in Myxomatous Mitral Valve Degeneration.	• Mitral valve prolapse manifests in dogs and humans after myxomatous degeneration. • It is among the major causes of heart failure due to high morbidity and mortality. • Several mechanistic studies *in vitro* and *in vivo* have been proposed.	• Pharmacological targeting is still missing.	Tang et al.
	Pigmentation Affects Elastic Fiber Patterning and Biomechanical Behavior of the Murine Aortic Valve	• Pigment content increases proportionally with elastin in heart valves • No echocardiographic modifications were appreciated. • No melanocyte cell content was correlated to pigmentation levels.	• Further studies are mandatory to understand the effect of pigmentation on valve micromechanical (dys)function.	Nasim et al.
	Mitral Plasticity: The Way to Prevent the Burden of Ischemic Mitral Regurgitation?	• Mechanical stress generated by mitral plasticity can be counteracted by surgical subvalvular correction • Pharmacological treatments, such as RAAS inhibitors (e.g., losartan), contrast valve remodeling consequent to acute myocardial infarction.	• Blocking EndMT in valve endothelial cells and valve fibrosis is effective to prevent mitral plasticity.	Vinciguerra et al.
	Functional Tricuspid Regurgitation: Behind the Scenes of a Long-Time Neglected Disease.	• Tricuspid regurgitation has a strong impact on cardiovascular disease prognosis.	• Three-dimensional echocardiography allows for severity stratification.	Vinciguerra et al.

(Continued)

TABLE 1 (Continued)

Heart valve disease management	Article title	Key points	Possible implications	Reference
		• Characterization of the tricuspid regurgitation subtypes is now possible by current sophisticated imaging. • Cardiac magnetic resonance renders feasible quantitative studies on right heart remodeling, and associated valve regurgitation.		
Heart valve disease treatment	Hemodynamic Performance of Sutureless vs. Conventional Bioprostheses for Aortic Valve Replacement: The 1-Year Core-Lab Results of the Randomized PERSIST-AVR Trial.	• Perceval sutureless valves show good pressure gradients, valve effective orifice area, and paravalvular leak.	• A non-inferiority of the Perceval sutureless valve compared to stented sutured counterparts is disclosed in terms of haemodynamic performances.	Fischlein et al.
	Residual Bioprosthetic Valve Immunogenicity: Forgotten, Not Lost.	• Valve degeneration might be immunogenicity-related. • Residual bioburden might induce immunogenic responses by the host toward the xenoantigens displayed by colonizing bacteria. • Bioprosthetic dystrophic calcification and rheumatic fever might parallel in their manifestations.	• Further analyses are needed to establish whether residual bioburden might be causal to bioprosthetic valve degeneration. • If this hypothesis is valid, improvements in terminal sterilization protocols are compulsory.	Human et al.
	Characterization of Turbulent Flow Behind a Transcatheter Aortic Valve in Different Implantation Positions.	• Turbulent flow induced by different TAVI device deployment modalities can be studied in pulse replicator to typify the three-dimensional flow field generated.	• Such *in vitro* experimental analyses are essential to simulate the pathological peculiarities of the patient's root. • Their results are informational for the best deployment strategy to use and for the prevision of the functional behavioral fate of TAVI devices.	Pietrasanta et al.
	Mitral and Aortic Regurgitation in Patients Undergoing Kidney Transplantation: The Natural Course and Factors Associated With Progression.	• Renal functional improvement after transplantation generally exerts favorable effects on left heart valve regurgitation. • In less than 10% of patients, mitral and aortic regurgitations might progress.	• It is necessary to investigate why a few patients with initial successful kidney transplantation require a second procedure due to the maintenance of a hypertensive state, valve calcifications, and reduced LV end-systolic dimensions.	Kim et al.

End-MT, endothelial-mesenchymal transition; ECM, extracellular matrix; SM, smooth muscle; RAAS, renin-angiotensin-aldosterone system; TAVI, transcatheter aortic valve insertion; LV, left ventricle.

replacements, have reached a routinary application for the therapeutic management of heart valve disease. In their 1-year PERSIST-AVR clinical trial, Fischlein et al. evaluated the performance of one of the most recent bioprosthetic valve concepts, i.e., sutureless replacements, with respect to conventional ones in the treatment of aortic valve regurgitation (Fischlein et al.). This study disclosed a non-inferiority of the Perceval sutureless valve compared to stented sutured counterparts in several hemodynamic parameters, such as pressure gradients, valve effective orifice area, and paravalvular leak.

Nevertheless, there are still some unsolved flaw in the usage of animal-derived valve bioprostheses and their dystrophic evolution in the mid/long term. In this regard, several hypotheses were proposed over time, as emphasized by Human et al. in their review article (Human et al.). In the last years, several pieces of evidence are corroborating the notion of immunogenicity-related valve degeneration. Although different technologies are finding applications to possibly reduce this animal burden (from simple alcohol-mediated glycolipid washout, passing through decellularization, to more sophisticated animal genetic engineering to silence or modify the signaling relevant for the expression of sugar xenoantigens), the studies performed in animal models likely suggest that something is still beyond the comprehension of the link between various xenoantigens and a sustained immune reply by the host. Fascinatingly, this review motions a further standpoint: xenoantigenicity might be not only related to the peculiar sugar moiety intrinsic to animal cells, their remnants, and/or extracellular matrix but also tissue bioburden. Sterilization protocols, standardly employed for medical devices, might be too detrimental for natural tissues to be employed for replacement manufacturing, thus maintenance of microorganisms, such as bacteria and viruses, might be probable after the application of milder decontamination treatments. This residual bioburden might match a remaining load of the same xenoantigens endowed in the animal tissues since several colonizing bacteria expose these glucidic groups on their cell membranes. In the support of this hypothesis, a parallel between bioprosthetic dystrophic calcification and rheumatic fever is provided in the review to point out the potential association of inflammation, pannus overgrowth, and/or autoimmunity observed in the progress of both diseases. While more studies are compulsory to confirm this, a quest for more effective sterilization treatments for natural tissues is undeniable.

In their original article (Pietrasanta et al.). Apart from the substitutes intended for classic surgery, the last decades have been characterized by the incredible technological revolution in valve disease therapy led by mini-invasive transcatheter replacement approaches, more commonly TAVI when intended for aortic valve treatment. The undisputable benefit for high mortality risk patients in advanced age might lessen its strength in younger subjects, for which a longer-term evaluation is foreseen. Possible dysfunctions might be associated again with the proneness to inflammatory/immune degeneration in those TAVI devices produced with animal tissues. Pietrasanta et al. reflected on the detrimental effects caused by the turbulent flow induced by different device deployment modalities. This wet-lab research performed through the use of a pulse replicator allowed to typify the three-dimensional flow field generated by different implantation configurations of a self-expandable TAVI valve in porcine pericardium. Such *in vitro* experimental analyses are essential to simulate the pathological peculiarities of the patient's root and, thus, their results are strongly informational for the best deployment strategy to use and for the prevision of the functional behavioral fate of TAVI devices, once implanted in the patient.

In addition, cardiac hemodynamic load and particularly valve regurgitation might find relief in most patients when their comorbidities are clinically treated, as proved by Kim et al. in their original research article focusing on left heart valve regurgitation and the favorable effects exerted by renal functional improvement after transplantation (Kim et al.). Interestingly, in a small percentage of patients (<10%), mitral and aortic regurgitations might progress although the initial success of the kidney transplantation and lead to the need for a second procedure due to the maintenance of a hypertensive state, valve calcifications, and reduced left ventricle (LV) end-systolic dimensions.

Take-home message

As a conclusive remark, all the original and reviewed knowledge reported in this Research Topic has shed more light on the physiology and pathophysiology of heart valve disease and associated cardiac and non-cardiac pathologies (Table 1). Based on these advances, it is evident that the standard of clinical care, as well as novel therapeutic approaches, should be fine-tuned thereof worldwide to have a more positive impact on the natural history and prognosis of cardiovascular diseases, the life quality of affected patients, and socio-economical health management programs.

Author contributions

LI conceived and wrote the editorial. AC, RS, and EA wrote and approved the editorial. All

authors contributed to the article and approved the submitted version.

Conflict of interest

The authors declare that the research was conducted in the absence of any commercial or financial relationships that could be construed as a potential conflict of interest.

Publisher's note

frontiers in Cardiovascular Medicine

ORIGINAL RESEARCH
published: 11 October 2021
doi: 10.3389/fcvm.2021.748137

Trends in Mortality From Aortic Stenosis in Europe: 2000–2017

Adam Hartley[1,2,3]*, *Matthew Hammond-Haley*[4], *Dominic C. Marshall*[1,2,5], *Justin D. Salciccioli*[6], *Iqbal S. Malik*[2,3], *Ramzi Y. Khamis*[1,2,3] and *Joseph Shalhoub*[2,7,8]

[1] National Heart and Lung Institute, Imperial College London, London, United Kingdom, [2] Imperial College Healthcare NHS Trust, London, United Kingdom, [3] Department of Cardiology, Hammersmith Hospital, London, United Kingdom, [4] British Heart Foundation Centre of Excellence, King's College London, London, United Kingdom, [5] Department of Respiratory Medicine, St Mary's Hospital, London, United Kingdom, [6] Pulmonary and Critical Care Medicine, Brigham and Women's Hospital and Harvard Medical School, Boston, MA, United States, [7] Academic Section of Vascular Surgery, Department of Surgery and Cancer, Imperial College London, London, United Kingdom, [8] Department of Vascular Surgery, St Mary's Hospital, London, United Kingdom

Background: Trends in mortality from aortic stenosis across European countries are not well-understood, especially given the significant growth in transcatheter aortic valve implantation (TAVI) in the last 10 years.

Methods: Age-standardised death rates were extracted from the World Health Organisation Mortality Database, using the International Classification of Diseases 10th edition code for non-rheumatic aortic stenosis for those aged > 45 years between 2000 and 2017. The UK and countries from the European Union with at least 1,000,000 inhabitants and at least 50% available datapoints over the study period were included: a total of 23 countries. Trends were described using Joinpoint regression analysis.

Results: No reductions in mortality were demonstrated across all countries 2000–2017. Large increases in mortality were found for Croatia, Poland and Slovakia for both sexes (>300% change). Mortality plateaued in Germany from 2008 in females and 2012 in males, whilst mortality in the Netherlands declined for both sexes from 2007. Mortality differences between the sexes were observed, with greater mortality for males than females across most countries.

Conclusions: Mortality from aortic stenosis has increased across Europe from 2000 to 2017. There are, however, sizable differences in mortality trends between Eastern and Western European countries. The need for health resource planning strategies to specifically target AS, particularly given the expected increase with ageing populations, is highlighted.

Keywords: aortic stenosis, mortality, Europe, transcatheter aortic valve implantation (TAVI), aortic valve replacement (AVR)

OPEN ACCESS

Edited by:
Bart Meuris,
University Hospitals Leuven, Belgium

Reviewed by:
Najma Latif,
The Magdi Yacoub Institute, United Kingdom
Francesca Bartoli-Leonard,
Brigham and Women's Hospital and Harvard Medical School, United States

***Correspondence:**
Adam Hartley
adam.hartley12@imperial.ac.uk

Specialty section:
This article was submitted to Heart Valve Disease, a section of the journal Frontiers in Cardiovascular Medicine

Received: *27 July 2021*
Accepted: *15 September 2021*
Published: *11 October 2021*

Citation:
Hartley A, Hammond-Haley M, Marshall DC, Salciccioli JD, Malik IS, Khamis RY and Shalhoub J (2021) Trends in Mortality From Aortic Stenosis in Europe: 2000–2017. Front. Cardiovasc. Med. 8:748137. doi: 10.3389/fcvm.2021.748137

INTRODUCTION

Aortic stenosis (AS) is the most prevalent valvular heart disease in Europe (1). Although rheumatic heart disease is the most common aetiology worldwide, degenerative calcification of native trileaflet valves and congenital bicuspid valves are the primary causes in developed countries. AS prevalence increases significantly with advancing age and is ∼10% over the age of 80 (2). Moreover, with ageing populations, the burden is expected to increase further (3).

AS prognosis relates predominantly to severity and symptoms, with over 50% mortality at 1-year with conservative treatment for severe symptomatic AS (4). Although traditionally the outlook for asymptomatic AS has been considered favourable, frequently managed with routine surveillance, this has been brought into focus in a recent meta-analysis which demonstrated significant cardiovascular mortality in this patient group (5).

Until relatively recently, the only treatment available for AS that provided prognostic benefit was surgical aortic valve replacement (SAVR). However, the first transcatheter aortic valve implantation (TAVI) was performed in 2002 (6), offering potential intervention to those who were previously denied invasive treatment based on advancing age or high operative risk, with a dramatic improvement in mortality in these patients (7). Widespread uptake of TAVI has subsequently been seen, with excellent outcomes and increasing procedural scope, and is now even indicated in patients with low surgical risk (8). Indeed, across Western Europe, TAVI procedures have increased almost 350% from 2010 to 2019 (9). Yet access to TAVI is not universal, and there is significant regional variation, strongly related to healthcare resource availability (10). A recent analysis of mortality in the USA demonstrated declining mortality trends in older patients with AS (in line with increased TAVI procedures), which was not seen in patients from non-metropolitan areas (11).

We sought to explore changing trends in AS mortality across Europe between 2000 and 2017, given the introduction, exponential uptake and expanding indications of TAVI. This will aim to demonstrate changing patterns of mortality with access to modern therapies and highlight regional healthcare inequalities that require targeted intervention.

METHODS

Data Sources

Data were extracted from the World Health Organisation (WHO) Mortality Database for the years 2000–2017. Data quality is continuously assessed by the WHO to ensure reliability and usability. Birth and population recording must exceed 90% for countries to be included in the database. Details of data collection and validation for the database have been described extensively previously (12, 13). The WHO Mortality Database uses International Classification of Disease (ICD) codes to classify causes of death. The tenth revision ICD code for non-rheumatic AS (I35.0) was used, whilst ICD codes pertaining to aortic insufficiency or mixed aortic valve disease were excluded.

Member states of the European Union (EU) as well as the United Kingdom, with populations > 1,000,000, were included in the study. EU countries Malta, Cyprus and Luxembourg were not included owing to having <1,000,000 inhabitants. Greece and Ireland were excluded due to more than 50% missing datapoints for the study period. All included countries had high quality cause of death data, except Bulgaria, Poland and Portugal (medium quality). Data are considered high quality if the country reports at least 5 years of data, uses ICD codes for at least the latest year, and has data usability (as defined by the WHO) of at least 80%. Data are considered medium quality using the same criteria as high quality, but with average data usability of at least 60% (12).

Therefore, 23 countries were included in the final analysis. The estimated level of completeness of death registration reported to the WHO Mortality Database for all included countries was at least 97% up to 2010, and 100% for the most recent year, up to 2016 (14). Death rates were computed from vital registration data for all included countries, with the exception of Lithuania which was based on annual estimates informed by completeness-adjusted vital registration data and United Nations population assessments (12). Mortality data were further restricted to those above the age of 45 years, to limit the effects of more severe congenital disease, and focus on a generalisable population that may be suitable for conventional medical and surgical interventions. This age restriction has been utilised previously (11). Not all countries had data available for 2017, and as such, four countries (Belgium, Estonia, Italy, and UK) reported up to 2016, three (Bulgaria, Denmark, and Latvia) reported up to 2015 and two (France and Slovakia) reported up to 2014.

Data Handling

Crude annual national mortality data with annual national population data were extracted from the WHO Mortality Database. Following this, the age standardised death rate (ASDR) was calculated. This relates the distribution of mortality per 5-year age group per country, weighted according to the WHO standard population (15). This standardisation process is commonly used in mortality epidemiological studies and controls for differences in age structure, permitting more robust comparison between countries. In this study we report ASDR per 1,000,000 population, as performed previously (11). The data underlying this article are available in the article and can be found at https://www.who.int/data/data-collection-tools/who-mortality-database. Patients or the public were not involved in the design or conduct of this study. Ethical approval was not required for this study, given that the data is collected from widely available, internationally collected mortality certification.

Statistical Analysis

Sex-specific trends for AS age-standardised mortality were established and analysed for 3-year periods at the start and end of the observation period. Where 3-year data were missing, at either the start or end of the observation period, the 2-year or 1-year averages were calculated, as appropriate. Where no data were available for any timepoint for either of these periods (2000–2002 or 2015–2017), the earliest and latest available timepoints were used. Percentage change was assessed between the earliest and latest values.

Mortality trends were assessed using Joinpoint Version 4.5.0.1 Command (US National Cancer Institute Surveillance Research Program). For the purpose of Joinpoint analysis, missing data were imputed in a last observation carried forward method. Joinpoint regression analysis assesses changes in linear gradients for ASDR over time, as performed previously (16). In brief, Joinpoint analysis initially assesses the overall trends in mortality without any joinpoints, and then evaluates for changes in the model, with the addition of further joinpoints for each

statistically significant slope change. A log-linear transformation is performed, permitting approximation to normal distributions and each additional joinpoint is tested for significance using a Monte Carlo permutation method. Estimated annual percentage change (EAPC) for each trend is calculated by fitting a regression line to the natural logarithm of the rates. Each EAPC is assessed to determine whether a significant difference exists compared to no change in mortality. The final model consists of multiple joinpoints, each representing a significant change in trend, with each trend described by EAPC and confidence intervals. A statistically significant difference was defined as a two-sided p-value < 0.05.

Differences in the change in ASDR per sex between newer EU joining countries and older countries from 2000 to 2017 were assessed with the Mann-Whitney test. EU-joining nations from 2004 or later were deemed new, as has been used previously (16).

RESULTS

Over the study period between 2000 and 2017, there were significant changes in AS mortality across European countries in those aged > 45 years, for both males and females. Twenty-three countries from the EU and UK were included in the final analysis, after exclusion of countries with significant missing data or with <1,000,000 inhabitants. The quality of the mortality data in the WHO Mortality Database has been reviewed previously to ensure sufficient reliability and robustness (13). In total, mortality data were missing for 8.7% of all potential values during the observation period.

Overall Changes in Mortality From Aortic Stenosis

Between 2000 and 2017 there were increases in mortality from AS in all countries, for both sexes. The differences in ASDRs between the start and end of the study period are shown in **Table 1**. Very large increases in mortality were reported in Croatia, Czech Republic, Estonia, Poland, Slovakia, and Slovenia for both sexes (>100% change). Small increases in mortality were reported for the majority of countries, including Belgium, Denmark, Finland, Hungary, Italy and UK (15–50% change for both sexes). The Netherlands was the only country that reported no substantial changes (<5% change for both sexes).

Figure 1 displays the percentage change in ASDR 2000–2017 for both males (A) and females (B) from **Table 1**, divided into earlier (pre-2004) and later (post-2004) EU joining nations. Although there is an apparent trend only for males ($p = 0.17$), there is a strongly statistically significant difference for females

TABLE 1 | Change in age-standardised death rates from non-rheumatic aortic stenosis for those aged > 45 years in Europe from 2000 to 2017.

Country	Start		End		Raw change		% change	
	Male	Female	Male	Female	Male	Female	Male	Female
Austria	17.64	15.58	27.76	26.56	10.12	10.98	57.4	70.48
Belgium	19.49	19.49	22.43	24.15	2.94	4.66	15.06	23.93
Bulgaria*	3.05	1.31	3.11	2.83	0.06	1.52	2.12	115.51
Croatia	5.69	1.97	33.81	26.86	28.12	24.89	493.93	1,265.62
Czech Republic	7.68	4.29	24.25	16.25	16.57	11.97	215.87	279.26
Denmark	19.03	18.89	28.09	24.99	9.06	6.1	47.62	32.28
Estonia	13.09	5.07	30.49	18.08	17.4	13.01	132.97	256.58
Finland	30.87	24.45	43.03	31.86	12.16	7.41	39.4	30.32
France†	17.97	13.68	20.81	15.69	2.85	2	15.84	14.63
Germany	15.55	14.5	29.61	26.53	14.06	12.03	90.47	82.97
Hungary	22.35	14.92	28.63	21.83	6.29	6.91	28.13	46.35
Italy	7.83	8.03	9.94	12.02	2.11	3.99	26.95	49.72
Latvia	7.92	4.39	8.61	9.42	0.69	5.02	8.7	114.45
Lithuania	7.09	1.34	8.86	6.25	1.77	4.91	24.95	367.28
Netherlands	21.66	20.45	21.82	20.92	0.16	0.47	0.75	2.3
Poland	3.42	1.72	14.79	11.08	11.37	9.36	333.02	545.1
Portugal€	12.21	11.51	19.57	20.52	7.36	9.01	60.28	78.32
Romania	3.2	2.19	4.68	4.18	1.47	1.99	46.01	90.91
Slovakia§	3.82	0.85	17.04	14.41	13.22	13.55	346.19	1,587.77
Slovenia	34.7	26.12	71.35	63.8	36.65	37.68	105.64	144.24
Spain	10.87	12.5	22.55	19.46	11.68	6.96	107.44	55.68
Sweden	23.2	19.09	25.79	20.48	2.59	1.39	11.18	7.28
United Kingdom	18.86	13.8	26.18	19.07	7.32	5.27	38.82	38.15

*Average estimated annual percentage change (EAPC) between 2000–2002 and 2015–2017 used, where data available. The following countries did not have available EAPC for one of those periods, and therefore the following intervals were used: *Bulgaria 2005–2015; †France 2000–2014; €Portugal 2007–2017; §Slovakia 2000–2014.*

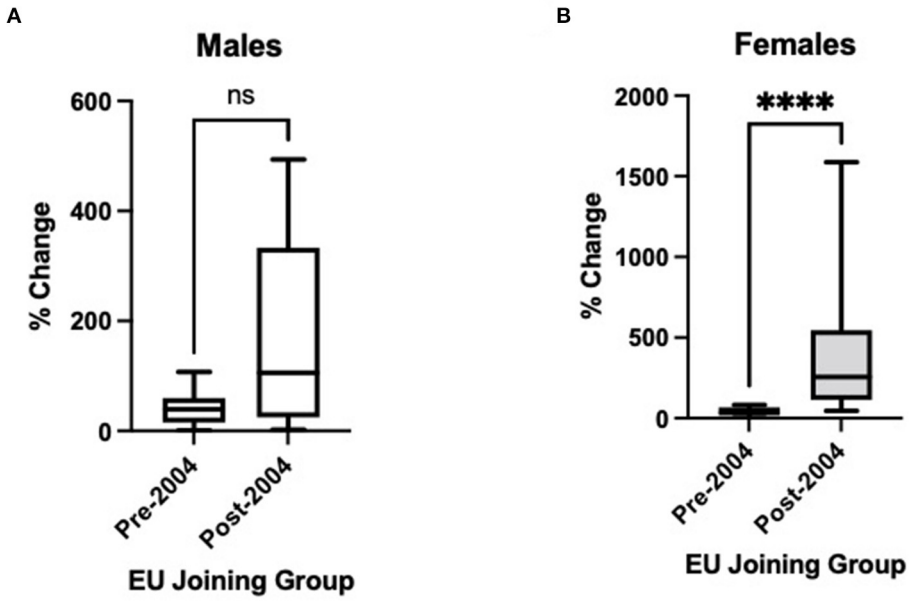

FIGURE 1 | Changes in age-standardised death certification rates per 1,000,000 for countries joining the European Union (EU) before 2004 and 2004 or later, 2000 to 2017, for non-rheumatic aortic stenosis for those aged > 45 years in **(A)** males and **(B)** females. Pre-2004 countries: Austria, Belgium, Denmark, Finland, France, Germany, Italy, Netherlands, Portugal, Spain, Sweden, and the United Kingdom. Post-2004 countries: Bulgaria, Croatia, Czech Republic, Estonia, Hungary, Latvia, Lithuania, Poland, Romania, Slovakia, and Slovenia. Rather than 2000–2017, the following intervals are used owing to data availability: Bulgaria 2005–2015; France 2000–2014; Portugal 2007–2017; Slovakia 2000–2014. Mann-Whitney test used to assess statistical significance. ns, non-significant ($p = 0.17$); ****, statistical significance at $p < 0.0001$.

($p < 0.0001$), with much greater increases in ASDR for later EU joining countries.

Joinpoint Regression Analysis of Mortality From Aortic Stenosis

Figure 2 displays the results of Joinpoint regression analysis for trends in mortality for each country per sex. The most common trend was for a slow sustained increased ASDR over the study period, as can be seen in Belgium, Hungary, Italy, Lithuania, Spain and the UK, for both sexes, and Latvia and Denmark for females. Steeper increases in mortality over the study period are observed in both sexes in the Czech Republic, Slovakia, Poland and Portugal, as well as Estonia for females and Austria for males. However, the steepest increases are seen in Croatia and Slovenia for both sexes. Of note, very low levels of mortality are reported in Bulgaria and Romania, with ASDRs < 10 per 1,000,000 population throughout the observation period. The death rates in Sweden and France for both sexes, as well as Latvia for males, were relatively static.

Despite there being no mortality reductions from the start to end of the study period, some improving mortality trends are observed. Mortality plateaued in Germany from 2008 in females and 2012 in males, whilst in the Netherlands mortality declined for both sexes from 2007. For males in Denmark mortality declined from 2008 and there was also a small decline in Estonian males from 2007. Lastly, there was a reduction in mortality for Austrian females from 2014.

Mortality differences between the sexes were also observed, with consistently greater mortality for males than females in a large proportion of countries. This sex gap appears to be narrowing in some countries (for example Denmark, Estonia and Latvia), but not all (for example Czech Republic and UK, where the difference is growing), and is stable in most.

Estimated Annual Percentage Change in Mortality From Aortic Stenosis

The EAPCs, shown in **Table 2**, highlight the differing trends between Eastern and Western European countries. Mortality in both sexes is consistently and statistically significantly increasing with an EAPC of >5 in Croatia, Czech Republic, Lithuania, Poland, Portugal, Slovakia and Slovenia. For males in Austria, as well as females in Estonia and Latvia, statistically significant increasing trends are also seen. The largest single trend increasing EAPCs in males are seen in Croatia {12.8 [95% confidence interval (95% CI) +10.2 to −15.5]}, Poland [+10.6 (95% CI +9.4 to −11.8)] and Czech Republic [+8.5 (95% CI +7.2 to −9.8)]. The largest single trend EAPCs in females are observed in Croatia [+17.6 [95% CI +14.3 to −21.0)], Slovakia [+15.9 (95% CI +9.9 to −22.4)] and Bulgaria [+10.8 [95% CI +2.4 to −19.9)].

Although consistent declining trends are seen Estonia, France, Italy and Netherlands for males, Netherlands and Austria are the only countries with declining female

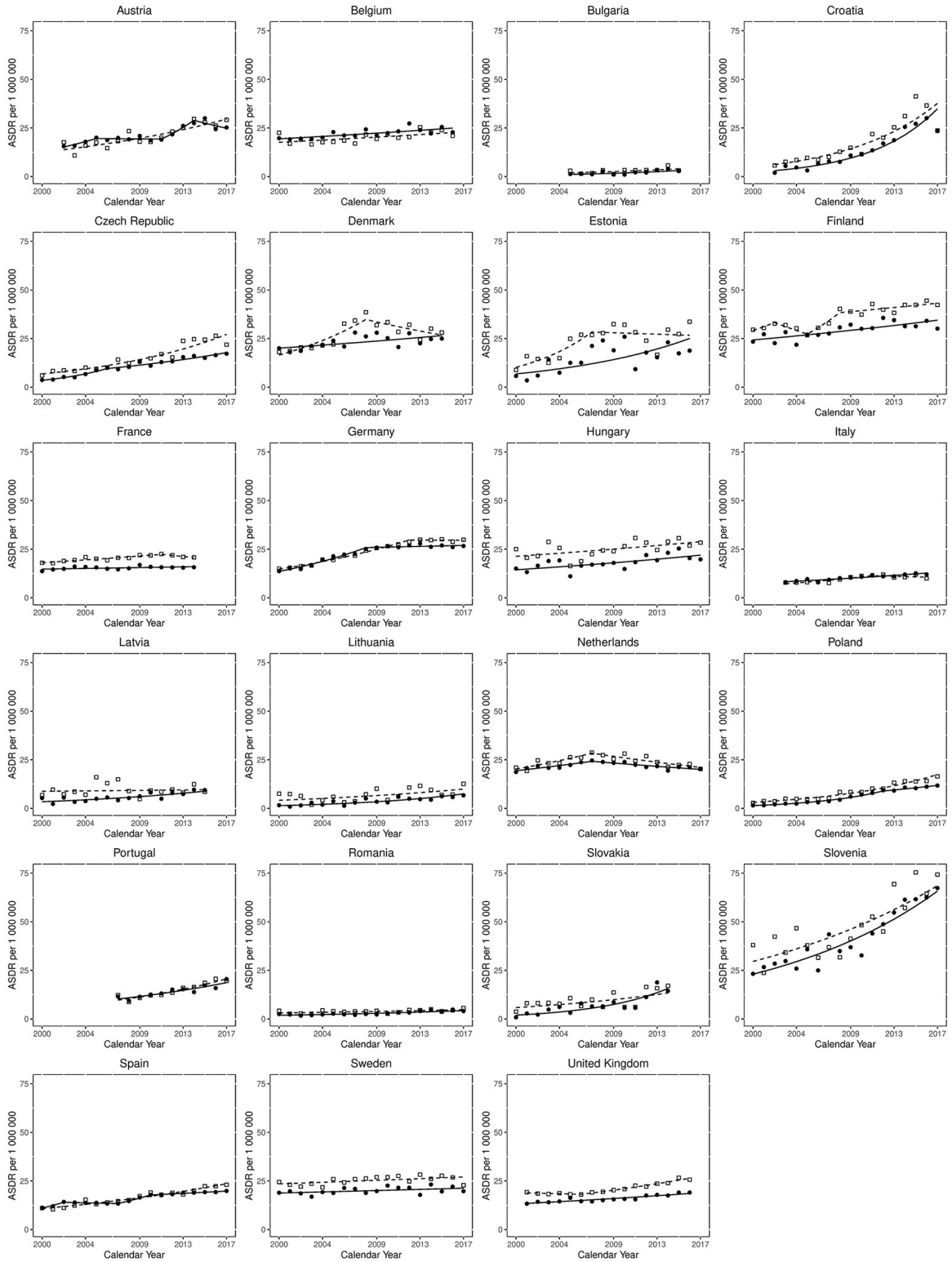

FIGURE 2 | Joinpoint regression analysis for trends in age-standardised death rates from non-rheumatic aortic stenosis for those aged > 45 years in Europe from 2000 to 2017. Clear squares indicate males; filled circles indicate females. The lines (dotted for males, solid for females) represent modelled trends based on joinpoint data.

TABLE 2 | Joinpoint regression analysis for mortality from non-rheumatic aortic stenosis for those aged > 45 years in Europe from 2000 to 2017.

Country	Sex	Trend 1		Trend 2		Trend 3		Trend 4	
		Years	EAPC	Years	EAPC	Years	EAPC	Years	EAPC
Austria	Males	2002–2017	5.2 (3.4–7.0)*						
	Females	2002–2005	8.8 (−3.0 to 22.1)	2005–2011	−0.2 (−5.2 to 5.0)	2011–2014	14.4 (−9.1 to 44.0)	2014–2017	−4.9 (−15.2 to 6.7)
Belgium	Males	2000–2016	1.6 (0.5–2.7)*						
	Females	2000–2016	1.6 (0.9–2.3)*						
Bulgaria	Males	2005–2015	7.8 (−0.6 to 16.8)						
	Females	2005–2015	10.8 (2.4–19.9)*						
Croatia	Males	2002–2017	12.8 (10.2–15.5)*						
	Females	2002–2017	17.6 (14.3–21.0)*						
Czech	Males	2000–2017	8.5 (7.2–9.8)*						
Republic	Females	2000–2006	18.3 (13.5–23.3)*	2006–2017	5.8 (4.0–7.5)*				
Denmark	Males	2000–2008	9.8 (5.8–13.9)*	2008–2015	−3.7 (−8.0 to 0.8)				
	Females	2000–2015	1.9 (0.5–3.3)*						
Estonia	Males	2000–2007	15.7 (5.5–26.9)*	2007–2016	−0.7 (−6.7 to 5.8)				
	Females	2000–2016	8.5 (3.7–13.4)*						
Finland	Males	2000–2002	6.7 (−8.5 to 24.6)	2002–2005	−6.4 (−19.8 to 9.3)	2005–2008	12.0 (−4.0 to 30.7)	2008–2017	1.3 (−0.1 to 2.8)
	Females	2000–2017	2.1 (1.2–3.0)*						
France	Males	2000–2011	2.0 (1.3–2.7)*	2011–2014	−2.5 (−7.3 to 2.6)				
	Females	2000–2014	0.6 (0.0–1.2)*						
Germany	Males	2000–2012	6.0 (5.4–6.6)*	2012–2017	−0.1 (−2.1 to 2.0)				
	Females	2000–2008	8.4 (7.0–9.8)*	2008–2017	0.5 (−0.6 to 1.6)				
Hungary	Males	2000–2017	1.8 (0.4–3.2)*						
	Females	2000–2017	2.5 (1.0–4.0)*						
Italy	Males	2003–2011	5.9 (2.8–9.1)*	2011–2016	−1.4 (−7.3 to 4.8)				
	Females	2003–2016	3.4 (2.5–4.3)*						
Latvia	Males	2000–2015	0.6 (−3.1 to 4.4)						
	Females	2000–2015	6.5 (3.4–9.7)*						
Lithuania	Males	2000–2017	5.2 (1.2–9.4)*						
	Females	2000–2017	10.3 (7.3–13.5)*						
Netherlands	Males	2000–2007	4.9 (2.2–7.7)*	2007–2017	−2.9 (−4.4 to −1.4)*				
	Females	2000–2007	3.2 (1.5–5.0)*	2007–2017	−1.9 (−2.8 to −0.9)*				
Poland	Males	2000–2017	10.6 (9.4–11.8)*						
	Females	2000–2012	16.6 (14.9–18.3)*	2012–2017	5.7 (−0.1 to 11.8)				
Portugal	Males	2007–2017	7.8 (5.3–10.3)*						
	Females	2007–2017	6.2 (4.0–8.4)*						
Romania	Males	2000–2017	2.5 (0.7–4.3)*						
	Females	2000–2017	5.0 (3.4–6.6)*						
Slovakia	Males	2000–2014	6.1 (1.3–11.0)*						
	Females	2000–2014	15.9 (9.9–22.4)*						
Slovenia	Males	2000–2017	5.1 (3.2–7.0)*						
	Females	2000–2017	6.4 (5.0–7.7)*						
Spain	Males	2000–2017	4.7 (4.0–5.3)*						
	Females	2000–2002	12.7 (7.9–17.7)*	2002–2007	−0.9 (−2.3 to 0.4)	2007–2010	10.0 (5.3–14.8)*	2010–2017	1.5 (1.0–2.1)*
Sweden	Males	2000–2017	0.8 (0.1–1.5)*						
	Females	2000–2017	0.7 (0.0–1.5)						
United	Males	2001–2006	−0.8 (−2.5 to 0.8)	2006–2016	3.8 (3.2–4.4)*				
Kingdom	Females	2001–2016	2.2 (1.6–2.7)*						

*Where data are available. EAPC, estimated annual percentage change. *Statistical significance, $p < 0.05$.*

mortality. Indeed, Netherlands is the only country with any statistically significant decreasing trend for any period across the study, with EAPC of −2.9 (95% CI −4.4 to −1.4) and −1.9 (95% CI −2.8 to −0.9) for males and females, respectively.

DISCUSSION

This study of deaths from AS between 2000 and 2017 identifies increases in mortality in all European countries. There are however substantially differing trends between countries, with

some reporting stable ASDRs across the observation period, some reporting changing trends towards reduction in mortality, whilst others report rapidly worsening mortality rates. Mortality from AS is shown to increase significantly in many Eastern European countries, for example Croatia, Czech Republic, Poland, Slovakia and Slovenia for both sexes. This divide is evident when examining earlier and later EU-joining nations (**Figure 1**), particularly in females. Of note, Estonia has the smallest population of all included countries, which may explain the more variable datapoints. In addition, the low level of mortality from AS in Bulgaria and Romania may represent under-reporting, perhaps due to a lower AS diagnosis rate. However, many Western European countries also demonstrate increasing trends, most notably Portugal. Germany and Netherlands are the only countries that have plateauing or declining mortality rates for both sexes, and Netherlands is the only country where the decreasing trends were statistically significant. Nonetheless, increases in mortality over the whole study period are observed in all countries; possibly related to population ageing or an increased likelihood of AS diagnosis with greater access to diagnostics.

The only countries with plateauing or declining mortality for both sexes (Germany and Netherlands) were early TAVI adopters, and have well-established TAVI practise and registries. Indeed, Germany performs the most TAVIs in Europe, whilst TAVI far exceeds SAVR in the Netherlands (17, 18). Procedural complications and mortality reduce with greater TAVI experience (19), which may contribute, along with the greater TAVI numbers, to the declining AS mortality in these countries. Conversely, Croatia had only performed 87 TAVIs by 2014 (20), Slovenia was a slow adopter and had only performed procedures in one centre in 2015 (21) and Poland has among the lowest numbers of TAVI procedures in Europe (22). Portugal, a Western European country with increasing AS mortality, had the lowest number of TAVI procedures in Europe (7 per 1,000,000 population/year) in 2013 (23). More recently, in a survey of TAVI practise from 20 European countries for 2018, Slovenia (6 per million inhabitants) and Poland (22 per million inhabitants) had the lowest reported figures (Croatia was not included in the study), whilst Germany had the highest (187 per million inhabitants). Portugal performed only 30 per million inhabitants (24).

However, the link between developments in TAVI practise and trends in mortality from AS cannot be assumed to be causal. For example, a possible explanation is that TAVI uptake could be a surrogate for other indicators of good clinical practise. Moreover, TAVI and SAVR rates are not collected uniformly, and are gained from multiple sources. There are also other potential factors that influence AS mortality. For example, experience and practise of SAVR, frequency of AS diagnosis, as well as the prevalence and management of AS risk factors (e.g., chronic renal disease, hypercholesterolaemia, diabetes, and smoking) (25). There is significant overlap between these risk factors and those for atherosclerotic cardiovascular disease. Of note, we have previously demonstrated growing disparity in mortality from cardiovascular disease between Western and Eastern European countries (16).

An interesting observation from the present study is the difference in mortality between males and females that, for the majority of countries, is not narrowing. This sex disparity contradicts the current belief that females have worse outcomes from AS. Theories behind this include that females are more likely to be older and frailer at presentation; have higher pulmonary pressures and more concomitant mitral valve disease (26); and that AS may be more common in females, related to longer life expectancy as well as smaller aortic root dimensions (27). However, males have a much higher preponderance of cardiovascular risk factors (which are mostly shared with AS) and have a lower left ventricular ejection fraction at presentation (28). Females present later into the disease course with more insidious symptoms; thus AS incidence, and therefore mortality, may be under-represented in this group (26). Procedural factors suggest more inherent risks during TAVI on female patients, for example smaller cardiac structures increasing technical complexity and more difficult vascular access (29). Despite this, TAVI outcomes are actually superior in females and indeed may be the preferred treatment modality in older women (30).

Challenges to wider adoption of TAVI in less economically developed countries include the availability of resources, education, infrastructure and diagnostic services. TAVI procedures are expensive, due to high device costs, necessary infrastructure including cardiothoracic surgical services, and the need for dedicated multi-disciplinary Heart teams. Any increase in TAVI use has to be justified in terms of both survival and quality of life benefits.

The morbidity and mortality related to AS in Europe and North America is likely to be very different to that of lower income countries. This relates to aetiology, where degenerative rather than infectious causes (infective endocarditis or rheumatic disease) predominate, the population affected (elderly vs. younger), as well as the healthcare resources available to detect and treat the condition. Although no worldwide comparisons of AS mortality have been performed, mortality from rheumatic heart diseases does appear to be decreasing (31).

Limitations of this study include the reliability of large scale retrospective data; however accuracy is assessed by the WHO, and there is at least medium quality data reporting and at least 98% death coverage for all included countries in this analysis (12). Nonetheless, data coding may be of differing quality between countries and this may impact on the observed results. There is also the potential for missed mortality trends, with absent datapoints for some countries. In addition, there may be a significant diagnosis bias in reporting of mortality. For example, AS will be detected at a greater rate with more widespread access to echocardiography, and therefore will feature more commonly on death certification. It is possible that more developed healthcare systems have more established echocardiography services. Another potential factor is the improving quality of contemporary cardiac ultrasound machines; AS may be detected more frequently on images with greater spatial and temporal resolution. As stated above, a causal

link between mortality rates and TAVI use cannot be inferred from this study. The effect of underdiagnosis on the treatment of AS unfortunately cannot be assessed in this study, as the WHO collect data on mortality with no information available on reported prevalence.

CONCLUSION

Mortality from aortic stenosis has increased across Europe between 2000 and 2017. There are, however, sizable differences in mortality trends between Eastern and Western European countries. Significant plateauing or declining mortality is observed for recent years in countries with greater access to TAVI, whilst increasing trends are observed in countries with the least TAVI use. The need for health resource planning strategies to specifically target AS, due to the expected increase in incidence with ageing populations, is highlighted.

DATA AVAILABILITY STATEMENT

The raw data supporting the conclusions of this article are freely available from the World Health Organisation (WHO) Mortality Database.

AUTHOR CONTRIBUTIONS

JS, JDS, DM, and AH designed the study. JDS and DM performed data analysis. AH wrote the manuscript, which was reviewed and edited by MH-H, JS, JDS, DM, IM, and RK. AH is the guarantor of the manuscript. All authors contributed to the article and approved the submitted version.

FUNDING

This work was supported by a Wellcome Trust Clinical Research Fellowship (220572/Z/20/Z) (AH).

REFERENCES

1. Iung B, Baron G, Butchart EG, Delahaye F, Gohlke-Bärwolf C, Levang OW, et al. A prospective survey of patients with valvular heart disease in Europe: the Euro Heart Survey on Valvular Heart Disease. *Eur Heart J.* (2003) 24:1231–43. doi: 10.1016/S0195-668X(03)00201-X
2. Eveborn GW, Schirmer H, Heggelund G, Lunde P, Rasmussen K. The evolving epidemiology of valvular aortic stenosis. The Tromsø study. *Heart.* (2013) 99:396–400. doi: 10.1136/heartjnl-2012-302265
3. Danielsen R, Aspelund T, Harris TB, Gudnason V. The prevalence of aortic stenosis in the elderly in Iceland and predictions for the coming decades: the AGES-Reykjavík study. *Int J Cardiol.* (2014) 176:916–22. doi: 10.1016/j.ijcard.2014.08.053
4. Leon MB, Smith CR, Mack M, Miller DC, Moses JW, Svensson LG, et al. Transcatheter aortic-valve implantation for aortic stenosis in patients who cannot undergo surgery. *New Engl J Med.* (2010) 363:1597–607. doi: 10.1056/NEJMoa1008232
5. Gahl B, Çelik M, Head SJ, Vanoverschelde JL, Pibarot P, Reardon MJ, et al. Natural history of asymptomatic severe aortic stenosis and the association of early intervention with outcomes: a systematic review and meta-analysis. *JAMA Cardiol.* (2020) 5:1–11. doi: 10.1001/jamacardio.2020.2497
6. Cribier A. Development of transcatheter aortic valve implantation (TAVI): a 20-year odyssey. *Arch Cardiovasc Dis.* (2012) 105:146–52. doi: 10.1016/j.acvd.2012.01.005
7. Kapadia SR, Leon MB, Makkar RR, Tuzcu EM, Svensson LG, Kodali S, et al. 5-year outcomes of transcatheter aortic valve replacement compared with standard treatment for patients with inoperable aortic stenosis (PARTNER 1): a randomised controlled trial. *Lancet*. (2015) 385:2485–91. doi: 10.1016/S0140-6736(15)60290-2
8. Mack MJ, Leon MB, Thourani VH, Makkar R, Kodali SK, Russo M, et al. Transcatheter aortic-valve replacement with a balloon-expandable valve in low-risk patients. *New Engl J Med.* (2019) 380:1695–705. doi: 10.1056/NEJMoa1814052
9. BIBA MedTech. *TAVI Monitor*. London: BIBA MedTech (2020). Available online at: https://www.bibamedtech.com/contact-us/
10. Durko AP, Osnabrugge RL, Van Mieghem NM, Milojevic M, Mylotte D, Nkomo VT, et al. Annual number of candidates for transcatheter aortic valve implantation per country: current estimates and future projections. *Eur Heart J.* (2018) 39:2635–42. doi: 10.1093/eurheartj/ehy107
11. Bevan GH, Zidar DA, Josephson RA, Al-Kindi SG. Mortality due to aortic stenosis in the United States, 2008-2017. *JAMA*. (2019) 321:2236–8. doi: 10.1001/jama.2019.6292
12. World Health Organisation. *WHO Methods and Data Sources for Country-Level Causes of Death 2000-2016*. World Health Organisation (2018). Available online at: https://www.who.int/healthinfo/global_burden_disease/GlobalCOD_method_2000-2016.pdf
13. Mathers CD, Fat DM, Inoue M, Rao C, Lopez AD. Counting the dead and what they died from: an assessment of the global status of cause of death data. *Bull World Health Organ.* (2005) 83:171–7.
14. World Health Organisation. *WHO Methods and Data Sources for Life Tables 1990-2016*. World Health Organisation (2018).
15. Ahmad OB, Boschi-Pinto C, Lopez AD, Murray CJ, Lozano R, Inoue M. *Age Standardization of Rates: A New WHO Standard*. Geneva: World Health Organization. (2001). p. 9.
16. Hartley A, Marshall DC, Salciccioli JD, Sikkel MB, Maruthappu M, Shalhoub J. Trends in mortality from ischemic heart disease and cerebrovascular disease in Europe: 1980 to 2009. *Circulation.* (2016) 133:1916–26. doi: 10.1161/CIRCULATIONAHA.115.018931
17. den Heijer P. Transcatheter aortic valve implantation: first choice for aortic stenosis? *Neth Heart J.* (2020) 28:227–8. doi: 10.1007/s12471-020-01419-9
18. Hamm CW, Beyersdorf F. GARY-the largest registry of aortic stenosis treatment worldwide. *Eur Heart J.* (2020) 41:733–5. doi: 10.1093/eurheartj/ehaa048
19. Eggebrecht H, Mehta RH. Transcatheter aortic valve implantation (TAVI) in Germany 2008-2014: on its way to standard therapy for aortic valve stenosis in the elderly? *EuroIntervention.* (2016) 11:1029–33. doi: 10.4244/EIJY15M09_11
20. Mirat J, Hrvatsko kardiološko d, Croatian Cardiac S, Alfirević I, Hrvatsko kardiološko d, Croatian Cardiac S, et al. Aortic valve diseases in croatia in 2014 and their treatment. *Cardiologia Croatica.* (2020) 10:126–8. doi: 10.15836/ccar.2015.126
21. Kogoj P, Furlan T, Lakič N, Mušič Š, Kontestabile B, AmbroŽič J, et al. Most relevant complications of transcatheter aortic valve implantation related to the site of implantation: results of Slovenian national registry. *Srce i krvni sudovi.* (2015) 34:18–23. doi: 10.5937/siks1501018K
22. Cardiology ESo. *Valve for Life Initiative in Poland: ESC.* (2020). Available online at: https://www.escardio.org/Sub-specialty-communities/European-Association-of-Percutaneous-Cardiovascular-Interventions-(EAPCI)/Advocacy/valve-for-life-poland (accessed March 1, 2021).
23. Campante Teles R, Gama Ribeiro V, Patrício L, Neves JP, Vouga L, Fragata J, et al. Position statement on transcatheter aortic valve implantation in Portugal. *Rev Port Cardiol.* (2013) 32:801–5. doi: 10.1016/j.repce.2013.02.012
24. Abraha I, Chiarolla E, Corio M, Gillespie F, Migliore A, Cerbo M, et al. *Rapid Assessment of Other (Non-Pharmaceuticals) Health Technologies Using the HTA Core Model for Rapid Relative Effectiveness Assessment: EUnetHTA Project ID: OTCA06.* (2018). Available online at: https://www.eunethta.eu/wp-content/uploads/2018/12/OTCA06-TAVI-FOR-THE-TREATMENT-

OFPATIENTS-AT-INTERMEDIATE-SURGICAL-RISK-FINAL-1.pdf (accessed March 1, 2021).
25. Palta S, Pai AM, Gill KS, Pai RG. New insights into the progression of aortic stenosis: implications for secondary prevention. *Circulation.* (2000) 101:2497–502. doi: 10.1161/01.CIR.101.21.2497
26. Mihos CG, Klassen SL, Yucel E. Sex-specific considerations in women with aortic stenosis and outcomes after transcatheter aortic valve replacement. *Curr Treat Options Cardiovasc Med.* (2018) 20:52. doi: 10.1007/s11936-018-0651-x
27. Toyofuku M, Taniguchi T, Morimoto T, Yamaji K, Furukawa Y, Takahashi K, et al. Sex differences in severe aortic stenosis- clinical presentation and mortality. *Circ J.* (2017) 81:1213–21. doi: 10.1253/circj.CJ-16-1244
28. Laricchia A, Bellini B, Romano V, Khawaja S, Montorfano M, Chieffo A. Sex and transcatheter aortic valve implantation: impact of female sex on clinical outcomes. *Interv Cardiol.* (2019) 14:137–41. doi: 10.15420/icr.2019.07.R1
29. Onorati F, D'Errigo P, Barbanti M, Rosato S, Covello RD, Maraschini A, et al. Different impact of sex on baseline characteristics and major periprocedural outcomes of transcatheter and surgical aortic valve interventions: results of the multicenter Italian OBSERVANT registry. *J Thorac Cardiovasc Surg.* (2014) 147:1529–39. doi: 10.1016/j.jtcvs.2013.05.039
30. Gaglia MA Jr, Lipinski MJ, Torguson R, Gai J, Ben-Dor I, et al. Comparison in men versus women of co-morbidities, complications, and outcomes after transcatheter aortic valve implantation for severe aortic stenosis. *Am J Cardiol.* (2016) 118:1692–7. doi: 10.1016/j.amjcard.2016.08.049
31. Coffey S, Cairns BJ, Iung B. The modern epidemiology of heart valve disease. *Heart.* (2016) 102:75–85. doi: 10.1136/heartjnl-2014-307020

Conflict of Interest: The authors declare that the research was conducted in the absence of any commercial or financial relationships that could be construed as a potential conflict of interest.

The reviewer FB-L declared a shared affiliation, with one of the authors JDS to the handling editor at the time of the review.

frontiers in Cardiovascular Medicine

ORIGINAL RESEARCH
published: 10 December 2021
doi: 10.3389/fcvm.2021.754560

Pigmentation Affects Elastic Fiber Patterning and Biomechanical Behavior of the Murine Aortic Valve

Sana Nasim[1], *Popular Pandey*[2,3], *Rosemeire M. Kanashiro-Takeuchi*[4], *Jin He*[2,3], *Joshua D. Hutcheson*[1,2*†] *and Lidia Kos*[2,5*†]

[1] Department of Biomedical Engineering, Florida International University, Miami, FL, United States, [2] Biomolecular Sciences Institute, Florida International University, Miami, FL, United States, [3] Department of Physics, Florida International University, Miami, FL, United States, [4] Department of Molecular and Cellular Pharmacology, Leonard M Miller School of Medicine, University of Miami, Miami, FL, United States, [5] Department of Biological Sciences, Florida International University, Miami, FL, United States

OPEN ACCESS

Edited by:
Adrian Chester,
The Magdi Yacoub Institute,
United Kingdom

Reviewed by:
Claudia Dittfeld,
Technical University
Dresden, Germany
Ana Maria Porras,
Cornell University, United States

***Correspondence:**
Lidia Kos
kosl@fiu.edu
Joshua D. Hutcheson
jhutches@fiu.edu

†These authors have contributed equally to this work

Specialty section:
This article was submitted to Heart Valve Disease, a section of the journal Frontiers in Cardiovascular Medicine

Received: 06 August 2021
Accepted: 04 November 2021
Published: 10 December 2021

Citation:
Nasim S, Pandey P, Kanashiro-Takeuchi RM, He J, Hutcheson JD and Kos L (2021) Pigmentation Affects Elastic Fiber Patterning and Biomechanical Behavior of the Murine Aortic Valve. Front. Cardiovasc. Med. 8:754560. doi: 10.3389/fcvm.2021.754560

The aortic valve (AoV) maintains unidirectional blood distribution from the left ventricle of the heart to the aorta for systemic circulation. The AoV leaflets rely on a precise extracellular matrix microarchitecture of collagen, elastin, and proteoglycans for appropriate biomechanical performance. We have previously demonstrated a relationship between the presence of pigment in the mouse AoV with elastic fiber patterning using multiphoton imaging. Here, we extended those findings using wholemount confocal microscopy revealing that elastic fibers were diminished in the AoV of hypopigmented mice (Kit^{Wv} and albino) and were disorganized in the AoV of K5-Edn3 transgenic hyperpigmented mice when compared to wild type C57BL/6J mice. We further used atomic force microscopy to measure stiffness differences in the wholemount AoV leaflets of mice with different levels of pigmentation. We show that AoV leaflets of K5-Edn3 had overall higher stiffness (4.42 ± 0.35 kPa) when compared to those from Kit^{Wv} (2.22 ± 0.21 kPa), albino (2.45 ± 0.16 kPa), and C57BL/6J (3.0 ± 0.16 kPa) mice. Despite the striking elastic fiber phenotype and noted stiffness differences, adult mutant mice were found to have no overt cardiac differences as measured by echocardiography. Our results indicate that pigmentation, but not melanocytes, is required for proper elastic fiber organization in the mouse AoV and dictates its biomechanical properties.

Keywords: atomic force microscopy, echocardiography, pigment, extracellular matrix, elastin

INTRODUCTION

The aortic valve (AoV) functions to maintain unidirectional blood flow between the left ventricle and the aorta for the systemic distribution. The AoV undergoes constant pressure, stress, flexure, biaxial tension, and compression during a cardiac cycle, which requires the AoV to be durable for $\sim 3 \times 10^9$ cardiac cycles over the course of an average lifetime. The AoV is composed of highly structured cellular and extracellular matrix (ECM) components required to maintain appropriate biomechanics. The AoV ECM is mainly composed of collagen, elastin, and proteoglycans. In the AoV, radially aligned elastic fibers and circumferentially aligned collagen fibers dictate AoV function (1). Pathological alterations in alignment and composition compromise AoV biomechanics. In human

AoV, elastic fibers on the left ventricular side of the leaflets confer elasticity, allowing extension when the valve opens and recoiling when the valve closes. The proteoglycans in the internal spongiosa layer absorb compressive forces and lubricate interactions between the highly structured elastic fibers and fibrous collagen of the aortic side, fibrosa layer. The fibrosa layer with rich collagen fibers provides tensile strength to the AoV leaflets. Lastly, elastic fibers maintain the tissue load at low strains, allowing the collagen fibers and the leaflet to stretch passively before bearing the load at maximum loading (2). The structure-function relationship of elastin and collagen is critical for proper valve function but underscoring the need for a full understanding of leaflet fiber interactions and their dynamic behavior.

Along with the highly specialized ECM, cells within the AoV leaflets sense and respond to mechanical stresses and strains. The cellular responses to mechanical stresses play an important role in valve development and remodeling (3). Two major cellular components are found in the AoV leaflets: valvular endothelial cells (VECs) and valvular interstitial cells (VICs). The AoV leaflets consist of an outer layer of VECs on both fibrosa and ventricular sides that interact with blood and associated hemodynamic forces. The inner layers of VICs are responsible for producing and maintaining the ECM. The VICs comprise a heterogeneous population of cells that include smooth muscle cells, fibroblasts, myofibroblasts, neurons and glia (4, 5). Besides these subpopulations of VICs, murine heart valves contain melanin producing cells, the melanocytes (6). The location of these melanocytes coincided with another ECM protein, Versican B, in the atrioventricular valve (AV) leaflets, suggesting that melanocytes may regulate or be regulated by ECM molecules (7). Moreover, pigmented regions within the AV valves are significantly stiffer than non-pigmented regions establishing an association between pigment and the biomechanical properties of the valve (7, 8). Using nanoindentation, the elastic modulus of AV leaflets was found to be higher in hyperpigmented leaflets (11.5GPa) as compared to hypopigmented (5.5GPa) and wild type (7.5GPa) leaflets (8).

We recently showed that the elastic fiber network of the mouse AoV is affected by pigmentation (4). We compared the pigmented AoV of C57BL/6J wild-type with the AoV of two other mouse models that show variations in pigmentation levels. The K5-Edn3 transgenic mouse expresses the cytokine endothelin 3 (Edn3) under the control of the keratin 5 promoter (K5) leading to hyperpigmentation in cutaneous and non-cutaneous locations such as the heart valves. The Kit^{Wv} mouse harbors a spontaneous mutation in the receptor tyrosine kinase Kit locus leading to the complete lack of pigmentation in cutaneous and non cutaneous locations. Excessive pigmentation in the leaflets of the K5-Edn3 hyperpigmented mice associated with disorganized elastic fibers while the leaflets of the Kit^{Wv} hypopigmented mice had less elastic fibers when compared to wild-type mie as demonstrated by two-photon imaging. Given the changes in elastin fiber patterning and alterations in the biomechanical properties observed in the AoV leaflets of K5-Edn3 and Kit^{Wv} mice, a more detailed investigation of the valve phenotypes can lead to a better understanding of the underlying causes of AoV disease including fibrosis and calcification (9). The goal of this study was to further demonstrate the correlation between pigmentation and AoV leaflet stiffness and structure. We extended the analysis of the relationship between pigmentation and ECM organization by employing wholemount confocal imaging and another hypopigmented model, albino mice, where melanocytes are present but melanogenesis is blocked by a mutation in the pigment rate limiting enzyme tyrosinase. We also show how varying pigmentation levels affect regional stiffness using atomic force microscopy (AFM) on wholemount freshly dissected leaflets. Finally, we performed echocardiography to identify potential cardiac physiological manifestations resulting from the elastin phenotypes observed in the pigmentation mutant mice.

MATERIALS AND METHODS

Animals

All mice were housed in the Florida International University Animal Care Facility. The animal protocol for this study was approved by the Institutional Animal Care and Use Committee (IACUC 19-017). IACUC regulations were followed throughout the study. C57BL/6J wild type mice (WT for simplicity; Stock number 000664), B6(Cg)-Tyr^{c-2J}/J mice (albino for simplicity; stock number: 000058), and C57BL/6J-Kit^{W-v}/J mice (Kit^{Wv} for simplicity (only the homozygous spontaneous mutants were used); Stock number: 000049) were purchased from Jackson Laboratory (BarHabor, ME). The K5-tTA; TRE-Edn3-lacZ (K5-Edn3, for simplicity) transgenic mice were generated in our laboratory (10). Ten to twelve-week-old mice (strains: WT, K5-Edn3, Kit^{Wv}, albino) ($N = 5$–6; 3F and 3M) were utilized for the mechanical and functional assessment of the AoV leaflets.

Genotyping

Genomic DNA was isolated from tail biopsies of K5-Edn3 mice. Genotyping was performed using the primers: 5′ CCAGGTGGAGTCACAGGATT 3′, 5′ ACAGAGACTGTGGACCACCC 3′, for the recognition of the K5-tTA gene and, 5′ GGCCTGTGCACACTTCTGT 3′, 5′ TCCTTGTGAAACTGGAGCCT 3′ for the TRE-Edn3-LacZ transgene. Routine PCR conditions were used (45 cycles of 94°C for 30 s, 60°C for 60 s, and 72°C for 60 s) with an initial 3 min hold at 94°C. PCR product was then visualized in 1.5% agarose gel containing 0.5 μg/ml ethidium bromide (Thermo Fisher Scientific, Pittsburgh, PA). The K5-tTA produced a 244 bp band, whereas the TRE-Edn3-LacZ produced a 463 bp band. WT, Kit^{Wv}, albino were identified phenotypically and did not require a genotype assessment.

ECM Structural Staining and Quantification

ECM Staining

Alexa Fluor 633 (AF 633) hydrazide (Invitrogen, Waltham, MA, Cat# A30634) for elastic fiber staining was used as previously described (11, 12). 0.2 μM concentration of AF633 probe in PBS was used along with 10 μM CNA-488 probe for collagen fiber staining (CNA-488 was kindly gifted by Chris Reutelingsperger from Maastricht University, Netherlands) (13). The wholemount

AoV tissue staining was carried out for 45 min at room temperature prior to 4% paraformaldehyde (PFA) fixation and pigment bleaching in 10% H_2O_2 overnight. Tissues were then placed on a glass side with the three leaflets of the AoV facing up and sealed with a coverslip. Z-stack images were taken using an Olympus Confocal BX61 microscope.

Staining Quantification

The obtained Z-stack images were utilized for 3D reconstruction and image processing. In brief, Z-project plugin in NIH ImageJ (14) was used to compile the z-stacks, and the ROI manager plugin was used to quantify the fluorescence signals from each stack after tracing a region around the leaflet.

Angle Quantification

A spectral based Cytospectre tool box was used to quantify the orientation of the elastin and collagen fiber angles from the z-stack images (15). For angle quantification, high magnification regional images were taken in all the four mouse models (**Supplementary Figure 1**). Collagen and elastic fiber alignment were separately measured in the green and red channel, respectively. All the collagen fibers were used as reference to elastic fibers, where the collagen fiber angles for each of the mouse model leaflet was set to zero and elastic fibers were rotated accordingly.

Atomic Force Microscopy

Mouse Aortic Valve Isolation and Setup

Ten to twelve-week-old mice (strains: WT, K5-Edn3, Kit^{Wv}, albino) ($N = 4$–5) were euthanized and the hearts were immediately washed in cold PBS. Within 5 min, AoV leaflets were isolated and placed on a coverslip in a 60 mm petri dish. Coverslips were glued with clear silicon waterproof sealant to the petri dish to avoid any movement of the coverslip. During the analyses, leaflets were kept in cold PBS, and all measurements were taken within 30–45 min of leaflet isolation. Following the AFM measurements, all samples were fixed in 4% PFA for 5–10 min (**Supplementary Figure 2**).

AFM Set Up

An XE-Bio system (Park systems, Santa Clara, CA, USA) in contact mode was used for all AFM measurements. Pre-calibrated gold-coated bead AFM probe (Novascan Technologies, Ames IA, USA) with a 1 μm diameter SiO_2 microsphere were used for the indentation measurements. The spring constant of the tip was 0.1 N/m. Force curves measurements at the targeted region of AoV leaflet were performed with a probe approaching speed of 0.3 μm/s and peak force range 0.4–2.4nN. Each targeted point was measured three to five times to ensure the accuracy of the measurement.

Data Analysis

The sample's Young modulus of elasticity (Y_E) was calculated using a Hertz model:

$$F = \frac{4Y_E R^{0.5}}{3\left(1-\nu^2\right)}\delta^{1.5}$$

Where, ν is the Poisson's ratio, which was set to be 0.5, and R of 0.5 μm is the radius of the tip. Sample indenting force (F) and deformation (δ) were calculated as follows:

$$F = k\left(d - d_0\right)$$

$$\delta = (z - z_0) - \left(d - d_0\right)$$

A custom MATLAB script was used to fit the measured force curves to obtain the Y_E values for each region.

Regional Pigment Quantification From Resected Leaflets

For the quantification of pigment, all the wholemount leaflets were oriented in the same direction and four regions were labeled: tip, belly, base, and commissure. All images were converted into 8-bit and each region was identified based on the intensity of the darker and lighter regions associated with pigment using ImageJ. Percent regional pigment was normalized with total leaflet pigment.

Echocardiography

Animal Preparation and Imaging Setup

Prior to image acquisition, mouse chest fur was removed by applying hair removal cream. Each animal was shaved immediately before the image acquisition and placed under 1–2% isoflurane. For consistency and comparability, all imaging conditions were controlled between animals. Mouse body temperature was monitored and maintained around 37°C during the entirety of the protocol. Since cardiac function is influenced by heart rate (HR), the HR was maintained at a similar level (450 ± 50 bpm) within each strain during imaging. Additionally, echo measurements were performed at similar times after anesthesia was administered to minimize differences in anesthesia-related effects to cardiac function.

The imaging setup included applying warm gel on the shaved chest and placing the mouse on a heating platform. ECG was continuously monitored. The heart was imaged with MX400, 20–46MHz linear transducer, with an axial resolution of 50 μm. Images were taken at 300–400 frames per second. All the imaging were done using a Vevo 3,100 (FUJIFILM Visual Sonics, Toronto Canada) imaging system under the IACUC rules and regulation at Sylvester Comprehensive Cancer Center at University of Miami.

Echocardiographic Assessments and Data Analysis

M-mode images in the left ventricle short-axis view and B-mode long-axis view were obtained for each mouse in a blinded fashion. Pulsed wave Doppler images were taken by placing the sample volume parallel to flow direction, which was assisted by Color Doppler-mode during long-axis view into left ventricular outflow tract and ascending aorta for AoV function. For mitral valve assessment, the apical four-chamber view was used (**Supplementary Table 1**). Quantified measures of function were obtained by averaging three consecutive heartbeats during the echocardiographic examination. From the M-mode, the left ventricular anterior, posterior, and inner wall during systolic and

diastolic peaks were taken to assess the LV thickness. Aortic valve measurements included peak AoV pressure, mean AoV velocity, peak AoV velocity, velocity across the AoV. Mitral valve Doppler was used to assess diastolic function by measuring intraventricular relaxation (IVRT)/contraction time (IVCT), the mitral peak velocity of early filling ratio to peak velocity flow in late diastole (E/A), and ejection time (ET). All data were analyzed using the Vevo Lab software (FUJIFILM Visual Sonics, Toronto Canada).

Tail Cuff Measurements

A non-invasive small animal blood pressure monitoring system (CODA Kent Scientific, Torrington, CT) was used to measure heart rate, systolic and diastolic blood pressure, and mean arterial blood pressure in ten- to twelve-week-old mice. In brief, the CODA tail-cuff system uses a specialized volume-pressure recording sensor to determine the tail blood volume to measure the blood pressure. All animals were kept anesthetized under 1–2% isoflurane. 10–15 consecutive readings were taken per animal to obtain stable blood pressure measurements.

Statistical Analysis

All quantitative data are given as mean ± standard error mean (SEM). For AFM results, each color point within the strain represents a biological replicate calculated from a mean of $N = 3$–4. "N" indicates the number of biological replicates within each strain and "n" indicates the technical replicates. For AFM and echocardiography results, statistical packages in GraphPad were used to assess data normality and variance between the groups (GraphPad Prism6 Software, LaJolla, CA). Statistical differences were determined using either the student's t-test or one-way analysis of variance (ANOVA) along with Tukey's *post hoc* HSD test with significance considered as $p < 0.05$. All the shown percent differences were normalized by the specified comparison.

RESULTS

Elastic Fiber Patterning of The Aortic Valve Leaflets Is Affected by Pigmentation

To assess the organization of elastic and collagen fibers in wholemount AoV leaflets, we used AF633 and CNA488, respectively. As in human AoV, murine wild type AoV had radially aligned elastic fibers and circumferentially aligned collagen fibers (**Figure 1A**). In the K5-Edn3 transgenic mouse Edn3 overexpression is under the control of keratin 5 promoter, resulting in excess pigment production by both cutaneous and non-cutaneous melanocytes (**Figure 1B**). The patterning of elastic fibers in the leaflets of K5-Edn3 mice appeared disoriented with fibers misaligned and ectopically located (**Figure 1B**). Kit^{Wv} and albino hypopigmented mice were assessed to further understand the role of pigment in elastic fiber patterning. Kit^{Wv} mice lack melanocytes in hair follicles leading to a white coat color, whereas albino mice have melanocytes that are unable to produce pigment due to a mutation in the *Tyrosinase* gene. The AoVs of both mutants are hypopigmented (**Figures 1C,D**). Compared to WT, Kit^{Wv} and albino AoV leaflets had fewer elastic fibers (**Figures 1C,D**). Quantification of elastic fiber fluorescence indicated that the elastic fibers was significantly reduced in the leaflets of Kit^{Wv} (66.3 ± 27.8%, $N = 7$, $n = 3$) and albino (64 ± 54.8%, $N = 3$, $n = 8$) compared to WT ($p = 0.0026$, $N = 4$, $n = 9$). In comparison to the leaflets of K5-Edn3 ($p < 0.01$, $N = 4$, $n = 7$), Kit^{Wv} (64.4 ± 29.8%) and albino (62 ± 56%) leaflets also had significantly reduced amounts of elastic fiber fluoresence (**Figure 1E**). We did not find statistically significant differences among the four groups for the collagen fiber staining (**Figure 1F**). Alignment of elastic fibers in relationship to the collagen fibers was also found to be mostly orthogonal in all four mouse models (**Figure 1G**). The elastic fiber alignment in WT was found to be 83.57 ± 7.18°, K5-Edn3 to be 67.74 ± 5.46°, Kit^{Wv} to be 58.08 ± 6.79° and lastly, albino to be 77.39 ± 7.72° with the collagen fibers referenced as 0°.

Micromechanical Properties of the Aortic Valve Leaflets Are Affected by Pigmentation

As expected, we found K5-Edn3 to have significantly higher overall leaflet pigmentation as compared to WT ($p = 0.023$), Kit^{Wv} ($p < 0.0001$) and albino ($p < 0.0001$) (**Figure 2A**). Similar to our previously published observations in the AV valve (8) (7), the overall stiffness of the AoV leaflet of the hyperpigmented K5-Edn3 showed a 30.9 ± 34.6% ($p = 0.0004$) higher stiffness compared to that of WT. Whereas hypopigmented Kit^{Wv} and albino were found to have significantly lower overall stiffness of 28.6 ± 25.4% ($p = 0.004$) and 22.8 ± 28.3% ($p = 0.0183$), respectively, in the AoV leaflet as compared to WT (**Figure 2B**). Moreover, compared to K5-Edn3, the hypopigmented Kit^{Wv} ($p < 0.0001$) and albino ($p < 0.0001$) AoV leaflets were found to have significantly lower stiffness of 45 ± 44.6% and 41.06 ± 46.80%, respectively (**Figure 2B**).

To further explore the relationship between pigment and the associated stiffness in wholemount AoV leaflets, the regional distribution of pigment (**Figure 2C**) was quantified. In WT leaflets pigment was found to be significantly lower in the commissure region compared to the same region in K5-Edn3 leaflets ($p = 0.0026$). In the tip region, pigment there was more pigment in WT leaflets when compared to those of K5-Edn3 ($p = 0.0837$) (**Figure 2D**). Of note, pigmentation was distributed more uniformly throughout the K5-Edn3 leaflets.

Among the four mouse models, there were no significant differences in stiffness within the tip region (**Figure 2E**), whereas K5-Edn3 showed significantly higher stiffness in the belly region compared to Kit^{Wv} mice ($p = 0.0205$) (**Figure 2F**). In the base region, K5-Edn3 exhibited higher stiffness ($p < 0.0001$) compared to WT, $Kit^{Wv,}$ and albino mice (**Figure 2G**). Furthermore, in the commissure region, WT stiffness was significantly higher than Kit^{Wv} ($p = 0.0432$) and albino ($p = 0.0047$) mice. Lastly, regional commissure stiffness of K5-Edn3 mice was comparable to that of WT and significantly higher compared to that of Kit^{Wv} ($p = 0.0075$) and albino ($p = 0.0003$) mice (**Figure 2H**). Overall we did not find any differences among the biological replicates in the mouse models (**Supplementary Figure 3**).

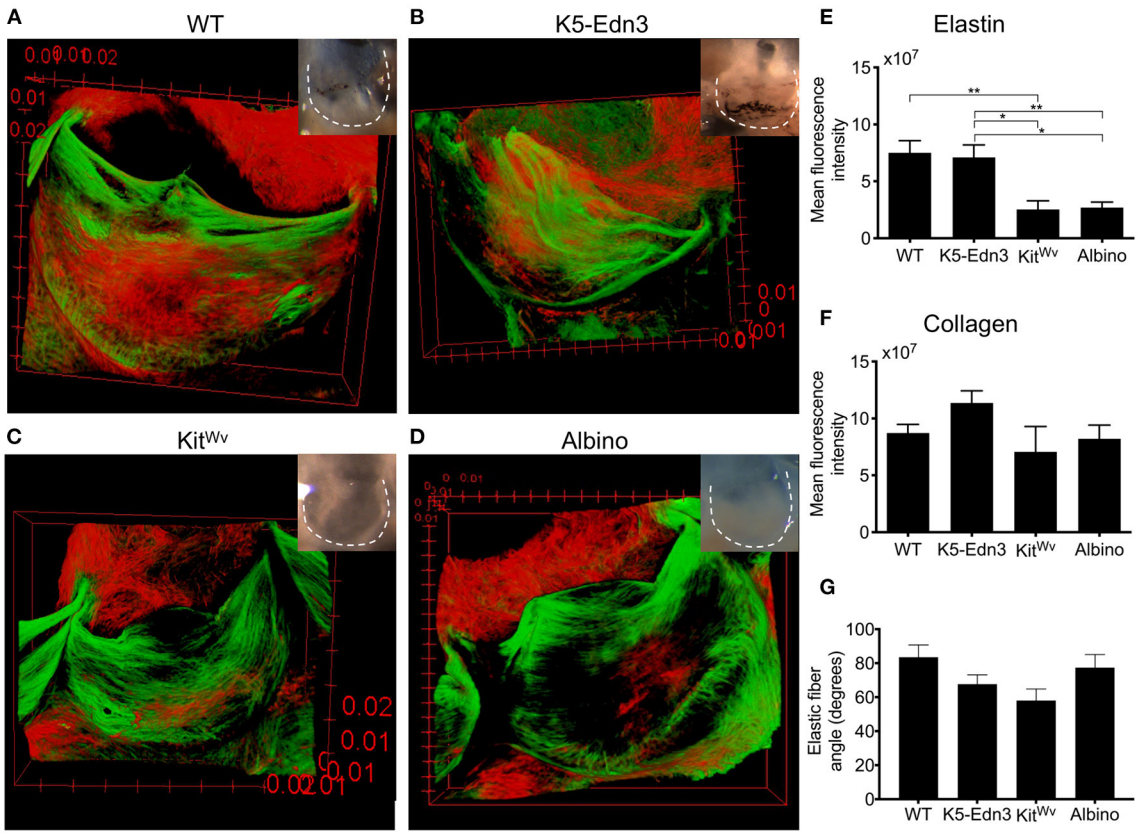

FIGURE 1 | Relationship between pigment variation and ECM in the AoV leaflet. Elastin (red) and collagen (green) staining of 12–13 weeks old mouse wholemount AoV leaflets of **(A)** WT, **(B)** K5-Edn3, **(C)** Kit^{Wv}, and **(D)** albino. Leaflets in the optical microscope images correspond to those in the images of the stained leaflets. Quantification of **(E)** elastin and **(F)** collagen fluorescence staining. **(G)** Elastic fiber angle quantification. MAG = 10X. Mean ± SEM shown; $^{**}p < 0.001$, $^{*}p < 0.05$. N = 4–5 biological replicates.

No Overt Aortic Valve Functional Differences Found With the Variation of Pigmentation

Using M-mode, B-mode, and pulsed wave Doppler imaging, cardiac functional parameters were assessed. No parameters traditionally associated with AoV function were found to be different between the mouse genotypes studied (**Figures 3A,B**). However, mitral valve ejection time was found to be significantly lower in K5-Edn3 mice compared to WT ($p = 0.018$) and Kit^{Wv} ($p = 0.0126$). There was also a significant difference ($p < 0.05$) between the E/A ratio of WT and Kit^{Wv} mice (**Supplementary Table 2**). We also assessed heart rate, systolic/diastolic blood pressure, and mean arterial pressures with conventional non-invasive tail-cuff blood pressure measurements. There was a significant increase in heart rate ($p = 0.0001$) and body weight/heart weight ratio ($p < 0.01$) among K5-Edn3 and Kit^{Wv} mice compared to WT mice (**Figures 3C,D**).

DISCUSSION

The AoV cells and ECM microstructure confer the appropriate biomechanical properties for valvular function. In the current study, we assessed wholemount AoV ECM patterning, specifically elastin and collagen in four different mouse models (WT, K5-Edn3, Kit^{Wv} and albino). We further show the biomechanical properties in the mouse models using AFM in freshly dissected wholemount AoV leaflets. The mechanical properties of murine AoV have been previously explored with other techniques such as micropipette aspiration and atomic force microscopy on fixed tissue sections (16, 17). This is the first study to report the relationship of ECM patterning and its associated biomechanical properties in freshly dissected wholemount AoV leaflets.

Using multiphoton imaging, we recently showed that the hypopigmented Kit^{Wv} mice lacked elastic fibers and had reduced elastin gene expression, whereas hyperpigmented K5-Edn3 mice with overabundant pigment had increased elastic fibers and elastin gene expression (4). The analysis presented here corroborates and extends these findings to another hypopigmented model, albino mice. We show that hypopigmented AoV leaflets (Kit^{Wv} and albino) have diminished elastic fibers. The addition of albino mice indicate that pigment production—rather than the presence of melanocytic populations—lead to the observed changes in elastic fiber patterning. We also found that elastic fibers in the WT leaflets

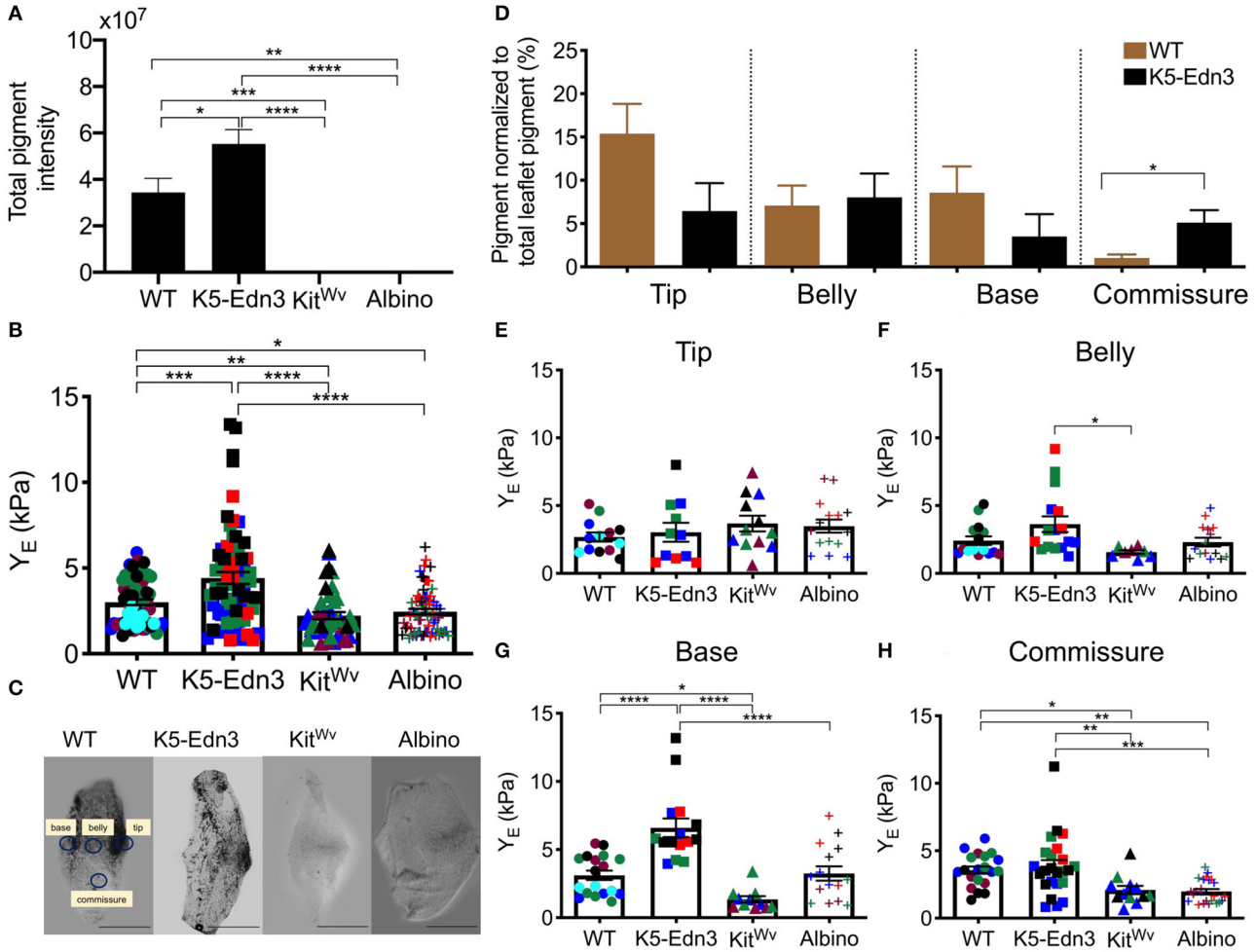

FIGURE 2 | Relationship between pigment variation and stiffness of the AoV leaflet. **(A)** Total pigment in the wholemount AoV leaflets in the four mouse models. **(B)** Stiffness measurements of wholemount AoV leaflets of WT, K5-Edn3 (hyperpigmented), Kit^{Wv} and albino (hypopigmented) mice. **(C)** Optical microscope image of resected wholemount AoV leaflet from the four mouse models. All the four leaflets are oriented in the same direction. WT label of the four regions corresponds to the other three leaflets, and stiffness and pigment quantification **(D)** Regional pigment quantification in all four mouse models. Regional stiffness of wholemount AoV leaflets of the four moue models in the **(E)** Tip **(F)** Belly **(G)** Base **(H)** Commissure. Mean ± SEM shown; $^{****}p < 0.0001$, $^{***}p < 0.0005$, $^{**}p < 0.001$, $^{*}p < 0.05$; N = 4–5 biological replicates per condition. Each color represents a biological replicate, and each color point represents an average of technical replicates of N = 3–4. Scale bar = 100 μm.

were orthogonal to the collagen fibers, similar to the alignment known in human AoV (4, 18). While not significantly different, we observed trends that indicate less orthogonality in the K5-Edn3 and Kit^{Wv} elastic fibers. To be noted, although pigment has not been observed in human valves, cells expressing melanocyte phenotypic markers [including dopachrome tautomerase (DCT) and tyrosinase related protein 1 (TRP1)] have been observed (4). These melanocytic markers exist within leaflets in a manner that mirrors the localization observed in murine leaflets. Future studies are needed to fully understand how these cells contribute to AoV patterning across species. Understanding the mechanisms associated with elastogenesis is critical as elastin abnormalities result in congenital AoV defects and elastin degradation can initiate AoV disease (19–21). The emilin1 deficient mouse has been proposed as a model for human fibrotic aortic valve disease (9). Emilin 1 is an elastin-binding glycoprotein involved in the process of elastogenesis. Its deficiency is associated with early postnatal elastic fiber fragmentation in the AoV and leaflet stiffening prior to full onset of fibrotic disease (22). The elastic fiber phenotype of the mouse models used in this study and its association to the presence of pigmentation may offer another avenue for the identification of factors important in the progression of aortic valve disease and provide potential therapeutic targets.

Previously pigment has been shown to be important in conferring biomechanical properties of the porcine retinal pigment epithelium using AFM and spectroscopy (23). Melanin granules were shown to be critical in maintaining the stiffness of the epithelium layer which is important in the mechanical separation between the retina from the

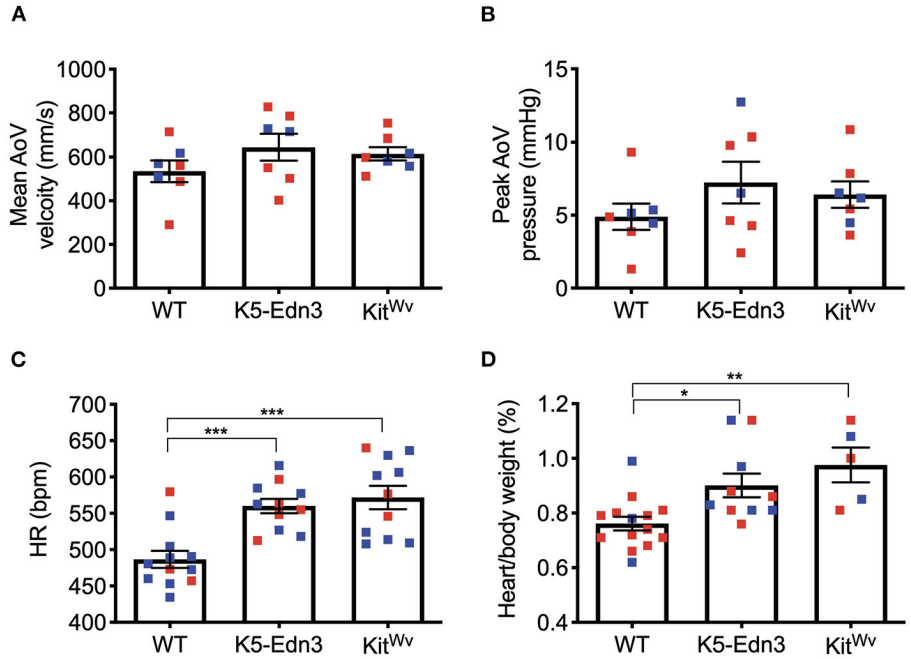

FIGURE 3 | Functional cardiac assessment of mouse models with varying levels of pigmentation in the AoV (WT, K5-Edn3, Kit^{Wv}). AoV blood flow measurement by pulse wave Doppler imaging **(A)** Mean AoV velocity **(B)** Peak AoV pressure **(C)** Non-invasive tail-cuff method to assess the heart rate. **(D)** Cardiac hypertrophy was determined by the ratio of heart weight (mg) to body weight (g). Mean ± SEM shown; $^{***}p < 0.0005$, $^{**}p < 0.001$, $^{*}p < 0.05$; $N = 7$ animals per group; Male (blue) and female (red); Age: 12–13 weeks old mice.

choroid. Using nanoindentation by AFM we showed that pigmented regions of AV leaflets are stiffer than non-pigmented regions, suggesting that pigment affects valve biomechanics (8). Moreover, we previously showed that hyperpigmented AV leaflets are stiffer than WT or hypopigmented valve leaflets, suggesting a contribution of pigment to the overall mechanical properties of murine heart valves (7). Here, we cooroborate the previous finding that hypopigmented leaflets are less stiff than WT and hyperpigmented leaflets by adding the albino hypopigmented model. These results further demonstrate that the presence of pigmentation affects the overall biomechanical properties, mainly the base and the commissure regions of the AoV leaflet. It has also previously been reported that the commissures of the human AoV have higher elastic modulus using uniaxial tensile testing (24). We found regional differences in stiffness among the mouse models suggesting that the changes in the biomechanical properties and ECM patterning could alter gross leaflet properties. We observed a strong positive correlation between total amount of pigment and leaflet stiffness in WT mice (**Supplementary Figure 4A**, $R^2 = 0.9582$). The overall stiffness was higher in the hyperpigmented mice and lower in the hypopigmented mice, as expected (**Supplementary Figure 4B**, $R^2 = 0.5765$). Individual differences in relation between pigment and stiffness, however, may indicate that the microstructural differences observed in these mice affect the stiffness beyond differences in pigmentation. AoV leaflets are heterogenous, which presents challenges for the localization of the AFM probe for consistent AFM measurements. AFM quantifies stiffness with micron spatial resolution; therefore, small differences in the chosen regions of interest could yield different results. Despite challenges with assessing small regions of interest for micromechanical testing, this is the first study to compare localized stiffness with corresponding ECM fiber patterning in freshly isolated wholemount murine AoV. Although we previously reported that unequal levels of pigmentation may occur amongst the left, right and coronary leaflets of the AoV (25), in this study all WT and K5-Edn3 leaflets that were used for biomechanical analyses were pigmented and we did not tract their anatomical position within the valve. We recognize this may have introduced some biases in the results and suggest that future studies take into consideration leaflet position to account for potential ontogenetic and histological differences among the three leaflets. Overall, this study has found a novel role for pigment in proper ECM deposition and biomechanics of the AoV.

Cardiac function assessed by echocardiography was found to be similar between the mouse models despite the drastic elastic fiber phenotypic difference observed. Cardiac imaging in mouse models are challenging due to their small size and high heart rate. We speculate that the lack of overt differences could potentially be explained by some compensatory mechanism that allows cardiac function to remain normal such as hypertrophy represented by an increase in HW/BW ratio (**Figure 3D**) or stiffer heart muscle, which we did not explore in this study. Alternatively, it is possible that differences between the groups would manifest in later adulthood or in response to pathological cues. In addition, in our study,

we used males and females which could explain the lack of differences between mouse strains since sex differences have been reported in preclinical (26) and clinical studies (27, 28). A diet variation may be used to create pathological conditions; for example, mice could be put under different types of diets such as celecoxib to manipulate glucocorticoid signaling to create a more permissive environment for the appearance of cardiac diseases (29). To further access if there were differences related to early stages of valve diseases particularly VIC activation, we found that the tip region of Kit^{Wv} was mostly devoid of α-SMA positive cells, which were also few in the belly and base regions (**Supplementary Figure 5**). However, no significant differences in the number of α-SMA positive cells were detected among the three mouse models. Future studies should assess cellular-level differences at developmental timepoints that correspond with elastin synthesis to understand associated mechanisms. A recent study showed that the expression of ECM components such as decorin, osteopontin, Cthrc1 and Ddr1 which are involved in collagen metabolism as well as TGFb signaling change in an age dependent manner potentially underlying cardiac functional differences observed in older mice (30). Metalloproteinase driven elastic fiber degradation has previously been shown to contribute to heart valve mineralization leading to progression of calcific aortic stenosis (31). Future studies that explore the mechanisms associated with elastic fiber differences and implications in pathological valve remodeling could lead to new insight into AoV homeostasis and disease.

DATA AVAILABILITY STATEMENT

The raw data supporting the conclusions of this article will be made available by the authors, without undue reservation.

ETHICS STATEMENT

The animal study was reviewed and approved by IACUC Florida International University.

AUTHOR CONTRIBUTIONS

SN designed the experiments, drafted the manuscript, conducted the aortic valve dissections, staining, confocal imaging, and AFM data analysis. PP conducted the AFM force curve measurements. RK-T imaged echocardiography and analyzed the echo data. JH supervised PP and provided feedback on AFM experiments. LK and JH equally designed the experiments, supervised SN and reviewed all the versions of the manuscript. All authors read and approved the final manuscript.

FUNDING

This work was supported by the Florida Heart Research Foundation. SN was partially funded by Florida International University Graduate School. PP was partially supported by NSF CBET 1454544 and FIU CASE distinguished postdoctoralfellowship.

ACKNOWLEDGMENTS

We would like to thank the FIU Confocal Core Facility.

SUPPLEMENTARY MATERIAL

The Supplementary Material for this article can be found online at: https://www.frontiersin.org/articles/10.3389/fcvm.2021.754560/full#supplementary-material

REFERENCES

1. Sacks MS, Yoganathan AP. Heart valve function: a biomechanical perspective. *Philos Trans R Soc B Biol Sci.* (2007) 362:1369–91. doi: 10.1098/rstb.2007.2122
2. Stella JA, Sacks MS. On the biaxial mechanical properties of the layers of the aortic valve leaflet. *J Biomech Eng.* (2007) 129:757–66. doi: 10.1115/1.2768111
3. Arjunon S, Rathan S, Jo H, Yoganathan AP. Aortic valve: mechanical environment and mechanobiology. *Ann Biomed Eng.* (2013) 41:1331–46. doi: 10.1007/s10439-013-0785-7
4. Hutcheson JD, Schlotter F, Creager MD Li X, Pham T, Vyas P, Higashi H, et al. Elastogenesis correlates with pigment production in murine aortic valve leaflets. *Front Cardiovasc Med.* (2021) 8:533. doi: 10.3389/fcvm.2021.678401
5. Schlotter F, Halu A, Goto S, Blaser MC, Body SC, Lee LH, et al. Spatiotemporal multi-omics mapping generates a molecular atlas of the aortic valve and reveals networks driving disease. *Circulation.* (2018) 138:377–93. doi: 10.1161/CIRCULATIONAHA.117.032291
6. Brito FC, Kos L. Timeline and distribution of melanocyte precursors in the mouse heart. *Pigment Cell Melanoma Res.* (2008) 21:464–70. doi: 10.1111/j.1755-148X.2008.00459.x
7. Carneiro F, Kruithof BP, Balani K, Agarwal A, Gaussin V, Kos L. Relationships between melanocytes, mechanical properties and extracellular matrix composition in mouse heart valves. *J Long Term Eff Med Implants.* (2015) 25:17–26. doi: 10.1615/JLongTermEffMedImplants.2015011748
8. Balani K, Brito FC, Kos L, Agarwal A. Melanocyte pigmentation stiffens murine cardiac tricuspid valve leaflet. *J R Soc Interface.* (2009) 6:1097–102. doi: 10.1098/rsif.2009.0174
9. Munjal C, Opoka AM, Osinska H, James JF, Bressan GM, Hinton RB. TGF- mediates early angiogenesis and latent fibrosis in an Emilin1-deficient mouse model of aortic valve disease. *Dis Model Mech.* (2014) 7:987–96. doi: 10.1242/dmm.015255
10. Garcia RJ, Ittah A, Mirabal S, Figueroa J, Lopez L, Glick AB, et al. Endothelin 3 induces skin pigmentation in a keratin-driven inducible mouse model. *J Invest Dermatol.* (2008) 128:131–42. doi: 10.1038/sj.jid.5700948
11. Sierra H, Cordova M, Chen C-SJ, Rajadhyaksha M. Confocal imaging–guided laser ablation of basal cell carcinomas: an *ex vivo* study. *J Invest Dermatol.* (2015) 135:612–5. doi: 10.1038/jid.2014.371
12. Clifford PS, Ella SR, Stupica AJ, Nourian Z, Li M, Martinez-Lemus LA, et al. Spatial distribution and mechanical function of elastin in resistance arteries. *Arterioscler Thromb Vasc Biol.* (2011) 31:2889–96. doi: 10.1161/ATVBAHA.111.236570
13. Aper SJA, van Spreeuwel ACC, van Turnhout MC, van der Linden AJ, Pieters PA, van der Zon NLL, et al. Colorful protein-based fluorescent probes for collagen imaging. *PLoS ONE.* (2014) 9:e114983. doi: 10.1371/journal.pone.0114983
14. Rasband WS. *ImageJ*. U.S. National Institutes of Health, Bethesda, Maryland, US. Available online at: https://imagej.nih.gov/ij/
15. Kartasalo K, Pölönen RP, Ojala M, Rasku J, Lekkala J, Aalto-Setälä K, et al. CytoSpectre: a tool for spectral analysis of oriented structures on cellular and subcellular levels. *BMC Bioinformatics.* (2015) 16:1–23. doi: 10.1186/s12859-015-0782-y

16. Krishnamurthy VK, Guilak F, Narmoneva DA, Hinton RB. Regional structure–function relationships in mouse aortic valve tissue. *J Biomech.* (2011) 44:77–83. doi: 10.1016/j.jbiomech.2010.08.026
17. Sewell-Loftin M-K, Brown CB, Baldwin HS, Merryman WD. A novel technique for quantifying mouse heart valve leaflet stiffness with atomic force microscopy. *J Heart Valve Dis.* (2012) 21:513–20.
18. Wiltz D, Arevalos CA, Balaoing LR, Blancas AA, Sapp MC, Zhang X, et al. Extracellular matrix organization, structure, and function. In: *Calcific Aortic Valve Disease*. Hicksville: IntechOpen (2013). doi: 10.5772/52842
19. Sherratt MJ. Tissue elasticity and the ageing elastic fibre. *Age (Omaha).* (2009) 31:305–25. doi: 10.1007/s11357-009-9103-6
20. Krettek A, Sukhova GK, Libby P. Elastogenesis in human arterial disease: A role for macrophages in disordered elastin synthesis. *Arterioscler Thromb Vasc Biol.* (2003) 23:582–7. doi: 10.1161/01.ATV.0000064372.78561.A5
21. Debelle L, Tamburro AM. Elastin: molecular description and function. *Int J Biochem Cell Biol.* (1999) 31:261–72. doi: 10.1016/S1357-2725(98)00098-3
22. Angel PM, Narmoneva DA, Sewell-Loftin MK, Munjal C, Dupuis L, Landis BJ, et al. Proteomic Alterations Associated with Biomechanical Dysfunction are Early Processes in the Emilin1 Deficient Mouse Model of Aortic Valve Disease. *Ann Biomed Eng.* (2017) 45:2548–62. doi: 10.1007/s10439-017-1899-0
23. Sarna M, Olchawa M, Zadlo A, Wnuk D, Sarna T. The nanomechanical role of melanin granules in the retinal pigment epithelium. *Nanomedicine.* (2017) 13:801–7. doi: 10.1016/j.nano.2016.11.020
24. Stradins P, Lacis R, Ozolanta I, Purina B, Ose V, Feldmane L, et al. Comparison of biomechanical and structural properties between human aortic and pulmonary valve. *Eur J Cardiothorac Surg.* (2004) 26:634–9. doi: 10.1016/j.ejcts.2004.05.043
25. Chaparro D, Dargam V, Alvarez P, Yeung J, Saytashev I, Bustillo J, et al. A method to quantify tensile biaxial properties of mouse aortic valve leaflets. *J Biomech Eng.* (2020) 142:100801. doi: 10.1115/1.4046921
26. Walker CJ, Schroeder ME, Aguado BA, Anseth KS, Leinwand LA. Matters of the heart: cellular sex differences. *J Mol Cell Cardiol.* (2021) 160:42–55. doi: 10.1016/j.yjmcc.2021.04.010
27. Kong WK, Regeer MV, Ng AC, McCormack L, Poh KK, Yeo TC, et al. Sex differences in phenotypes of bicuspid aortic valve and aortopathy: insights from a large multicenter, international registry. *Circ Cardiovasc Imaging.* (2017) 10:e005155. doi: 10.1161/CIRCIMAGING.116.005155
28. Myasoedova VA, Di Minno A, Songia P, Massaiu I, Alfieri V, Valerio V, et al. Sex-specific differences in age-related aortic valve calcium load: a systematic review and meta-analysis. *Ageing Res Rev.* (2020) 61:101077. doi: 10.1016/j.arr.2020.101077
29. Vaidya KA, Donnelly MP, Gee TW, Ibrahim Aibo M-A, Byers S, Butcher JT. Induction of aortic valve calcification by celecoxib and its COX-2 independent derivatives is glucocorticoid-dependent. *Cardiovasc Pathol.* (2020) 46:107194. doi: 10.1016/j.carpath.2019.107194
30. Grilo GA, Shaver PR, Stoffel HJ, Morrow CA, Johnson OT, Iyer RP, et al. Age- and sex-dependent differences in extracellular matrix metabolism associate with cardiac functional and structural changes. *J Mol Cell Cardiol.* (2020) 139:62–74. doi: 10.1016/j.yjmcc.2020.01.005
31. Perrotta I, Russo E, Camastra C, Filice G, Di Mizio G, Colosimo F, et al. New evidence for a critical role of elastin in calcification of native heart valves: immunohistochemical and ultrastructural study with literature review. *Histopathology.* (2011) 59:504–13. doi: 10.1111/j.1365-2559.2011.03977.x

Conflict of Interest: The authors declare that the research was conducted in the absence of any commercial or financial relationships that could be construed as a potential conflict of interest.

Publisher's Note: All claims expressed in this article are solely those of the authors and do not necessarily represent those of their affiliated organizations, or those of the publisher, the editors and the reviewers. Any product that may be evaluated in this article, or claim that may be made by its manufacturer, is not guaranteed or endorsed by the publisher.

frontiers in Cardiovascular Medicine

REVIEW
published: 04 January 2022
doi: 10.3389/fcvm.2021.760635

Residual Bioprosthetic Valve Immunogenicity: Forgotten, Not Lost

Paul Human[1,2]*, *Deon Bezuidenhout*[1,2], *Elena Aikawa*[3] and *Peter Zilla*[1,2,4]

[1] Chris Barnard Division of Cardiothoracic Surgery, University of Cape Town and Groote Schuur Hospital, Cape Town, South Africa, [2] Cardiovascular Research Unit, Faculty of Health Sciences, University of Cape Town, Cape Town, South Africa, [3] Division of Cardiovascular Medicine, Brigham and Women's Hospital and Harvard Medical School, Boston, MA, United States, [4] Faculty of Health Sciences, Cape Heart Institute, University of Cape Town, Cape Town, South Africa

Despite early realization of the need to control inherent immunogenicity of bioprosthetic replacement heart valves and thereby mitigate the ensuing host response and its associated pathology, including dystrophic calcification, the problem remains unresolved to this day. Concerns over mechanical stiffness associated with prerequisite high cross-link density to effect abrogation of this response, together with the insinuated role of leaching glutaraldehyde monomer in subsequent dystrophic mineralization, have understandably introduced compromises. These have become so entrenched as a benchmark standard that residual immunogenicity of the extracellular matrix has seemingly been relegated to a very subordinate role. Instead, focus has shifted toward the removal of cellular compartment antigens renowned for their implication in the failure of vascularized organ xenotransplants. While decellularization certainly offers advantages, this review aims to refocus attention on the unresolved matter of the host response to the extracellular matrix. Furthermore, by implicating remnant immune and inflammatory processes to bioprosthetic valve pathology, including pannus overgrowth and mineralization, the validity of a preeminent focus on decellularization, in the context of inefficient antigen and possible residual microbial remnant removal, is questioned.

Keywords: bioprosthetic, valve, extracellular matrix, decellularization, immunogenicity, pathology, inflammation, calcification

OPEN ACCESS

Edited by:
Bart Meuris,
University Hospitals Leuven, Belgium

Reviewed by:
Simon Kraler,
University of Zurich, Switzerland
Laura Iop,
University of Padua, Italy

***Correspondence:**
Paul Human
paul.human@uct.ac.za

Specialty section:
This article was submitted to Heart Valve Disease, a section of the journal Frontiers in Cardiovascular Medicine

Received: *18 August 2021*
Accepted: *13 December 2021*
Published: *04 January 2022*

Citation:
Human P, Bezuidenhout D, Aikawa E and Zilla P (2022) Residual Bioprosthetic Valve Immunogenicity: Forgotten, Not Lost. Front. Cardiovasc. Med. 8:760635. doi: 10.3389/fcvm.2021.760635

INTRODUCTION

Despite deployment of valve heterografts as native valve replacement prostheses more than a half century ago (1), understanding of the specific mechanisms involved in the most pernicious of observed xenogeneic valve substitute pathologies, namely dystrophic mineralization, remains elusive to this day. Remarkably, none of the initial grafts implanted, prepared either by chemical sterilization or by formalin treatment and retrieved after 3 months to 3 years, demonstrated any evidence of mineralization but did exhibit moderate inflammatory infiltrates (2). The authors of that pioneering study quickly recognized that the observed host response was indicative of persistent antigenicity in the heterograft tissue and elimination of antigenic components was highlighted as one of the key criteria for ensuring graft longevity. With respect to the use of formalin, it was also recognized that both its susceptibility for cross-link reversibility and its inefficacy in eliminating glycoprotein and collagen non-helical terminal telopeptide antigenicity detracted from its potential use. The bifunctional dialdehyde glutaraldehyde (GA) (0.65%; w:v) was identified as a suitable alternative, together with periodate oxidation to create zero-length

cross-links with structural glycoproteins (2). These innovations were ground-breaking, arriving within 4 years of the initial implants but, apart from decellularization and the introduction of variations of cross-link chemistries deployed in contemporary counterparts, in general remain little changed.

DISTRACTION, DIVISION, AND DECELLULARIZATION

Due to the quest for organ donor alternatives and the experiences with solid organ xenografts, which highlighted the catastrophic phenomenon of hyperacute rejection, attention has recently refocused on the cell surface molecule galactose-α-1,3-galactose (α-Gal) found in New World monkeys and candidate non-primate mammal donors (3) such as the pig, cow and sheep. This molecule was identified as the target for preformed, naturally occurring, antibodies (PFNAb) found in humans and Old World primates, such as the baboon and rhesus and vervet monkeys, and was quickly labeled as the principal "xeno-antigen." This preoccupation, together with the assumption that the problem of extracellular matrix (ECM) antigenicity in bioprosthetic valve tissue was satisfactorily resolved through chemical cross-linking, appeared to translate into the belief that persistent valve pathologies could be ascribed entirely to the presence of donor cells found in tissue valve heterografts, and that remnant immunogenicity could simply be addressed by cell removal alone.

Ironically, evidence has been presented which suggested that myocardial, but not valvular, tissue in the domestic pig expressed the α-Gal epitope and, in a pig to primate xenotransplant model, unfixed valvular tissue was seen to be immunologically privileged (4). However, since hyperacute rejection rapidly occurred due to microvascular binding of IgM and complement, the exact long-time outcome potential of porcine valvular tissue could not be confirmed. Despite this, the suggestion to use unfixed porcine valves for valve replacement as an alternative to mechanical and chemically treated bioprosthetic valves was proffered (5). In contrast, evidence of the mineralization of unfixed, acellular, pig and kangaroo tissue, implanted in sheep, both confirmed the immunogenicity of decellularized tissue and the role thereof in mineralization (6).

A study which evaluated the subdermal *in vivo* response in juvenile rats to glutaraldehyde (0.6%; w:v) cross-linked pericardial tissue from α-Gal knockout pigs, determined calcium levels to be significantly lower than in the corresponding wild-type equivalent after 1 month (7). Moreover, detergent-treated and cross-linked wild-type pericardium, arguably therefore decellularized, resulted in negligible levels of mineralization but which were again significantly increased following pre-incubation with purified human anti-α-Gal antibody. This not only confirmed the role of tissue-specific immunoglobulin in accelerating calcification of bioprosthetic pericardial tissue in accordance with our rabbit serum pre-incubation study (8), but also highlighted the problem of insufficient washout of xeno-antigens following detergent treatment. In that study, where porcine aortic wall implants were pre-incubated with sera obtained from rabbits immunized with extracts of the same tissue and implanted sub-dermally, tissue-specific immunoglobulin would undoubtedly not have been directed at the α-Gal epitope, given the rabbit recipients were α-Gal positive and, thereby, anti-α-Gal negative.

Detection of α-Gal based on lectin binding is common practice but is questionable in detergent-treated tissue due to its specificity for non-α-Gal carbohydrate structures likely to be exposed through that denaturing process (9). Development of the M86 monoclonal antibody and its application in a quantitative enzyme linked immunosorbent assay (ELISA) assay (10) aided in providing more definitive evidence of the distribution of the α-Gal epitope in porcine (11) and bovine (3) tissues, although lack of evidence for its presence in heart valve tissue was conspicuously absent. It is, however, apparent, based on monoclonal anti-α-Gal immunostaining and more quantitative studies, that porcine valvular tissue appears to contain at least a modicum, if not more, of α-Gal epitopes, albeit less in aortic compared to pulmonary tissue (9). It is difficult to discern whether this extends beyond the vascular endothelium to stromal tissue but, if predominant in the former, may be inconsequential or easily lost as a result of denudation of lumenal endothelium during commercial processing.

Additionally, not only does the α-Gal epitope appear resilient to both GA fixation and decellularization, but the cross-reactivity of anti-α-Gal PFNAb against so-called "competitor" epitopes, themselves equally pervasive, may also contribute to long-term failure (12). Naso et al. (13) have more recently provided evidence, based on an adapted M86 ELISA, of native and contemporary bioprosthetic valve construct tissues, including from the porcine, valve-based, Epic and bovine pericardial Mitroflow tissue valves, not only highlighting the presence of α-Gal in both native bovine and porcine tissue but, importantly, its diminution following commercial processing. The apparent elimination of this epitope in the Epic valve is, however, offset by its reported early mineralization (14). Furthermore, Moczar et al. (15) provided evidence of IgG and complement in 20/22 failed Mitroflow valves, despite the 75% reduction in α-Gal epitope reported by Naso et al. While we would concede that the presence of α-Gal, capable of eliciting a host response, may indeed contribute to ensuing pathology of the implanted tissue, it likely does not represent the quintessential xeno-antigen and its depletion should not be held as the sole benchmark for determining xeno-reactivity. Certainly, given the inherent resistance to adequately remove such immunogens from tissue where they exist, the promise may well lie in the use of purpose-bred knockout animals, particularly targeting not only α-Gal but the full "trifecta" of known xeno-antigens, including N-glycolylneuraminic acid (NeuGc) and the glycan products of beta-1,4-N-acetyl-galactosaminyl transferase 2 (16). While the cytidine monophosphate-N-acetyl-neuraminic acid hydroxylase enzyme involved in the synthesis of NeuGc is lacking in humans, it exists in other mammals, including non-human primates (17). Consequently in humans, as with α-Gal, preformed natural antibody to NeuGc potentially exists, likely due to dietary uptake of this antigen present in red meat and dietary products (17). It has been demonstrated in both porcine aortic valve leaflet and pericardium as well as in bovine pericardium (16, 18) with

effective knockout of the respective enzyme and antigen genes abrogating human immunoglobulin binding *in vitro* (16, 19, 20).

Removal of α-Gal is not limited to knockout technology and, while GA treatment alone is purported to diminish the antigen exposure by half (21), enzymatic treatment with green coffee bean alpha-galactosidase (22), or a recombinant human equivalent (23), has been shown to effectively remove it completely. Kim et al. showed reduction, but not abolition, of calcium in GA cross-linked, decellularized and alpha-galactosidase treated bovine pericardium after 4 months in α-Gal knockout mice, designed to simulate the clinical scenario (24). It is likely that this was due to the presence of xeno-antigens other than α-Gal since calcium levels in concurrently implanted primate tissue were statistically equivalent. Therefore, enzymatic treatment offers an alternative to employment of α-Gal knockout donors with potential benefit but equally fails to represent a panacea for achieving immunologically inert bioprosthetic tissue.

Although work has focused on the development of transgenic pigs for solid organ xenotransplantation incorporating human decay accelerating factor, which promises to mitigate complement fixation (25) and other regulatory molecules, application of this technology is unlikely to benefit devitalised bioprosthetic valves. However, a preclinical heterotopic cardiac xenotransplant study in baboons (*Papio anubis*) involving donor pig hearts transgenic for human complement regulatory factors CD59 and decay accelerating factor demonstrated intact valve tissue and confirmed by immunohistology to be immunoglobulin free and with a confluent endothelium, despite failure of the myocardium itself after up to 11 days due to IgM binding and establishment of membrane attack complexes (5). Manji et al. postulate that, provided α-Gal and NeuGc are eliminated in knockout strains of donor pigs, transfer of human genes associated with regulation of complement may suffice to protect against the response to what they term "minor antigens" (26). They further highlighted the need for such genetically engineered bioprosthetic heart valves in children and young patients where structural valve destruction is likely linked to a xenograft-like rejection of the prosthesis (27).

Nevertheless, the enthusiastic push for a decellularized bioprosthetic tissue valve does hold merit. Firstly, it offers a potentially pristine, standardized, three-dimensional scaffold uncluttered with the detritus associated with the consequences of inevitable cell death due to a combination of processing artifacts, including warm ischaemia, hypotonic shock, autolysis, and microbial degeneration. Immediate processing combined with high GA concentrations offers reduced mineralization (28), which has been shown to be coincidental with improved ultrastructural preservation (29). Since these approaches, while ideal from a reduced immunogenicity perspective, are impractical due to logistical and aortic wall stiffness considerations, an acellular prosthesis is arguably preferable. The promise of repopulation of such material with host cells is tantalizing and holds great promise, especially in young children where a growing valve might avoid multiple valve replacement procedures during their lifespan (30), but is yet elusive and seemingly dependent on a macrophage driven response (31).

Despite some early successes (32), the perplexing question of whether inflammation is a prerequisite for repopulation remains, as does the matter of the suitability of the composition of that ingrowth when donor tissue is anatomically different from that of the intended target. For example, the use of pericardial tissue to replace the complex triple-layered design of tricuspid leaflets with the beneficial damping qualities of the spongiosa and the overdistention avoidance of the ventricularis, may be too ambitious, despite the successes of contemporary non-decellularized, cross-linked, pericardial valve constructs. Many of the reports suggestive of the repopulation potential of acellular xenogeneic tissue typically misinterpret an inflammatory infiltrate with "regenerative potential," which is yet to be adequately defined. It is conceivable that inflammation may lay down some of the necessary "guide-rails" suited to subsequent infiltration and establishment of the correct connective tissue. However, the degradation products of an inflammatory response, especially when unresolved, will, through a process of defective phagocytosis, lead to pathological tissue remodeling, including apoptotic bodies, extracellular vesicles and other debris-all typical initiators of dystrophic calcification. Through mechanical forces exerted by the hydroxyapatite crystals on the scaffold, irreversible tissue disruption and delamination will be inevitable.

In addition, the complex mix of detergents, enzymes and inhibitors used in decellularization can themselves induce an immune response and care needs to be taken to adequately wash these from the tissue (33). In addition to the retention of these exogenous reagents, the incomplete washout of disrupted endogenous lipid membrane micelles, typically also associated with partially solubilized cellular antigens, which may have otherwise been less exposed, can induce a sterile granulocytic response with catastrophic consequences (34). Further evidence confirms that incomplete immunogen washout in porcine pulmonary valve tissue is capable of eliciting both a substantial foreign-body reaction on the luminal surface as well as a lymphoproliferative response, comprising T- and B-lymphocytes and plasma cells with evidence of marked immunoglobulin secretion, in children (35). We have observed a severe, sterile, pus-like granulocytic response to porcine aortic wall tissue decellularized using the anionic detergent Sodium dodecyl sulfate (SDS) in rabbit, rat, and primate (baboon and vervet) subdermal implant models, despite exhaustive washout (**Figure 1**).

SDS is a logical choice for ensuring thorough removal of cellular and non-structural proteins, as it impacts both cytoplasmic and nuclear membranes and results in extensive denaturation of tertiary and secondary conformation. However, it is equally capable of deleterious effects to collagen and elastin and thereby, not only altering the mechanical properties of the tissue but, also limiting the ingrowth potential of the tissue to allow for desirable cell repopulation (36). The bile acid/salt detergent, deoxycholate, offers advantages in solubilizing lipid membranes and being more compatible with the ECM, but their subsequent efficient washout can prove difficult. The non-ionic detergent, Triton-X, is less effective than SDS at cell component removal (37) and is facing a legislative ban due to ecotoxicity safety issues. Compared to others, SDS and deoxycholate were the only detergents capable of total removal of cells from porcine

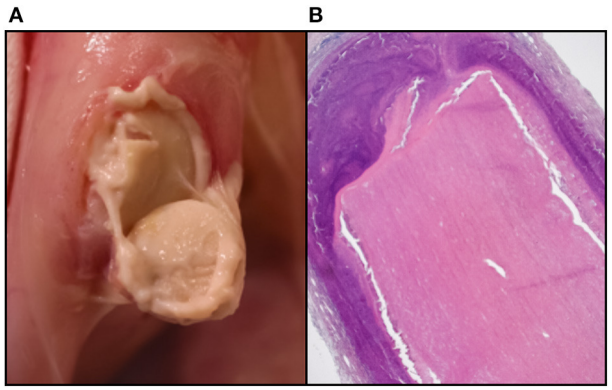

FIGURE 1 | Sterile granulocytic pus response to SDS-based decellularization of porcine aortic wall in the rabbit subdermal model. **(A)** Macro photo at time of retrieval. **(B)** Haematoxylin & Eosin histology showing thick granulocytic rim surrounding the implant.

aortic leaflet tissue (38) with their combination being reported as optimally anti-inflammatory to macrophage and T-lymphocyte infiltration (37). In contrast, our experience with decellularized porcine and bovine pericardial tissue using a combination of Triton–X and sodium deoxycholate, suggested only scanty involvement of granulocytes, with the response involving predominantly a mixed macrophage/lymphocyte response after six-week subdermal implantation in the rat.

Enhanced methods of decellularization have been used to bridge the problem of inefficient washout of disrupted components, including vacuum assisted (39) and electrophoretic approaches (40, 41). Our own exploration into enhanced electrophoretic washout following decellularization using a semi-dry method following decellularization of bovine pericardium with SDS demonstrated negligible inflammatory infiltrates within the interior of the tissue but with a moderate rim of surface inflammatory cells in the subdermal rat model (**Figure 2**).

Accurate methods of validating the efficiency of decellularization are paramount and this, by necessity, requires a detailed knowledge of the identity of the immunogens present in the respective tissues. Quantitative DNA analysis, for example, has been shown to be a poor litmus test for residual immunogenicity (42) and evaluating extractable soluble protein provides little assurance of the removal of lipid soluble ones. Other structural proteins, such as fibronectin mentioned above, and which appear resilient to extraction or indeed adequate cross-linking, are highly immunogenic (43).

Clearly, a "marriage of convenience" between decellularization and chemical cross-linking is required to adequately address residual immunogenicity, especially of the ECM. Despite concerns to the contrary, the use of GA, long thought to promote bioprosthetic mineralization, as an adjunct to decellularization of bovine pericardium, failed to undo the anti-calcification benefit of decellularization in our hands (44). Whether this suggests that leaching of monomeric GA is diminished in acellular tissue, or perhaps is confounded by the presence of the cellular compartment in intact tissue, or both, remains to be determined.

EXTRACELLULAR MATRIX IMMUNOGENICITY

We had previously demonstrated in a subdermal rabbit model that residual immunogenicity of porcine aortic wall led to an acquired humoral immune response in tissue fixed with a GA concentration applied commercially (45). Immunoglobulin specific to porcine fibronectin, a structural glycoprotein known to associate with collagen in the ECM and distinctly present in the basement membrane and therefore principally exposed in denuded bioprosthetic valves, persisted in rabbits immunized with tissue cross-linked with a range of GA concentrations spanning and far exceeding those used commercially. It was only abrogated when cross-links were further extended between free aldehyde groups using the diamine L-Lysine, which was confirmed to increase shrink temperature and therefore, hypothetically, cross-link density (43). Decellularization of bovine pericardium, a tissue widely used in minimally invasive transcatheter aortic valve implantation, has demonstrated a resilience in the removal of this structural glycoprotein, despite diminishment of other ECM components collagen IV and laminin (46), suggesting that both cell removal techniques and commercial cross-linking practices may likely fail to fully abolish this tenacious xeno-antigen.

There are mixed reports regarding immunogenicity of the principal structural components of the ECM, namely collagen and elastin. Bayrak et al. report an absence of *in vitro* evidence for dendritic cell maturation or B- and T-lymphocyte response to bovine and porcine type 1 collagen and elastin (47). In contrast, Biermann et al. report acute T-lymphocyte infiltration in acellular, unfixed, cryopreserved porcine pulmonary valve xenografts implanted in sheep (48). While anecdotal, we have observed *in vitro* evidence for post-implant rabbit IgG binding under transmission electron microscopy to both collagen and elastin in 0.2% GA fixed porcine aortic wall using gold-labeled anti-IgG (**Figure 3**). The calcium observed by Van Nooten et al. in acellular pig and kangaroo aortic valves after implantation in sheep for 4 months was seen to be in close association with collagen fibers while non-decellularized porcine valves failed to calcify (6). Electrophoretic analysis of decellularized porcine valve tissue confirmed the presence of residual proteins and proteoglycans distinct from those found in decellularized human valves, with persistent mononuclear infiltration in the former but which was completely eliminated in the latter (49).

Additional data on the immunogenicity of proteoglycans is scanty, although *in vitro* co-culture experiments using peripheral blood mononuclear cells with electrospun decorin was indicative of low immunogenicity (50).

Demonstration of the undisputed role of bioprosthesis-specific immunoglobulin as a key contributor of subsequent mineralisation (8), and the recent finding that calcification and degeneration of GA-fixed porcine bioprosthetic tissue in a macrophage-depleted mouse model were decreased (51) are equally noteworthy in highlighting the absolute requirement to diminish residual immunogenicity as a means of increasing longevity of bioprosthetic valves, especially in children.

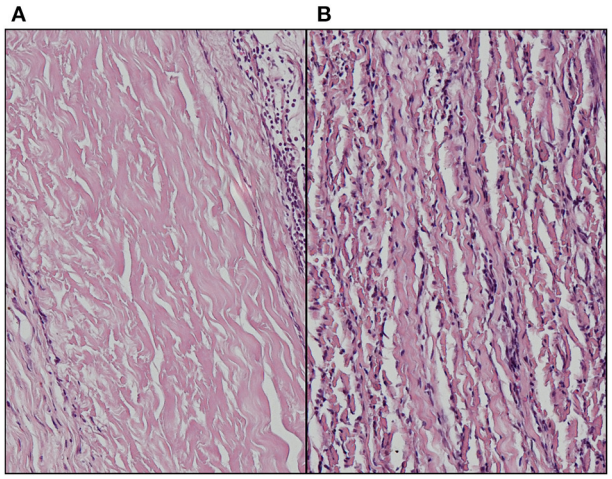

FIGURE 2 | Absence of inflammatory infiltrate in **(A)** electrophoretically enhanced anionic detergent decellularization of bovine pericardium following 6-week subdermal implantation in the rat compared to **(B)** non-ionic decellularization with exhaustive washing (Haematoxylin & Eosin stain).

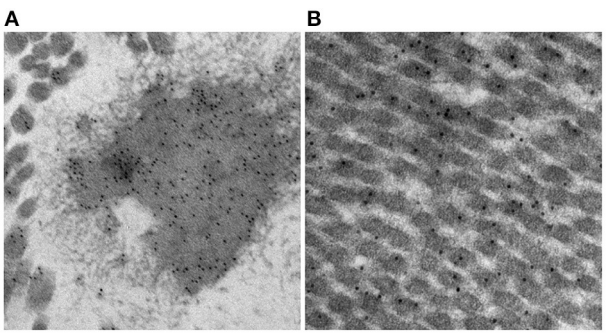

FIGURE 3 | *In vitro* evidence of post-implant rabbit sera specificity to elastin **(A)** and collagen **(B)** in GA fixed (0.2%) porcine aortic wall using gold-labeled anti-IgG.

IMMUNOGENICITY AND PHYLOGENETIC DISPARITY

It is undisputed that, apart from the inflammatory response associated with surgical trauma and the response to synthetic material such as valve skirts and sutures, transplantation of viable valve tissue between syngeneic donor/recipient pairs is intrinsically successful and typically requires minimal or no immunosuppression. This is also clinically evident from the realization that the longevity of conjoined homozygous twins remains unchallenged, at least from an immunological perspective. The approach is understandably cautious when transplantation of solid organs is performed between dizygotic twins or between closely matched individuals despite zero-HLA-mismatch, with low-level immunosuppressive regimens still being advocated (52), although successful outcomes following renal transplantation between homozygous pairs have been reported without continuous immunotherapy (53, 54), but long-term studies are lacking.

Pulmonary autografts represent the perfect matching tissue for valve replacement, typically used in the aortic (Ross procedure) or even the mitral position (55). Seven-year follow-up of the latter confirmed non-calcified leaflets. In Ross procedure patients, the limited ability of the wall of a living autograft root to adapt to the demands of the aortic position may sometimes overshadow its success (56). Yet, most importantly, remodeling has been reported in the absence of inflammation (57, 58).

Allogeneic (homograft) valves, on the other hand, have been reported to be associated with both post-operative fever and valvular dysfunction, which correlated with the extent of MHC Class 2 HLA-DR mismatches (59). Indeed, experimentally, cytotoxic alloreactive T-cell involvement has been implicated in the thickening and destruction of allogeneic leaflets in valves implanted infra-renally in rats compared to syngeneic and T-cell deficient animals (60). Clinically, in a small retrospective study, five infants, but none of the adults, who underwent aortic valve replacement with homograft valves and which failed within 8 months, all exhibited distinct T- and, in three cases, B-lymphocytic infiltrates (61). Curiously, only the adults, as well as a 13-month-old child showed evidence of calcium, despite the absence of inflammatory cells.

One of the original reports in 1996, which hinted at an immune mechanism underlying dystrophic calcification of bioprosthetic tissue, evaluated the outcome of a small cohort (eight GA-fixed bovine pericardial and two GA-fixed porcine aortic valve prostheses) of aortic valve replacement patients with aortitis, and who had received a long-term regimen of steroid therapy (62). Despite a mean follow-up exceeding 11 years, no re-operations were required for stenosis of the replacement prosthesis, and mineralization was "minimal" in three of the pericardial valves requiring replacement.

The success or failure of solid organ xenotransplantation was loosely categorized by Calne as either "concordant" or "discordant," implying potential success or potential failure dependent on phylogenetic heterogeneity between donor and recipient (63). Using a heterotopic cervical cardiac xenotransplant model in the Chacma Baboon (*Papio ursinus*), we were able to demonstrate distinct histopathological differences associated with increasing genetic disparity between donor and recipient (64). The response to Vervet Monkey (*Cercopithecus aethiops*) myocardium was partially analogous to allogeneic transplant pathology, being mainly mononuclear with aggregations of T-lymphocytes. Rejection episodes were successfully treated with short duration prednisolone rescue therapy but presented with additional features of vascular rejection (interstitial hemorrhage, oedema, and myocyte necrosis). This, however, differed from the histopathological features associated with full-blown hyperacute rejection, typical of pig to baboon transplantation of vascular organs, which included vascular microthrombi, worsened oedema and hemorrhage and rapid vascular congestion and cyanosis, but without the cellular infiltrates. Nevertheless, while the cellular response could be averted with treatment in the vervet to baboon model, the humoral response eventually dominated,

leading to inevitable failure. The potential survival times of such "concordant" grafts inversely correlated with titres of PFNAb, suggesting that success could be more accurately and definitively ascertained by their relative titer than the genetic donor-recipient disparity. Clearly, however, a widely divergent pair, such as the pig and baboon combination, might arguably be more accurately classified as "discordant" without knowledge of specific titer, given the higher likelihood of a lack of phylogenetic conservation. Inevitably, even with ingenious attempts at minimizing the deleterious effects of PFNAbs, which offer short-term success (65), all forms of cross-species transplantation are potentially unsuccessful without genetic engineering approaches to avoid known immunogens.

The same principal likely applies to devitalized tissues used in the fabrication of bioprosthetic valves. Certainly, donor and recipient choice was demonstrated by Carpentier et al. (66) to affect levels of subsequent calcification following subcutaneous implantation in a variety of species. However, despite recognition of the role played by graft immunogenicity in the ensuing inflammatory response, the same connection was not assumed with respect to the process of mineralization. Furthermore, a realization of the interrelationship between donor and recipient was not apparent. Logic might be expected to predict the pig to be most related to the cow but less so to the chicken. However, calcium levels in porcine cusps were significantly higher when implanted in the rabbit and rat, compared to the cow and hen, which showed equally negligible levels. Phylogenetic disparity needs to be taken into context, therefore, with respect to the conservation of specific epitopes present in the tissue in question, rather than donor-recipient evolutionary distance. The specific realization of the conservation of the α-Gal antigen in pigs, but not in humans therefore, together with the coincidental existence of PFNAb in the latter, likely directed toward a microbial epitope but capable of cross-reactivity with α-Gal, is critical in predicting outcome.

NeuGc is a case in point, occurring not only in potentially discordant donors such as the pig, but in the more otherwise phylogenetically closer non-human primate. It's relevant absence in corneal endothelial cells and pancreatic islets in wild-type pigs suggests use of NeuGc knockout donors (or combined with α-Gal knockout) of corneal or pancreatic tissue to be inappropriate compared to heart and aortic valves, for example, where significant reduction of the antigen holds much promise (19). While bioprosthetic valves, by their non-vascularized nature, are not at risk for hyperacute rejection, the opsonisation thereof by immunoglobulin directed at xenoantigen, whether α-Gal, NeuGc, fibronectin, or other residual or insufficiently masked epitope, will fix complement and/or induce macrophage and polymorphonuclear neutrophil adhesion with subsequent infiltration and phagocytosis or latent damage through frustrated phagocytosis and the formation of foreign body giant cells. This often insidious process, which continues beyond an early acute lymphocyte phase (67), underlies the importance of ensuring complete abrogation of tissue immunogenicity, either through complete removal (decellularization with extensive washing or enhanced electrophoretic removal), modification (through epitope capping) or masking (chemical cross-linking) of xeno-antigens.

With regard to the latter, we have advocated an engineered approach toward cross-linking decellularized xenogenic pericardium with GA, specifically through incorporation of extender diamine molecules, such as L-Lysine, and reduction of labile Schiff bases to avoid monomer leaching (44) which may again lead to exposure of epitopes over time. While GA remains the principal cross-linking agent used in contemporary bioprosthetic valves, alternatives, including genipin, which has shown potential for reduction of calcification (68), have been explored. However, decellularized porcine aortic valve scaffolds cross-linked with genipin and implanted in the pulmonary position of sheep for 6 weeks, while displaying significantly attenuated inflammatory infiltration, demonstrated persistent immunoglobulin binding (69).

MICROBIAL CONTAMINATION

While it is not the intent to suggest that commercial bioprosthetic valves contain viable microorganisms, one must assume that microbial remnants could likely be contained therein. Whereas, abattoirs are not unclean, they are decidedly not sterile environments and contamination, either from the slaughtered animal itself, or from the processing area, is inevitable. Although the problem of porcine endogenous retroviruses is well-realized, especially in the field of xenotransplantation (70), bacteria may additionally contribute to bioprosthesis pathology. Other than gut and skin flora, endogenous bacteria too are known to exist in domestic pigs and may be associated with a foreign body response and/or dystrophic mineralization (71). Furthermore, tissue used in the fabrication of bioprosthesis typically remains in cold saline, potentially up to 48 h before being processed, which may permit colony expansion. Decellularization and/or GA fixation may remove the likelihood of transfer of viable endogenous bacteria or viruses to the human recipient, but remnants of these organisms will likely persist. We have certainly observed positive immunostaining in un-implanted commercial valve tissue using a monoclonal antibody specific for Gram-positive (Gram+) bacteria (**Figure 4**). In cases of contamination of bovine pericardial valves in the mitral position, colocalization between areas of positive Gram+ staining and positive Von Kossa staining depicting calcium deposits (**Figure 5**) and positive immunoglobulin G staining was observed (**Figure 6**). Contamination with Gram-negative bacteria or fungi was not associated with calcium deposits, suggesting an interplay between Gram+ bacteria, humoral immune response, and dystrophic mineralization. Mineralization of passenger bacteria in GA fixed tissue may also rely on an "inhibitor exclusion" mechanism whereby Fetuin, normally an inhibitor of crystal formation, is size-excluded from the Gram+ cell wall as well as additionally promoting their phagocytosis by neutrophils and macrophages (72, 73). This is highly speculative with respect to mineralization of bioprosthetic tissue, but the evidence of the pro-calcific nature of a yet unidentified, Gram + bacterium, is worthy of further investigation.

Certainly, while it is arguable that sterilization and cross-linking methods adequately render tissues used in the construction of bioprosthetic valves, free of any viable microbial organisms, further studies will be required to assess the relevant role of residual contaminants. Contemporary GA concentrations are incapable of total inactivation of bacterial spores, but added bioburden reduction strategies using alcohol, gamma radiation and other proprietary protocols are already unquestionably efficient at removing such a microbial risk. Should bacterial remnants, however, indeed represent initiation points for inflammatory migration and hydroxyapatite crystal growth, methods would need to be developed to limit or exclude these from the tissue. Prevention in the abattoir is unlikely, given strict controls disallowing chemical reagents at these locations. Shortening of the delay to processing is equally limited by the logistics of the expertise required for dissection and cleaning of valves and pericardial sacks. It would seem, therefore, that improved methods of decellularization and efficient washout, for acellular valves at least, offers the best hope for microbial antigenic determinant removal.

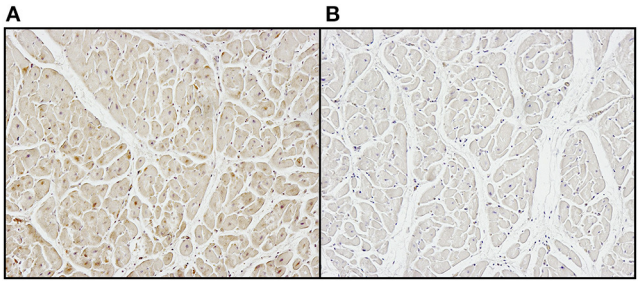

FIGURE 4 | Positive immunostaining **(A)** to Gram+ bacteria in unimplanted commercial bioprosthetic valve tissue compared to **(B)** negative control.

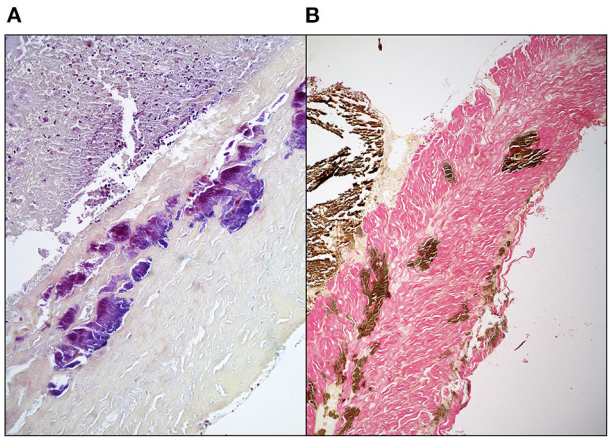

FIGURE 5 | Suspected colocalization of areas of Gram + bacterial contamination of GA-fixed bovine pericardial tissue and mineralization in a stented mitral valve replacement bioprosthesis retrieved after 112 days **(A)** Brown & Brenn stain **(B)** Von Kossa & Van Gieson stain.

INFLAMMATION AND PANNUS OVERGROWTH

Intimal hyperplasia, encouraged by smooth muscle cell migration through severed elastic lamellae during the surgical implantation of freestyle aortic roots is also seen to occur in transcatheter aortic valve implantation cases (74) where there is no such trauma, and which suggests a different underlying mechanism. Furthermore, while a foreign body response to synthetic components has been shown to provide a sustained myointimal stimulus (75), the involvement of macrophages in inducing myointimal proliferation in transplant recipients (76) suggests that the same may be true for opsonisation of bioprosthetic tissue through immunoglobulin binding. Macrophage and foreign body giant cell formation are hallmarks of GA-fixed bioprosthetic heart valve pathology, and we have observed diminished pannus formation when high GA concentrations together with diamine extension were applied (43). Improved tissue fixation through increased cross-link density with resulting surface inflammation quiescence was concomitantly associated with diminished

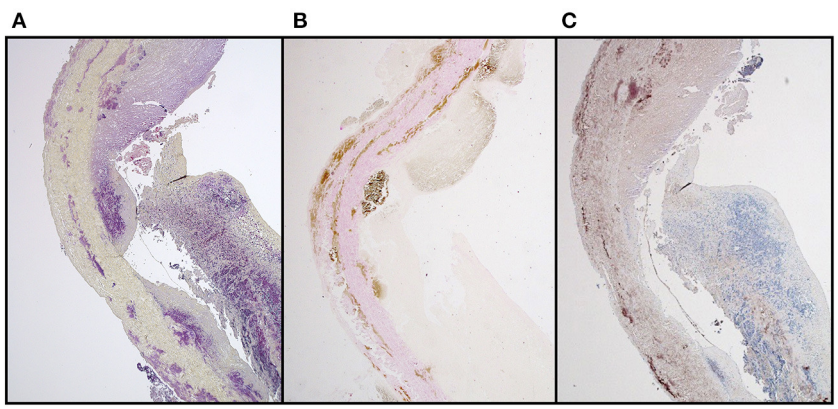

FIGURE 6 | IgG binding in areas of Gram-positive bacterial contamination together with mineralization in a stented, GA-fixed, mitral valve pericardial bioprosthesis retrieved after 112 days **(A)** Brown & Brenn stain **(B)** Von Kossa & Van Gieson stain **(C)** Anti-Sheep IgG.

pannus overgrowth. Therefore, not only inflammation with ensuing degradation, nor immune-mediated calcification, but also leaflet stenosis through pannus overgrowth will benefit from insurances of reduced bioprosthetic immunogenicity.

RHEUMATIC HEART DISEASE ANALOGY

Much of the pathology observed in rheumatic deterioration is analogous to that seen in failed bioprosthetic heart valves. Dystrophic mineralization, stenosis and unresolved chronic inflammation are prominent features of both. Despite it being undisputed that rheumatic heart disease represents the autoimmune consequence of poorly managed rheumatic fever and that the associated calcification is not an inactive process but instead highly regulated through inflammation (77), acknowledgment of a host immune response as the central feature of bioprosthetic pathology, while increasingly undeniable, is seemingly still partially ignored.

DISCUSSION

Bioprosthetic replacement heart valves, whether sourced as anatomical porcine aortic valves or fabricated from bovine parietal pericardium are, by definition, xenogeneic and potentially highly immunogenic. If attempts at antigen masking, removal and/or modification are not employed, their implantation in humans should certainly be classified as "discordant." Limited progress regarding cross-link masking has been made since the first use of GA five decades ago. In addition, the deployment of new and innovative chemistries has been withheld clinically, presumably due to corporate risk assessments including expensive and lengthy regulatory approvals. Antigen removal, through decellularization, may represent a similar concern, which likely stemmed from well-intentioned but failed attempts at the introduction of this technology to leave the door open to repopulation with host tissue by not combining it with antigen masking through cross-linking of the extracellular matrix. **Figure 7** provides an overview of the progression of tissue treatments, based on animal studies, from non-crosslinked fresh tissue which undergoes rapid phagocytosis, followed by cross-linking with contemporary GA concentrations incapable of complete antigen masking with its characteristic infiltrating inflammatory and humoral immune response and widespread mineralization. High cross-link density completely removes inflammatory infiltration and tissue-specific immunoglobulin but renders the tissue impractically stiff and subject to "frustrated" phagocytosis with possible latent tissue damage. Decellularization, even with contemporary GA fixation, fails to adequately remove or mask solubilized cellular antigen and introduces problems of microbial remnant

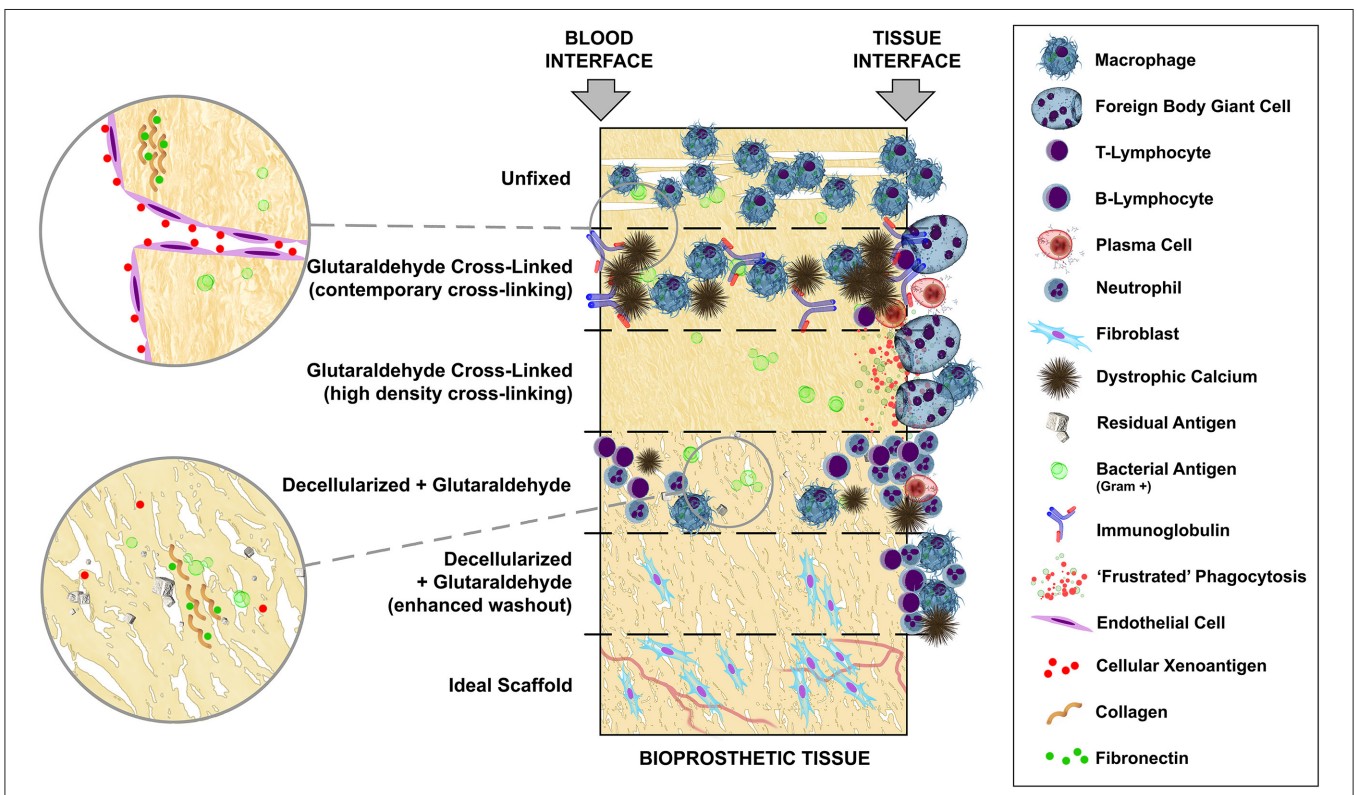

FIGURE 7 | Hypothetical mechanistic overview, based on animal models, of the potential impact of a residual immunogen presence on inflammatory and immune sequelae in bioprosthetic tissue and the ensuing potential for mineralization.

antigen (especially when contemporary GA concentrations are used) and other contaminants despite a significant reduction in mineralization. Enhanced passive washout, or via active electrophoresis, of decellularization products may best approach the ideal scaffold, potentially immunologically inert and capable of repopulation and revascularisation.

However, the distinction between cross-species vascularized organ transplantation and the use of largely structural, non-vital tissue used in the replacement of diseased heart valves has become blurred with the consequence that residual immunogenicity of the extracellular matrix has been, unconsciously perhaps, deemed to be inconsequential. Unlike the catastrophic consequences observed in vascularized organs, the pathological response to the bioprosthetic valve is often far more insidious and latent in nature, although can be accelerated in children. The idealistic belief that acellular scaffolds will repopulate and grow with the patient, while desirable, must be tempered with the realization that, while residual immunogens remain, decellularization alone will be inadequate. The growing acceptance of the contribution of an immune-mediated mechanism of dystrophic mineralization together with the potential for pannus-mediated stenosis advocates caution in disregarding the consequences of residual immunogenicity, irrespective of which compartment, cellular or extracellular, that might reside in.

AUTHOR CONTRIBUTIONS

PH conceptualized and composed the bulk of the manuscript, it is based on insights acquired through related research performed together with PZ and DB. EA provided valuable insight into inflammatory mechanisms suspected to play a role in the pathology of bioprosthetic heart valves with all three having also intensively reviewed the manuscript. All authors contributed to the article and approved the submitted version.

REFERENCES

1. Binet JP, Carpentier A, Langlois J, Duran C, Colvez P. Implantation de valves heterogenes dans le traitement d e cardiopathies aortiques. *C R Acad Hebd Seances Acad Sci D.* (1965) 261:5733–4.
2. Carpentier A, Lemaigre G, Robert L, Carpentier S, Dubost C. Biological factors affecting long-term results of valvular heterografts. *J Thorac Cardiovasc Surg.* (1969) 58:467–83. doi: 10.1016/S0022-5223(19)42561-0
3. Galili U, Clark MR, Shohet SB, Buehler J, Macher BA. Evolutionary relationship between the natural anti-Gal antibody and the Gal alpha 1-3Gal epitope in primates. *Proc Natl Acad Sci USA.* (1987) 84:1369–73. doi: 10.1073/pnas.84.5.1369
4. Chen RH, Kadner A, Mitchell RN, Adams DH. Fresh porcine cardiac valves are not rejected in primates. *J Thorac Cardiovasc Surg.* (2000) 119:1216–20. doi: 10.1067/mtc.2000.106526
5. Chen RH, Adams DH. Transgenic porcine valves show no signs of delayed cardiac xenograft rejection. *Ann Thorac Surg.* (2001) 71:S389–92. doi: 10.1016/S0003-4975(01)02505-X
6. Van Nooten G, Somers P, Cornelissen M, Bouchez S, Gasthuys F, Cox E, et al. Acellular porcine and kangaroo aortic valve scaffolds show more intense immune-mediated calcification than cross-linked Toronto SPV valves in the sheep model. *Interact Cardiovasc Thorac Surg.* (2006) 5:544–9. doi: 10.1510/icvts.2006.136267
7. Lila N, McGregor CG, Carpentier S, Rancic J, Byrne GW, Carpentier A. Gal knockout pig pericardium: new source of material for heart valve bioprostheses. *J Heart Lung Transplant.* (2010) 29:538–43. doi: 10.1016/j.healun.2009.10.007
8. Human P, Zilla P. The possible role of immune responses in bioprosthetic heart valve failure. *J Heart Valve Dis.* (2001) 10:460–6.
9. Naso F, Gandaglia A, Iop L, Spina M, Gerosa G. First quantitative assay of alpha-Gal in soft tissues: presence and distribution of the epitope before and after cell removal from xenogeneic heart valves. *Acta Biomater.* (2011) 7:1728–34. doi: 10.1016/j.actbio.2010.11.030
10. Galili U, LaTemple DC, Radic MZ. A sensitive assay for measuring alpha-Gal epitope expression on cells by a monoclonal anti-Gal antibody. *Transplantation.* (1998) 65:1129–32. doi: 10.1097/00007890-199804270-00020
11. Sandrin MS, Vaughan HA, Dabkowski PL, McKenzie IF. Anti-pig IgM antibodies in human serum react predominantly with Gal(alpha 1-3)Gal epitopes. *Proc Natl Acad Sci USA.* (1993) 90:11391–5. doi: 10.1073/pnas.90.23.11391
12. Naso F, Gandaglia A, Iop L, Spina M, Gerosa G. Alpha-Gal detectors in xenotransplantation research: a word of caution. *Xenotransplantation.* (2012) 19:215–20. doi: 10.1111/j.1399-3089.2012.00714.x
13. Naso F, Gandaglia A, Bottio T, Tarzia V, Nottle MB, d'Apice AJ, et al. First quantification of alpha-Gal epitope in current glutaraldehyde-fixed heart valve bioprostheses. *Xenotransplantation.* (2013) 20:252–61. doi: 10.1111/xen.12044
14. Izzat MB, Sabbagh N, Aljasem H. Early calcific degeneration of the St. Jude Medical Epic aortic bioprosthesis. *Clin Case Rep.* (2020) 8:387–8. doi: 10.1002/ccr3.2664
15. Moczar M, Lecerf L, Mazzucotelli JP, Loisance D. Immunoglobulins and complement deposits in mitroflow pericardial bioprosthetic heart valves–a contributing factor to structural deterioration. *J Heart Valve Dis.* (1996) 3:S276–83.
16. Zhang R, Wang Y, Chen L, Wang R, Li C, Li X, et al. Reducing immunoreactivity of porcine bioprosthetic heart valves by genetically-deleting three major glycan antigens, GGTA1/beta4GalNT2/CMAH. *Acta Biomater.* (2018) 72:196–205. doi: 10.1016/j.actbio.2018.03.055
17. Salama A, Evanno G, Harb J, Soulillou JP. Potential deleterious role of anti-Neu5Gc antibodies in xenotransplantation. *Xenotransplantation.* (2015) 22:85–94. doi: 10.1111/xen.12142
18. Reuven EM, Leviatan Ben-Arye S, Marshanski T, Breimer ME, Yu H, Fellah-Hebia I, et al. Characterization of immunogenic Neu5Gc in bioprosthetic heart valves. *Xenotransplantation.* (2016) 23:381–92. doi: 10.1111/xen.12260
19. Lee W, Hara H, Ezzelarab MB, Iwase H, Bottino R, Long C, et al. Initial *in vitro* studies on tissues and cells from GTKO/CD46/NeuGcKO pigs. *Xenotransplantation.* (2016) 23:137–50. doi: 10.1111/xen.12229
20. Lee W, Long C, Ramsoondar J, Ayares D, Cooper DK, Manji RA, et al. Human antibody recognition of xenogeneic antigens (NeuGc and Gal) on porcine heart valves: could genetically modified pig heart valves reduce structural valve deterioration? *Xenotransplantation.* (2016) 23:370–80. doi: 10.1111/xen.12254
21. Naso F, Stefanelli U, Buratto E, Lazzari G, Perota A, Galli C, et al. Alpha-gal inactivated heart valve bioprostheses exhibit an anti-calcification propensity similar to knockout tissues<sup/>. *Tissue Eng Part A.* (2017) 23:1181–95. doi: 10.1089/ten.tea.2016.0474
22. LaVecchio JA, Dunne AD, Edge ASB. Enzymatic removal of alpha-galactosyl epitopes from porcine endothelial cells diminishes the cytotoxic effect of natural antibodies. *Transplantation.* (1995) 60:841–7. doi: 10.1097/00007890-199510270-00014
23. Park S, Kim WH, Choi SY, Kim YJ. Removal of alpha-Gal epitopes from porcine aortic valve and pericardium using recombinant human alpha galactosidase A. *J Korean Med Sci.* (2009) 24:1126–31. doi: 10.3346/jkms.2009.24.6.1126

24. Kim MS, Lim HG, Kim YJ. Calcification of decellularized and alpha-galactosidase-treated bovine pericardial tissue in an alpha-Gal knock-out mouse implantation model: comparison with primate pericardial tissue. *Eur J Cardiothorac Surg.* (2016) 49:894–900. doi: 10.1093/ejcts/ezv189
25. Schmoeckel M, Nollert G, Shahmohammadi M, Muller-Hocker J, Young VK, Kasper-Konig W, et al. Transgenic human decay accelerating factor makes normal pigs function as a concordant species. *J Heart Lung Transplant.* (1997) 16:758–64.
26. Manji RA, Ekser B, Menkis AH, Cooper DK. Bioprosthetic heart valves of the future. *Xenotransplantation.* (2014) 21:1–10. doi: 10.1111/xen.12080
27. Manji RA, Lee W, Cooper DKC. Xenograft bioprosthetic heart valves: Past, present and future. *Int J Surg.* (2015) 23:280–4. doi: 10.1016/j.ijsu.2015.07.009
28. Zilla P, Zhang Y, Human P, Koen W, von Oppell. U. Improved ultrastructural preservation of bioprosthetic tissue. *J Heart Valve Dis.* (1997) 6:492–501.
29. Human P, Weissenstein C, Trantina A, Zilla P. Fixation-related autolysis and bioprosthetic aortic wall calcification. *J Heart Valve Dis.* (2001) 10:656—65.
30. Ueda Y, Torrianni MW, Coppin CM, Iwai S, Sawa Y, Matsuda H. Antigen clearing from porcine heart valves with preservation of structural integrity. *Int J Artif Organs.* (2006) 29:781–9. doi: 10.1177/039139880602900808
31. Paniagua Gutierrez JR, Berry H, Korossis S, Mirsadraee S, Lopes SV, da Costa F, et al. Regenerative potential of low-concentration SDS-decellularized porcine aortic valved conduits in vivo. *Tissue Eng Part A.* (2015) 21:332–42. doi: 10.1089/ten.tea.2014.0003
32. Iwai S, Torikai K, Coppin CM, Sawa Y. Minimally immunogenic decellularized porcine valve provides in situ recellularization as a stentless bioprosthetic valve. *J Artif Organs.* (2007) 10:29–35. doi: 10.1007/s10047-006-0360-1
33. Grebenik EA, Gafarova ER, Istranov LP, Istranova EV, Ma X, Xu J, et al. Mammalian pericardium-based bioprosthetic materials in xenotransplantation and tissue engineering. *Biotechnol J.* (2020) 15:e1900334. doi: 10.1002/biot.201900334
34. Simon P, Kasimir MT, Seebacher G, Weigel G, Ullrich R, Salzer-Muhar U, et al. Early failure of the tissue engineered porcine heart valve SYNERGRAFT in pediatric patients. *Eur J Cardiothorac Surg.* (2003) 23:1002–6. doi: 10.1016/S1010-7940(03)00094-0
35. Cicha I, Ruffer A, Cesnjevar R, Glockler M, Agaimy A, Daniel WG, et al. Early obstruction of decellularized xenogenic valves in pediatric patients: involvement of inflammatory and fibroproliferative processes. *Cardiovasc Pathol.* (2011) 20:222–31. doi: 10.1016/j.carpath.2010.04.006
36. Naso F, Gandaglia A. Different approaches to heart valve decellularization: A comprehensive overview of the past 30 years. *Xenotransplantation.* (2018) 25:12354. doi: 10.1111/xen.12354
37. Liu X, Li N, Gong D, Xia C, Xu Z. Comparison of detergent-based decellularization protocols for the removal of antigenic cellular components in porcine aortic valve. *Xenotransplantation.* (2018) 25:e12380. doi: 10.1111/xen.12380
38. Booth C, Korossis SA, Wilcox HE, Watterson KG, Kearney JN, Fisher J, et al. Tissue engineering of cardiac valve prostheses I: development and histological characterization of an acellular porcine scaffold. *J Heart Valve Dis.* (2002) 11:457–62.
39. Luo Y, Ma L. Bioprosthetic heart valves with reduced immunogenic residuals using vacuum-assisted decellularization treatment. *Biomed Mater.* (2020) 15:065012. doi: 10.1088/1748-605X/abaabf
40. Duran CJ. *Tissue Electrophoresis for Generation of Porcine Acellular Dermal Matrices* [dissertation/master's thesis]. Colorado State University (2013).
41. Arai S, Lacerda C, Orton EC. Tissue-gel electrophoresis enhances antigen removal from porcine aortic valve and bovine pericardium. *J Heart Valve Dis.* (2010) 19:753–8.
42. Wong ML, Leach JK, Athanasiou KA, Griffiths LG. The role of protein solubilization in antigen removal from xenogeneic tissue for heart valve tissue engineering. *Biomaterials.* (2011) 32:8129–38. doi: 10.1016/j.biomaterials.2011.07.030
43. Human P, Zilla P. Inflammatory and immune processes: the neglected villain of bioprosthetic degeneration? *J Long Term Eff Med Implants.* (2001) 11:199–220. doi: 10.1615/JLongTermEffMedImplants.v11.i34.80
44. Human P, Ofoegbu C, Ilsley H, Bezuidenhout D, de Villiers J, Williams DF, et al. Decellularization and engineered crosslinking: a promising dual approach towards bioprosthetic heart valve longevity. *Eur J Cardiothorac Surg.* (2020) 58:1192–200. doi: 10.1093/ejcts/ezaa257
45. Human P, Zilla P. Characterization of the immune response to valve bioprostheses and its role in primary tissue failure. *Ann Thorac Surg.* (2001) 71:S385–8. doi: 10.1016/S0003-4975(01)02492-4
46. Mirsadraee S, Wilcox HE, Watterson KG, Kearney JN, Hunt J, Fisher J, et al. Biocompatibility of acellular human pericardium. *J Surg Res.* (2007) 143:407–14. doi: 10.1016/j.jss.2007.01.026
47. Bayrak A, Pruger P, Stock UA, Seifert M. Absence of immune responses with xenogeneic collagen and elastin. *Tissue Eng Part A.* (2013) 19:1592–600. doi: 10.1089/ten.tea.2012.0394
48. Biermann AC, Marzi J, Brauchle E, Schneider M, Kornberger A, Abdelaziz S, et al. Impact of T-cell-mediated immune response on xenogeneic heart valve transplantation: short-term success and mid-term failure. *Eur J Cardiothorac Surg.* (2018) 53:784–92. doi: 10.1093/ejcts/ezx396
49. Simon P, Kasimir MT, Rieder E, Weigel G. Tissue Engineering of heart valves-Immunologic and inflammatory challenges of the allograft scaffold. *Progress Pediatric Cardiol.* (2006) 21:161–5. doi: 10.1016/j.ppedcard.2005.11.004
50. Hinderer S, Schesny M, Bayrak A, Ibold B, Hampel M, Walles T, et al. Engineering of fibrillar decorin matrices for a tissue-engineered trachea. *Biomaterials.* (2012) 33:5259–66. doi: 10.1016/j.biomaterials.2012.03.075
51. Liu Z, Wang Y, Xie F, Liu X, Li F, Dong N. Elimination of macrophages reduces glutaraldehyde-fixed porcine heart valve degeneration in mice subdermal model. *Pharmacol Res Perspect.* (2021) 9:e00716. doi: 10.1002/prp2.716
52. Blitzer D, Yedlicka G, Manghelli J, Dentel J, Caldwell R, Brown JW. Twin-to-twin heart transplantation: a unique event with a 25-year follow-up. *Ann Thorac Surg.* (2017) 103:e341–2. doi: 10.1016/j.athoracsur.2016.09.060
53. Lim WH, Gray NA, Chadban SJ, Pilmore H, Wong G. Graft and patient outcomes of zero-human leucocyte-antigen-mismatched deceased and live donor kidney transplant recipients. *Transpl Int.* (2015) 28:610–8. doi: 10.1111/tri.12542
54. Krishnan N, Buchanan PM, Dzebisashvili N, Xiao H, Schnitzler MA, Brennan DC. Monozygotic transplantation: concerns and opportunities. *Am J Transplant.* (2008) 8:2343–51. doi: 10.1111/j.1600-6143.2008.02378.x
55. Kanzaki T, Yamagishi M, Yashima M, Yaku H. Seven-year outcome of pulmonary valve autograft replacement of the mitral valve in an infant. *J Thorac Cardiovasc Surg.* (2011) 141:e33–5. doi: 10.1016/j.jtcvs.2011.01.049
56. El-Hamamsy I, Eryigit Z, Stevens LM, Sarang Z, George R, Clark L, et al. Long-term outcomes after autograft versus homograft aortic root replacement in adults with aortic valve disease: a randomised controlled trial. *Lancet.* (2010) 376:524–31. doi: 10.1016/S0140-6736(10)60828-8
57. Mookhoek A, de Heer E, Bogers AJ, Takkenberg JJ, Schoof PH. Pulmonary autograft valve explants show typical degeneration. *J Thorac Cardiovasc Surg.* (2010) 139:1416–9. doi: 10.1016/j.jtcvs.2010.01.020
58. Rabkin-Aikawa E, Aikawa M, Farber M, Kratz JR, Garcia-Cardena G, Kouchoukos NT, et al. Clinical pulmonary autograft valves: pathologic evidence of adaptive remodeling in the aortic site. *J Thorac Cardiovasc Surg.* (2004) 128:552–61. doi: 10.1016/j.jtcvs.2004.04.016
59. Dignan R, O'Brien M, Hogan P, Passage J, Stephens F, Thornton A, et al. Influence of HLA matching and associated factors on aortic valve homograft function. *J Heart Valve Dis.* (2000) 9:504–11.
60. Legare JF, Lee TD, Creaser K, Ross DB. T lymphocytes mediate leaflet destruction and allograft aortic valve failure in rats. *Ann Thorac Surg.* (2000) 70:1238–45. doi: 10.1016/S0003-4975(00)01677-5
61. Rajani B, Mee RB, Ratliff NB. Evidence for rejection of homograft cardiac valves in infants. *J Thorac Cardiovasc Surg.* (1998) 115:111–7. doi: 10.1016/S0022-5223(98)70449-0
62. Eishi K, Ishibashi-Ueda H, Nakano K, Kosakai Y, Sasako Y, Kobayashi J, et al. Calcific degeneration of bioprosthetic aortic valves in patients receiving steroid therapy. *J Heart Valve Dis.* (1996) 5:668–72.
63. Calne RY. Organ transplantation between widely disparate species. *Transplant Proc.* (1970) 2:550–6. doi: 10.1136/bmj.2.5701.111-a
64. Rose AG, Cooper DK, Human PA, Reichenspurner H, Reichart B. Histopathology of hyperacute rejection of the heart: experimental and clinical observations in allografts and xenografts. *J Heart Lung Transplant.* (1991) 10:223–34.

65. Cooper DK, Human PA, Lexer G, Rose AG, Rees J, Keraan M, et al. Effects of cyclosporine and antibody adsorption on pig cardiac xenograft survival in the baboon. *J Heart Transplant.* (1988) 7:238–46.
66. Carpentier SM, Monier MH, Shen M, Carpentier AF. Do donor or recipient species influence calcification of bioprosthetic tissues? *Ann Thorac Surg.* (1995) 60:S328–30. doi: 10.1016/0003-4975(95)00244-F
67. Grabenwoger M, Grimm M, Eybl E, Kadletz M, Havel M, Kostler P, et al. New aspects of the degeneration of bioprosthetic heart valves after long-term implantation. *J Thorac Cardiovasc Surg.* (1992) 104:14–21. doi: 10.1016/S0022-5223(19)34831-7
68. Jeong S, Yoon EJ, Lim HG, Sung SC, Kim YJ. The effect of space fillers in the cross-linking processes of bioprosthesis. *Biores Open Access.* (2013) 2:98–106. doi: 10.1089/biores.2012.0289
69. Somers P, De Somer F, Cornelissen M, Bouchez S, Gasthuys F, Narine K, et al. Genipin blues: an alternative non-toxic crosslinker for heart valves? *J Heart Valve Dis.* (2008) 17:682–8.
70. Fiebig U, Fischer K, Bahr A, Runge C, Schnieke A, Wolf E, et al. Porcine endogenous retroviruses: Quantification of the copy number in cell lines, pig breeds, and organs. *Xenotransplantation.* (2018) 25:e12445. doi: 10.1111/xen.12445
71. Jensen HE, Gyllensten J, Hofman C, Leifsson PS, Agerholm JS, Boye M, et al. Histologic and bacteriologic findings in valvular endocarditis of slaughter-age pigs. *J Vet Diagn Invest.* (2010) 22:921–7. doi: 10.1177/104063871002200611
72. Arellano CK. *The Calcification of Staphylococcus aureus Bacteria: A Potential Defense Mechanism Against Infections* [dissertation/master's thesis]. University of California, San Diego (2010).
73. Truong LY. *The Calcification of Staphylococcus aureus Bacteria by the Mineralization by Inhibitor Exclusion Mechanism: A Potential Defense Mechanism Against Bacterial Infections* [dissertation/master's thesis]. University of California, San Diego (2011).
74. Koo HJ, Choe J, Kang DY, Ko E, Ahn JM, Park DW, et al. Computed tomography features of cuspal thrombosis and subvalvular tissue ingrowth after transcatheter aortic valve implantation. *Am J Cardiol.* (2020) 125:597–606. doi: 10.1016/j.amjcard.2019.11.015
75. Greisler HP, Dennis JW, Endean ED, Ellinger J, Friesel R, Burgess W. Macrophage/biomaterial interactions: the stimulation of endothelialization. *J Vasc Surg.* (1989) 9:588–93. doi: 10.1016/0741-5214(89)90478-3
76. Wewers MD, Marsh CB. Role of the antibody in the pathogenesis of transplant vascular sclerosis: a hypothesis. *Transpl Immunol.* (1997) 5:283–8. doi: 10.1016/S0966-3274(97)80009-3
77. Chopra P, Gulwani H. Pathology and pathogenesis of rheumatic heart disease. *Indian J Pathol Microbiol.* (2007) 50:685–97.

Conflict of Interest: The authors declare that the research was conducted in the absence of any commercial or financial relationships that could be construed as a potential conflict of interest.

Publisher's Note: All claims expressed in this article are solely those of the authors and do not necessarily represent those of their affiliated organizations, or those of the publisher, the editors and the reviewers. Any product that may be evaluated in this article, or claim that may be made by its manufacturer, is not guaranteed or endorsed by the publisher.

frontiers in Cardiovascular Medicine

REVIEW
published: 04 January 2022
doi: 10.3389/fcvm.2021.794574

Mitral Plasticity: The Way to Prevent the Burden of Ischemic Mitral Regurgitation?

Mattia Vinciguerra[1]*, *Silvia Romiti*[1], *Eleonora Wretschko*[1], *Mizar D'Abramo*[1], *David Rose*[2], *Fabio Miraldi*[1] and *Ernesto Greco*[1]

[1] Department of Clinical, Internal Medicine, Anesthesiology and Cardiovascular Sciences, Sapienza University of Rome, Rome, Italy, [2] Lancashire Cardiac Centre, Blackpool Victoria Hospital, Blackpool, United Kingdom

The ischemic impairment of the left ventricular contractility, followed by an adverse remodeling leading to the displacement of the papillary muscles (PMs), increased tethering forces and loss of valve competence has been the long-term accepted definition of ischemic mitral regurgitation (IMR). Over the years, different approaches of management have attempted to address valve regurgitation, nevertheless failing to achieve satisfactory outcomes. Recent studies have observed some structural and molecular changes of the mitral valve (MV), challenging the concept of a bystander passive to the subvalvular involvement. Indeed, the solely mechanical stretch of the PMs, as in the dilated left ventricle because of the aortic valve regurgitation, is not enough in causing relevant MV regurgitation. This setting triggers a series of structural changes called "mitral plasticity," leaflets increase in their size among others, ensuring an adequate systolic area closure. In contrast, the ischemic injury not only triggers the mechanical stretch on the subvalvular apparatus but is also a powerful promotor of profibrotic processes, with an upregulation of the transforming growth factor (TGF)-β signaling pathway, leading to a MV with exuberant leaflet thickness and impaired mobility. In this article, we revise the concept of IMR, particularly focusing on the new evidence that supports dynamic changes in the MV apparatus, discussing the consequent clinical insights of "mitral plasticity" and the potential therapeutic implications.

Keywords: mitral valve, ischemic mitral regurgitation, left ventricle remodeling, mitral plasticity, myocardial infarction

OPEN ACCESS

Edited by:
Bernard Chevalier, Institut Cardiovasculaire Paris Sud, France

Reviewed by:
Antonio Maria Calafiore, Henry Dunant Hospital, Greece
Antonino S. Rubino, University of Campania Luigi Vanvitelli, Italy

***Correspondence:**
Mattia Vinciguerra
mattia_vinciguerra@libero.it

Specialty section:
This article was submitted to Heart Valve Disease, a section of the journal Frontiers in Cardiovascular Medicine

Received: *13 October 2021*
Accepted: *07 December 2021*
Published: *04 January 2022*

Citation:
Vinciguerra M, Romiti S, Wretschko E, D'Abramo M, Rose D, Miraldi F and Greco E (2022) Mitral Plasticity: The Way to Prevent the Burden of Ischemic Mitral Regurgitation? Front. Cardiovasc. Med. 8:794574. doi: 10.3389/fcvm.2021.794574

INTRODUCTION

Ischemic mitral regurgitation (IMR) is a complex syndrome caused by unbalanced closing and tethering forces, that affects 1.6–2.8 million people in the United States and may complicate the 10–20% of patients with the ischemic heart disease (1, 2).

Several surgical approaches have been described and used over the years to address valve incompetence caused by ischemic injury. Nevertheless, mitral valve (MV) surgery is still associated with unsatisfactory outcomes; MV replacement and MV repair, including restrictive annuloplasty, were associated with a not negligible in-hospital mortality and mostly a high recurrence rate of MR in long-term follow-up (1, 3). The target of the medical therapy has been focused on improving LV contractility, following the long-term accepted idea that FMR depended solely on LV impairment, in the absence of a tailored categorization of IMR etiology and subtypes (4).

Current literature focuses to describe in detail IMR phenotypes, differentiating them according to the direction of the tethering forces on MV leaflets and LV dimensions, in order to offer targeted strategies of approach (5).

In the IMR phenotype with asymmetric tethering of valve leaflets, the altered geometry of MV due to the prevalent restricted motion of the posterior mitral leaflets (PML) may be the main driver of MR progression, in the setting of LV not dilated globally. In contrast, symmetric tethering, involving both MV leaflets are often linked to displacement of PMs and LV dilatation, which leads to a progressive impairment of the LV contractility and subsequent poor prognosis (5).

Nevertheless, MV apparatus and leaflets are not a passive bystander, they have the capacity to counteract mechanical stress triggered by LV dilatation, highlighting that the main driver in MR progression may be searched in the biological pathways activated.

In this article, we revise the concept of IMR, initially reporting the pathophysiology of LV adverse remodeling after AMI or chronic ischemia and then focusing on the new evidence that supports dynamic changes in the MV apparatus, finally discussing the consequent clinical insights of "MV plasticity."

ISCHEMIC LEFT VENTRICULAR ADVERSE REMODELING

Left ventricular adverse remodeling occurring after acute myocardial infarction (AMI) or chronic ischemia is defined by the loss of normal architecture and function of the cardiac chamber secondary to an ischemic injury. Although the clinical course is typically silent for a long period, symptomatic heart failure (HF) is the main adverse outcome, potentially leading to death.

Left ventricular impaired contractility results from changes first in the molecular pathways, cellular and interstitial arrangement, and consequently size, shape, and function (6, 7).

In the early phases after AMI, an inflammatory response involving infiltration of leukocytes and granulocytes and finalized to remove necrotic cell debris is activated. This early lytic and scavenger phase is followed by an anti-inflammatory reparative phase, which ultimately leads to scar formation (8).

The disorder in the delicate balance at the basis of these molecular mechanisms leads to adverse LV remodeling. Contractility may be affected by both the exuberant proinflammatory response leading to an exacerbation of cytokines expression and proteolytic activity, and by the overactivation of cardiac fibroblasts causing an expansion of the fibrotic area (9, 10).

Infarct expansion might also be promoted by changes in LV pressure and shape during the lytic phase because of the higher vulnerability of the cardiac chamber (8).

In particular, the increased wall stress with the release of matrix metalloproteinases from activated inflammatory cells, causes the degradation of collagen matrix, and the consequent loss of physiological cardiomyocytes junctions.

As an effect of tissue rearrangement, an expansion of the infarcted zone occurs in the absence of additional necrosis leading to wall thinning and regional LV cavity dilatation, further worsened by apposition of collagen by the cardiac fibroblasts (7).

The loss of contractile function, how happens in chronic ischemia, triggers compensatory responses involving the non-infarcted myocardium, to maintain the stroke volume, thus increasing the LV loading (11).

Neurohormonal agents belonging to the adrenergic system and renin-angiotensin-aldosterone system (RAAS) among others, are mainly responsible for adaptive mechanisms that occur during and immediately after AMI; an increased plasma concentration promotes inotropic and chronotropic activity, which ensures respectively cardiac output and blood pressure according to the Frank-Starling mechanism; but worsens infarct size expansion due to long-standing volume overload (12).

The temporary beneficial effects brought by compensatory mechanisms, contribute first to an expansion of the infarcted area and in the long term, to postinfarction LV adverse remodeling (11).

The chronic activation of the autonomic system and renin-angiotensin axis exacerbate ventricular dilatation, triggering eccentric hypertrophy, through re-expression of the fetal gene program (13).

Indeed, the chronic neurohormones concentration, produces a hypertrophic stimulus because of the overexpression of sarcoplasmic contractile units, including non-contractile and contractile proteins identifiable only in the fetal period and in the context of global cellular hyperplasia (13).

Hypertrophy and the lack of adequate perfusion, with a consequent imbalance in the oxygen supply, triggers a vicious circle leading to a proapoptotic phase and adverse ventricular remodeling.

Adverse LV remodeling is typically defined by transthoracic echocardiography as a 15–20% increase in both the LV end-diastolic (LVEDV) and end-systolic (LVESV) volumes vs. baseline (14).

The grade of impaired contractility and the infarct size are valid predictors of adverse remodeling and are crucial in the evolution of the global ventricular dilatation. The involvement of more than 10% of the myocardial mass was indicated as the threshold beyond which the regional infarct expansion is followed by eccentric hypertrophy of non-infarcted myocardium, leading to the change of LV from elliptical to a spherical shape, echocardiographically estimated through three-dimensional sphericity index ($EDV/(4/3 \times \pi \times (D/2)^3)$) (13–15). However, the recent evidence suggests that the relationship is not exactly proportional. Data derived from the cardiac magnetic resonance, although have shown an increased incidence of LV remodeling when infarct size affects more than 18.5% of LV mass, have failed to demonstrate absolute criteria. Approximately only 40% of patients in this group underwent progressive LV adverse remodeling. Therefore, could exist an interindividual variability related to predisposing risk factors and an excessive inflammatory response post-AMI, leading to a change in the architecture of the ventricle (16, 17).

Furthermore, it should be considered the crucial role of the mechanical desynchrony decisive for the progression of LV dysfunction. Besides the structural rearrangement of contractile units, LV desynchrony, caused by balance disorder in ion channels, alteration of intercellular communication, and collagen deposition, is a strong indicator for the remodeling severity (18, 19).

MITRAL VALVE DYNAMIC STRUCTURAL CHANGES

Disorder balance caused by LV remodeling between closing and tethering forces, which normally ensures optimal mitral leaflet coaptation, has been the long-accepted origin of IMR (20).

The recent literature has challenged our knowledge regarding IMR, making obsolete the concept that the MV apparatus is only a passive bystander.

The active role played by the MV appears clear when we consider the lack of predictivity emerging from the link between LV dilatation, papillary muscles (PMs) displacement, and severity of MR.

The increased sphericity of the LV and tethering forces are widely observable in the chronic aortic valve regurgitation (AVR); surprisingly showing only a low incidence of functional mitral regurgitation (FMR) (21–23).

First through a necroscopic study, Mautner et al. (24) have documented a significant independent association between LV dilatation and mitral leaflet area. A subgroup analysis showed that AV disease associated with enlargement of the LV cavity, was followed by a compensatory change in the MV morphology. In this group of patients larger and heavier dimensions of the mitral leaflet area, the anterior mitral leaflet (AML) length, and the overall mitral circumference were observed, conversely, this was not observed in a control group of subjects and in those with AV stenosis without LV dilatation.

An increase greater than 30% in the mitral leaflet area, varying proportionally with LV volume and ensuring an adequate systolic closure area, has been shown in the subjects with chronic aortic regurgitation (AR) by Beaudoin et al. (25). In the group of FMR, affected by ischemic cardiomyopathy in more than 80% of cases, although the increase in LV volume was comparable with the group with chronic AR, the authors observed relatively smaller dimensions of the MV; without an adequate enlargement of the leaflet as a request by the increased systolic closure area.

The mechanical elasticity working on the MV, which follows LV cavity enlargement and remodeling with PMs displacement in the setting of chronic AR, may promote an adaptive MV active growth with a slow and compensative evolution. Dal Bianco et al. (26) demonstrated, with a comprehensive experimental evaluation of MV morphology, that PMs tethering leads to a cellular change in the valvular tissue, responsible for the active adaptive mechanisms, later called "MV plasticity."

Endothelial cells of the leaflets, normally quiescent, stimulated by the mechanical stress of remodeling, may increase the expression of signal factors typical of the embryogenic developmental pathways. This active adaptation depends on the molecular process of the endothelial-mesenchymal trans differentiation (EndMT), detected by the expression of mesenchymal markers such as smooth muscle alpha-actin (α-SMA).

In contrast, the MV plasticity results are often not adequate to compensate for the LV remodeling following AMI, although this latter is a powerful trigger of the process (27). These findings are expressions of the delicate balance underlying the reactivation of the embryogenetic biological pathways; this latter, when excessively stimulated in a concentration and time-dependent manner, lead to prevalent fibrotic changes with an unfavorable adaption of MV apparatus.

The inflammatory response following AMI probably plays a crucial role in the altered adaption. The valve tissues infiltration by the cells from the circulating blood, which ultimately differentiate into macrophages, promotes TGF-β upregulation (28).

Therefore, the altered leaflet adaptation with consequent MR post-MI is caused by a vicious cycle triggered by the dysregulation of the post-MI compensatory mechanisms, RAAS among others, which leads to profibrotic changes in the valvular cells with an excessive TGF-β concentration (27).

The molecular changes associated with the altered valve tissue response include an exuberant induction of α-SMA expression involving the endothelium of valvular leaflets on the atrial side. Differently by the solely mechanical stretching/tethering, a deep interstitial penetration involving the valvular interstitial cells (VICs) is present (27).

The infiltration of α-SMA myofibroblasts cells, with increased endothelial neovascularization induces an extracellular matrix (ECM) remodeling with changes in the collagen composition (27).

The adaptive activation of EndMT that stimulates collagen production by the valvular endothelial cells (VECs) and may allow to counteract the mechanical displacement of PMs, is significantly influenced by the environmental context (29).

The inflammatory response seems to be the main driver of the maladaptive process, although in the absence of clear evidence, leading to excessive Angiotensin II (Ang II) concentration (27, 28).

Angiotensin II stimulates the production of growth factors with the conversion of TGF-β to active TGF-β, the principal profibrotic cytokine, in a concentration-dependent manner, increasing the sensitivity of VICs to the fibrogenic actions of TGF-β (30, 31).

The activation of the TGF-β signaling cascade is progressively amplified by paracrine/autocrine stimulation, involving canonical, non-canonical pathways and the expression of endoglin, a transmembrane receptor that modulates the binding of TGF-β to the receptors (31).

Therefore, the initially compensatory mechanism might become counter-productive leading to thickness mitral leaflets and chordae which fail to compensate demanded increased systolic closure area, ultimately impairing coaptation.

The natural history of this molecular rearrangement and structural changes of the MV after an ischemic injury can potentially provide important clinical implications.

THERAPEUTIC IMPLICATIONS

Evolving therapies are following the improvements in the knowledge around IMR. From the surgical point of view, subvalvular and surgical mitral plasticity techniques, with the aim to complete the inadequate valvular adaption, are receiving the greater endorsement, counteracting mechanically the progressive displacement of PMs, mainly in the setting of minimally invasive approach (32–37).

In particular, surgical mitral plasticity includes techniques such as second-order chordal cut (CC) and AML, which plan to compensate ineffectiveness of the molecular process. The increased surface area of the coaptation demanded by the restricted mobility and the consequent leaflet malcoaptation in the setting of IMR may be adequately covered augmenting anterior leaflet with a pericardial patch. Nevertheless, a limitation in performing the solely AML technique is represented by the reduced leaflets mobility secondary to excessive chordal tethering, with chordae not sufficiently remodeled in length to avoid restricted mobility, which can hamper a more physiological coaptation (33). These observations have been highlighted by Calafiore et al. (33), who approached MV using CC, AML, and restrictive MV annuloplasty, demonstrating excellent outcomes.

Although basing our knowledge on still limited literature, a surgical approach inclusive of subvalular correction is mandatory to restore the leaflet coaptation. Indeed, besides the improved leaflet mobility with a more physiologic curvature, the use of second-order CC has shown to determine significant benefit also to the LV contractility (38).

The mechanical stress imposed with MV leaflets because of the increased tethering forces only partially explain the consequent tissue impairment, as aforementioned, with the inflammatory response and TGF-β upregulation that play a crucial role. Therefore, a potential additional management strategy could aim to modulate the TGF-β biological pathway. The TGF-β production is significantly stimulated by Ang II in several cell types, working as a growth factor also in the cardiac fibroblasts, binding the AT1 receptor (39, 40).

The fibrogenic effects of TGF-β may potentially be modulated by RAAS inhibitors such as Angiotensin-Converting Enzyme inhibitor (ACEi) and Ang II receptor blocker (ARBs), certain drugs.

A significant reduction in the infarct size has been observed in ischemic-reperfusion models when ACEi or ARBs have been provided early after percutaneous intervention (41).

Yu et al. (42) conducted an animal study to analyze the effects of RAAS inhibitors in modulating histopathologic changes leading to the ventricular remodeling after AMI. They distributed the population in the three groups according to the received drugs, differentiating between ACEi, ARBs, and a combination therapy group. Regardless of the specific drugs, the study revealed a significant reduction of activated myofibroblasts, rather than the control group (no treatment). Interestingly, the therapy based solely on the ARB (valsartan) or in combination with fosinopril (ACEi) was importantly shown to completely prevent pathological collagen deposition after AMI and the decrease TGF-β mRNA expression, as demonstrated by other authors (43–46).

The treatment with ACEi may be limited by different factors: the production of Ang II in a non-ACE–dependent pathways and the major beneficial effects made through bradykinin production rather than by suppressing Ang II pathways, among others (47).

ARBs, in particular Losartan, have demonstrated, through blocking the interaction of Ang II with its AT1 receptor, to decrease the release of latent TGF-β and to modulate signaling through Smad pathway (47, 48). Furthermore, the expression of endoglin, a powerful promoter of TGF-β fibrogenic effects, and the inhibition in the ERK 1/2 signaling for non-canonical production represents the main drivers of the beneficial effects (31, 49–51).

These results were encouraging for a potential effect on MV endothelium when TGF-β stimulates EndMT; whereas initially favorable, as contributing to an increase in the leaflet size minimizing MR after ischemic injury, but disadvantageous when upregulated in the long term as mainly responsible for exuberant leaflet thickness and impaired mobility.

Wylie-Sears et al. (30) observed a useful ability of Losartan in manipulating EndMT, avoiding excessive fibrotic growth of leaflets. Losartan, in clonal VEC blocked TGF-β signaling; the inhibition of the non-canonical pathway through phosphorylation of ERK, in mitral VEC, was successful to regulate positively EndMT.

These molecular findings have been later confirmed in an animal test by Bartko et al. (52); Losartan can modulate profibrotic changes of the tethered MV leaflets post-MI leading to the solely positive adaptive growth.

The expression of EndMT has been studied, assessing the effect of Losartan in shams affected by IMR produced through apical MI and PMs retraction. In the Losartan-treated group a significant reduction in the thickness of the leaflets, decreasing cell proliferation, collagen deposition, and neovascularization have been demonstrated.

The maladaptive fibrotic changes may be the catalytic factor in the vicious cycle triggered between MR and LV remodeling. The therapeutical accessibility of the profibrotic processes in positively shaping MV after ischemic injury might be potentially revolutionary, considering the unsatisfactory results achieved by most of the current approaches.

CONCLUSION

The burden of IMR is importantly associated with the impairment in the LV contractility often linked to HF, with an important role in worsening patient prognosis. Although evidence is still limited, medical therapy

targeted to modulate TGF-β signaling might open new horizons in the management of MR post-MI. In a not-too-distant future, we can hypothesize of targeted medical therapy, that by promoting mitral plasticity could reduce the incidence of the mitral regurgitation secondary to ischemic cardiomyopathy.

AUTHOR CONTRIBUTIONS

MV and EG: conceptualization. MV and SR: writing—original draft preparation. DR, EG, EW, MD'A, and FM: review and editing. All authors contributed to the article and approved the submitted version.

REFERENCES

1. Acker MA, Parides MK, Perrault LP, Moskowitz AJ, Gelijns AC, Voisine P, et al. Mitral-valve repair versus replacement for severe ischemic mitral regurgitation. *N Engl J Med.* (2014) 370:23–32. doi: 10.1056/NEJMoa1312808
2. Boyd JH. Ischemic mitral regurgitation. *Circ J.* (2013) 77:1952–6. doi: 10.1253/circj.CJ-13-0743
3. Mick SL, Keshavamurthy S, Gillinov AM. Mitral valve repair versus replacement. *Ann Cardiothorac Surg.* (2015) 4:230. doi: 10.3978/j.issn.2225-319X.2015.03.01
4. Otto CM, Nishimura RA, Bonow RO, Carabello BA, Erwin III, Gentile JPF, et al. 2020 ACC/AHA guideline for the management of patients with valvular heart disease: executive summary: a report of the American College of Cardiology/American Heart Association Joint Committee on Clinical Practice Guidelines. *J Am Coll Cardiol.* (2021) 77:450–500. doi: 10.1016/j.jacc.2020.11.035
5. Grayburn PA, Sannino A, Packer M. Proportionate and disproportionate functional mitral regurgitation: a new conceptual framework that reconciles the results of the MITRA-FR and COAPT trials. *JACC: Cardiovascular Imaging.* (2019) 12:353–62. doi: 10.1016/j.jcmg.2018.11.006
6. Konstam MA, Kramer DG, Patel AR, Maron MS, Udelson JE. Left ventricular remodeling in heart failure: current concepts in clinical significance and assessment. *JACC: Cardiovascular Imaging.* (2011) 4:98–108. doi: 10.1016/j.jcmg.2010.10.008
7. Gajarsa JJRA. Left ventricular remodeling in the post-infarction heart: a review of cellular, molecular mechanisms, and therapeutic modalities. *Heart Fail Rev.* (2011) 16:13–21. doi: 10.1007/s10741-010-9181-7
8. Ong SB, Hernández-Reséndiz S, Crespo-Avilan GE, Mukhametshina RT, Kwek XY, Cabrera-Fuentes HA, et al. Inflammation following acute myocardial infarction: multiple players, dynamic roles, and novel therapeutic opportunities. *Pharmacol Ther.* (2018) 186:73–87. doi: 10.1016/j.pharmthera.2018.01.001
9. Bujak M, Dobaczewski M, Chatila K, Mendoza LH, Li N, Reddy A, et al. Interleukin-1 receptor type I signaling critically regulates infarct healing and cardiac remodeling. *Am J Pathol.* (2008) 173:57–67. doi: 10.2353/ajpath.2008.070974
10. Dobaczewski M, Xia Y, Bujak M, Gonzalez-Quesada C, Frangogiannis NG. CCR5 signaling suppresses inflammation and reduces adverse remodeling of the infarcted heart, mediating recruitment of regulatory T cells. *Am J Pathol.* (2010) 176:2177–87. doi: 10.2353/ajpath.2010.090759
11. Sutton MGSJ, Sharpe N. Left ventricular remodeling after myocardial infarction: pathophysiology and therapy. *Circulation.* (2000) 101:2981–8. doi: 10.1161/01.CIR.101.25.2981
12. Yousef ZR, Redwood SR, Marber MS. Postinfarction left ventricular remodelling: where are the theories and trials leading us? *Heart.* (2000) 83:76–80. doi: 10.1136/heart.83.1.76
13. Braunwald E. Ribonucleic acid biomarkers for heart failure: is there a correlation between heart and blood transcriptomics? *JACC: Heart Failure CME.* (2013) 1:20. doi: 10.1016/j.jchf.2013.10.002
14. Huttin O, Coiro S, Selton-Suty C, Juillière Y, Donal E, Magne J. Prediction of left ventricular remodeling after a myocardial infarction: role of myocardial deformation: a systematic review and meta-analysis. *PLoS ONE.* (2016) 11:e0168349. doi: 10.1371/journal.pone.0168349
15. Mannaerts HF, van der Heide JA, Kamp O, Stoel MG, Twisk J, Visser CA. Early identification of left ventricular remodelling after myocardial infarction, assessed by transthoracic 3D echocardiography. *Eur Heart J.* (2004) 25:680–7. doi: 10.1016/j.ehj.2004.02.030
16. Wu E, Ortiz JT, Tejedor P, Lee DC, Bucciarelli-Ducci C, Kansal P. Infarct size by contrast enhanced cardiac magnetic resonance is a stronger predictor of outcomes than left ventricular ejection fraction or end-systolic volume index: prospective cohort study. *Heart.* (2008) 94:730–6. doi: 10.1136/hrt.2007.122622
17. Westman PC, Lipinski MJ, Luger D, Waksman R, Bonow RO, Wu E, et al. Inflammation as a driver of adverse left ventricular remodeling after acute myocardial infarction. *J Am Coll Cardiol.* (2016) 67:2050–60. doi: 10.1016/j.jacc.2016.01.073
18. Azevedo PS, Polegato BF, Minicucci MF, Paiva SA, Zornoff LA. Cardiac remodeling: concepts, clinical impact, pathophysiological mechanisms and pharmacologic treatment. *Arq Bras Cardiol.* (2016) 106:62–9. doi: 10.5935/abc.20160005
19. Ko JS, Jeong MH, Lee MG, Lee SE, Kang WY, Kim SH. Left ventricular dyssynchrony after acute myocardial infarction is a powerful indicator of left ventricular remodeling. *Korean Circ J.* (2009) 39:236–42. doi: 10.4070/kcj.2009.39.6.236
20. Agricola E, Oppizzi M, Pisani M, Meris A, Maisano F, Margonato A. Ischemic mitral regurgitation: mechanisms and echocardiographic classification. *Eur J Echocardiogr.* (2008) 9:207–21. doi: 10.1016/j.euje.2007.03.034
21. Kochav JD, Kim J, Judd R, Kim HW, Klem I, Heitner J. Ischemia-mediated dysfunction in subpapillary myocardium as a marker of functional mitral regurgitation. *Cardiovasc Imag.* (2021) 14:826. doi: 10.1016/j.jcmg.2021.01.007
22. Bonow RO, Lakatos E, Maron BJ, Epstein SES. Assessment of the natural history of asymptomatic patients with chronic aortic regurgitation and normal left ventricular systolic function. *Circulation.* (1991) 84:1625–35. doi: 10.1161/01.CIR.84.4.1625
23. Ishii K, Hirota Y, Suwa M, Kita Y, Onaka H, Kawamura K. Natural history and left ventricular response in chronic aortic regurgitation. *Am J Cardiol.* (1996) 78:357–61. doi: 10.1016/S0002-9149(96)00295-0
24. Mautner SL, Klues HG, Mautner GC, Proschan MA, Roberts WC, Maron BJC. Mitral valve dimensions in adults with valvular aortic stenosis, pure aortic regurgitation and hypertrophic cardiomyopathy. *Am J Cardiol.* (1993) 71:949–53. doi: 10.1016/0002-9149(93)90912-V
25. Beaudoin J, Handschumacher MD, Zeng X, Hung J, Morris EL, Levine RA, et al. (2013). Mitral valve enlargement in chronic aortic regurgitation as a compensatory mechanism to prevent functional mitral regurgitation in the dilated left ventricle. *J Am Coll Cardiol.* 61:1809–16. doi: 10.1016/j.jacc.2013.01.064
26. Dal-Bianco JP, Aikawa E, Bischoff J, Guerrero JL, Handschumacher MD, Sullivan S, et al. Active adaptation of the tethered mitral valve: insights into a compensatory mechanism for ischemic mitral regurgitation. *Am Heart Assoc.* (2008) 2008:S_649. doi: 10.1161/circ.118.suppl_18.S_649
27. Dal-Bianco JP, Aikawa E, Bischoff J, Guerrero JL, Hjortnaes J, Beaudoin J, et al. (2015). Myocardial infarction adaptation of the tethered mitral valve. *J Am Coll Cardiol.* 67:275–87. doi: 10.1016/j.jacc.2015.10.092
28. Calafiore AM, Totaro A, Testa N, Sacra C, Castellano G, Guarracini S. The secret life of the mitral valve. *J Card Surg.* (2021) 36:247–59. doi: 10.1111/jocs.15151
29. Campbell SE, Katwa LC. Angiotensin II stimulated expression of transforming growth factor-β1in cardiac fibroblasts and myofibroblasts. *J Mol Cell Cardiol.* (1997) 29:1947–58. doi: 10.1006/jmcc.1997.0435
30. Wylie-Sears J, Levine RA, Bischoff J. Losartan inhibits endothelial-to-mesenchymal transformation in mitral valve endothelial cells by blocking transforming growth factor-β-induced phosphorylation of ERK. *Biochem Biophys Res Commun.* (2014) 446:870–5. doi: 10.1016/j.bbrc.2014.03.014

31. Chen K, Mehta JL, Joseph LD, Joseph LJ. Transforming growth factor beta receptor endoglin is expressed in cardiac fibroblasts and modulates profibrogenic actions of angiotensin II. *Circ Res.* (2004) 95:1167–73. doi: 10.1161/01.RES.0000150369.68826.2f
32. Vinciguerra M, Grigioni F, Romiti S, Benfari G, Rose D, Spadaccio C. Ischemic mitral regurgitation: a multifaceted syndrome with evolving therapies. *Biomedicines.* (2021) 9:447. doi: 10.3390/biomedicines9050447
33. Calafiore AM, Totaro A, Amicis D, Pelini V, Pinna P, Testa GN, et al. Surgical mitral plasticity for chronic ischemic mitral regurgitation. *J Cardiac Surg.* (2020) 35:772–8. doi: 10.1111/jocs.14487
34. Calafiore AM, Totaro A, Paparella D, Gaudino M, Prapas S, Mick SL, et al. Mimicking natural mitral adaptation to ischaemic regurgitation: a proposed change in the surgical paradigm. *Eur J Cardio-Thorac Surg.* (2020) 58:35–9. doi: 10.1093/ejcts/ezaa163
35. Chirichilli I, D'Ascoli R, Rose D, Frati G, Greco E. Port Access (Thru-Port System) video-assisted mitral valve surgery. *J Thorac Dis.* (2013) 5 Suppl 6:S680–5. doi: 10.3978/j.issn.2072-1439.2013.10.14
36. Marullo AG, Irace FG, Vitulli P. Recent developments in minimally invasive cardiac surgery: evolution or revolution? *Biomed Res Int.* (2015) 2015:483025. doi: 10.1155/2015/483025
37. Cimino S, Guarracino F, Valenti V, Frati G, Sciarretta S, Miraldi F, et al. Echocardiography and correction of mitral regurgitation: an unbreakable link. *Cardiology.* (2020) 145:110–20. doi: 10.1159/000504248
38. Dobre M, Koul B, Rojer A. Anatomic and physiologic correction of the restricted posterior mitral leaflet motion in chronic ischemic mitral regurgitation. *J Thorac Cardiovasc Surg.* (2000) 120:409–11. doi: 10.1067/mtc.2000.106521
39. Ketteler M, Noble NA. Transforming growth factor-β and angiotensin II: the missing link from glomerular hyperfiltration to glomerulosclerosis? *Annu Rev Physiol.* (1995) 57:279–95. doi: 10.1146/annurev.ph.57.030195.001431
40. Vracko R. Contractile cells in rat myocardial scar tissue. *Lab Invest.* (1991) 65:214–27.
41. Weidenbach R, Schulz R, Gres P, Behrends M, Post H, Heusch G. Enhanced reduction of myocardial infarct size by combined ACE inhibition and AT1-receptor antagonism. *Br J Pharmacol.* (2000) 131:138–44. doi: 10.1038/sj.bjp.0703544
42. Yu CM, Tipoe GL, Wing-Hon Lai K. Effects of combination of angiotensin-converting enzyme inhibitor and angiotensin receptor antagonist on inflammatory cellular infiltration and myocardial interstitial fibrosis after acute myocardial infarction. *J Am Coll Cardiol.* (2001) 38:1207–15. doi: 10.1016/S0735-1097(01)01518-2
43. Schieffer B, Wirger A, Meybrunn M, Seitz S, Holtz J, Riede UN, et al. Comparative effects of chronic angiotensin-converting enzyme inhibition and angiotensin II type 1 receptor blockade on cardiac remodeling after myocardial infarction in the rat. *Circulation.* (1994) 89:2273–82. doi: 10.1161/01.CIR.89.5.2273
44. Richer C, Mulder P, Fornes P, Domergue V, Heudes D, Giudicelli JF. Long-term treatment with trandolapril opposes cardiac remodeling and prolongs survival after myocardial infarction in rats. *J Cardiovasc Pharmacol.* (1992) 20:147–56. doi: 10.1097/00005344-199207000-00019
45. van Krimpen C, Smits JF, Cleutjens JP, Debets JJ, Schoemaker RG, Boudier HAS. DNA synthesis in the non-infarcted cardiac interstitium after left coronary artery ligation in the rat: effects of captopril. *J Mol Cell Cardiol.* (1991) 23:1245–53. doi: 10.1016/0022-2828(91)90082-W
46. Michel JB, Lattion AL, Salzmann JL, Cerol MD, Philippe M, Camilleri JP, et al. Hormonal and cardiac effects of converting enzyme inhibition in rat myocardial infarction. *Circ Res.* (1988) 62:641–50. doi: 10.1161/01.RES.62.4.641
47. Hartman JC. The role of bradykinin and nitric oxide in the cardioprotective action of ACE inhibitors. *Ann Thorac Surg.* (1995) 60:789–92. doi: 10.1016/0003-4975(95)00192-N
48. Rosenkranz S. TGF-β1 and angiotensin networking in cardiac remodeling. *Cardiovasc Res.* (2004) 63:423–32. doi: 10.1016/j.cardiores.2004.04.030
49. Habashi JP, Doyle JJ, Holm TM, Aziz H, Schoenhoff F, Bedja D. Angiotensin II type 2 receptor signaling attenuates aortic aneurysm in mice through ERK antagonism. *Science.* (2011) 332:361–5. doi: 10.1126/science.1192152
50. Holm TM, Habashi JP, Doyle JJ, Bedja D, Chen Y, Van Erp C. Noncanonical TGFβ signaling contributes to aortic aneurysm progression in Marfan syndrome mice. *Science.* (2011) 332:358–61. doi: 10.1126/science.1192149
51. Rodríguez-Vita J, Sánchez-López E, Esteban V, Rupérez M, Egido J, Ruiz-Ortega M. Angiotensin II activates the Smad pathway in vascular smooth muscle cells by a transforming growth factor-β-independent mechanism. *Circulation.* (2005) 111:2509–17. doi: 10.1161/01.CIR.0000165133.84978.E2
52. Bartko PE, Dal-Bianco JP, Guerrero JL, Beaudoin J, Szymanski C, Kim DH. Transatlantic Mitral Network Effect of losartan on mitral valve changes after myocardial infarction. *J Am Coll Cardiol.* (2017) 70:1232–44. doi: 10.1016/j.jacc.2017.07.734

Conflict of Interest: The authors declare that the research was conducted in the absence of any commercial or financial relationships that could be construed as a potential conflict of interest.

Publisher's Note: All claims expressed in this article are solely those of the authors and do not necessarily represent those of their affiliated organizations, or those of the publisher, the editors and the reviewers. Any product that may be evaluated in this article, or claim that may be made by its manufacturer, is not guaranteed or endorsed by the publisher.

frontiers in Cardiovascular Medicine

ORIGINAL RESEARCH
published: 13 January 2022
doi: 10.3389/fcvm.2021.796041

Trends in Ischemic Mitral Regurgitation Following ST-Elevation Myocardial Infarction Over a 20-Year Period

Leor Perl[1,2]*, *Tamir Bental*[1,2], *Katia Orvin*[1,2], *Hana Vaknin-Assa*[1,2], *Gabriel Greenberg*[1,2], *Pablo Codner*[1,2], *Yaron Shapira*[1,2], *Mordehay Vaturi*[1,2], *Alexander Sagie*[1,2] and *Ran Kornowski*[1,2]

[1] Department of Cardiology, Rabin Medical Center – Beilinson Hospital, Petach Tikva, Israel, [2] Affiliated to Sackler Faculty of Medicine, Tel Aviv University, Tel Aviv, Israel

Background: Ischemic mitral regurgitation (IMR) is a common complication of acute ST-elevation myocardial infarction (STEMI). Little is known regarding the impact of IMR over a long period of follow up.

Methods: Of 3,208 consecutive STEMI patients from a prospective registry, full echocardiographic information was available for 2,985 patients between the years 2000 and 2020. We compared the two decades- 2001 to 2010 and 2011 to 2020, and assessed for the presence of IMR at baseline, 3 (range 2–6) months and 12 (range 10–14) months after the index event.

Results: One thousand six hundred and sixty six patients were included in the first decade, 1,319 in the second. Mean patient age was 61.3 ± 12.3 years, 21.1% female patients in the first decade vs. 60.9 ± 12.0 years and 22.2% female in the second ($p = 0.40$ and $p = 0.212$, respectively). Rates of moderate IMR or above during the index admission were 17.2% in the first period and 9.3% in the second one ($p < 0.001$). After 3 months, the rate of IMR was 48.5% for those who suffered from IMR at baseline, vs. 9.5% for those without IMR at baseline (HR- 4.2, $p < 0.001$). Death rates for those with moderate IMR or above were 14.7% and 17.8% after 1 and 2 years, respectively, vs. 7.3 and 9.6% for those without ($p < 0.001$ for both). IMR was associated with 1 year mortality in multivariate analysis (HR-1.37; 1.09–2.20, $p = 0.009$), as well as in propensity score matched analysis (HR 1.29; CI: 1.07–1.91; $p < 0.001$).

Conclusions: IMR is a common complication following acute STEMI, impacting prognosis. Rates of IMR have declined significantly over the years.

Keywords: ischemic mitral regurgitation, myocardial infarction, primary percutaneous coronary, remodeling, ST-segment elevation myocardial infarction

OPEN ACCESS

Edited by:
Bernard Chevalier, Institut Cardiovasculaire Paris Sud, France

Reviewed by:
Prakash P. Punjabi, Imperial College London, United Kingdom
Antonio Miceli, Istituto Clinico Sant'Ambrogio, Italy

***Correspondence:**
Leor Perl
leorperl@gmail.com;
leorper@clalit.org.il

Specialty section:
This article was submitted to Heart Valve Disease, a section of the journal Frontiers in Cardiovascular Medicine

Received: *15 October 2021*
Accepted: *21 December 2021*
Published: *13 January 2022*

Citation:
Perl L, Bental T, Orvin K, Vaknin-Assa H, Greenberg G, Codner P, Shapira Y, Vaturi M, Sagie A and Kornowski R (2022) Trends in Ischemic Mitral Regurgitation Following ST-Elevation Myocardial Infarction Over a 20-Year Period. Front. Cardiovasc. Med. 8:796041. doi: 10.3389/fcvm.2021.796041

INTRODUCTION

Ischemic mitral regurgitation (IMR, **Figure 1**) is a common complication of myocardial infarction (MI) and is caused by left ventricular (LV) remodeling affecting the mitral valve apparatus (1). The estimated incidence of IMR is 11–59% following MI, while moderate to severe IMR appear in 6.3–12.0% of the cases (2–4). The presence of IMR is of grave importance, as it increases the risk for the development of symptomatic heart failure as well as mortality (3, 5–7).

Little is known regarding the natural course of IMR and the tendency of acute IMR to remain permanently. Previous studies suggested that shorter onset-to-reperfusion time and non-total occlusion were found to be independent predictors of early improvement of IMR, whereas higher cardiac biomarker levels, older age, global longitudinal strain and global LV infarct extent were found to have a negative impact in the chronic phase (5, 8). In addition, in some studies IMR was more frequent in patients with an inferior infarction compared with an anterior infarction (9, 10). However, many of the studies have been published based on a limited cohort, both in terms of number of patients and the observation period.

Our aims, therefore, were to investigate the rates of IMR over a 20 year period, based on a large prospective registry of patients suffering from STEMI treated by primary percutaneous coronary intervention (pPCI), in order to study the natural course of IMR following the event.

MATERIALS AND METHODS

Study Design

The present study is based on a prospectively collected STEMI registry from Rabin Medical Center in Petach Tikva—Israel, which includes two campuses—Beilinson and Hasharon hospitals. The registry includes consecutive patients suffering from STEMI who were treated with pPCI from January 2001 through December 2020. The data is continuously entered into an ongoing registry for purposes of recording and monitoring patient-related parameters, clinical events, and angiographic findings.

Of the patients in the registry, we included all patients who have had echocardiographic information during the initial admission, including a proposed mechanism for mitral regurgitation. Patients were excluded if they were treated with thrombolysis instead of pPCI (<1% of cases), if they had known IMR prior to the index event or if they were found to have primary mitral regurgitation prior to MI diagnosis. We then collected information on the echocardiographic exams they have had in the first year, in two more time periods: 3 months (range 2–6 months, period 2) and 12 months (range 10–14 months, period 3). Comparisons were made between the two decades: from January 2001 through December 2010 and from January 2011 through December 2020. The study protocol was approved by the local Institutional Review Board.

Interventional Procedure

All patients provided explicit written informed consent to undergo cardiac catheterization. Pre-catheterization treatment consisted of aspirin and unfractionated heparin (70 U/kg). Clopidogrel 300 or 600 mg, prasugrel 60 mg, or ticagrelor 180 mg was administered as a loading dose before or immediately after PCI. The utilization of glycoprotein IIb/IIIa inhibitors (GP2b3a) and choice of stent, as well as other therapeutic modalities such as mechanical thrombectomy and distal protection devices, were left to the discretion of the primary operator. All stents were implanted with moderate-to-high deployment pressure (12 to 16 atm). All patients received dual antiplatelet therapy with aspirin 100 mg daily and a thienopyridine (clopidogrel, prasugrel, or ticagrelor) for at least 12 months after PCI.

Endpoints

Immediate and in-hospital events were prospectively collected in the institutional database. During follow-up, patients completed standardized questionnaires for clinical events either by telephone or in the outpatient clinics at 6 month intervals. When indicated, records from peripheral hospitals were acquired to verify the events in the follow-up period. All events were further confirmed and adjudicated by the institutional clinical events adjudication committee. Survival status at follow-up was assessed by review of municipal civil registries at 30 days and 3 years. Clinical outcomes included all-cause mortality and major adverse cardiac events (MACE), which comprised death, MI, target vessel revascularization (TVR), subsequent coronary artery bypass graft (CABG) and renal failure (defined as glomerular filtration rate below 50 ml/min/1.73 m^2, according to the Modification of Diet in Renal Disease formula).

Statistical Analysis

Continuous data are summarized as mean and standard deviation (SD) or median and interquartile range (IQR) and were compared using Student *t*-tests or analyses of variance. Categorical variables are presented as frequency and were compared by chi-square or Fisher's exact tests. The normality of variable distributions was assessed using the Kolmogorov–Smirnov test. Time-to-event curves were constructed using the Kaplan–Meier method and compared using log-rank test. Cox regression analyses were performed to identify independent predictors of the primary end point. Covariates for the Cox model were chosen according to their known association with IMR and outcomes, and included age, sex, diabetes mellitus, hypertension, renal failure, peripheral artery disease (PAD), previous CABG, previous PCI, left ventricular ejection fraction (LVEF, for each 1% increase), the 2011–2020-decade, deployment of drug eluting stents, trans radial access and moderate or above MR at baseline. Effect sizes are presented as odds ratios and 95% confidence intervals. Step-wise variable selection of significant univariate predictors ($P < 0.1$) was used to identify variables for inclusion in the multivariate model. Multivariate logistic regression analyses were performed to determine independent predictors of the primary end point, accounting for known baseline cardiovascular risk differences. Finally, due to several differences in baseline characteristics, we compiled a cohort of propensity score matched patients with a 1:1 ratio between the two decades. The propensity score was derived from a multivariate logistic regression model that included the decade of the admission, considered as the independent (outcome)

Abbreviations: IMR, Ischemic mitral regurgitation; STEMI, ST-elevation myocardial infarction; MI, myocardial infarction; LV, left ventricle; pPCI, primary percutaneous coronary intervention; MACE, major adverse cardiac events; TVR, target vessel revascularization; CABG, coronary artery bypass graft; PAD, peripheral artery disease; LVEF, left ventricular ejection fraction; MVP, mitral valve prolapse; CAD, coronary artery disease; GFR, glomerular filtration rate; CPK, creatine phosphokinase; IABP, intra-aortic balloon pump; TIMI, Thrombolysis in Myocardial Infarction, FMC, first medical contact.

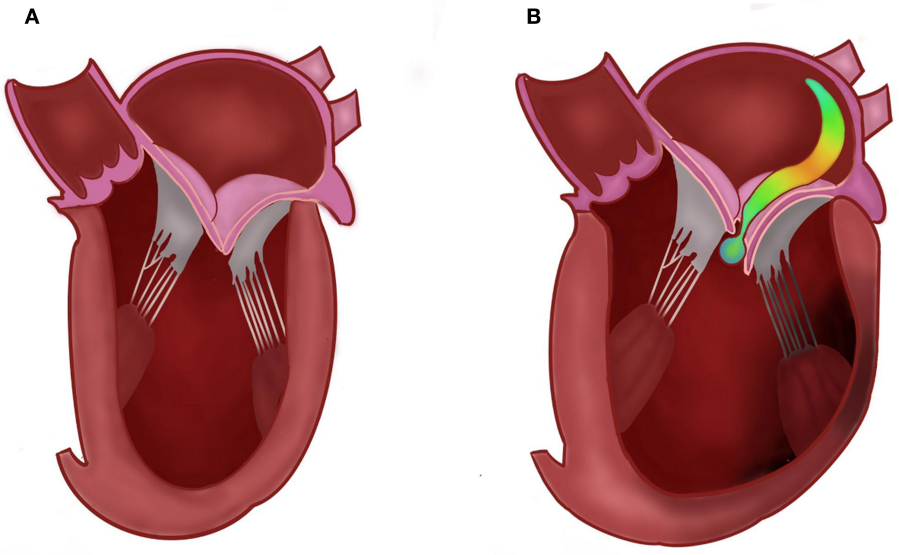

FIGURE 1 | Normal **(A)** vs. ischemic mitral regurgitation **(B)**, demonstrating an eccentric jet due to left ventricular remodeling, displacement of the papillary muscles and tethering of the leaflets.

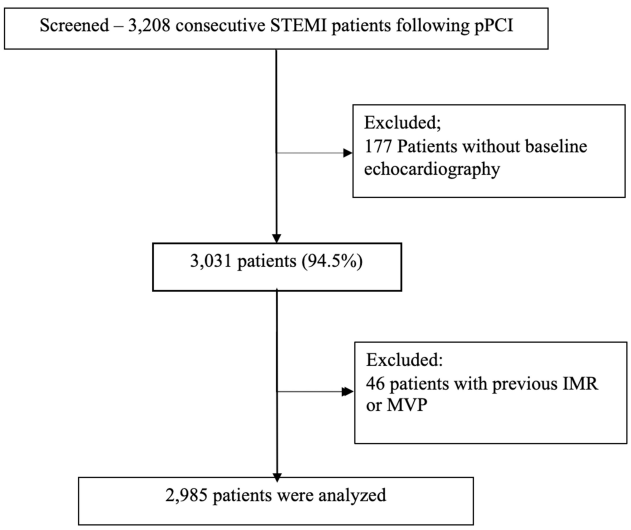

FIGURE 2 | Study cohort.

variable, and all baseline clinical characteristics and procedural characteristics as covariates. The propensity score matched cohort was analyzed for the main combined outcome. Author Leor Perl had full access to all the data in the study and takes responsibility for its integrity and the data analysis. All statistical analyses were performed with IBM SPSS statistics V.27 software. A $P < 0.05$ was considered statistically significant.

RESULTS

Of 3,208 patients in the Rabin Medical Center STEMI registry, detailed echocardiographic information existed at baseline for 3,031 (94.5%) of the patients. Following exclusion of patients with known IMR prior to the event, mitral valve prolapse and the other exclusion detailed above, 2,985 patients remained (n-1,666 for the first decade and 1,319 for the latter, **Figure 2**).

Mean patient age was 61.3 years between 2001 and 2010 and 60.9 during the period of 2011–2020 ($p = 0.40$), 22.2% were female patients at the second period vs. 21.1% at the first ($p = 0.212$), 27.6% suffered from diabetes mellitus vs. 27.2% ($p = 0.634$, **Table 1**). A higher proportion of the patients in the second period also had previous PCI (18.2% vs. 15.0%, $p = 0.041$). Other baseline characteristics were similar (**Table 1**).

As for their presentation during the index event, patients in the second decade had lower rates of peak CPK (1569.5 ± 351.5 vs. 2089.7 ± 331.2 mcg/L, $p = 0.01$) and higher LV ejection fraction at baseline (51.3% vs. 48.4%, $p = 0.031$) than patients in the first decade. Patients in the second period were also treated faster (mean presentation to reperfusion time 1.0 h vs. 1.3 h, $p = 0.041$) and by higher rates of transradial PCI (68.2% vs. 21.4%, $p < 0.001$), drug eluting stents (93.2% vs. 38.2%, $p < 0.001$) and prasugrel pharmacotherapy (61.2% vs. 0.0%, $p < 0.001$) than in the first period (**Table 2**).

Rates of moderate IMR or above during the index admission were 17.2% in the first period and 9.3% in the second one ($p < 0.001$, **Figure 3**). After 3 (range 2–6) months, information was available for 554 of the patients (18.6% of the cohort). The rate of moderate IMR or above was 48.5% for those who suffered from IMR at baseline, vs. 9.5% for those without IMR at baseline ($p < 0.001$). After 12 (range 10–14) months, information existed for 379 patients (12.7% of the baseline). At that point in time, the rate of IMR decreased and was 15.4% for those with significant IMR at baseline, vs. 1.6% for those without ($p < 0.001$).

Death rates for those with moderate IMR or above at baseline were 14.7 and 17.8% after one and two years, respectively, vs. 7.3 and 9.6% for those without (**Figure 4**, $p < 0.001$ for both). Mortality rates for those who also presented with moderate IMR

TABLE 1 | Baseline characteristics according to decade.

Parameter	Period 1 (2001–2010) *n*-1,666	Period 2 (2011–2020) *n*-1,319	*P*-Value
Age (years)	61.3 ± 12.3	60.9 ± 12.0	0.400
Female Sex (%)	21.1	22.2	0.212
BMI*	30.221 ± 9.1	28.884 ± 9.4	0.151
Family History of CAD† (%)	31.9	32.6	0.452
Diabetes Mellitus (%)	27.2	27.6	0.634
Hypertension (%)	49.5	55.3	0.138
Smoking (%)	0.434	0.478	0.392
Hyperlipidemia (%)	0.493	0.517	0.283
Obesity (%)	0.359	0.380	0.356
Renal Failure (%)	0.097	0.080	0.241
Past Stroke (%)	0.056	0.064	0.090
PAD‡ (%)	0.051	0.044	0.385
Previous PCI§ (%)	0.150	0.182	0.041
Previous CABG‖ (%)	0.029	0.035	0.231
Previous MI# (%)	12.3	17.3	0.127
Valvular Surgery (%)	4.5	3.8	0.832

**BMI, body mass index; †CAD, coronary artery disease; ‡PAD, peripheral arterial disease; §PCI, percutaneous coronary intervention; ‖CABG, coronary artery bypass graft; #MI, myocardial infarction.*

TABLE 2 | Presentation and procedural details according to decade.

Parameter	Period 1 (2001–2010) *n*-1,666	Period 2 (2011–2020) *n*-1,319	*P*-Value
Systolic blood pressure (mmHg ± SD)	133.4 ± 40.7	135.1 ± 42.5	0.473
Diastolic blood pressure (mmHg ± SD)	77.3 ± 38.2	78.7 ± 37.8	0.383
GFR* (mL/min/1.73 m^2)	86.3 ± 20.2	86.5 ± 19.4	0.472
Hemoglobin (g/dL ± SD)	13.4 ± 2.4	13.2 ± 3.1	0.274
Platelets ($\times 10^9$/L. ±SD)	182.1 ± 45.2	186.2 ± 41.6	0.167
Glucose (mg/L±SD)	128.2 ± 47.4	134.2 ± 52.6	0.121
Peak-CPK† (mcg/L±SD)	2089.7 ± 331.2	1569.5 ± 351.5	0.010
Transradial approach (%)	21.4	68.2	<0.001
Symptoms to presentation (hours ± SD)	4.2 ± 2.0	3.9 ± 1.8	0.088
Presentation to PCI‡ (hours ± SD)	1.3 ± 0.5	1.0 ± 0.6	0.041
Anterior territory of infarction (%)	48.5%	49.2%	0.425
Inferior territory of infarction (%)	34.2%	33.9%	0.523
Cardiogenic Shock (%)	8.1	4.9	0.091
LVEF§ (%)	48.4 ± 12.4	51.3 ± 14.5	0.031
Aspirin (%)	91.0	95.1	0.410
Plavix (%)	88.1	34.1	0.002
Prasugrel (%)	0.0	61.2	<0.001
Ticagrelor (%)	0.0	2.4	0.202
Amines (%)	4.8	2.8	0.448
Number of vessels (N±SD)	1.8	1.8	0.285
Thrombus (%)	69.2	68.4	0.684
Drug eluting Stent (%)	38.2	93.2	<0.001
IABP‖ (%)	4.0	3.2	0.420
Temporary Pacemaker (%)	5.3	3.9	0.083
Thrombectomy (%)	13.5	9.8	0.344
Bifurcation (%)	14.8	16.6	0.952
Mean TIMI# pre-procedural (±SD)	1.5 ± 0.9	1.5 ± 0.8	0.960
Mean TIMI post-procedural (±SD)	2.9 ± 0.2	2.9 ± 0.1	0.324

**GFR, glomerular filtration rate; †CPK, creatine phosphokinase; ‡PCI, percutaneous coronary intervention; §LVEF, left ventricular ejection fraction; ‖IABP, intra-aortic balloon pump; #TIMI, Thrombolysis in Myocardial Infarction.*

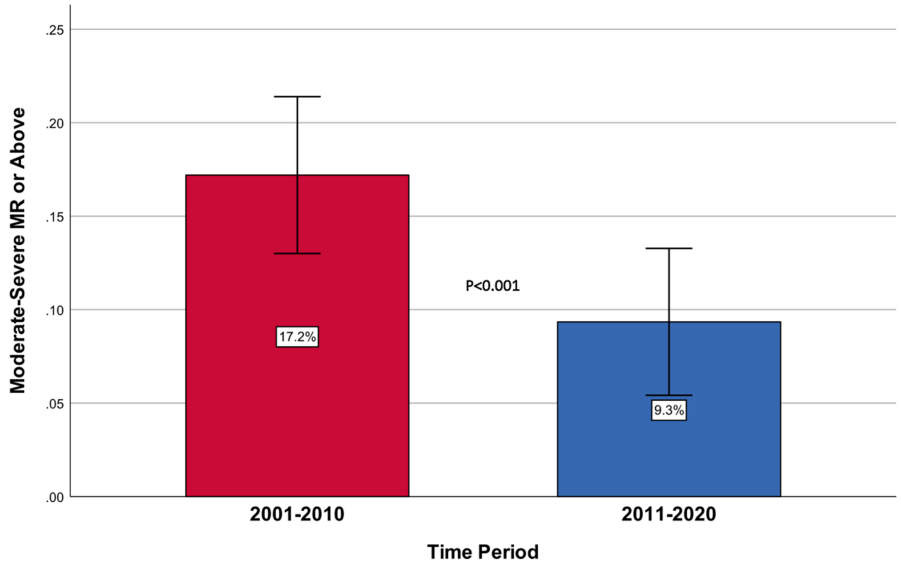

FIGURE 3 | Rates of moderate-severe or above IMR by period.

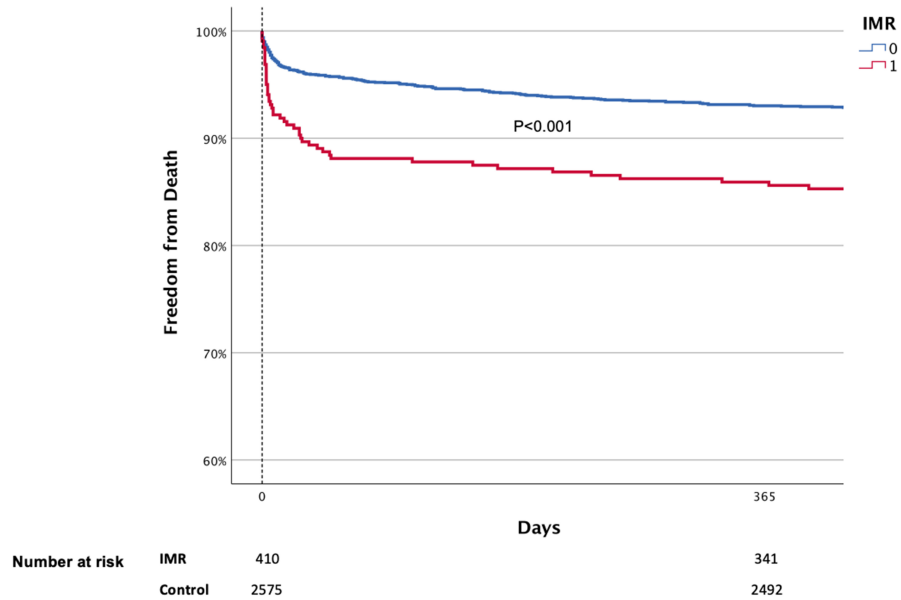

FIGURE 4 | Kaplan Meier curves of survival by IMR.

or above after 3 months was 17.9 and 28.7% after 1 and 2 years, respectively, vs. 10.7 and 17.9% for those without IMR ($p < 0.001$ for both).

In a multivariate analysis, IMR was found to have an independent impact on 1 year mortality rates (HR-1.37; SD 1.09–2.20, $p = 0.009$), as well as age (HR-1.04; 1.03–1.05, $p < 0.001$), diabetes mellitus (HR-1.58; 1.18–2.12, $p = 0.002$), renal failure (HR-2.79; 2.02–3.85, $p < 0.001$), LVEF (HR-0.920; 0.91–0.93, $p < 0.001$), application of drug eluting stents (HR-0.64; 0.44–0.94, $p = 0.022$), first medical contact (FMC)-to balloon time (HR-1.83; 1.09–2.99, $p = 0.02$) and trans-radial approach (HR-0.83; 0.38–0.99, $p = 0.044$). However, after correcting for these confounding factors, the 2001–2010 decade was not found to negatively impact the risk of 1 year death (HR-1.00; 0.71–1.41, $p = 0.999$, **Table 3**). Importantly, at both time periods, IMR significantly increased the likelihood of death (**Figure 5**).

The propensity match score was able to form 288 matched pairs of first- and second-decade patients, showing similar

TABLE 3 | Multivariate analysis for the risk of 1-year mortality.

Parameter	HR	*P*-value
Age	1.042 (1.029–1.054)	0.000
Sex (female)	1.217 (0.888–1.668)	0.222
Diabetes Mellitus	1.584 (1.180–2.124)	0.002
Hypertension	0.871 (0.637–1.190)	0.385
Renal Failure	2.788 (2.019–3.849)	0.000
PAD*	1.448 (0.951–2.205)	0.085
S/P CABG†	1.115 (0.626–1.984)	0.712
Previous PCI‡	0.847 (0.580–1.237)	0.390
FMC§ to Balloon	1.825 (1.092–2.987)	0.02
LVEF‖%	0.920 (0.907–0.933)	0.000
Time period	1.000 (0.711–1.407)	0.999
Drug Eluting Stent	0.640 (0.436–0.938)	0.022
Trans-Radial Access	0.832 (0.384–0.992)	0.044
MR# at Baseline	1.365 (1.094–2.202)	0.009

PAD, peripheral arterial disease; †CABG, coronary artery bypass graft; ‡PCI, percutaneous coronary intervention; §FMC, first medical contact; ‖LVEF, left ventricular ejection fraction; #MR, mitral regurgitation.

results; Rates of IMR in these two matched cohorts were not significantly different (12.6% in the first decade vs. 9.8% in the second, $p = 0.08$). Following Cox regression, patients presenting with IMR demonstrated higher rates 1 year death than patients without IMR (HR 1.29; CI: 1.07–1.91; $p < 0.001$).

A separate regression was performed to predict the risk of the development of moderate or above IMR at baseline, and following correction for these above factors, the 2001–2010 decade was not associated with risk of IMR (HR-0.93; 0.63–1.22, $p = 0.08$). Factors associated with IMR were LVEF (HR-0.83 for each 1%; 0.46–0.94, $p < 0.001$) and FMC-to balloon time (HR-1.69 for each passing hour; 1.04–2.48, $p = 0.04$, **Table 4**). The territory of infarct (anterior vs. inferior) did not impact the risk of IMR.

DISCUSSION

In this study, we examined the impact of IMR on clinical outcomes in patients presenting with STEMI over a period of two decades, treated at our 2 hospitals in a single combined medical center. We have shown that mortality had changed dramatically over the years, as the time to revascularization, rates of transradial access, P2Y12 and implantation of drug eluting stents have changed. However, the deleterious effect of IMR on death remained profound.

In recent years, there have been significant improvements in the rates of timely revascularization and outcomes for patients suffering from acute coronary syndrome worldwide (11–14). Furthermore, studies assessing the temporal trends following myocardial infarction show a reduction in the rates of mechanical complications over the years. However, when these events occur, they continue to be associated with high mortality rates, which have not improved over the years (15–17).

Mitral regurgitation, whether apparent during the acute or chronic phase of myocardial infarction, increases the rate of adverse events, including all-cause mortality and the risk of the development of congestive heart failure (3, 5–7, 18, 19).

In our study, we have attempted to describe the rates of IMR over a long period of time, and correlate it with mortality. We have seen that rates of IMR have reduced significantly over time, but that in those who present with IMR at baseline, only around half recover after 3 months. We also witnessed a strong impact of IMR on survival, regardless of time period. In our two medical campuses, standard echocardiographic exams are performed immediately after a patient's arrival at the cardiac intensive care unit by skilled sonographers as a protocolized patient care for acute coronary syndrome. In addition, all STEMI patients' clinical course and outcomes are recorded and followed-up for adverse events in a dedicated registry. This allows for the serial follow-up of all patients and comparison of outcomes with echocardiography. Similarly, in the study by Nishino et al. (5), a trend for improvement was witnessed over time in close to 40% of patients, but for those who present with IMR at baseline, the risk for chronic IMR remains. In addition, the presence of IMR in the acute phase worsens prognosis. Also, in similar fashion to the results by Nishino et al. we have found no correlation between the infarction territory and the risk for IMR, as opposed to the outcomes published previously, mostly during the thrombolysis era of STEMI. However, in that study, as well as in the study by Zhang et al. (8), an increased risk of IMR was correlated with older age and higher CPK levels, but in our study these factors did not affect the risk of IMR. Risk factors that were shown to increase the risk of IMR included reduced LVEF and longer FMC-to balloon time. In fact, when correcting for the differences in these factors, the risk of IMR is similar between the years 2001–2010 and 2011–2020.

We have previously shown that in our cohort, the transradial approach improves survival in our PCI patients (20), as was evident in numerous other studies, including in cohorts of STEMI (21–25). Additionally, 2nd generation DES in primary PCI was shown to improve outcomes as compared to 1st generation or bare metal stents (26–28). Both of these factors predicted improved prognosis in our patient population as well, but had no impact on the risk of development of IMR. In our study, the risk for IMR is correlated with a longer FMC-to-balloon time and reduced LVEF. It was previously shown that the extent of global LV infarction extent independently predicts IMR following STEMI (8), mostly due to geometric changes in the mitral valve apparatus with greater displacement of posterior papillary muscle (1). These changes are dependent upon the amount of rescued myocardium by emergency revascularization. The earlier the FMC-to-reperfusion time, the greater the degree of rapid LV improvement is expected. Therefore, improvement in the techniques to achieve timely reperfusion worldwide may continue to reduce the rates of mechanical complications, including IMR, in the years to come. In addition, thanks to advancements in the percutaneous methods to correct functional MR, we may also soon witness a true therapeutic option for IMR directly, in patients with STEMI. New preliminary data now suggests edge-to-edge mitral valve repair may benefit patients with IMR who are hemodynamically unstable (29–31). Conceivably, these and other new therapeutic

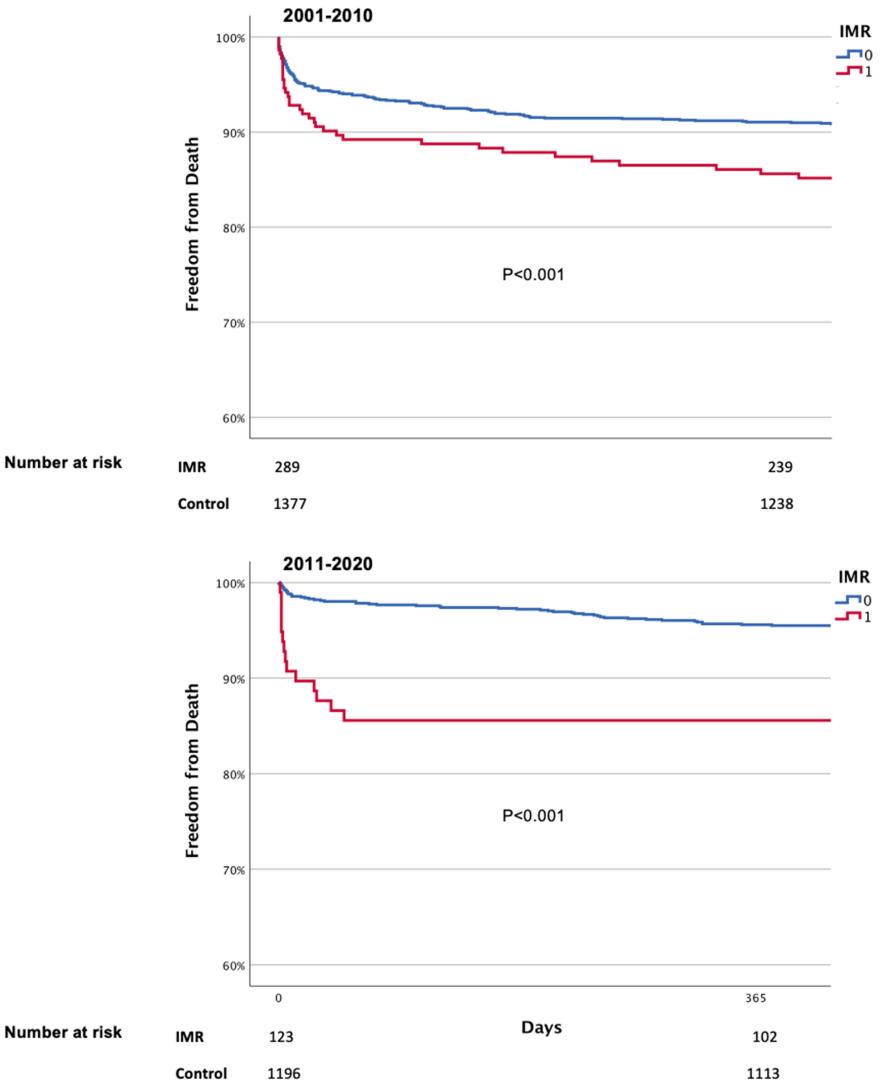

FIGURE 5 | Kaplan Meier curves of survival by decade.

modalities may potentially become a viable option in reducing the risk for this menacing complication. However, the basic etiology of IMR is ischemia, and it is also possible that more complete revascularization may reduce potential residual ischemia. Whether IMR is a surrogate of myocardial jeopardy or an independent factor for worse prognosis remains to be proven in future trials. Finally, improved adherence to medications attenuating progressive ventricular remodeling, such as beta blockers and angiotensin converting enzyme inhibitors after STEMI may reduce rates of IMR.

Limitations

In this observational study, we have baseline information, data on the interventional procedure and outcomes for all patients. However, since this data is gathered from a real-world setting, echocardiographic information is missing for a significant portion of the patients after several months. In fact, <20% have full echocardiographic data at the two time points, after 6 and 12 months. We thus are forced to limit the validity of our conclusions regarding the natural course of IMR over a long period of time for each patient, but convincingly adhere to our conclusions related to the findings at baseline, i.e., the impact of IMR at presentation on outcomes over the course of 20 years. In fact, this is the first study to assess the impact the presence and influence of IMR on outcomes over such a long period of time. While examining the impact of changes in practice over a time span of two decades, we have discovered several key factors for improved outcomes and the risk of IMR. These include a shorter FMC to balloon and LVEF. We also employed propensity matching to correct for differences in time periods. These included all factors related to prognosis. However, it is important to mention that Prasugrel was not available at

TABLE 4 | Multivariate analysis for the risk of IMR.

Parameter	HR	*P*-value
Age	1.034 (0.914–1.363)	0.071
Sex (female)	1.217 (0.888–1.668)	0.222
Diabetes Mellitus	1.356 (0.872–3.561)	0.002
Hypertension	0.894 (0.527–2.556)	0.855
Renal Failure	2.135 (0.923–5.525)	0.120
PAD*	1.241 (0.951–2.213)	0.311
S/P CABG†	1.323 (0.515–1.673)	0.329
Previous PCI‡	0.924 (0.633–1.592)	0.390
FMC§ to Balloon	1.689 (1.038–2.482)	0.040
LVEF‖%	0.830 (0.457–0.942)	0.000
Time period	0.930 (0.629–1.219)	0.079
Drug Eluting Stent	0.841 (0.350–1.432)	0.121
Trans-Radial Access	0.910 (0.492–1.549)	0.231

**PAD, peripheral arterial disease; †CABG, coronary artery bypass graft; ‡PCI, percutaneous coronary intervention; §FMC, first medical contact; ‖LVEF, left ventricular ejection fraction.*

the early time period, but became the most common anti-$P2Y_{12}$ agent in the second period. This was not a factor we could have included in the matching process. Finally, we do not have detailed information on the extent of LV infarction, beyond the extent of cardiac enzymes/biomarkers data. Future studies incorporating data from cardiac magnetic resonance imaging, in particular, may shed more light on the natural course of IMR post STEMI.

CONCLUSIONS

IMR is a common complication following acute STEMI, impacting prognosis, remaining in about half of the patients after 3 months and 15.4% after 12 months among surviving patients. Rates of IMR have declined over the years, mediated by improved rates of early reperfusion, but it remains a significant risk factor for mortality.

DATA AVAILABILITY STATEMENT

The raw data supporting the conclusions of this article will be made available by the authors, without undue reservation.

ETHICS STATEMENT

The studies involving human participants were reviewed and approved by Rabin Medical Center IRB. Written informed consent for participation was not required for this study in accordance with the national legislation and the institutional requirements.

AUTHOR CONTRIBUTIONS

LP and RK: idea conception. LP, TB, HV-A, GG, PC, YS, MV, and AS: data collection. LP and TB: data analysis. LP, YS, and RK: drafting the manuscript. All authors revised the final version and approved it for publication.

REFERENCES

1. Kumanohoso T, Otsuji Y, Yoshifuku S, Matsukida K, Koriyama C, Kisanuki A, et al. Mechanism of higher incidence of ischemic mitral regurgitation in patients with inferior myocardial infarction: quantitative analysis of left ventricular and mitral valve geometry in 103 patients with prior myocardial infarction. *J Thorac Cardiovasc Surg.* (2003) 125:135–13503ac Card1067/mtc.2003.78
2. Bursi F, Enriquez-Sarano M, Nkomo VT, Jacobsen SJ, Weston SA, Meverden RA, et al. Heart failure and death after myocardial infarction in the community: the emerging role of mitral regurgitation. *Circulation.* (2005) 111:295–301. doi: 10.1161/01.CIR.0000151097.30779.04
3. López-Pérez M, Estévez-Loureiro R, López-Sainz A, Couto-Mallón D, Soler-Martin MR, Bouzas-Mosquera A, et al. Long-term prognostic value of mitral regurgitation in patients with ST-segment elevation myocardial infarction treated by primary percutaneous coronary intervention. *Am J Cardiol.* (2014) 113:907–12. doi: 10.1016/j.amjcard.2013.11.050
4. Aronson D, Goldsher N, Zukermann R, Kapeliovich M, Lessick J, Mutlak D, et al. Ischemic mitral regurgitation and risk of heart failure after myocardial infarction. *Arch Intern Med.* (2006) 166:2362–8. doi: 10.1001/archinte.166.21.2362
5. Nishino S, Watanabe N, Kimura T, Enriquez-Sarano M, Nakama T, Furugen M, et al. The course of ischemic mitral regurgitation in acute myocardial infarction after primary percutaneous coronary intervention: from emergency room to long-term follow-up. *Circ Cardiovasc Imaging.* (2016) 9:e004841. doi: 10.1161/CIRCIMAGING.116.004841
6. Mentias A, Raza MQ, Barakat AF, Hill E, Youssef D, Krishnaswamy A, et al. Outcomes of ischaemic mitral regurgitation in anterior versus inferior ST elevation myocardial infarction. *Open Heart.* (2016) 3:e000493. doi: 10.1136/openhrt-2016-000493
7. Lamas GA, Mitchell GF, Flaker GC, Smith SC, Gersh BJ, Basta L, et al. Clinical significance of mitral regurgitation after acute myocardial infarction. Survival and ventricular enlargement investigators. *Circulation.* (1997) 96:827–33. doi: 10.1161/01.CIR.96.3.827
8. Zhang C, Zhao L, Zhu E, Schoenhagen P, Tian J, Lai Y, et al. Predictors of moderate to severe ischemic mitral regurgitation after myocardial infarction: a cardiac magnetic resonance study. *Eur Radiol.* (2021) 31:5650–8. doi: 10.1007/s00330-020-07658-z
9. Kumanohoso T, Otsuji Y, Yoshifuku S, Matsukida K, Koriyama C, Kisanuki A, et al. Mechanism of higher incidence of ischemic mitral regurgitation in patients with inferior myocardial infarction: quantitative analysis of left ventricular and mitral valve geometry in 103 patients with prior myocardial infarction. *J Thorac Cardiovasc Surg.* (2003) 125:135–43. doi: 10.1067/mtc.2003.78
10. Gillinov AM, Wierup PN, Blackstone EH, Bishay ES, Cosgrove DM, White J, et al. Is repair preferable to replacement for ischemic mitral regurgitation? *J Thorac Cardiovasc Surg.* (2001) 122:1125–41. doi: 10.1067/mtc.2001.116557
11. Neumann JT, Goßling A, Sörensen NA, Blankenberg S, Magnussen C, Westermann D. Temporal trends in incidence and outcome of acute coronary syndrome. *Clin Res Cardiol.* (2020) 109:1186–92. doi: 10.1007/s00392-020-01612-1
12. Wang TKM, Grey C, Jiang Y, Jackson RT, Kerr AJ. Nationwide trends in acute coronary syndrome by subtype in New Zealand 2006-2016. *Heart.* (2020) 106:221–7. doi: 10.1136/heartjnl-2019-315655
13. Lauridsen MD, Rørth R, Lindholm MG, Kjaergaard J, Schmidt M, Møller JE, et al. Trends in first-time hospitalization, management, and short-term

mortality in acute myocardial infarction-related cardiogenic shock from 2005 to 2017: a nationwide cohort study. *Am Heart J.* (2020) 229:127–37. doi: 10.1016/j.ahj.2020.08.012
14. Grinberg T, Bental T, Hammer Y, Assali A, Vaknin-Assa H, Kornowski R, et al. Temporal trends of the management and outcome of patients with myocardial infarction according to the risk for recurrent cardiovascular events. *Am J Med.* (2020) 133:839–847.e2. doi: 10.1016/j.amjmed.2019.12.027
15. Sanmartín-Fernández M, Raposeiras-Roubin S, Anguita-Sánchez M, Marín F, Garcia-Marquez M, Fernández-Pérez C, et al. In-hospital outcomes of mechanical complications in acute myocardial infarction: analysis from a nationwide Spanish database. *Cardiol J.* (2020) 28:589–97. doi: 10.5603/CJ.a2020.0181
16. Puerto E, Viana-Tejedor A, Martínez-Sellés M, Domínguez-Pérez L, Moreno G, Martín-Asenjo R, et al. Temporal trends in mechanical complications of acute myocardial infarction in the elderly. *J Am Coll Cardiol.* (2018) 72:959–66. doi: 10.1016/j.jacc.2018.06.031
17. Elbadawi A, Elgendy IY, Mahmoud K, Barakat AF, Mentias A, Mohamed AH, et al. Temporal trends and outcomes of mechanical complications in patients with acute myocardial infarction. *JACC Cardiovasc Interv.* (2019) 12:1825–36. doi: 10.1016/j.jcin.2019.04.039
18. Grigioni F, Enriquez-Sarano M, Zehr KJ, Bailey KR, Tajik AJ. Ischemic mitral regurgitation: long-term outcome and prognostic implications with quantitative Doppler assessment. *Circulation.* (2001) 103:1759–64. doi: 10.1161/01.CIR.103.13.1759
19. Chua S, Hung J, Chung S-Y, Lin Y-C, Fu M, Wu C-J, et al. Primary percutaneous coronary intervention lowers the incidence of ischemic mitral regurgitation in patients with acute ST-elevated myocardial infarction. *Circ J.* (2010) 74:2386–92. doi: 10.1253/circj.CJ-10-0435
20. Perl L, Bental T, Assali A, Vaknin-Assa H, Greenberg G, Witberg G, et al. Temporal trends in the practice of the transradial approach for percutaneous coronary intervention in a large tertiary center. *Coron Artery Dis.* (2020) 31:40–8. doi: 10.1097/MCA.0000000000000764
21. Di Santo P, Simard T, Wells GA, Jung RG, Ramirez FD, Boland P, et al. Transradial versus transfemoral access for percutaneous coronary intervention in ST-segment–elevation myocardial infarction. *Circ Cardiovasc Interv.* (2021) 14:e009994. doi: 10.1161/CIRCINTERVENTIONS.120.009994
22. Jolly SS, Yusuf S, Cairns J, Niemelä K, Xavier D, Widimsky P, et al. Radial versus femoral access for coronary angiography and intervention in patients with acute coronary syndromes (RIVAL): a randomised, parallel group, multicentre trial. *Lancet.* (2011) 377:1409–20. doi: 10.1016/S0140-6736(11)60404-2
23. Romagnoli E, Biondi-Zoccai G, Sciahbasi A, Politi L, Rigattieri S, Pendenza G, et al. Radial versus femoral randomized investigation in ST-segment elevation acute coronary syndrome: the RIFLE-STEACS (Radial Versus Femoral Randomized Investigation in ST-Elevation Acute Coronary Syndrome) study. *J Am Coll Cardiol.* (2012) 60:2481–9. doi: 10.1016/j.jacc.2012.06.017
24. Singh S, Singh M, Grewal N, Khosla S. Transradial vs transfemoral percutaneous coronary intervention in ST-segment elevation myocardial infarction: a systemic review and meta-analysis. *Can J Cardiol.* (2016) 32:777–90. doi: 10.1016/j.cjca.2015.08.019
25. Zhang Q, Qiu J-P, Zhang R-Y, Hu J, Yang Z-K, Ding F-H, et al. Improved outcomes from transradial over transfemoral access in primary percutaneous coronary intervention for patients with acute ST-segment elevation myocardial infarction and upstream use of tirofiban. *Chin Med J.* (2013) 126:1063–8. doi: 10.3760/cma.j.issn.0366-6999.20130037
26. Philip F, Stewart S, Southard JA. Very late stent thrombosis with second generation drug eluting stents compared to bare metal stents: network meta-analysis of randomized primary percutaneous coronary intervention trials. *Catheter Cardiovasc Interv.* (2016) 88:38–48. doi: 10.1002/ccd.26458
27. Kim YH, Her A-Y, Jeong MH, Kim B-K, Hong S-J, Kim J-S, et al. Impact of stent generation on 2-year clinical outcomes in ST-segment elevation myocardial infarction patients with multivessel disease who underwent culprit-only or multivessel percutaneous coronary intervention. *Catheter Cardiovasc Interv.* (2020) 95:E40–55. doi: 10.1002/ccd.28440
28. Sabaté M, Räber L, Heg D, Brugaletta S, Kelbaek H, Cequier A, et al. Comparison of newer-generation drug-eluting with bare-metal stents in patients with acute ST-segment elevation myocardial infarction: a pooled analysis of the EXAMINATION (clinical Evaluation of the Xience-V stent in Acute Myocardial INfArcTION) and COMFORTABLE-AMI (Comparison of Biolimus Eluted From an Erodible Stent Coating With Bare Metal Stents in Acute ST-Elevation Myocardial Infarction) trials. *JACC Cardiovasc Interv.* (2014) 7:55–63. doi: 10.1016/j.jcin.2013.07.012
29. Estévez-Loureiro R, Shuvy M, Taramasso M, Benito-Gonzalez T, Denti P, Arzamendi D, et al. Use of MitraClip for mitral valve repair in patients with acute mitral regurgitation following acute myocardial infarction: effect of cardiogenic shock on outcomes (IREMMI Registry). *Catheter Cardiovasc Interv.* (2021) 97:1259–67. doi: 10.1002/ccd.29552
30. Adamo M, Curello S, Chiari E, Fiorina C, Chizzola G, Magatelli M, et al. Percutaneous edge-to-edge mitral valve repair for the treatment of acute mitral regurgitation complicating myocardial infarction: a single centre experience. *Int J Cardiol.* (2017) 234:53–7. doi: 10.1016/j.ijcard.2017.02.072
31. Haberman D, Estévez-Loureiro R, Benito-Gonzalez T, Denti P, Arzamendi D, Adamo M, et al. Conservative, surgical, and percutaneous treatment for mitral regurgitation shortly after acute myocardial infarction. *Eur Heart J.* (2021) ehab496. doi: 10.1093/eurheartj/ehab496

Conflict of Interest: The authors declare that the research was conducted in the absence of any commercial or financial relationships that could be construed as a potential conflict of interest.

frontiers in Cardiovascular Medicine

ORIGINAL RESEARCH
published: 13 January 2022
doi: 10.3389/fcvm.2021.804565

Characterization of Turbulent Flow Behind a Transcatheter Aortic Valve in Different Implantation Positions

Leonardo Pietrasanta[1]*, *Shaokai Zheng*[1], *Dario De Marinis*[1,2], *David Hasler*[1] and *Dominik Obrist*[1]

[1] ARTORG Center for Biomedical Engineering Research, University of Bern, Bern, Switzerland, [2] Dipartimento di Meccanica Matematica e Management, Centro di Eccellenza in Meccanica Computazionale, Politecnico di Bari, Bari, Italy

The development of turbulence after transcatheter aortic valve (TAV) implantation may have detrimental effects on the long-term performance and durability of the valves. The characterization of turbulent flow generated after TAV implantation can provide fundamental insights to enhance implantation techniques. A self-expandable TAV was tested in a pulse replicator and the three-dimensional flow field was extracted by means of tomographic particle image velocimetry. The valve was fixed inside a silicone phantom mimicking the aortic root and the flow field was studied for two different supra-annular axial positions at peak systole. Fluctuating velocities and turbulent kinetic energy were compared between the two implantations. Velocity spectra were derived at different spatial positions in the turbulent wakes to characterize the turbulent flow. The valve presented similar overall flow topology but approximately 8% higher turbulent intensity in the lower implantation. In this configuration, axial views of the valve revealed smaller opening area and more corrugated leaflets during systole, as well as more accentuated pinwheeling during diastole. The difference arose from a lower degree of expansion of the TAV's stent inside the aortic lumen. These results suggest that the degree of expansion of the TAV *in-situ* is related to the onset of turbulence and that a smaller and less regular opening area might introduce flow instabilities that could be detrimental for the long-term performance of the valve. The present study highlights how implantation mismatches may affect the structure and intensity of the turbulent flow in the aortic root.

Keywords: TAVI, tomographic particle image velocimetry, turbulence, implantation position, pinwheeling, turbulent spectra

OPEN ACCESS

Edited by:
Philippe Sucosky, Kennesaw State University, United States

Reviewed by:
Vrishank Raghav, Auburn University, United States
Diego Gallo, Politecnico di Torino, Italy

***Correspondence:**
Leonardo Pietrasanta
leonardo.pietrasanta@unibe.ch

Specialty section:
This article was submitted to Heart Valve Disease, a section of the journal Frontiers in Cardiovascular Medicine

Received: *29 October 2021*
Accepted: *14 December 2021*
Published: *13 January 2022*

Citation:
Pietrasanta L, Zheng S, De Marinis D, Hasler D and Obrist D (2022) Characterization of Turbulent Flow Behind a Transcatheter Aortic Valve in Different Implantation Positions. Front. Cardiovasc. Med. 8:804565. doi: 10.3389/fcvm.2021.804565

1. INTRODUCTION

Aortic stenosis is the primary valvular disease with increasing prevalence due to an aging population (1, 2). Untreated severe symptomatic aortic stenosis has a fatal prognosis with a mortality rate up to 50% in the first year and higher than 90% after 5 years (3). Transcatheter aortic valve implantation (TAVI) is an established treatment for high-risk patients which are not eligible for surgery. Recently, guidelines were updated and TAVI was introduced as a possible treatment for a larger population which include intermediate-risk patients (4–7). TAVI demonstrated significant survival benefit in the short-term follow ups across the spectrum of intermediate and high-risk patients when compared to the classical surgical valve replacement (SVR) (8, 9). More recent studies based on longer follow ups also showed promising improvements in patients' quality of

life (10) and health status (11). Current debates focus on the expansion of TAVI to patients with low operative risk which have a longer life expectancy (12). Consequently, long-term structural device integrity is an important goal for transcatheter aortic valve (TAV) design. Turbulence might be considered as one of the detrimental phenomena that could affect the long-term performance of TAV and lead over time to clinically adverse events. Turbulent flow is not only directly related to increased transvalvular pressure gradients (13) but also to structural valve deterioration (SVD) caused by excessive stress loads on the valve's leaflets (14, 15). Turbulence could also lead to endothelial lesions and aorta remodeling due to unphysiological wall shear stress (16), as well as thrombus formation due to the activation of platelets (17, 18). The high degree of freedom present during implantation makes TAVs particularly prone to the development of turbulent flows due to potential geometrical mismatches. Even though guidelines are given to practitioners, the final geometrical configuration of the TAV is highly patient-specific due to the specific anatomy and different degree of calcification of the aortic root (19). Different implantation configurations may lead to different degree of turbulent flow. Despite the important role of turbulence there is a lack of understanding of this phenomenon. In theory, direct numerical simulations can resolve the smallest scales of turbulent flow structures providing the information for a full characterization of turbulence. However, the available numerical findings focus on surgical valves (SVs) (13, 20–22) and the ones on TAV are limited and need to be cross-validated with experimental results (23–26). One of the first fluid structure interaction (FSI) simulations on TAV was performed by Mao et al. (23) who investigated the leaflets' kinematics and stress distribution on a simplified TAV model without considering the stent geometry. A comparison between FSI simulation and *in-vitro* measurements of a self-expandable TAV was obtained for an idealized experimental condition by Wu et al. (24), yet the comparison was limited to the quantitative analysis of the TAV's opening area and did not investigate the flow field. A FSI simulation of a CoreValve (*Medtronic Inc, Minneapolis, Minnesota, USA*) in a more realistic geometry was performed by Kandail et al. (25), who considered an anatomically correct aortic arch but focused on the flow patterns in the coronary arteries. More recently, Basri et al. (26) studied the impact of paravalvular leakage using the FSI approach. None of the mentioned works investigated the role of turbulence generated after TAVI. On the other hand, experimental studies are often limited by the measurement technology which often lack sufficient resolution and only allow for one or two-dimensional analysis of turbulent flow (27–30). Therefore, further investigations are needed to better characterize the turbulent three-dimensional flow and its potential effect on the long-term performance of TAVs. To the best of our knowledge, this study is the first experimental investigation that attempts to characterize the turbulent wake generated by a TAV with tomographic particle image velocimetry (Tomo-PIV).

TAVs may block the electrical signal in the atrio-ventricular node or in the left bundle branch due to balloon dilatation or prosthesis implantation. Conduction abnormalities have to be treated with the implantation of pacemakers. Furthermore, TAVs may impair the coronary flow due the displacement of the calcified native cusp over the coronary ostium or due to the TAV's skirt which prevent the blood flow from entering the sinus of Valsalva. As suggested by Yerasi et al. (31) and Ribeiro et al. (32) a higher TAV implantation is related to a higher risk for coronary obstruction. From this perspective, a lower implantation should be preferred. However, Van Rosendael et al. (33) and Mauri et al. (34) reported higher pacemaker implant rate in lower implantations. Indipendent of this important discussion, we will discuss here the effect of the longitudinal positioning and the resulting turbulence for two different implantation heights.

2. METHODS

In-vitro measurements of the three-dimensional flow field in the aortic root generated by a TAV were performed in a validated pulse replicator with a multi-view imaging system for Tomo-PIV (35). The experimental apparatus already used by the authors for studies of surgical heart valve (36) was further adapted for TAV testing.

2.1. Pulse Replicator

The tested TAV was crimped at 0 $^{\circ}C$ and released in a semi-rigid silicone phantom (SP) with an idealized aortic root geometry (**Figure 1**) at 37 $^{\circ}C$. The silicone phantom was characterized by an aortic annulus diameter $D_a = 23\ mm$, three hemispherical bulges mimicking the sinuses of Valsalva and a straight ascending aorta with a diameter of 29 *mm*. More details on the aortic root phantom can be found in **Table 1**. The silicone phantom and the TAV were inserted in the test section of a pulse replicator which reproduced physiological pulsatile flow using a computer-controlled volumetric pump (VP). The motion of the VP's piston was tuned to replicate physiological flow profiles characterized by 1/3 of systolic phase and 2/3 of diastolic phase. A schematic of the operation of the pulse replicator is shown in **Figure 2A** for the systolic phase and in **Figure 2B** for the diastolic phase. During systole, a silicone left ventricle (LV) was compressed by the forward motion of the VP's piston and the fluid was directed toward the test section. After passing through the test section, the fluid reached a sealed compliance chamber (CC) and a tunable resistor (TR) mimicking the arterial compliance and the peripheral resistance of the systemic circulation, respectively. Finally, the fluid was collected in an open chamber exposed to atmospheric pressure simulating the left atrium (LA). During diastole the silicone ventricle was expanded to its original relaxed state by the backward motion of the VP's piston and the fluid was returned from the open chamber to the silicone ventricle. To mimic the function of the mitral valve a mechanical bi-leaflet valve (MV) was installed between the open chamber and the silicone ventricle. Pressure sensors (PSs) were positioned in the left ventricle and in the compliance chamber to estimate the left ventricular pressure and the aortic pressure. A blood analog test fluid with a density of $\rho_f = 1,200\ kg/m^3$ and a kinematic viscosity $\nu = 4.7\ mm^2/s$ at 22 $^{\circ}C$ was used. The test fluid consisted of 49.4 *w*% water, 34 *w*% glycerol (*Dr. Grogg Chemie AG, Deisswil, Switzerland*) and 16.6 *w*% sodium chloride (*Sigma-Aldrich Corporation, St. Louis, MO, USA*) by weight. The test fluid

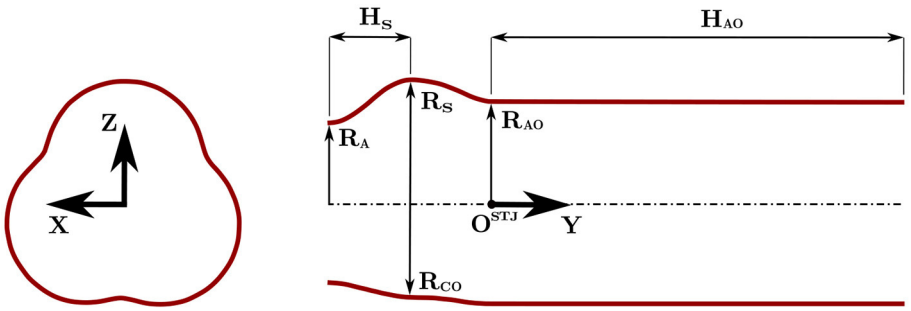

FIGURE 1 | Inner lumen geometry of the silicone phantom mimicking the aortic root with reference to the main geometrical parameters of **Table 1**.

TABLE 1 | Relevant geometrical parameters of the aortic root silicone phantom.

Parameter	Value [*mm*]	Description
H_S	11.6	Sinus half-height
H_{AO}	58.9	Ascending aorta height
R_A	11.5	Aortic annulus radius
R_S	17.6	Sinus radius
R_{CO}	13.1	Commissure radius
R_{AO}	14.5	Ascending aorta radius

had a refraction index similar to the one of silicone to reduce distortion during image acquisition.

2.2. TAV Model

The TAV featured three leaflets made of porcine pericardium sutured onto a self-expandable Nitinol stent frame. The nominal valve prosthesis size was 29 *mm* which is suitable for implantation in aortic roots with an aortic annulus diameter $D = 23 - 26$ *mm* according to manufacturer's recommendation. To ensure the correct axial position, the TAV was positioned over a stopper (ST). The stopper was designed as a tubular structure with the same wall thickness as the valve's stent struts. The lower extremities of the TAV's struts touched the upper end of the stopper avoiding migration toward the ventricle. The TAV was oriented in a "native configuration" with the leaflets facing the sinuses of Valsalva. The axial positioning, or implantation height (IH), was controlled through the stopper such that the lower extremities of the TAV's stent were 10 *mm* distal to the aortic annulus of the silicone phantom ("lower implantation," LI, **Figure 3A**). A second configuration ("upper implantation," UI, **Figure 3B**) 4 *mm* distal to the annulus was considered to span the full range of IH suggested by the manufacturer.

A high-speed camera (*Photron AX 100, Tokyo, Japan*) was used to capture axial top view images of the tested TAV. Valve kinematics was assessed by direct inspection of the axial high speed recordings. The geometric orifice area (*GOA*) was defined by a contour line along the TAV's leaflet tips and was manually selected from the axial images. The projected orifice area (*POA*) was defined as the open area seen by the axial camera and was estimated with the same procedure. The presented results are mean values over five consecutive pulses. The pinwheeling index (*PI*) of Midha et al. (37) was used to quantify localized bending of TAV's leaflets along the coaptation edge during diastole:

$$PI = \frac{L_{actual} - L_{ideal}}{L_{ideal}} \quad (1)$$

where L_{actual} is the length of the coaptation edge and L_{ideal} is the distance between the commisures and the center of the valve. The presented results are mean values of the three coaptation edges. The *PI* of each of the three coaptation edges was evaluated as an average over five consecutive pulses.

2.3. Tomo-PIV Measurement System

Two 8M 12 bit CCD Digital Cameras (*Imager LX, LaVision, Gttingen, Germany*) and a set of mirrors were used to image the aortic root flow domain. The field of view of each camera was split into two images such that four different viewing angles were captured simultaneously with only two cameras. The cameras were equipped with prime lenses with a focal length of $f = 100$ *mm* and a maximum aperture of F2.8 (*Kenko Tokina, Tokyo, Japan*). Each of the four recorded images had a resolution of 1656×2488 pixels. The pixel size was $\Delta_{px} = 5.5\ \mu m$, while the magnification factor M resulting from the focal length f and the object distance $S = 0.7\ m$ was $M = f/(S - f) = 0.167$. The test fluid was seeded with fluorescent PMMA micro particles of mean diameter $D_p = 35\ \mu m$ (density $\rho_p = 1180\ kg/m^3$) with Rhodamin B coating (*Microparticles GmbH, Berlin, Germany*) that has an excitation peak at wavelength $\lambda = 560\ nm$ and emission peak at wavelength $\lambda = 584\ nm$. A dual cavity Nd:YAG laser (*Nano L 200-15 PIV, Litron Systems Ltd, Rugby, UK*) was used to excite the fluorescent particles at $\lambda = 532\ nm$ with a power of 235 *mJ/pulse*. The time width of the laser was set to 7 *ns* and the interframe time between consecutive laser pulses was set to 200 μs. A low-pass filter (570 *nm* cut-off wavelength) in front of the cameras ensured that only the emitted light from the particles was collected by the camera sensors. The side views of the CCD cameras where used to capture the light emitted by the fluorescent particles, as well as to measure the expansion rate of the TAV in the silicon phantom.

The software *DaVis 8.4* (*LaVision GmbH, Gttingen, Germany*) was used for camera calibration, raw image pre-processing,

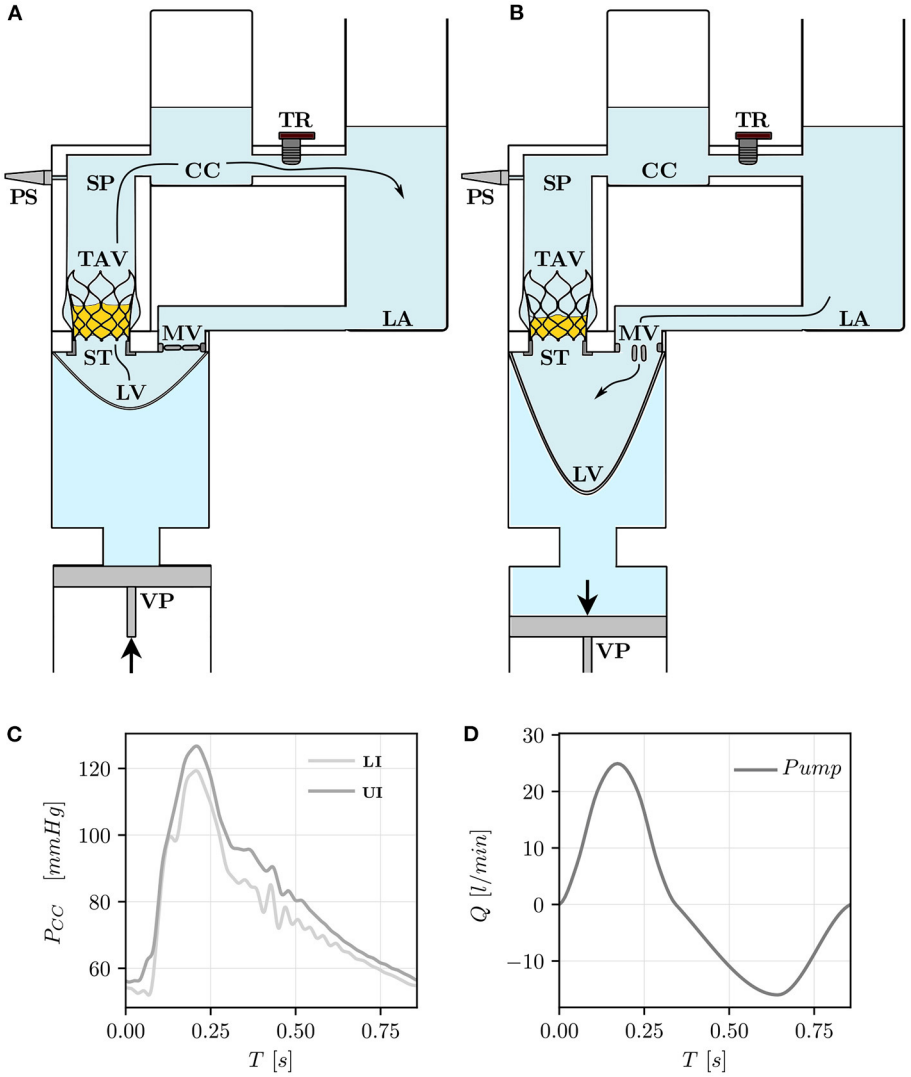

FIGURE 2 | Pulse replicator and its elements during the systolic phase **(A)** and the diastolic phase **(B)**. The pulse replicator is a hydraulic flow loop consisting of the volumetric pump (VP), the left ventricle (LV), the transcatheter aortic valve (TAV), the stopper (ST), the compliance chamber (CC), the tunable resistor (TR), the left atrium (LA), the mitral valve (MV), and the pressure sensors (PSs). Pressure signals in the CC (P_{CC}) are shown in **(C)** for the UI and the LI. The flow rate (Q) prescribed at the outlet of the VP (*Pump*) is shown in **(D)**.

volume reconstruction and for the computation of the 3D instantaneous velocity vector fields with a 3D cross-correlation algorithm (tomographic particle image velocimetry, Tomo-PIV). The resulting 3D instantaneous velocity vector field

$$\boldsymbol{v}(\boldsymbol{x}, t) \quad \text{where} \quad \boldsymbol{v} = [v_x, v_y, v_z] \quad \text{and} \quad \boldsymbol{x} = [x, y, z] \qquad (2)$$

was defined on a Cartesian voxel grid. As shown in **Figure 3**, the origin O_{STJ} of the Cartesian coordinate system was located on the centerline of the aortic root at the height of the sinotubular junction (STJ). Because the TAV leaflets' trailing edge during systole was 3 *mm* below O_{STJ} in the LI and 3 *mm* above O_{STJ} in the UI, two additional coordinates systems were defined to have a correspondence with respect to the valve's trailing edge. Thus, a coordinate system O_{LI} for the LI was placed 3 *mm* below O_{STJ} while a coordinate system O_{UI} for the UI was positioned 3 *mm* above O_{STJ}:

O_{LI} reference system: $\boldsymbol{x}_{LI} = [x, y_{LI}, z]$ where $y_{LI} = y - 3\ mm$;

O_{UI} reference system: $\boldsymbol{x}_{UI} = [x, y_{UI}, z]$ where $y_{UI} = y + 3\ mm$.

A schematic of the main components of the hardware for image acquisition and processing of the experimental apparatus with reference to the measurement Cartesian reference system can be found in **Figure 4**.

The experimental resolution δ was the same in all spatial directions ($\delta_x = \delta_y = \delta_z$) and was estimated from the voxel size ($\Delta_{vx} = \Delta_{px}/M$) and from the dimension of the spherical interrogation volume and overlap set for the last step of the 3D

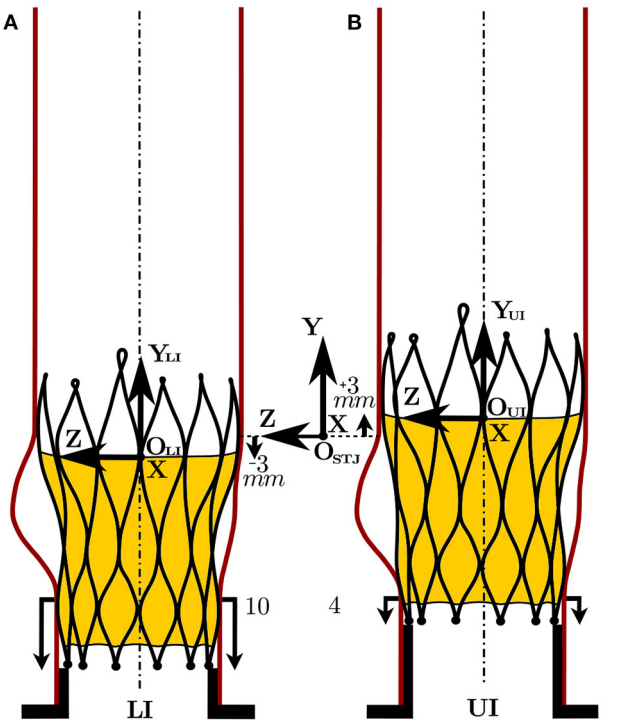

FIGURE 3 | TAV axial positioning in the LI **(A)** and in the UI **(B)** and the relative positioning of the LI (O^{LI}) and the UI (O^{UI}) reference systems with respect to the measurement reference system (O^{STJ}).

cross-correlation routine. The interrogation volume was set to 48 *voxels*, which is equivalent to 1.58 *mm*. With 75% correlation overlap, the final resolution of the velocity field was:

$$\delta = 48 \times (1 - 0.75) \times \Delta_{vx} \approx 0.43\ mm. \tag{3}$$

Further details on Tomo-PIV are given in [1].

2.4. Experimental Protocol

The experiments were performed at room temperature ($\approx 22\,^{\circ}C$) with a heart rate of 70 *bpm* which led to a heart cycle of period $T = 0.86\ s$. **Figures 2C,D** show the hemodynamics boundary conditions (averaged over five consecutive pulses) under which the TAV operated during the measurements. A cardiac output of approximately 5 l/min with $Q_{\max} \approx 25\ l/min$ resulted from the prescribed pump settings. The pressure in the compliance chamber (CC) ranged between 50 and 130 *mmHg* for both implantation configurations. The Reynolds number (Re) and the Womersley number (Wo) at peak flow were:

$$Re = \frac{4Q_{\max}}{D_a \pi \nu} \approx 5000 \quad \text{and} \quad Wo = R_a \sqrt{\frac{2\pi}{T\nu}} \approx 14 \tag{4}$$

where $D_a = 23\ mm$ and $R_a = D_a/2 = 11.5\ mm$ are the diameter and radius of the aortic annulus, respectively.

At this Reynolds number, turbulent flow is expected. N acquisitions of the instantaneous flow field at different phases (ϕ) of the cardiac cycle were performed with a phase-locked approach such that every acquisition was obtained at time $t = t_\phi + nT$ where $n = 1, 2, ..., N$ indicates the repetition number.

The mean velocities $\overline{\boldsymbol{v}}(\boldsymbol{x})$ were computed by *phase-averaging* the instantaneous velocity field such that:

$$\overline{\boldsymbol{v}}(\boldsymbol{x}) = \frac{1}{N} \sum_{n=1}^{N} \boldsymbol{v}(\boldsymbol{x}, t_\phi + nT) \tag{5}$$

where $\bar{\cdot}$ denotes the *phase-averaging* operation over the N repetitions of the experiment. At peak flow phase ($t_{\text{peak}} = 0.17\ s$) $N = 64$ realizations were acquired; $N = 24$ acquisitions were also performed at t_ϕ between $0.05 - 0.17\ s$ with $\Delta t_\phi = 0.01\ s$, and between $0.20 - 0.40\ s$ with an interval $\Delta t_\phi = 0.05\ s$.

2.5. Flow Field Analysis

The overall topology of the flow field in the different phases of the heart cycle was assessed by studying the mean streamwise velocity component $\overline{v}_y$ and the mean velocity magnitude:

$$|\overline{\boldsymbol{v}}| = \sqrt{\overline{v}_x^2 + \overline{v}_y^2 + \overline{v}_z^2}. \tag{6}$$

From the velocity fields $\boldsymbol{v}$, the velocity fluctuations fields $\boldsymbol{v}'$ were computed according to the Reynolds decomposition (38):

$$\boldsymbol{v} = \overline{\boldsymbol{v}} + \boldsymbol{v}' \tag{7}$$

where $'$ indicates the velocity fluctuation. Note that the fluctuations $\boldsymbol{v}'$ may include turbulent fluctuations, as well as pulse-to-pulse fluctuations. The standard deviation σ_i of the velocity fluctuations v_i' was defined as:

$$\sigma_i = \sqrt{\overline{v_i'^2}} \quad \text{with} \quad i = x, y, z; \tag{8}$$

while the root mean square of the velocity fluctuations was computed as:

$$v'_{rms} = \sqrt{\overline{v_x'^2} + \overline{v_y'^2} + \overline{v_z'^2}}. \tag{9}$$

At peak flow, sufficient convergence of the $v'_{rms}(\boldsymbol{x})$ was obtained on the centerline of the flow domain ($\boldsymbol{x} = [0, y, 0]$) already with $N = 50$ repetitions (see **Supplementary Material**).

The mean kinetic energy density $mke(\boldsymbol{x})$ $[J/kg]$ and the turbulent kinetic energy density $tke(\boldsymbol{x})$ $[J/kg]$ were defined as:

$$mke = \frac{1}{2}(\overline{v}_x^2 + \overline{v}_y^2 + \overline{v}_z^2) = \frac{1}{2}\,|\overline{\boldsymbol{v}}|^2 \tag{10}$$

$$tke = \frac{1}{2}(\overline{v_x'^2} + \overline{v_y'^2} + \overline{v_z'^2}) = \frac{1}{2}\,v'^2_{rms}. \tag{11}$$

Integration over the volume V yielded the total mean kinetic energy MKE $[J]$ and the total turbulent kinetic energy TKE $[J]$:

$$MKE = \rho \int_{\mathrm{V}} mke\ d\mathrm{v} \tag{12}$$

$$TKE = \rho \int_{\mathrm{V}} tke\ d\mathrm{v}. \tag{13}$$

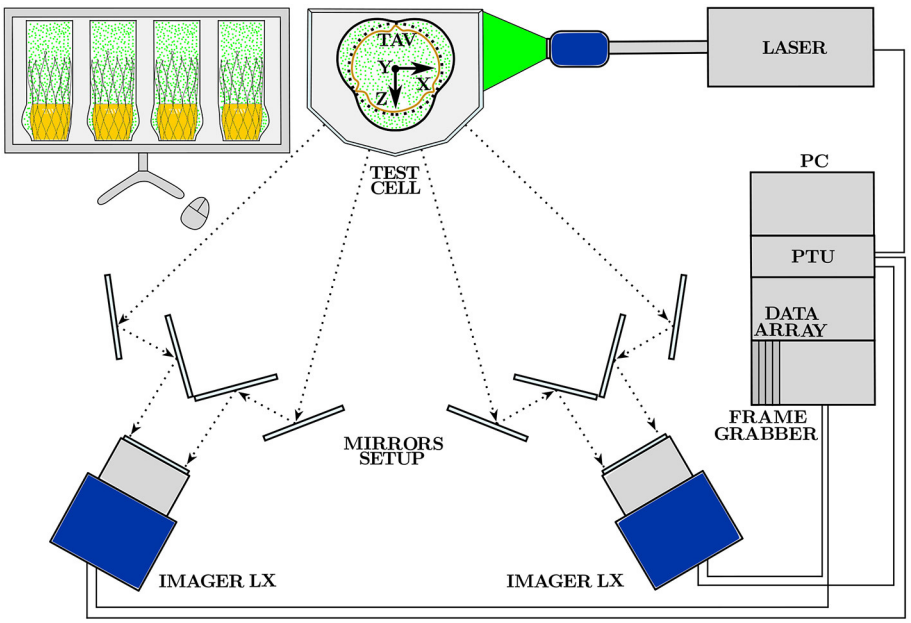

FIGURE 4 | Scheme of the Tomo-PIV hardware together with the measurement reference system. The main components for image acquisition are: two CCD Digital Camera, a set of mirrors and a dual cavity Nd:YAG laser with optics for volumetric illumination. Image storage and processing is performed with the software *DaVis 8.4* installed on the PC workstation.

The turbulence intensity (*TI* [%]) was estimated as the ratio of *TKE*/*MKE*.

A pointwise auto-covariance $\Gamma_{ii}(\boldsymbol{l})$ between fluctuations at different locations separated by a distance $\boldsymbol{l}$ was computed according to:

$$\Gamma_{ii}(\boldsymbol{l};\boldsymbol{x},t_\phi)=\overline{v_i'(\boldsymbol{x}+\boldsymbol{l},t_\phi)v_i'(\boldsymbol{x},t_\phi)}\quad\text{with}\quad\boldsymbol{l}=[l_x,l_y,l_z]. \tag{14}$$

The turbulent velocity spectrum $E_{ii}(\boldsymbol{k})$ was computed according to the Wiener-Khinchin theorem:

$$E_{ii}(\boldsymbol{k};\boldsymbol{x},t_\phi)=\frac{1}{2\pi}\int_{-\infty}^{+\infty}e^{-i\boldsymbol{k}\boldsymbol{l}}\Gamma_{ii}(\boldsymbol{l};\boldsymbol{x},t_\phi)d\boldsymbol{l}\quad\text{with}\quad\boldsymbol{k}=[k_x,k_y,k_z] \tag{15}$$

where $\boldsymbol{k}$ represents the wavenumber.

The energy dissipation rate ϵ was calculated from the rate of strain tensor of the velocity fluctuations as:

$$\epsilon=2\nu\overline{\sum_{ij}S_{ij}^2} \tag{16}$$

where S_{ij} is the symmetric component of the velocity fluctuation gradient tensor:

$$S_{ij}=\frac{1}{2}\left(\frac{\partial v_i'}{\partial x_j}+\frac{\partial v_j'}{\partial x_i}\right)\quad\text{with}\quad i=x,y,z\quad\text{and}\quad j=x,y,z. \tag{17}$$

Local isotropy and homogeneity was assumed to compute the Kolmogorov length scale η from the energy dissipation rate ϵ as:

$$\eta=\left(\frac{\nu^3}{\epsilon}\right)^{\frac{1}{4}}. \tag{18}$$

Finally, the integral length scale I_{ii} was estimated as:

$$I_{ii}(\boldsymbol{l})=\int_L R_{ii}(\boldsymbol{l})d\boldsymbol{l} \tag{19}$$

where L represents the maximum correlation distance along direction $\boldsymbol{l}$ and $R_{ii}(\boldsymbol{l})$ is the pointwise auto-covariance normalized with the standard deviations of the velocity fluctuations $\sigma_i(\boldsymbol{x})$:

$$R_{ii}(\boldsymbol{l};\boldsymbol{x},t_\phi)=\frac{\Gamma_{ii}(\boldsymbol{l};\boldsymbol{x},t_\phi)}{\sigma_i(\boldsymbol{x}+\boldsymbol{l})\sigma_i(\boldsymbol{x})}=\frac{\overline{v_i'(\boldsymbol{x}+\boldsymbol{l})v_i'(\boldsymbol{x})}}{\sqrt{\overline{v_i'(\boldsymbol{x}+\boldsymbol{l})^2}}\sqrt{\overline{v_i'(\boldsymbol{x})^2}}}. \tag{20}$$

3. RESULTS

3.1. TAV Characteristics

Valve opening and closing times were estimated as an average over five consecutive pulses from direct inspection of the recorded axial view. In the LI, the valve started opening at $t_\phi = 0.06\ s$ with respect to the beginning of the forward motion of the piston pump and was fully open at $t_\phi = 0.11\ s$. Valve closure started at $t_\phi = 0.24\ s$ and was completed at $t_\phi = 0.41\ s$. The resulting opening and closing time was 0.05 *s* and 0.17 *s*, respectively. In the UI the valve opened slightly earlier at $t_\phi = 0.05\ s$ but showed otherwise the same opening and

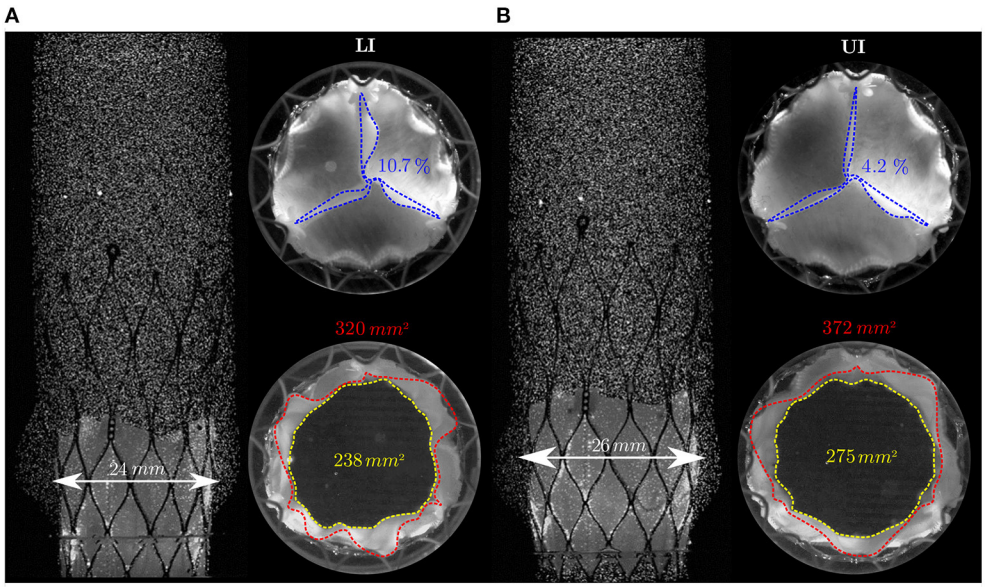

FIGURE 5 | Side and axial views of the TAV in the LI **(A)** and in UI **(B)**. The top views show the TAV at peak flow ($t_\phi = 0.17\ s$) and at the end of the diastole ($t_\phi = 0.86\ s$). The side view shows the TAV at peak flow. Red dashed lines highlight the TAV's leaflets tips during systole (*GOA*) while blue lines highlight the TAV's leaflets tips during diastole (*PI*). The *POA* is highlighted by yellow dashed lines. The white arrows denote the TAV's degree of expansion in the aortic root silicone phantom at the level of the sinus portion.

closing kinematics. The IH had an effect on the TAV expansion (**Figure 5**). At the level of the sinus of Valsalva, the TAV's stent struts in the LI expanded to a diameter of 24 *mm*, whereas they expanded to 26 *mm* in the UI. Consequently, the *GOA* in the UI ($GOA_{\mathrm{UI}} = 372\ mm^2$) was 14% larger than the the *GOA* in the LI ($GOA_{\mathrm{LI}} = 320\ mm^2$). A difference of 13.5% was observed from the POAs as well ($POA_{\mathrm{UI}} = 275\ mm^2, POA_{\mathrm{LI}} = 238\ mm^2$). The different opening areas affected the Reynolds number of the flow fields downstream the TAV in the two implantation configuration. Local Reynolds numbers were estimated close to the leaflets' leading edge at peak systole for both IH as:

$$Re_{\mathrm{LI}} = \frac{4Q_{\max}}{D_{\mathrm{LI}}^{GOA}\pi\nu} \approx 5600 \qquad Re_{\mathrm{UI}} = \frac{4Q_{\max}}{D_{\mathrm{UI}}^{GOA}\pi\nu} \approx 5200 \quad (21)$$

where $D_{\mathrm{LI}}^{GOA} = 20.2\ mm$ and $D_{\mathrm{UI}}^{GOA} = 21.8\ mm$ are diameters computed from circular openings with equivalent areas of GOA_{LI} and GOA_{UI}, respectively. Moreover, the TAV in LI showed corrugated and unevenly opened leaflets during systole and accentuated pinwheeling ($PI_{\mathrm{LI}} = 10.7\%$). Whereas, in UI, it had a more regular orifice area and less pinwheeling ($PI_{\mathrm{UI}} = 4.2\ \%$). The reported characteristics are summarized in **Table 2**.

3.2. Flow Characteristics

The streamwise velocity component $\overline{v}_y$, the velocity fluctuations v'_{rms} , the turbulent kinetic energy density *tke*, the turbulent velocity spectra together with the Kolmogorov and the integral scales are presented in this section for the peak flow phase ($t_\phi = 0.17\ s$).

TABLE 2 | Geometrical features of the expanded TAV's leaflet (*POA*, *GOA*, *PI*), estimated Reynolds number (*Re*) at leaflet tips and integral quantities in the front half of the flow domain (*MKE*, *TKE* and *TI* = *TKE*/*MKE* for $z > 0$).

	***POA* [mm^2]**	***GOA* [mm^2]**	***PI* [%]**	***Re***	***MKE* [*mJ*]**	***TKE* [*mJ*]**	***TI* [%]**
LI	238	320	10.7	5600	5.1	1.0	19.6
UI	275	372	4.4	5200	4.4	0.5	11.4

3.2.1. Mean Streamwise Velocity

The flow field in the aortic root was characterized by the presence of a confined forward core jet and regions of slow retrograde flow close to the aortic walls. In **Figure 6**, isocontour lines with $\overline{v}_y = 0.5\ m/s$ show a triangular cross-section of the core jet at 10 *mm* distal to the TAV for both IH (note that in **Figures 6**, **7**, some data in UI is not shown due to poor quality of the raw PIV data in this region). In both configurations the core jet attached to the aortic walls at $y \approx 25\ mm$. Compared to the LI, the core jet in the UI was wider and slower.

The retrograde flow regions are highlighted by $-0.2\ m/s$ contour lines in **Figure 6** and are located between the core jet and the aortic walls in correspondence to the leaflet commissures. Between the core jet and the retrograde flow, shear layers with high velocity gradients were present.

3.2.2. Velocity Fluctuations

Figure 7 shows v'_{rms} values which illustrate the turbulent nature of the flow field in the aortic root. Low v'_{rms} values characterized the flow in the core jet but high velocity fluctuations were found

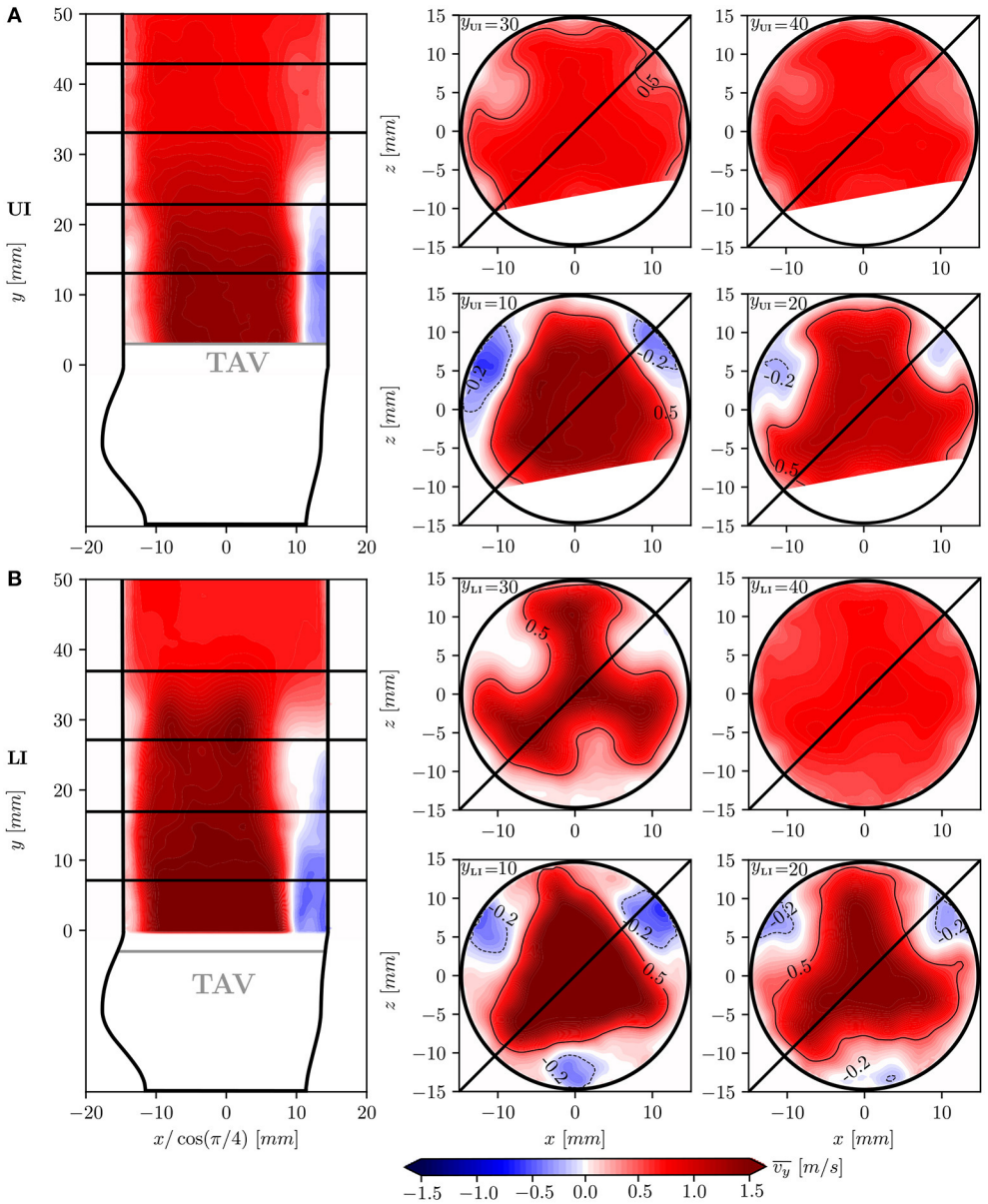

FIGURE 6 | Mean streawise velocity $\overline{v}_y$ in different cross-sections of the flow-domain: longitudinal plane at 45° together with transversal planes at $y_{LI} = y_{UI} = 10, 20, 30, 40\ mm$ for the UI **(A)** and for the LI **(B)**. The core jet is highlighted by contour lines which include $\overline{v}_y$ values higher than 0.5 m/s. High v'_{rms} values were found close to the aortic wall for the UI due to measurement artifacts. This portion of the flow domain was therefore discarded for subsequent analysis.

in the shear layers. Isocontour lines of $v'_{rms} = 0.3\ m/s$ enclose the turbulent regions with high velocity fluctuations. In the LI, the turbulent shear layer thickness increased in downstream direction, such that the potential core of the central jet closed at a distance of 30 mm from the TAV ($y_{LI} = 30\ mm$). In the UI, the shear layers were less pronounced and disappeared downstream of $y_{UI} = 25\ mm$.

3.2.3. Turbulent Kinetic Energy

The spatial arrangement of turbulent flow described for v'_{rms} can also be appreciated from the *tke* in **Figure 8**. In the turbulent shear layers the energy density is in the range of $0.1 - 0.3\ [J/kg]$ but local peak values of $0.5\ [J/kg]$ were found. **Table 2** reports the *MKE* and the *TKE* obtained by integrating the *mke* and the *tke* over the front half of the flow domain ($z > 0$) which excludes the region of low quality PIV data in the UI. For LI, *MKE* was 14% higher than in UI, and *TKE* was even 100% higher. The TI was 19.6% in the LI and 11.4% in UI.

3.2.4. Turbulent Velocity Spectrum

The one-dimensional spectra E_{yy} along wavenumber k_x at different positions distal to the TAV (**Figure 9**) show the energy

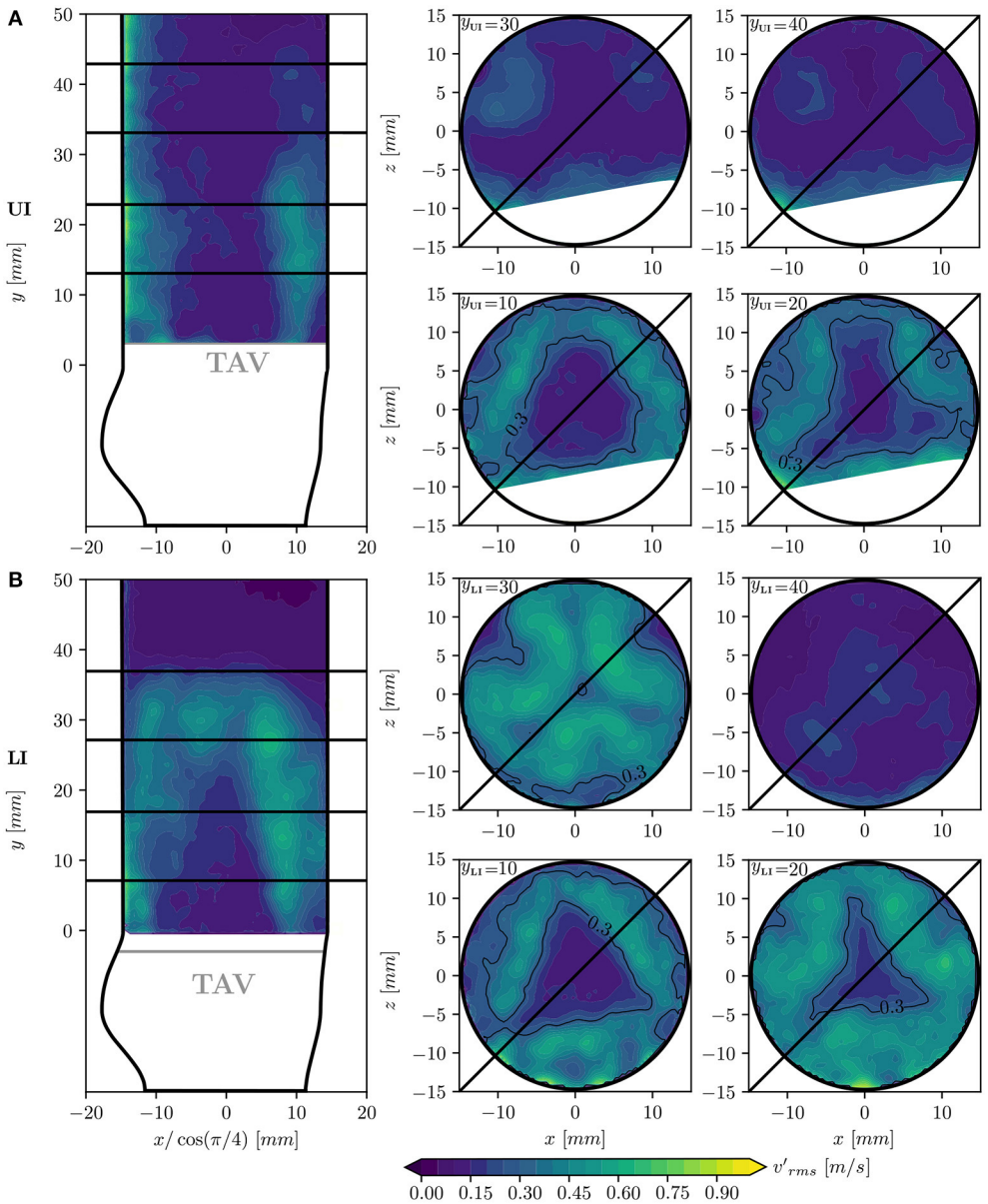

FIGURE 7 | Root mean square of velocity fluctuations v'_{rms} in different cross-sections of the flow-domain: longitudinal plane at 45° together with transversal planes at $y_{LI} = y_{UI} = 10, 20, 30, 40\ mm$ for the UI **(A)** and for the LI **(B)**. Shear layers are highlighted by contour lines which include v'_{rms} values higher than 0.3 m/s. High v'_{rms} values were found close to the aortic wall for the UI due to measurement artifacts. This portion of the flow domain was therefore discarded for subsequent analysis.

content of turbulent structures with different transversal length scales and are limited at large wavenumbers by the experimental resolution ($k_{max} = 2\pi/2\delta$) and at small wavenumbers by the diameter of the aortic root ($k_{min} = 2\pi/D_{ao}$). In the LI, the spectra show similarities with a $-5/3$ power-law and the spectral energy increases moving away from the TAV until $y_{LI} = 30\ mm$. Further downstream, at $y_{LI} = 40\ mm$, the spectral energy decays. In the UI, the spectra have a lower energy content. In **Figure 10** the one-dimensional spectra E_{yy} along wavenumber k_y show the energy content of turbulent structures at a distance of 10 mm from the valve trailing edge ($y_{LI} = y_{UI} = 10\ mm$) but at different transversal x-locations. They are limited at small wavenumbers by the length of the aortic root ($k_{min} = 2\pi/L_{ao}$). In the LI, the spectral energy increases moving from the center of the flow domain toward the aortic walls. The point $\boldsymbol{x}_{LI} = [10, 10, 0]\ mm$ is in the turbulent shear layer and the spectrum adheres to the -5/3 power-law for a wide range of wavenumbers k_y. Closer to the wall, at $\boldsymbol{x}_{LI} = [13, 10, 0]\ mm$, the spectral energy decreases. In UI, the turbulent energy is generally lower and only the points close to the wall ($\boldsymbol{x}_{UI} = [10, 10, 0]\ mm$, $\boldsymbol{x}_{UI} = [13, 10, 0]\ mm$)

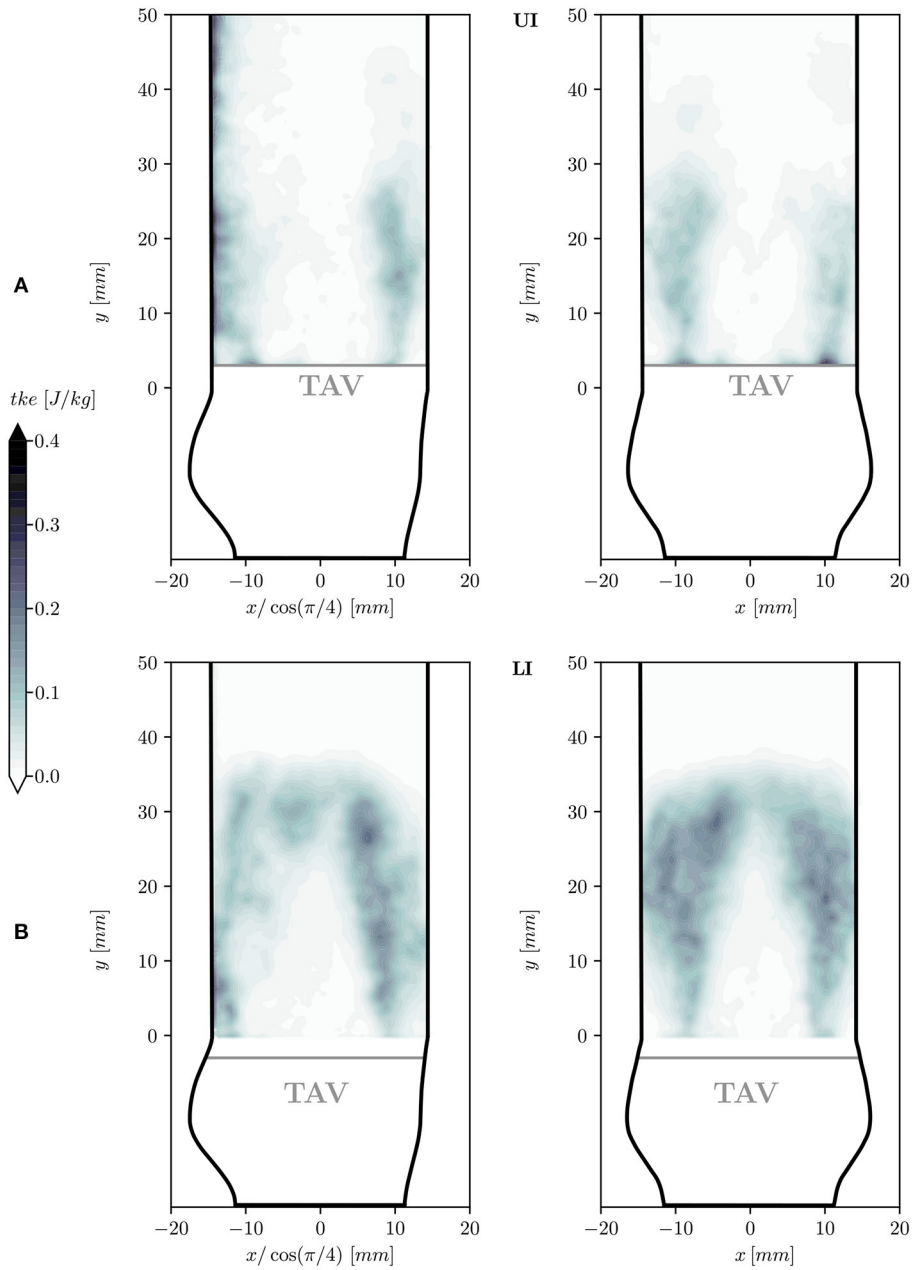

FIGURE 8 | Turbulent kinetic energy density *tke* in two longitudinal planes at 45° (left) and 0° (right) for the UI **(A)** and for the LI **(B)**.

show similarity with the -5/3 power-law for a small range of wavenumbers. The peaks in turbulent energy in the large wavenumbers should be interpreted as measurement artifacts.

3.2.5. Length Scales

The Kolmogorov scale η was calculated at $y_{\mathrm{LI}} = y_{\mathrm{UI}} = 10\ mm$ and $z = 0$ for $x = 0, 5, 10, 13\ mm$ (**Table 3**). It shows a decreasing size of the smallest turbulent structures moving from the center toward the aortic walls for both IH. The minimum values of η were found in the shear layer. The integral scales $I_{yy}(l_y)$ estimated in the same locations show a similar trend for large turbulent structures (**Table 3**).

4. DISCUSSION

4.1. TAV Expansion

The stopper controlled the longitudinal positioning of the TAV while the degree of expansion of the TAV was limited at the lower stent extremity by the aortic annulus and at the upper stent extremity by the aortic lumen. The interaction

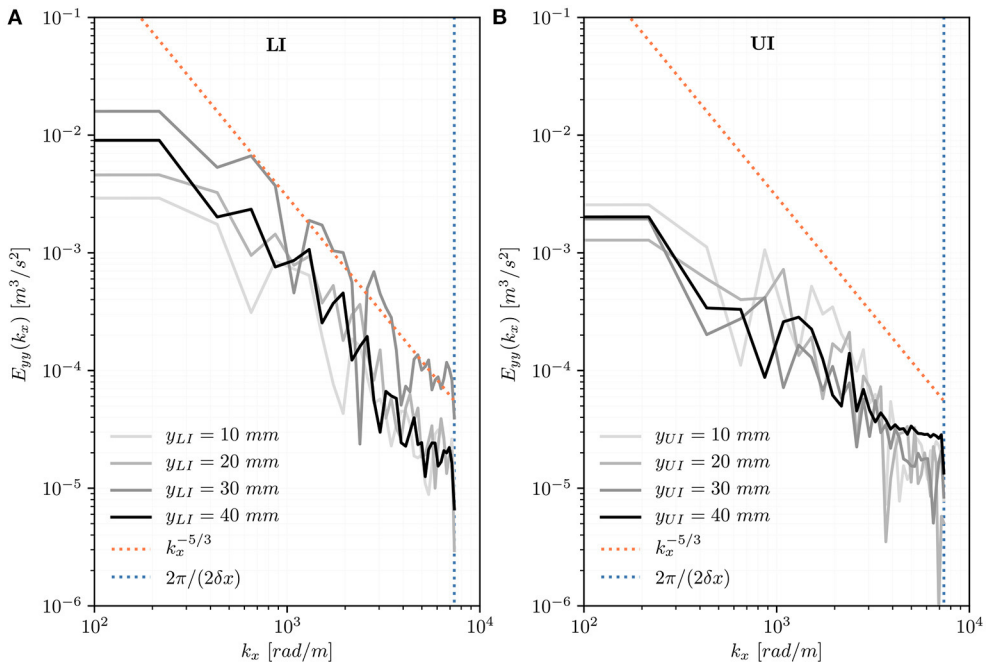

FIGURE 9 | Turbulent velocity spectra $E_{yy}(k_x)$ for points located at increasing distance from the valve ($y_{LI} = y_{UI} = 10, 20, 30, 40\ mm$) on the centerline of the flow domain ($x = z = 0\ mm$) for the LI **(A)** and for the UI **(B)**.

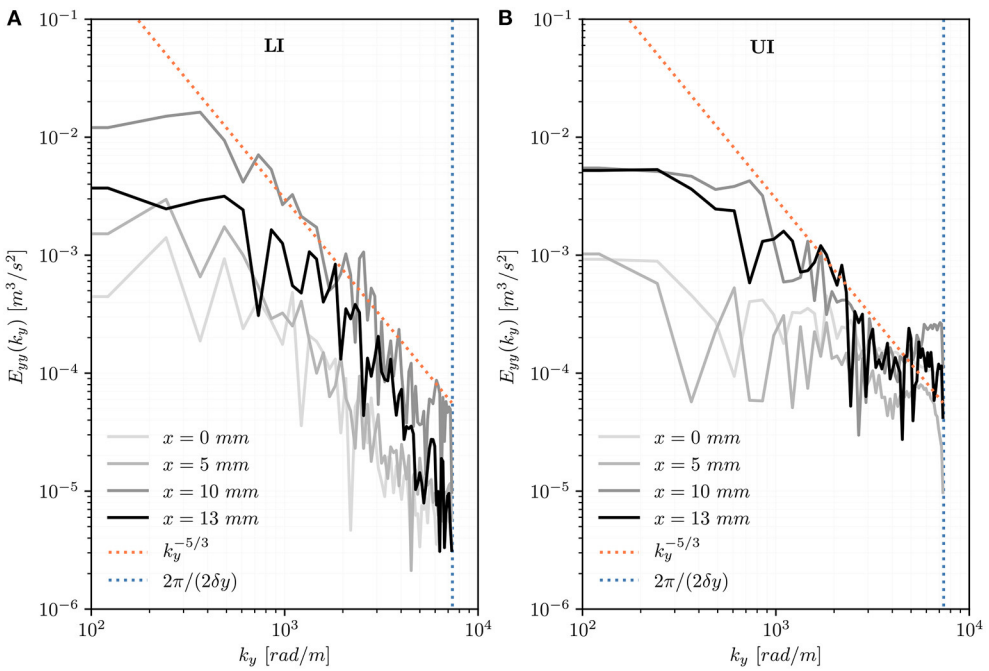

FIGURE 10 | Turbulent velocity spectra $E_{yy}(k_y)$ for points at different transversal locations ($x = 0, 5, 10, 13\ mm$) on the center plane ($z = 0\ mm$) at a distance of 10 *mm* from the valve's trailing edge ($y_{LI} = y_{UI} = 10\ mm$) for the LI **(A)** and for the UI **(B)**.

between the lower extremity of the TAV's stent and the aortic annulus ultimately determined the degree of expansion of the TAV. From visual inspection, the TAV's stent was not fully expanded in the 23 *mm* annulus of the aortic root phantom for neither IH. During systole, the valve presented unevenly opened leaflets while during diastole pinwheeling was observed. These characteristics suggest that the TAV was over-constrained although the size of the annulus was within the recommended

TABLE 3 | Kolmogorov η and integral length scales l_{yy} estimated at 10 *mm* distance from the TAV's trailing edge at $x = 0, 5, 10, 13$ *mm* and $z = 0$ *mm* for both IH.

x :	0 *mm*	5 *mm*	10 *mm*	13 *mm*
η_{LI} [μm]	142	174	83	98
η_{UI} [μm]	141	163	85	89
l_{yyLI} [mm]	11.08	9.82	3.17	3.03
l_{yyUI} [mm]	10.10	6.74	3.05	7.80

range for this valve. A similar leaflet configuration was oberved by Luraghi et al. (39) after performing FSI simulation with an high fidelity CoreValve Evolute R (*Medtronic Inc, Minneapolis, Minnesota, USA*) model in a patient-specific domain including aortic root and calcifications reconstructed from computed tomography images.

Moreover, different degrees of expansion of the TAV were observed between the upper and lower implantation due to the different anchoring surfaces at the annulus. In the UI, the anchoring surface was smaller, allowing the TAV to reach a higher degree of expansion at the level of the sinus portions. This led to a larger *GOA* and *POA* during the systolic phase and a less prominent pinwheeling (*PI*) during diastole compared to the LI (**Figure 5**).

These differences in TAV expansion (and all the effects that follow from this) are a result of the specific configuration of this experiment with an idealized aortic root geometry. Therefore, it would not be fair to conclude that a more distal IH generally leads to a higher degree of expansion (and possibly a less turbulent flow). However, the observed differences, which were induced in this experiment by modifying the IH, could arise in reality from a variety of implantation mismatches due to the high degree of freedom of implantation procedure and due to the variability between patients aortic root geometries and degree of calcification. Moreover, an incomplete stent expansion of $10 - 15\%$ is commonly considered acceptable in clinical practice (40). Therefore, incomplete TAV expansion with corrugated leaflets and reduced orifice area (as seen in the LI configuration) could be a common outcome of TAVI if the valve is not optimally positioned.

4.2. Flow Characteristics

4.2.1. Turbulent Kinetic Energy

The mean systolic flow field in the aortic root was characterized by the presence of a fast antegrade central jet and a slow retrograde flow close to the aortic walls (**Figure 6**). This overall flow topology has already been documented for surgical bioprosthetic valves (36). The antegrade and retrograde flow domains were separated by shear layers where the velocity fluctuations were predominant and showed high levels of *tke* (**Figure 8**). In the LI these turbulent shear layers converged and created a more homogeneous turbulent region at $y_{LI} = 30$ *mm*. In contrast, the turbulent shear layers in the UI were less pronounced and remained confined between the core jet and the aortic walls. This was connected to higher levels of turbulence in the LI for which *TKE* was twice as high as in UI. Likewise the turbulence intensity was higher for LI (19.6%) than for UI (11.4%).

We attribute these differences to the reduced stent expansion and the more marked leaflet corrugation in LI, because it constrained the jet to a smaller opening area with higher velocities and a higher Reynolds number in the central jet. Furthermore, the corrugated shape of the leaflets trailing edge represented an obstacle for the forward motion of the fluid and likely triggered instabilities which contributed to the onset of turbulence.

The increased turbulent flow generated in the LI could potentially have a negative effect on the durability of the valve. Moreover, fluttering of the leaflets was observed from the axial high speed recordings in both implantation configurations. This fluttering was similar to one found for surgical valves in experimental and numerical studies (13, 41) and may further compromise the TAVs long-term performance (42).

Hatoum et al. (29) performed 2D particle image velocimetry measurement of an annular (*SAPIEN 3 26-mm, Edwards Lifesciences*) and a supra-annular (*Evolut 26-mm, Medtronic*) TAV in different types of silicone phantoms: the supra-annular TAV showed consistently higher levels of *tke*. Similarly to what was observed in the present study, Hatoum et al. found turbulent wakes of different intensity which impinged on the aortic walls. At peak systole, Hatoum et al. reported peak *tke* values of $0.59\ J/kg$, which are similar to the peak values of $0.5\ J/kg$ found in the present study. Hatoum et al. concluded that efforts are needed to investigate the intrinsically three-dimensional nature of turbulence. The present work corroborate the findings of Hatoum et al., showing that turbulent flow develops during the systolic phase after TAVI and that turbulent wakes impinge the aortic walls, posing a risk for the endothelial cells that might be exposed to unphysiological stress loading (16).

Gülan et al. (43) tested two TAVs (*Strait Access Technologies, Cape Town, South Africa*) inside an anatomically shaped silicone phantom featuring the aortic arch. The velocity field was extracted with 3D particle tracking velocimetry (3D PTV) and a spatially averaged turbulent kinetic energy of $0.02 - 0.03\ J/kg$ during the systolic phase was found. This corresponds well to values in the present study of $0.03 - 0.04\ J/kg$ (UI) and $0.06 - 0.07\ J/kg$ (LI). Differences between experimental results may be attributed to the different valves, implantation positions, aortic root geometries and dimensions of regions of interests.

Recently, Bessa et al. (44) studied with stereoscopic particle image velocimetry the effect of tilting the aortic valve in the aortic root annulus. The influence of the inlet flow orientation was assessed also by considering the spatial distribution of the *tke* in the aortic root. In their study, G.M. Bessa et al. found that the maximum values of *tke* were distributed along the inlet jet boundary as described in the present work.

Finally, we compare our results with a recent computational investigation by Manchester et al. (45) who conducted large eddy simulations (LES) in a patient specific dilated ascending aorta with aortic valve stenosis and investigated the effect of turbulence in relation with energy losses and wall shear stresses. In their study, they recognize the high velocity jet entering the dilated

ascending aorta as one of the primary sources of turbulence production. Similarly to the present work, turbulent flow was concentrated in the shear layers surrounding the high velocity jet. Manchester et al. underlined that the turbulence production was further amplified by the dilated aortic root which provided space for turbulence to develop. This numerical evidence agrees with the results of the present study, where the higher level of turbulence in the LI was associated with a faster and narrower central jet which left more room for the turbulent shear layers to develop between the jet and the wall.

4.2.2. Length Scales and Spectra

Quinlan and Dooley (46) pointed out that the energy spectrum of turbulence must be considered as a whole when the effect of turbulence on biological structures is investigated. In the LI, the turbulent velocity spectra $E_{yy}(k_x)$ on the centerline showed increasing spectral energy in downstream direction until $y_{\mathrm{LI}} = 30\ mm$ (**Figure 9**). In the UI, no such trend could be observed and the spectra had lower energy than in the LI. In both IH, the spectra adhered reasonably well to the -5/3 spectrum suggesting the presence of a Kolmogorov-type energy cascade. Close to the leaflets' trailing edge ($y_{\mathrm{LI}} = y_{\mathrm{UI}} = 10\ mm$) the spectra showed a more differentiated situation (**Figure 10**): In the UI, the $k^{-5/3}$ behavior could only be observed within the shear layers for a small window of wavenumbers. Close to the centerline, the UI spectra did not exhibit a $-5/3$ slope. In the LI, all spectra showed a $-5/3$ slope. Their energy levels and the size of the inertial ranges increased from the center ($x = 0\ mm$) toward the shear layer ($x = 10\ mm$). For $x = 13\ mm$, the energy levels decreased probably due to the effect of the aortic wall. This quantitative evidence highlights the presence of well-developed turbulent flow mostly confined in the (growing) shear layers and it corroborates the earlier observation that LI leads to significantly higher levels of turbulence. The spectra agree reasonably well with the spectra presented by Becsek et al. (13) who studied a surgical bioprosthetic valve using a computational model. The quantitative agreement is best for the LI, whereas the UI shows lower energy levels than the data of Becsek et al.

The limited resolution of the experimental method can be interpreted as a low pass filter which affects the calculation of velocity gradients. Therefore, the energy dissipation might be underestimated and as a consequence the Kolmogorov scale may be overestimated. Nevertheless, the computed Kolmogorov scales (**Table 3**) are similar to those reported in previous experimental studies (27, 28). Lie et al. (28) conducted *in-vitro* tests on three clinically used bileaflet heart valves (*St. Jude Medical, CarboMedics and Edwards Tekna*) with 2D laser doppler anemometry. Performing the experiment at $Re = 12,000$ and applying the Taylor frozen eddy hypothesis they obtained the smallest length scale in the range of $20 - 70\ \mu m$. Li et al. (27) tested a St. Jude Medical valve with 2D particle image velocimetry and accounted for the limited resolution through a sub-grid scale model. They obtained a Kolmogorov scale of 75 μm at peak flow ($Re = 7500$). It must be noted, however, that both studies focused on mechanical valves at higher Reynolds numbers. In such conditions, the aortic flow is potentially more turbulent and the resulting Kolmogorov scale smaller.

4.3. Limitations

As indicated by Raghav et al. (47) it is important to estimate the uncertainty related to the measured quantities. To this end, the uncertainty of the mean streamwise velocity $U_{\overline{v}_y}(\boldsymbol{x})$ and the uncertainty of the turbulent kinetic energy density $U_{tke}(\boldsymbol{x})$ were computed according to Sciacchitano and Wieneke (48). Spatially averaging the normalized values of uncertainty an $U_{\overline{v}_y} < 1\%$ and an $U_{tke} < 11\%$ were found for both implantation configurations (see **Supplementary Material**).

The final TAV's configuration and stent expansion are strongly affected by the rigidity of the phantom annulus which limited the expansion of the TAV's stent. However, it must also be taken into account that during implantation, practitioners do not remove the calcified native leaflets which may introduce a similar rigid mechanical obstacle to the radial expansion of the TAV. Another limitation was the absence of the aortic arch which might have affected the impingement location of the turbulent wake in the aorta. Nevertheless, the turbulent wake was observed in the first part of the aortic root (within a distance of $2 - 3$ aortic diameters from the aortic annulus) where the effect of secondary flows generated by the curvature could be considered small. Furthermore, the experiments were performed at room temperature and not at human body temperature, potentially weakening the anchoring radial forces and reducing the final expansion state of the TAV. To mitigate this effect the silicone phantom together with the TAV were immersed for 5 minutes in water at 37° before integrating them in the pulse replicator.

The different implantation positions (LI, UI) were chosen *ad hoc* and the resulting effects on TAV expansion could be considered artificial. Therefore, we would like to emphasize again that this study did not intend to evaluate the clinical outcome of different implantation positions. The two configurations were chosen to highlight that small differences in implantation positions may lead to implantation mismatches resulting in significant changes in the turbulent flow behind TAV.

Finally, the effect of the limited experimental resolution on the estimation of the Kolmogorov scale was quantified assuming isotropy and homogeneity of turbulence and resulted to be approximately 5% in the LI and 20% in the UI (see **Supplementary Material**).

5. CONCLUSION

The present experimental study characterized the turbulent flow behind a self-expendable TAV. The valve was implanted in a semi-rigid silicone phantom mimicking the aortic root geometry in two different supra-annular configurations: a lower implantation position (LI) and an upper implantation position (UI). The TAV was tested in an experimental apparatus including a pulse replicator and hardware for image acquisition and processing. The three-dimensional flow field was extracted in the aortic root by means of Tomo-PIV at different phases of the cardiac cycle. The valve presented similar overall flow topology but different levels of turbulence in the two different implantation configurations. In the lower implantation the TAV showed approximately 8% higher turbulent kinetic energy. In

both configurations, turbulent flow was strongest in the shear layers surrounding the central jet. These turbulent shear layers impinged the aortic wall indicating that valve turbulence might play a detrimental role in the endothelial cell turnover. The turbulent energy content was presented by turbulent velocity spectra comprising well developed inertial ranges with $-5/3$ power-law decay. This illustrated the turbulent nature of the shear layers and the higher degree of turbulence of the TAV in the lower position. Axial views of the valve showed a smaller opening area with more corrugated leaflets during systole, as well as a more accentuated pinwheeling during diastole in the lower implantation position due to a reduced expansion of the TAV's stent in the aortic root. This suggested that the uneven opening of the leaflets and the resulting irregular orifice area amplified the onset of turbulence in the lower implantation position.

The present study highlights how implantation mismatches, which can be common in TAVI, may affect the structure and intensity of the turbulent flow in the aortic root. Leaflet corrugation during systole and pinwheeling during diastole could be considered as kinematic indicators for the presence of intensified turbulent flows that could contribute to the TAV's structural deterioration. Therefore, careful implantation planning by the heart team should also consider the patient-specific aortic root geometry and calcification degree which may lead to uneven or incomplete TAV expansion.

DATA AVAILABILITY STATEMENT

The raw data supporting the conclusions of this article will be made available by the authors, without undue reservation.

AUTHOR CONTRIBUTIONS

LP contributed in performing the experimental measurement, post-processing, analysis and interpretation of data, and writing and critical revision of the manuscript. SZ contributed to the post-processing, analysis of experimental data, and critical revision of the manuscript. DD contributed in the post- processing and analysis of experimental data. DH contributed in the study design and supervised the experimental campaign. DO contributed to the post-processing, analysis and interpretation of data, writing and critical revision of the manuscript, as well as study design and supervision. All authors contributed to the article and approved the submitted version.

SUPPLEMENTARY MATERIAL

The Supplementary Material for this article can be found online at: https://www.frontiersin.org/articles/10.3389/fcvm.2021.804565/full#supplementary-material

REFERENCES

1. Nkomo VT, Gardin JM, Skelton TN, Gottdiener JS, Scott CG, Enriquez-Sarano M. Burden of valvular heart diseases: a population-based study. *Lancet* (2006) 368:1005–11. doi: 10.1016/S0140-6736(06)69208-8
2. Baumgartner H, Falk V, Bax JJ, De Bonis M, Hamm C, Holm PJ, et al. 2017 ESC/EACTS guidelines for the management of valvular heart disease. *Eur Heart J.* (2017) 38:2739–91. doi: 10.1093/eurheartj/ehx391
3. Bonow RO, Leon MB, Doshi D, Moat N. Management strategies and future challenges for aortic valve disease. *Lancet* (2016) 387:1312–23. doi: 10.1016/S0140-6736(16)00586-9
4. Reardon MJ, Van Mieghem NM, Popma JJ, Kleiman NS, Søndergaard L, Mumtaz M, et al. Surgical or transcatheter aortic-valve replacement in intermediate-risk patients. *New England J Med.* (2017) 376:1321–31. doi: 10.1056/NEJMoa1700456
5. Thourani VH, Kodali S, Makkar RR, Herrmann HC, Williams M, Babaliaros V, et al. Transcatheter aortic valve replacement versus surgical valve replacement in intermediate-risk patients: a propensity score analysis. *Lancet* (2016) 387:2218–25. doi: 10.1016/S0140-6736(16)30073-3
6. Siemieniuk RA, Agoritsas T, Manja V, Devji T, Chang Y, Bala MM, et al. Transcatheter versus surgical aortic valve replacement in patients with severe aortic stenosis at low and intermediate risk: systematic review and meta-analysis. *BMJ* (2016) 354:1–10. doi: 10.1136/bmj.i5130
7. Spears J, Al-Saiegh Y, Goldberg D, Manthey S, Goldberg S. TAVR: a review of current practices and considerations in low-risk patients. *J Interventional Cardiol.* (2020) 2020: 2582938. doi: 10.1155/2020/2582938
8. Siontis GC, Praz F, Pilgrim T, Mavridis D, Verma S, Salanti G, et al. Transcatheter aortic valve implantation vs. surgical aortic valve replacement for treatment of severe aortic stenosis: a meta-analysis of randomized trials. *Eur Heart J.* (2016) 37:3503–12. doi: 10.1093/eurheartj/ehw225
9. Chakos A, Wilson-Smith A, Arora S, Nguyen TC, Dhoble A, Tarantini G, et al. Long term outcomes of transcatheter aortic valve implantation (TAVI): a systematic review of 5-year survival and beyond. *Ann Cardiothoracic Surgery* (2017) 6:432. doi: 10.21037/acs.2017.09.10
10. De Ronde-Tillmans MJ, de Jager TA, Goudzwaard JA, El Faquir N, van Mieghem NM, Zijlstra F, et al. Long-term follow-up of quality of life in high-risk patients undergoing transcatheter aortic valve implantation for symptomatic aortic valve stenosis. *J Geriatric Cardiol* (2018) 15:261. doi: 10.11909/j.issn.1671-5411.2018.04.003
11. Murray MIK, Hofmann E, De Rosa R, Mas-Peiro S, Seppelt P, Walther T, et al. Life beyond 5 years after TAVI: patients perceived health status and long-term outcome after transcatheter aortic valve implantation. *J Interventional Cardiol* (2019) 2019:4292987. doi: 10.1155/2019/4292987
12. Voigtländer L, Seiffert M. Expanding TAVI to low and intermediate risk patients. *Front Cardiovasc Med.* (2018) 5:92. doi: 10.3389/fcvm.2018.00092
13. Becsek B, Pietrasanta L, Obrist D. Turbulent systolic flow downstream of a bioprosthetic aortic valve: velocity spectra, wall shear stresses, and turbulent dissipation rates. *Front Physiol.* (2020) 11:577188. doi: 10.3389/fphys.2020.577188
14. Dvir D, Bourguignon T, Otto CM, Hahn RT, Rosenhek R, Webb JG, et al. Standardized definition of structural valve degeneration for surgical and transcatheter bioprosthetic aortic valves. *Circulation* (2018) 137:388–99. doi: 10.1161/CIRCULATIONAHA.117.030729
15. Gomel MA, Lee R, Grande-Allen KJ. Comparing the role of mechanical forces in vascular and valvular calcification progression. *Front Cardiovasc Med.* (2019) 5:197. doi: 10.3389/fcvm.2018.00197
16. Davies PF, Remuzzi A, Gordon EJ, Dewey CF, Gimbrone MA. Turbulent fluid shear stress induces vascular endothelial cell turnover in vitro. *Proc Nat Acade Sci.* (1986) 83:2114–7. doi: 10.1073/pnas.83.7.2114
17. Kameneva MV, Burgreen GW, Kono K, Repko B, Antaki JF, Umezu M. Effects of turbulent stresses on mechanical hemolysis: experimental and computational analysis. *ASAIO J (Amer Soc Artif Internal Organs 1992)* (2004) 50:418. doi: 10.1097/01.mat.0000136512.36370.b5
18. Bluestein D. Research approaches for studying flow-induced thromboembolic complications in blood recirculating devices. *Exp Rev Med Devices* (2004) 1:65–80. doi: 10.1586/17434440.1.1.65
19. Buellesfeld L, Stortecky S, Kalesan B, Gloekler S, Khattab AA, Nietlispach F, et al. Aortic root dimensions among patients with severe aortic stenosis

undergoing transcatheter aortic valve replacement. *JACC Cardiovasc Interv* (2013) 6:72–83. doi: 10.1016/j.jcin.2012.09.007
20. Borazjani I. Fluid–structure interaction, immersed boundary-finite element method simulations of bio-prosthetic heart valves. *Comput Methods Appl Mech Eng.* (2013) 257:103–16. doi: 10.1016/j.cma.2013.01.010
21. Hedayat M, Borazjani I. Comparison of platelet activation through hinge vs bulk flow in bileaflet mechanical heart valves. *J Biomech.* (2019) 83:280–90. doi: 10.1016/j.jbiomech.2018.12.003
22. Bailoor S, Seo JH, Dasi LP, Schena S, Mittal R. A computational study of the hemodynamics of bioprosthetic aortic valves with reduced leaflet motion. *J Biomech.* (2021) 120:110350. doi: 10.1016/j.jbiomech.2021.110350
23. Mao W, Li K, Sun W. Fluid–structure interaction study of transcatheter aortic valve dynamics using smoothed particle hydrodynamics. *Cardiovasc Eng Technol.* (2016) 7:374–88. doi: 10.1007/s13239-016-0285-7
24. Wu W, Pott D, Mazza B, Sironi T, Dordoni E, Chiastra C, et al. Fluid–structure interaction model of a percutaneous aortic valve: comparison with an in vitro test and feasibility study in a patient-specific case. *Ann Biomed Eng.* (2016) 44:590–603. doi: 10.1007/s10439-015-1429-x
25. Kandail HS, Trivedi SD, Shaikh AC, Bajwa TK, Daniel P, Jahangir A, et al. Impact of annular and supra-annular CoreValve deployment locations on aortic and coronary artery hemodynamics. *J Mech Behav Biomed Mater.* (2018) 86:131–42. doi: 10.1016/j.jmbbm.2018.06.032
26. Basri AA, Zuber M, Basri EI, Zakaria MS, Aziz AF, Tamagawa M, et al. Fluid structure interaction on paravalvular leakage of transcatheter aortic valve implantation related to aortic stenosis: a patient-specific case. *Comput Math Methods Med.* (2020) 2020:9163085. doi: 10.1155/2020/9163085
27. Li CP, Lo CW, Lu PC. Estimation of viscous dissipative stresses induced by a mechanical heart valve using PIV data. *Ann Biomed Eng.* (2010) 38:903–16. doi: 10.1007/s10439-009-9867-y
28. Liu J, Lu P, Chu S. Turbulence characteristics downstream of bileaflet aortic valve prostheses. *J Biomech Eng.* (2000) 122:118–24. doi: 10.1115/1.429643
29. Hatoum H, Yousefi A, Lilly S, Maureira P, Crestanello J, Dasi LP. An in vitro evaluation of turbulence after transcatheter aortic valve implantation. *J Thorac Cardiovasc Surgery* (2018) 156:1837–48. doi: 10.1016/j.jtcvs.2018.05.042
30. Groves EM, Falahatpisheh A, Su JL, Kheradvar A. The effects of positioning of transcatheter aortic valve on fluid dynamics of the aortic root. *ASAIO J (Amer Soc Artif Internal Organs 1992)* (2014) 60:545. doi: 10.1097/MAT.0000000000000107
31. Yerasi C, Forrestal BJ, Rogers T. TAVR pitfalls: addressing coronary obstruction risk. *Contemporary Issues in TAVR* (2021) 15:45–7. Available online at: https://citoday.com/articles/2021-mar-apr/tavr-pitfalls-addressing-coronary-obstruction-risk?c4src=archive:feed
32. Ribeiro HB, Nombela-Franco L, Urena M, Mok M, Pasian S, Doyle D, et al. Coronary obstruction following transcatheter aortic valve implantation: a systematic review. *JACC Cardiovasc Interv.* (2013) 6:452–61. doi: 10.1016/j.jcin.2012.11.014
33. Van Rosendael PJ, Delgado V, Bax JJ. Pacemaker implantation rate after transcatheter aortic valve implantation with early and new-generation devices: a systematic review. *Eur Heart J.* (2018) 39:2003–13. doi: 10.1093/eurheartj/ehx785
34. Mauri V, Reimann A, Stern D, Scherner M, Kuhn E, Rudolph V, et al. Predictors of permanent pacemaker implantation after transcatheter aortic valve replacement with the SAPIEN 3. *JACC Cardiovasc Interv* (2016) 9:2200–9. doi: 10.1016/j.jcin.2016.08.034
35. Hasler D, Landolt A, Obrist D. Tomographic PIV behind a prosthetic heart valve. *Exp Fluids* (2016) 57:80. doi: 10.1007/s00348-016-2158-0
36. Hasler D, Obrist D. Three-dimensional flow structures past a bio-prosthetic valve in an in-vitro model of the aortic root. *PLoS ONE* (2018) 13:e0194384. doi: 10.1371/journal.pone.0194384
37. Midha PA, Raghav V, Condado JF, Okafor IU, Lerakis S, Thourani VH, et al. Valve type, size, and deployment location affect hemodynamics in an in vitro valve-in-valve model. *JACC Cardiovasc Interv.* (2016) 9:1618–28. doi: 10.1016/j.jcin.2016.05.030
38. Pope SB. *Turbulent Flows*. (2001). New York: Cambridge University Press.
39. Luraghi G, Migliavacca F, García-González A, Chiastra C, Rossi A, Cao D, et al. On the modeling of patient-specific transcatheter aortic valve replacement: a fluid–structure interaction approach. *Cardiovasc Eng Technol.* (2019) 10:437–55. doi: 10.1007/s13239-019-00427-0
40. Kostyunin AE, Yuzhalin AE, Rezvova MA, Ovcharenko EA, Glushkova TV, Kutikhin AG. Degeneration of bioprosthetic heart valves: update 2020. *J Amer Heart Assoc.* (2020) 9:e018506. doi: 10.1161/JAHA.120.018506
41. Vennemann B, Rösgen T, Heinisch PP, Obrist D. Leaflet kinematics of mechanical and bioprosthetic aortic valve prostheses. *ASAIO J.* (2018) 64:651–61. doi: 10.1097/MAT.0000000000000687
42. Avelar AHdF, Canestri JA, Bim C, Silva MG, Huebner R, Pinotti M. Quantification and analysis of leaflet flutter on biological prosthetic cardiac valves. *Artif Organs* (2017) 41:835–44. doi: 10.1111/aor.12856 lan2019performance
43. Gülan U, Appa H, Corso P, Templin C, Bezuidenhout D, Zilla P, et al. Performance analysis of the transcatheter aortic valve implantation on blood flow hemodynamics: an optical imaging-based in vitro study. *Artif Organs* (2019) 43:E282–93. doi: 10.1111/aor.13504
44. Bessa GM, Fernandes LS, Gomes BA, Azevedo LF. Influence of aortic valve tilt angle on flow patterns in the ascending aorta. *Exp Fluids* (2021) 62:1–31. doi: 10.1007/s00348-021-03199-3
45. Manchester EL, Pirola S, Salmasi MY, ORegan DP, Athanasiou T, Xu XY. Analysis of turbulence effects in a patient-specific aorta with aortic valve stenosis. *Cardiovasc Eng Technol.* (2021) 12:1–16. doi: 10.1007/s13239-021-00536-9
46. Quinlan NJ, Dooley PN. Models of flow-induced loading on blood cells in laminar and turbulent flow, with application to cardiovascular device flow. *Ann Biomed Eng.* (2007) 35:1347–56. doi: 10.1007/s10439-007-9308-8
47. Raghav V, Sastry S, Saikrishnan N. Experimental assessment of flow fields associated with heart valve prostheses using particle image velocimetry (PIV): recommendations for best practices. *Cardiovasc Eng Technol.* (2018) 9:273–87. doi: 10.1007/s13239-018-0348-z
48. Sciacchitano A, Wieneke B. PIV uncertainty propagation. *Meas Sci Technol.* (2016) 27:084006. doi: 10.1088/0957-0233/27/8/084006

Conflict of Interest: The authors declare that the research was conducted in the absence of any commercial or financial relationships that could be construed as a potential conflict of interest.

Publisher's Note: All claims expressed in this article are solely those of the authors and do not necessarily represent those of their affiliated organizations, or those of the publisher, the editors and the reviewers. Any product that may be evaluated in this article, or claim that may be made by its manufacturer, is not guaranteed or endorsed by the publisher.

frontiers in Cardiovascular Medicine

ORIGINAL RESEARCH
published: 27 January 2022
doi: 10.3389/fcvm.2022.809707

Mitral and Aortic Regurgitation in Patients Undergoing Kidney Transplantation: The Natural Course and Factors Associated With Progression

*Minjeong Kim[1], Darae Kim[2], Juhan Lee[3], Dae-Young Kim[1], Jiwon Seo[1], Iksung Cho[1], Kyu Ha Huh[3], Geu-Ru Hong[1], Jong-Won Ha[1] and Chi Young Shim[1]**

[1] Division of Cardiology, Severance Cardiovascular Hospital, Yonsei University College of Medicine, Seoul, South Korea, [2] Division of Cardiology, Department of Medicine, Heart Vascular Stroke Institute, Samsung Medical Center, Sungkyunkwan University School of Medicine, Seoul, South Korea, [3] Departement of Surgery, Yonsei University College of Medicine, Seoul, South Korea

OPEN ACCESS

Edited by:
Sanjeev Bhattacharyya, Barts Heart Centre, United Kingdom

Reviewed by:
Sveeta Badiani, Barts Health NHS Trust, United Kingdom
Dimitrios Klettas, Hippokration General Hospital, Greece

***Correspondence:**
Chi Young Shim
cysprs@yuhs.ac

Specialty section:
This article was submitted to Heart Valve Disease, a section of the journal Frontiers in Cardiovascular Medicine

Received: *05 November 2021*
Accepted: *03 January 2022*
Published: *27 January 2022*

Citation:
Kim M, Kim D, Lee J, Kim D-Y, Seo J, Cho I, Huh KH, Hong G-R, Ha J-W and Shim CY (2022) Mitral and Aortic Regurgitation in Patients Undergoing Kidney Transplantation: The Natural Course and Factors Associated With Progression. Front. Cardiovasc. Med. 9:809707. doi: 10.3389/fcvm.2022.809707

Background: Valve regurgitation can decrease with resolution of hemodynamic loads on the left ventricle (LV) after kidney transplantation (KT). We aimed to investigate the natural course of left-side valve regurgitation after KT and factors associated with progression.

Methods: Among patients who underwent KT in two tertiary centers, 430 (224 men, mean age 50 ± 13 years) were examined by echocardiography within 3 months before KT and between 6 and 36 months after KT. Mitral regurgitation (MR) and aortic regurgitation (AR) were graded according to the current guidelines. Regression was defined as a decrease in regurgitation by one or more steps, and progression was an increase in one or more steps after KT. Clinical and echocardiographic factors associated with progression of MR and AR were analyzed.

Results: Mild or greater MR was observed in 216 (50%) patients before KT, and mild or greater AR was observed in 99 (23%). During the follow-up period of 23.4 ± 9.9 months, most patients experienced regression or no change in regurgitation after KT, but 34 patients (7.9%) showed MR progression and 37 (8.6%) revealed AR progression. Patients who showed MR progression were more likely to receive a second KT, have mitral annular calcifications, and show a smaller decrease in LV end-systolic dimension. Patients who showed AR progression were more likely to have persistent hypertension after KT, aortic valve calcifications, and a smaller reduction of LV end-systolic dimension.

Conclusions: Risk factors for progression of MR after KT include a second KT, MAC and a smaller decrease in LV end-systolic dimension after KT. Risk factors for progression of AR include valve calcification, persistent hypertension and a smaller decrease in LV end-systolic dimension after KT. Further echocardiographic surveillance and risk factor management after KT are warranted in these patients.

Keywords: left-side valve disease, mitral regurgitation, aortic regurgitation, ESRD, kidney transplantation

INTRODUCTION

Valve regurgitation is observed frequently in patients with chronic kidney disease or end stage renal disease (ESRD) (1, 2). Left-side valve regurgitation, including mitral regurgitation (MR) and aortic regurgitation (AR), is predicted to decrease when the hemodynamic load on the left ventricle (LV) decreases after kidney transplantation (KT). However, in some patients, left-side valve regurgitation does not decrease but persists or even progresses (3–5). In particular, degeneration and structural change of the valve start early in patients with ESRD because of the hemodynamic load and impaired calcium-phosphate homeostasis and progress faster than in those with normal kidney function (6–8). MR and AR are affected by different hemodynamic factors and structural alterations. MR is influenced more highly by preload and LV remodeling, while AR is affected most by afterload and aorta remodeling. Patients who have undergone KT are thought to have reduced or increased MR or AR depending on the clinical situation in pre-KT and post-KT periods (9). However, data regarding the prevalence of left-side valve regurgitation in patients undergoing KT and the natural course of MR and AR after KT are scarce.

In the present study, we investigated the prevalence of MR and AR before KT and the regression or progression rate of MR and AR after KT. We also identified clinical and echocardiographic factors associated with progression of MR and AR.

METHODS

Study Population

This study included patients with ESRD who received KT between 2005 and 2018 at two tertiary medical centers (Severance Hospital, Seoul, Korea; Samsung Medical Center, Seoul, Korea). Patients with a history of valve surgery or intervention, congenital heart disease, or combined transplantation with other organs were excluded, as were patients without follow-up transthoracic echocardiography (TTE) after KT. After applying exclusion criteria, 430 patients were analyzed retrospectively.

All patients underwent TTE at least twice. Pre-KT echocardiography was performed within 3 months before KT, and post-KT echocardiography was performed between 6 and 36 months after KT. If a patient underwent TTE more than twice after KT, we analyzed the most recent.

Clinical information was obtained from electronic medical records, and data were analyzed at baseline and follow-up TTE. Prior medical history was composed of hypertension, diabetes mellitus, dyslipidemia, atrial fibrillation, coronary artery disease, heart failure, duration of hemodialysis, and second KT. The diagnosis of heart failure was based on typical clinical symptoms and signs caused by a structural or functional cardiac abnormality, followed the current guideline, including both reduced EF and preserved EF (8). Systolic and diastolic blood pressures were measured at baseline and post-KT follow-up visits. Clinical factors after KT including new-onset hypertension, new-onset diabetes, renal dysfunction, graft failure, and cardiovascular medications were collected. Renal dysfunction was defined as a >1.5-fold increase in serum creatinine or an absolute increase in serum creatinine $\geq$ 0.3 mg/dL (9).

Echocardiography

Two-dimensional and Doppler echocardiography was performed using a commercially available ultrasound machine with a 2.5–3.5 MHz probe before and after KT. Standard measurements were performed following the current guideline recommendations (10). LV ejection fraction (EF) was measured using the biplane Simpson's method in apical four- and two-chamber views. Left atrial (LA) volume index was measured by the biplane method at the end of ventricular systole and indexed to body surface area. From the mitral inflow velocities, we obtained data on peak velocity of early (E) and late filling and deceleration time of E velocity. Early diastolic (e') velocities were measured at the septal mitral annulus (11).

The severity and mechanism of each valve regurgitation were assessed according to American Society of Echocardiography guidelines (12). The degrees of MR and AR, if present, were graded as no/trivial, mild, moderate, or severe using an integrated approach (12). The etiology of MR was categorized into primary or secondary MR. Primary MR was defined as degenerative MR directly affecting the mitral valve leaflets and/or chordae, and secondary MR was MR due to a pathological process of the LV or LA (12). Mitral annular calcification (MAC) was defined as the thick and echo-dense area of the mitral annulus, occasionally extending to mitral valve leaflets, as described in previous studies (13, 14). Aortic valve calcification was defined as a calcium deposit in the aortic root and valve regardless of restriction of leaflet mobility on parasternal short- and long-axis views (15, 16). The echocardiography reports were independently reviewed by 2 cardiologists blinded to the clinical data. All discrepancy of echocardiographic readings was resolved by consensus. In a consensus process, the 2 cardiologists reviewed the echocardiographic images and reached an agreement on the interpretation.

Regression of MR or AR was noted if severity decreased by one or more grades. Progression was defined as severity increase by one or more grades. Patients were categorized into three groups (regression, unchanged, progression) according to valve regurgitation.

Statistical Analysis

The baseline characteristics are expressed using frequencies and percentages for categorical variables using chi-square test. The continuous variables are summarized as mean $\pm$ standard deviation and were compared using analysis of variance (ANOVA) among the three groups. For pairwise comparisons, *post-hoc* test with Tukey's HSD was conducted. To identify factors associated with progression of valve regurgitation, a linear regression model was used. Univariable factors with $P < 0.10$ or the major relevant clinical factors were entered into multivariable analyses. The coefficient values were generated, and all two-sided p-values < 0.05 were considered statistically significant. The Hosmer–Lemeshow test for stepwise logistic regression was performed for incremental value of risk prediction. All statistical

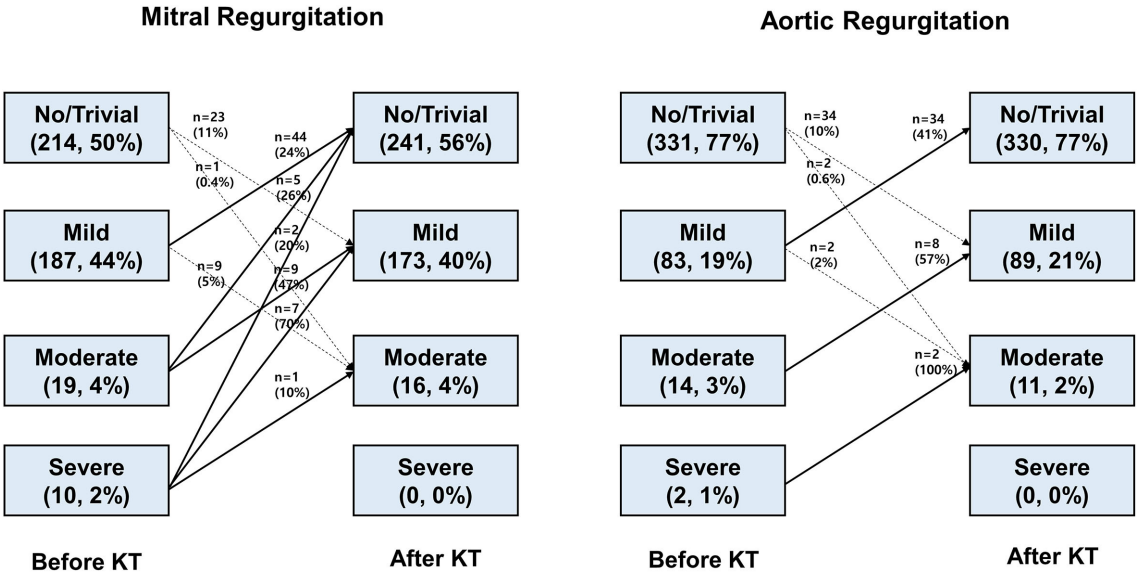

FIGURE 1 | Natural course of left-sided valvular regurgitation after kidney transplantation.

analyses were performed using SPSS software (version 25.0; IBM Corp., Armonk, NY, USA).

RESULTS

Severity and Changes of Left-Side Valve Regurgitation After KT

The severity of MR and AR before KT and the changes after KT are shown in **Figure 1**. Before KT, 187 (44%) patients had mild MR, 19 (4%) had moderate MR, and 10 (2%) showed severe MR. Factors related to MR severity before KT are presented in **Supplementary Table 1**. Female sex, history of heart failure, and larger LA volume index were associated with MR before KT. Before KT, 83 (19%) patients had mild AR, 14 (3%) had moderate AR, and 2 (1%) showed severe AR. Factors associated with AR severity before KT are described in **Supplementary Table 2**. Old age and history of heart failure were associated with AR grade before KT. Mild or greater MR was observed in 216 (50%) patients and mild or greater AR in 99 (23%) before KT. During the follow-up period of 23.4 ± 9.9 months, most patients experienced regression or no change in regurgitation after KT, but 34 (7.9%) showed MR progression and 37 (8.6%) revealed AR progression.

Factors Associated With MR Progression

Table 1 shows the baseline clinical and renal characteristics in the three groups according to change in MR after KT. A history of atrial fibrillation, history of heart failure and secondary MR tended to be more prevalent in the MR regression group compared with the other groups. Second KT and post-KT renal dysfunction were significantly different in the three groups, and these events tended to be more prevalent in the progression group. Most of the echocardiographic findings differed between the three groups. In patients with MR progression, LV chamber size was small, and E/e′ was lower than that in the other groups before KT, but these factors were significantly higher after KT. In the group showing MR progression, LV and LA size increased after KT, LVEF decreased, and E/e′ increased (**Table 2**).

Univariate linear regression analysis revealed that second KT, MAC before KT, renal dysfunction after KT, and a smaller decrease in LV end systolic dimension (LVESD) were associated with MR progression. After multivariable adjustment, second KT, baseline MAC, and smaller decrease in LVESD after KT were independent predictors for MR progression after KT (**Table 3**). Factors related to progression of MR showed statistically meaningful predictive values in a stepwise manner (**Figure 2A**).

These findings indicate that MR tended to show regression after KT for controlling volume overload. In contrast, MR progression can occur after KT if the volume overload is relatively low before KT or if valve degeneration represented by MAC is present before KT. Furthermore, progression of MR was related to subsequent elevation of LV filling pressure after KT.

Factors Associated With AR Progression

Table 4 shows the baseline clinical and renal characteristics of the three groups categorized by AR change after KT. Patients who showed AR progression experienced persistent hypertension, defined as systolic blood pressure ≥140 mmHg and diastolic blood pressure ≥90 mmHg after KT among those with hypertension. In echocardiographic findings, patients who showed AR progression showed larger LV and LA size after KT compared with the other groups. Similar to the results from the analysis of MR, smaller reductions in LV and LA sizes after KT, no improvement in LVEF, and an increase in E/e′ were observed in the AR progression group (**Table 5**).

TABLE 1 | Comparison of clinical and renal characteristics in the three groups according to change in mitral regurgitation.

	MR regression (n = 68)	MR unchanged (n = 328)	MR progression (n = 34)	p-value
Clinical characteristics				
Age, years	51.0 ± 11.6	49.5 ± 13.0	53.9 ± 10.7	0.128
Male sex, *n* (%)	28 (40.6)	180 (55.0)	16 (47.1)	0.076
Hypertension, *n* (%)	58 (84.1)	299 (91.7)	29 (85.3)	1.000
Diabetes mellitus, *n* (%)	24 (34.8)	114 (35.0)	16 (47.1)	0.368
Dyslipidemia, *n* (%)	16 (23.2)	62 (19.0)	3 (8.8)	0.214
Atrial fibrillation, *n* (%)	9 (13.0)	13 (4.0)*	0 (0.0)#	0.003
CAD, *n* (%)	9 (13.0)	37 (11.3)	7 (20.6)	0.292
Heart failure, *n* (%)	13 (18.8)	24 (7.3)*	2 (5.9)#	0.008
Renal characteristics				
Dialysis, *n* (%)	68 (100.0)	328 (100.0)	34 (100.0)	1.000
Hemodialysis, *n* (%)	62 (91.2)	282 (86.0)	31 (91.2)	0.664
Peritoneal dialysis, *n* (%)	6 (8.8)	46 (14.0)	3 (8.8)	0.306
HD duration, months	56.7 ± 58.2	65.2 ± 66.9	56.4 ± 62.1	0.577
Second KT, *n* (%)	2 (2.9)	23 (7.0)	7 (20.6)*#	0.005
Post-KT comorbidities, *n* (%)				
New-onset HTN	4 (5.8)	13 (4.0)	2 (5.9)	0.732
Persistent HTN	13 (18.8)	103 (31.5)*	17 (50.0)*#	0.005
New-onset DM	5 (7.2)	52 (16.0)	3 (8.8)	0.111
Renal dysfunction, *n* (%)	9 (13.0)	62 (19.0)	12 (35.3)*#	0.025
Graft failure, *n* (%)	11 (15.9)	33 (10.1)	6 (17.6)	0.202
Post-KT medications				
RAAS blocker, *n* (%)	12 (18.8)	74 (26.9)	5 (15.6)	0.186
Beta blocker, *n* (%)	23 (34.8)	145 (52.3)*	14 (43.8)	0.032
CCB, *n* (%)	25 (36.0)	108 (32.9)	17 (50.0)	0.470
Diuretics, *n* (%)	6 (9.4)	27 (9.9)	4 (12.1)	0.906
Statin, *n* (%)	17 (26.2)	85 (31.4)	12 (36.4)	0.556

*$P < 0.05$ compared with the MR regression group.
#$P < 0.05$ compared with the MR unchanged group.
MR, mitral regurgitation; CAD, coronary artery disease; HD, hemodialysis; KT, kidney transplantation; HTN, hypertension; DM, diabetes mellitus; RAAS, renin-angiotensin-aldosterone system; CCB, calcium channel blocker.

TABLE 2 | Comparison of echocardiographic characteristics in the three groups according to change in mitral regurgitation.

	MR regression (n = 68)	MR unchanged (n = 328)	MR progression (n = 34)	p-value
Pre-KT echocardiogram				
LVEDD, mm	56.6 ± 6.9	52.4 ± 5.9	51.3 ± 5.7*	<0.001
LVESD, mm	38.5 ± 9.3	34.1 ± 6.0	62.5 ± 6.1*	<0.001
LVEF, %	56.7 ± 12.8	62.3 ± 9.3	61.7 ± 10.6	<0.001
LV mass index, g/m^2	148.4 ± 51.1	124.9 ± 37.0	118.6 ± 36.4	<0.001
LA volume index, ml/m^2	51.6 ± 24.5	38.1 ± 15.1	39.5 ± 14.8	<0.001
E/e′	15.4 ± 6.9	12.4 ± 5.6*	12.2 ± 4.1*	0.001
PASP, mmHg	40.0 ± 11.8	30.3 ± 9.3*	35.4 ± 10.5	0.015
Degree of MR, *n* (%)				<0.001
No/trivial	0 (0)	190 (57.8)*	24 (70.6)*#	
Mild	46 (66.7)	131 (40.1)*	10 (29.4)*	
Moderate	12 (17.4)	7 (2.1)*	0 (0.0)*	
Severe	10 (14.5)	0 (0.0)*	0 (0.0)*	
Secondary MR, *n* (%)	68 (100.0)	111 (76.5)*	28 (82.3)*	<0.001
Presence of MAC, *n* (%)	6 (8.7)	19 (5.8)	6 (17.6)#	0.035
Post-KT echocardiogram				
LVEDD, mm	48.7 ± 5.6	48.9 ± 5.8	52.0 ± 5.8	0.011
LVESD, mm	30.3 ± 5.6	30.4 ± 5.1	33.5 ± 5.7	0.006
LVEF, %	65.4 ± 7.6	65.8 ± 7.8	58.4 ± 9.6	<0.001
LV mass index, g/m^2	108.3 ± 34.4	111.7 ± 33.5	125.6 ± 33.9	0.045
LA volume index, ml/m^2	36.8 ± 14.4	35.5 ± 16.3	45.0 ± 17.8	0.006
E/e′	11.6 ± 5.1	11.5 ± 4.8	16.6 ± 7.2*#	<0.001
PASP, mmHg	30.3 ± 11.6	29.5 ± 7.9	42.7 ± 13.4*#	0.003
Degree of MR, *n* (%)				<0.001
No/trivial	51 (73.9)	190 (58.1)*	0 (0.0)* #	
Mild	17 (24.6)	132 (40.4)*	24 (70.6)* #	
Moderate	1 (1.4)	5 (1.5)	10 (29.4)* #	
Severe	0 (0.0)	0 (0.0)	0 (0.0)	
Changes after KT				
Δ LVEDD, mm	−1.8 ± 9.6	1.1 ± 9.4	0.9 ± 5.8	0.082
Δ LVESD, mm	−8.1 ± 8.8	−3.7 ± 5.4*	0.9 ± 6.5*	<0.001
Δ LVEF, %	8.3 ± 13.6	3.5 ± 8.4	−3.3 ± 10.6*	<0.001
Δ E/e′	−4.4 ± 6.5	−1.1 ± 5.4*	4.2 ± 5.3*#	<0001
Δ LV mass index, g/m^2	−42.8 ± 53.4	−12.5 ± 46.6	7.4 ± 42.7*#	<0.001
Δ LA volume index, ml/m^2	−15.7 ± 24.7	−4.7 ± 13.8	1.0 ± 17.7*	<0.001

*$P < 0.05$ compared with the MR regression group.
#$P < 0.05$ compared with the MR unchanged group.
MR, mitral regurgitation; LVEDD, left ventricular end-diastolic diameter; LVESD, lefMRt ventricular end-systolic diameter; LVEF, left ventricular ejection fraction; LV, left ventricle; LA, left atrium; E/e′, ratio of early diastolic mitral velocity to early diastolic mitral annular velocity; PASP, pulmonary arterial systolic pressure; MAC, mitral annular calcification.

Univariate linear regression analysis revealed that presence of aortic valve calcification before KT, persistent HTN after KT, and a smaller decrease in LVESD after KT were associated with AR progression. All the above factors were independent predictors for AR progression after KT in multivariate analysis (**Table 6**). **Figure 2B** shows additive predictive values for AR progression after KT in a stepwise manner. These findings suggest that preexisting aortic valve degeneration accompanying unresolved afterload as well as less volume control after KT might affect AR progression.

DISCUSSION

The principal findings in the present multicenter study are as follows. (1) Left-side valve regurgitation is common in patients with ESRD undergoing KT, and MR is more common than AR. (2) After KT, MR and AR regress or do not change in most patients but progress in some patients. (3) Patients who receive second KT and who have MAC and a smaller decrease in LVESD

TABLE 3 | Factors associated with progression of mitral regurgitation after KT.

	Univariate analysis			Multivariate analysis		
	B	*t*	*p*-value	*B*	*t*	*p*-value
Age	0.002	1.82	0.070	0.001	1.29	0.198
Female sex	0.016	0.61	0.541			
Hypertension	−0.041	−0.95	0.345			
Diabetes mellitus	0.038	1.41	0.158			
Dyslipidemia	−0.052	−1.56	0.119			
Atrial fibrillation	−0.084	−1.41	0.158			
CAD	0.060	1.52	0.129			
Heart failure	−0.031	−0.67	0.501			
HD duration	−0.032	−0.59	0.558			
Second KT	0.151	3.07	0.002	0.114	2.31	0.022
New-onset HTN	0.027	0.43	0.669			
Persistent HTN	0.036	1.21	0.228			
New-onset DM	−0.034	−0.90	0.367			
Renal dysfunction	0.081	2.47	0.014	0.062	1.19	0.057
Graft failure	0.046	1.14	0.255			
Secondary MR	−0.068	−1.07	0.286			
Presence of MAC	0.123	2.46	0.014	0.110	2.20	0.028
Δ LVEDD	0.008	0.16	0.876			
Δ LVESD	0.009	4.57	<0.001	0.008	4.15	<0.001
Δ LVEF	−0.006	−4.21	<0.001			
Δ LV mass index	0.001	2.79	0.006			
Δ LA volume index	0.002	2.43	0.016			

CAD, coronary artery disease; HD, hemodialysis; KT, kidney transplantation; HTN, hypertension; DM, diabetes mellitus; MR, mitral regurgitation; MAC, mitral annular calcification; LVEDD, left ventricular end-diastolic diameter; LVESD, left ventricular end-systolic diameter; LVEF, left ventricular ejection fraction; LV, left ventricle; LA, left atrium.

after KT showed MR progression after KT. (4) Patients who had aortic valve calcification, persistent HTN after KT, and a smaller decrease in LVESD after KT showed AR progression. The present study suggests that pre-existing valve degeneration before KT, smaller volume changes, and specific conditions before or after KT affect the progression of regurgitation on each valve. As expected, MR was affected more highly by volume factor, and AR was affected most by afterload, such as persistent HTN after KT. Therefore, it is necessary to perform echocardiographic surveillance and risk factor control after KT according to individual characteristics before and after KT and presence of valve calcification.

Left-Side Valve Disease in Patients With ESRD

Patients with chronic kidney disease or ESRD show a high prevalence of left-side valve disease due to not only degeneration of the valve itself, but also chamber dilatation or dysfunction related with increased hemodynamic load and loss of LV contractility (8, 17). Previous studies demonstrated higher prevalence of premature aortic valve calcification and consequent aortic stenosis, as well as mitral annular calcification and functional mitral stenosis (18–21). In particular, increased calcium x phosphate product and long-term hemodialysis are associated with valve calcification (8, 17). Also, increased cardiac output caused by anemia and arteriovenous fistula and hypertension increase mechanical stress in the valve leaflets and modulate premature valve calcification (8, 17). In stenotic valve disease, primary degeneration is the main mechanism, whereas regurgitation is caused mainly by secondary causes. Therefore, because of preload and afterload reduction after KT

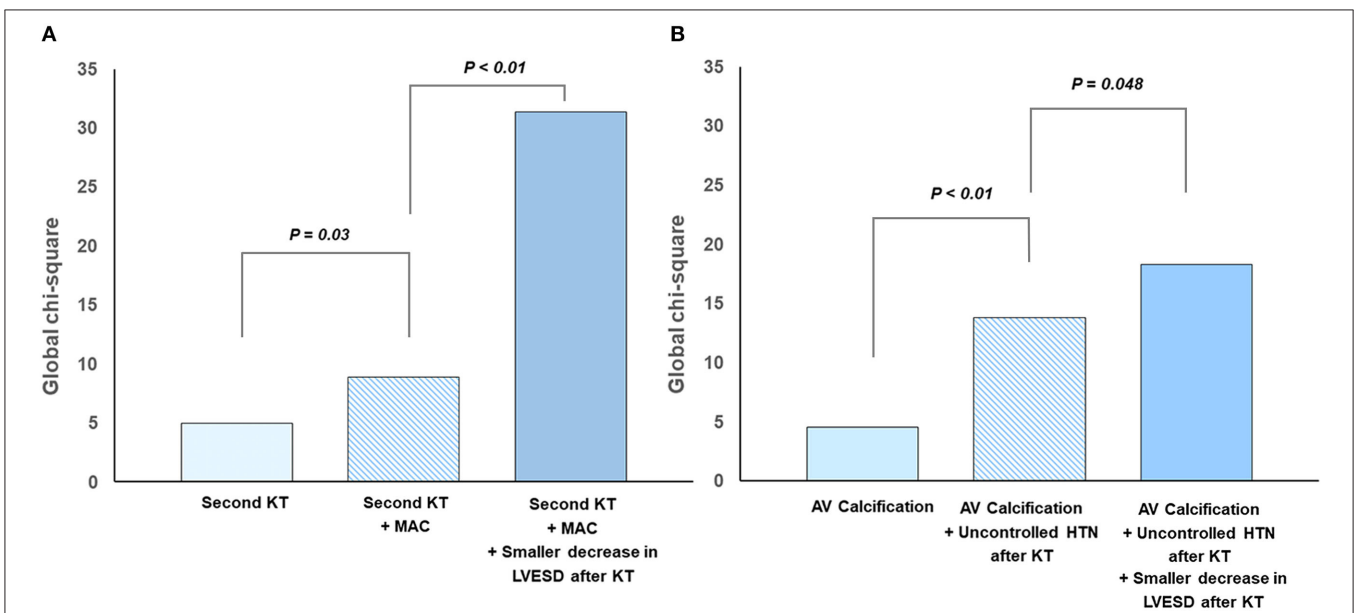

FIGURE 2 | Predictors for progression of left-sided valvular regurgitation after kidney transplantation: **(A)** mitral regurgitation and **(B)** aortic regurgitation.

and additional improvement of renin-angiotensin-aldosterone system (RAAS) activation, regression of valve regurgitation is expected after KT. If the patient does not show any specific clinical features after KT, regular echocardiographic follow-up is not performed; valve regurgitation sometimes progresses, and timely treatment can be delayed.

Natural Course of MR and AR in Patients Undergoing KT

Several previous studies have focused on valve disease in patients undergoing KT. A serial echocardiographic follow-up study in 95 patients undergoing KT reported no interval change in average MR fraction and volume after KT (22). However, this study was limited in that it did not provide information on patient characteristics or changes in chamber size and function. Another study conducted at a single center with 180 patients undergoing KT demonstrated that grade 2 MR decreased from 11% on pre-KT echocardiogram to 2% at 12 months after KT (23). Interestingly, valve calcification was detected preoperatively in 21.5% of the study population but was detected in 25.8% of the population at 6 months after KT and in 35.5% of the population 12 months after KT (23). Incidence of calcified valve was more common in patients with diabetes than in those without it (23). These results suggest that, even if hemodynamic load is resolved by KT, valve degeneration and calcification can have initiated and can proceed. It also suggests that risk factor modulation and echocardiographic follow-up are needed even after KT in patients who have calcification on the valve or surrounding annular structure. In this context, the present study showed on pre-KT echocardiogram that MR and AR can progress even after KT in patients with MAC or aortic valve calcification through a multicenter analysis. In addition, we found some differential risk factors between MR progression and AR progression after KT.

Risk Factors for Progression of MR and AR After KT

Smaller LVESD decrease after KT was related to progression of not only MR, but also AR in this study. Therefore, a smaller volume decrease after KT was a pre-condition of progression of left-side valve regurgitation. These results indicate the need for follow-up TTE for surveillance of chamber size and course of functional regurgitation after KT, especially for patients who have predisposing factors. Furthermore, prolonged optimal medical treatment might be necessary after KT, especially for patients with risk factors of progression. In our study, there might have been insufficient usage of RAAS inhibitor in patients with progression of AR compared with that in the unchanged AR group. Since RASS inhibitor can promote reverse LV remodeling after KT through both afterload reduction and inhibition of myocardial fibrosis, active use of RASS inhibitor after KT seems to be helpful for hemodynamic control.

MAC or aortic valve calcification shares biological links with atherosclerosis and is very common in patients with ESRD (18). Patients with valve or peri-valvular calcification in ESRD were more likely to have dyslipidemia and a broken mineral-bone axis, and this condition might not recover fully after KT (16). These conditions were thought to be due to valve dysfunction accompanied by valve calcification that could progress after KT. This might be related to greater use of statins in patients who showed progression of AR after KT.

After KT, hypertension remains widespread, with 56–93% of recipients consistently having a systolic blood pressure >140 mmHg. Multiple factors can lead to hypertension, including donor and recipient characteristics, immunosuppressive medications, and allograft function (17). Long-term exposure to high blood pressure is a strong and potentially modifiable risk factor for aortic stenosis and regurgitation (19). Our study also revealed persistent HTN after KT as a predictor of AR progression. This suggests that unresolved afterload and preload affect AR progression; therefore, strict anti-hypertensive treatment is important for preventing progression of AR after KT.

TABLE 4 | Comparison of clinical and renal characteristics in the three groups according to change in aortic regurgitation.

	AR regression ($n = 38$)	AR unchanged ($n = 355$)	AR progression ($n = 37$)	*p*-value
Clinical characteristics				
Age, years	53.2 ± 12.9	49.4 ± 12.8	53.7 ± 9.8	0.044
Male sex, *n* (%)	11 (28.9)	198 (55.8)*	15 (40.5)	0.002
Hypertension, *n* (%)	32 (84.2)	320 (90.4)	34 (91.9)	0.445
Diabetes mellitus, *n* (%)	14 (36.8)	124 (35.0)	16 (43.2)	0.607
Dyslipidemia, *n* (%)	6 (15.8)	71 (20.1)	4 (10.8)	0.345
Atrial fibrillation, *n* (%)	5 (13.2)	16 (4.5)	1 (2.7)	0.056
CAD, *n* (%)	6 (15.8)	43 (12.1)	4 (10.8)	0.775
Heart failure, *n* (%)	8 (21.1)	28 (7.9)*	3 (8.1)	0.027
Renal characteristics				
Dialysis, *n* (%)	38 (100.0)	355 (100.0)	37 (100.0)	1.000
Hemodialysis, *n* (%)	35 (92.1)	305 (85.9)	35 (94.6)	0.473
Peritoneal dialysis, *n* (%)	3 (7.9)	50 (14.1)	2 (5.4)	0.519
HD duration, months	62.9 ± 64.6	64.3 ± 66.6	55.0 ± 54.9	0.733
Second KT, *n* (%)	4 (10.5)	24 (6.8)	4 (10.8)	0.503
Post-KT comorbidities, *n* (%)				
New-onset HTN	3 (7.9)	15 (4.2)	1 (2.7)	0.504
Persistent HTN	9 (23.7)	103 (29.0)	21 (56.8)*#	0.001
New-onset DM	3 (7.9)	54 (15.3)	3 (8.1)	0.258
Renal dysfunction, *n* (%)	4 (10.5)	69 (19.4)	10 (27.0)	0.192
Graft failure, *n* (%)	10 (26.3)	33 (9.3)*	7 (18.9)	0.003
Post-KT medications, *n* (%)				
RAAS blocker	2 (5.2)	91 (30.3)*	3 (8.1)#	<0.001
Beta blocker	16 (43.2)	149 (49.5)	17 (45.9)	0.731
CCB	16 (34.0)	267 (33.7)	20 (37.0)	0.630
Diuretics	4 (10.8)	32 (10.8)	1 (2.7)	0.296
Statin	0 (0)	110 (36.9)*	4 (11.1)*#	<0.001

*$P < 0.05$ compared with the AR regression group.
#$P < 0.05$ compared with the AR unchanged group.
AR, aortic regurgitation; CAD, coronary artery disease; HD, hemodialysis; KT, kidney transplantation; HTN, hypertension; DM, diabetes mellitus; RAAS, renin-angiotensin-aldosterone system; CCB, calcium channel blocker.

TABLE 5 | Comparison of echocardiographic characteristics in the three groups according to change in aortic regurgitation.

	AR regression (n = 38)	AR unchanged (n = 355)	AR progression (n =37)	p-value
Pre-KT echocardiogram				
LVEDD, mm	55.6 ± 8.0	52.6 ± 6.1*	53.7 ± 4.5	0.018
LVESD, mm	36.4 ± 10.2	34.6 ± 6.5	32.9 ± 5.4	0.095
LVEF, %	58.7 ± 13.5	61.5 ± 9.9	63.4 ± 8.8	0.141
LV mass index, g/m^2	139.7 ± 55.8	127.0 ± 39.0	128.6 ± 34.4	0.195
LA volume index, ml/m^2	54.1 ± 29.8	38.5 ± 14.8*	45.3 ± 19.2	<0.001
E/e′	14.9 ± 6.9	12.7 ± 5.7	12.6 ± 5.1	0.113
PASP, mmHg	36.6 ± 11.2	30.0 ± 10.3	29.8 ± 9.1	0.006
Degree of AR, n (%)				<0.001
No/trivial	0 (0)	296 (83.4)*	35 (94.6)*	
Mild	34 (89.5)	47 (13.2)*	2 (5.4)*#	
Moderate	4 (10.5)	10 (2.8)*	0 (0)*	
Severe	0 (0)	2 (0.6)	0 (0)	
AV calcification, n (%)	4 (10.5)	33 (9.3)	8 (21.6)#	0.018
Post-KT echocardiogram				
LVEDD, mm	48.7 ± 6.7	48.8 ± 5.8	51.9 ± 4.7*#	0.008
LVESD. Mm	28.7 ± 5.5	30.7 ± 5.3	31.8 ± 5.1*	0.033
LVEF, %	66.5 ± 7.4	65.2 ± 8.2	63.1 ± 7.9	0.185
LV mass index, g/m^2	112.9 ± 34.9	111.8 ± 34.0	116.7 ± 31.7	0.706
LA volume index, ml/m^2	43.2 ± 18.6	35.0 ± 15.4*	44.0 ± 19.5#	<0.001
E/e′	12.0 ± 6.5	11.6 ± 4.7	14.7 ± 7.1	0.005
PASP, mmHg	33.1 ± 12.5	28.7 ± 9.9	31.0 ± 9.2	0.083
Degree of AR, n (%)				<0.001
No/trivial	34 (89.5)	296 (83.4)	0 (0)*#	
Mild	4 (10.5)	51 (14.4)	34 (91.9)*#	
Moderate	0 (0)	8 (2.2)	3 (8.1)*#	
Severe	0 (0)	0 (0)	0 (0)	
Changes after KT				
Δ LVEDD, mm	−4.5 ± 9.1	1.4 ± 9.7*	−1.1 ± 6.4	0.001
Δ LVESD, mm	−7.5 ± 9.8	−4.0 ± 6.0*	−1.2 ± 5.7*#	<0.001
Δ LVEF, %)	7.3 ± 13.6	3.7 ± 9.4	−0.2 ± 9.1*#	0.006
Δ E/e′	−3.6 ± 6.9	−1.3 ± 5.7	2.5 ± 5.6*	<0.001
Δ LV mass index, g/m^2	−30.4 ± 55.6	−14.3 ± 48.6	−11.2 ± 45.3	0.193
Δ LA volume index, ml/m^2	−13.4 ± 28.9	−5.7 ± 14.6*	0.2 ± 18.1*	0.004

*$P < 0.05$ compared with the AR regression group.
#$P < 0.05$ compared with the AR unchanged group.
AR, aortic regurgitation; LVEDD, left ventricular end-diastolic diameter; LVESD, left ventricular end-systolic diameter; LVEF, left ventricular ejection fraction; LV, left ventricle; LA, left atrium; E/e′, ratio of early diastolic mitral velocity to early diastolic mitral annular velocity; PASP; pulmonary arterial systolic pressure; AV, aortic valve.

TABLE 6 | Factors associated with progression of aortic regurgitation after KT.

	Univariate analysis			Multivariate analysis		
	B	t	p-value	B	t	p-value
Age	0.002	1.80	0.073	−0.002	−0.63	0.533
Female sex	0.040	1.47	0.142			
Hypertension	0.018	0.41	0.686			
Diabetes mellitus	0.028	0.97	0.331			
Dyslipidemia	−0.045	−1.13	0.190			
Atrial fibrillation	−0.043	−0.70	0.485			
CAD	−0.012	−0.30	0.766			
Heart failure	−0.010	−0.21	0.832			
HD duration	−0.042	−0.78	0.435			
New-onset HTN	−0.035	−0.53	0.594			
Second KT	0.042	0.82	0.415			
Persistent HTN	0.063	2.07	0.039	0.200	2.49	0.014
New-onset DM	−0.042	−1.08	0.282			
Renal dysfunction	0.043	1.25	0.214			
Graft failure	0.061	1.45	0.149			
AV calcification	0.330	2.66	0.009	0.274	0.12	0.029
Δ LVEDD	−0.002	−1.11	0.269			
Δ LVESD	0.006	2.73	0.007	0.010	2.01	0.046
Δ LVEF	−0.003	−2.46	0.014			
Δ LV mass index	0.027	0.52	0.603			
Δ LA volume index	0.002	2.21	0.028			

CAD, coronary artery disease; HD, hemodialysis; KT, kidney transplantation; HTN, hypertension; DM, diabetes mellitus; AV, aortic valve; LVEDD, left ventricular end-diastolic diameter; LVESD, left ventricular end-systolic diameter; LVEF, left ventricular ejection fraction; LV, left ventricle; LA, left atrium.

Study Limitations

First, this was a retrospective study and a significant number of patients were excluded because there was no echocardiographic follow-up within a specific time period after KT. Moreover, post-KT echocardiography was not performed according to the pre-specified period. However, we attempted to overcome these shortcomings by including a large number of patients from multiple centers who had undergone follow-up echocardiography between 6 and 36 months after KT.

Second, in this KT cohort, there were many cases of no or mild valve regurgitation before KT. If there was significant or severe valve regurgitation, it is possible that KT was postponed or not performed, and volume control by dialysis was attempted. Accordingly, there were many patients whose MR and AR did not change after KT. There was a limitation of the population in evaluating the dynamic change of AR and MR. Therefore, it is possible that we selected only relatively healthy ESRD patients. Nevertheless, we believe that we identified patient characteristics that reflect real clinical practice and the natural course of MR and AR.

Third, although we aimed to find factors that could influence progression of MR and AR, it is possible that some factors that were not investigated or that undetected confounding factors had an influence on the results.

CONCLUSIONS

Among patients undergoing KT, MR, and AR can progress in those patients with certain characteristics. Risk factors for progression of MR after KT include a second KT, MAC and a smaller decrease in LVESD after KT. Risk factors for progression of AR include valve calcification, persistent hypertension and a smaller decrease in LVESD after KT. Further echocardiographic

surveillance and risk factor management after KT are warranted in these patients.

DATA AVAILABILITY STATEMENT

The original contributions presented in the study are included in the article/**Supplementary Material**, further inquiries can be directed to the corresponding author.

ETHICS STATEMENT

The studies involving human participants were reviewed and approved by Institutional Review Board of the Yonsei University Health System (2021-0994-001). Written informed consent for participation was not required for this study in accordance with the national legislation and the institutional requirements.

AUTHOR CONTRIBUTIONS

MK reviewed the literature and wrote the first draft of the manuscript. CS supervised this paper, coordinated the multidisciplinary discussion, and critically reviewed the manuscript. DK provided the data of the Samsung medical center and reviewed the manuscript. JL, D-YK, JS, IC, KH, G-RH, and J-WH reviewed the manuscript, provided comments, and suggested modifications to the manuscript. All authors contributed to the article and approved the submitted version.

SUPPLEMENTARY MATERIAL

The Supplementary Material for this article can be found online at: https://www.frontiersin.org/articles/10.3389/fcvm.2022.809707/full#supplementary-material

REFERENCES

1. Marwick TH, Amann K, Bangalore S, Cavalcante JL, Charytan DM, Craig JC, et al. Chronic kidney disease and valvular heart disease: conclusions from a kidney disease: improving global outcomes (KDIGO) controversies conference. *Kidney Int.* (2019) 96:836–49. doi: 10.1016/j.kint.2019.06.025
2. Forman MB, Virmani R, Robertson RM, Stone WJ. Mitral anular calcification in chronic renal failure. *Chest.* (1984) 85:367–71. doi: 10.1378/chest.85.3.367
3. Straumann E, Meyer B, Misteli M, Blumberg A, Jenzer HR. Aortic and mitral valve disease in patients with end stage renal failure on long-term haemodialysis. *Br Heart J.* (1992) 67:236–9. doi: 10.1136/hrt.67.3.236
4. Samad Z, Sivak JA, Phelan M, Schulte PJ, Patel U, Velazquez EJ. Prevalence and outcomes of left-sided valvular heart disease associated with chronic kidney disease. *J Am Heart Assoc.* (2017) 6:44. doi: 10.1161/JAHA.117.006044
5. Cirit M, Ozkahya M, Cinar CS, Ok E, Aydin S, Akçiçek F, et al. Disappearance of mitral and tricuspid regurgitation in haemodialysis patients after ultrafiltration. *Nephrol Dial Transplant.* (1998) 13:389–92. doi: 10.1093/oxfordjournals.ndt.a027835
6. Abbott KC, Hshieh P, Cruess D, Agodoa LY, Welch PG, Taylor AJ, et al. Hospitalized valvular heart disease in patients on renal transplant waiting list: incidence, clinical correlates and outcomes. *Clin Nephrol.* (2003) 59:79–87. doi: 10.5414/CNP59079
7. Rangaswami J, Mathew RO, Parasuraman R, Tantisattamo E, Lubetzky M, Rao S, et al. Cardiovascular disease in the kidney transplant recipient: epidemiology, diagnosis and management strategies. *Nephrol Dial Transplant.* (2019) 34:760–73. doi: 10.1093/ndt/gfz053
8. Ponikowski P, Voors AA, Anker SD, Bueno H, Cleland JGF, Coats AJS, et al. (2016). ESC Guidelines for the diagnosis and treatment of acute and chronic heart failure: the task force for the diagnosis and treatment of acute and chronic heart failure of the European Society of Cardiology (ESC)Developed with the special contribution of the Heart Failure Association (HFA) of the ESC. *Eur Heart J.* (2016) 37:2129–200. doi: 10.1093/eurheartj/ehw128
9. Thomas ME, Blaine C, Dawnay A, Devonald MA, Ftouh S, Laing C, et al. The definition of acute kidney injury and its use in practice. *Kidney Int.* (2015) 87:62–73. doi: 10.1038/ki.2014.328
10. Cheitlin MD, Armstrong WF, Aurigemma GP, Beller GA, Bierman FZ, Davis JL, et al. ACC/AHA/ASE (2003). Guideline update for the clinical application of echocardiography: summary article. a report of the American College of Cardiology/American Heart Association Task Force on Practice Guidelines (ACC/AHA/ASE Committee to Update the (1997). Guidelines for the Clinical Application of Echocardiography). *J Am Soc Echocardiogr.* (2003). 16:1091–110. doi: 10.1016/S0894-7317(03)00685-0
11. Mitchell C, Rahko PS, Blauwet LA, Canaday B, Finstuen JA, Foster MC, et al. Guidelines for performing a comprehensive transthoracic echocardiographic examination in adults: recommendations from the american society of echocardiography. *J Am Soc Echocardiogr.* (2019) 32:1–64. doi: 10.1016/j.echo.2018.06.004
12. Zoghbi WA, Adams D, Bonow RO, Enriquez-Sarano M, Foster E, Grayburn PA, et al. Recommendations for noninvasive evaluation of native valvular regurgitation: a report from the American Society of Echocardiography Developed in collaboration with the society for cardiovascular magnetic resonance. *J Am Soc Echocardiogr.* (2017) 30:303–71. doi: 10.1016/j.echo.2017.01.007
13. Kim D, Shim CY, Hong GR, Jeong H, Ha JW. Morphological and functional characteristics of mitral annular calcification and their relationship to stroke. *PLoS ONE.* (2020) 15:e0227753. doi: 10.1371/journal.pone.0227753
14. Kohsaka S, Jin Z, Rundek T, Boden-Albala B, Homma S, Sacco RL, et al. Impact of mitral annular calcification on cardiovascular events in a multiethnic community: the Northern Manhattan Study. *JACC Cardiovasc Imag.* (2008) 1:617–23. doi: 10.1016/j.jcmg.2008.07.006
15. Lu ML, Gupta S, Romero-Corral A, Matejková M, De Venecia T, Obasare E, et al. Cardiac calcifications on echocardiography are associated with mortality and stroke. *J Am Soc Echocardiogr.* (2016) 29:1171–8. doi: 10.1016/j.echo.2016.08.020
16. Lu KC, Wu CC, Yen JF, Liu WC. Vascular calcification and renal bone disorders. *Sci World J.* (2014) 2014:637065. doi: 10.1155/2014/637065
17. Neale J, Smith AC. Cardiovascular risk factors following renal transplant. *World J Transpl.* (2015) 5:183–95. doi: 10.5500/wjt.v5.i4.183
18. Jesri A, Braitman LE, Pressman GS. Severe mitral annular calcification predicts chronic kidney disease. *Int J Cardiol.* (2008) 128:193–6. doi: 10.1016/j.ijcard.2007.05.015
19. Rahimi K, Mohseni H, Kiran A, Tran J, Nazarzadeh M, Rahimian F. et al. Elevated blood pressure and risk of aortic valve disease: a cohort analysis of 54 million UK adults. *Eur Heart J.* (2018) 39:3596–603. doi: 10.1093/eurheartj/ehy486

Conflict of Interest: The authors declare that the research was conducted in the absence of any commercial or financial relationships that could be construed as a potential conflict of interest.

frontiers in Cardiovascular Medicine

ORIGINAL RESEARCH
published: 18 February 2022
doi: 10.3389/fcvm.2022.844876

Hemodynamic Performance of Sutureless vs. Conventional Bioprostheses for Aortic Valve Replacement: The 1-Year Core-Lab Results of the Randomized PERSIST-AVR Trial

Theodor Fischlein[1†], Elena Caporali[2,3,4*†], Federico M. Asch[5], Ferdinand Vogt[1], Francesco Pollari[1], Thierry Folliguet[6], Utz Kappert[7], Bart Meuris[8], Malakh L. Shrestha[9], Eric E. Roselli[10], Nikolaos Bonaros[11], Olivier Fabre[12], Pierre Corbi[13], Giovanni Troise[14], Martin Andreas[15], Frederic Pinaud[16], Steffen Pfeiffer[1], Sami Kueri[17], Erwin Tan[18], Pierre Voisine[19], Evaldas Girdauskas[20], Filip Rega[8], Julio García-Puente[21], Laurent De Kerchove[22], Roberto Lorusso[4,23] and on behalf of the PERSIST-AVR Investigators[‡]*

[1] Cardiac Surgery, Klinikum Nürnberg, Paracelsus Medical University, Nuremberg, Germany, [2] Department of Cardiology, Istituto Cardiocentro Ticino, Lugano, Switzerland, [3] Department of Cardiac Surgery, Istituto Cardiocentro Ticino, Lugano, Switzerland, [4] Department of Cardio-Thoracic Surgery, Heart and Vascular Centre, Maastricht University Medical Centre (MUMC+), Maastricht, Netherlands, [5] MedStar Health Research Institute, Washington Hospital Center, Washington D.C., DC, United States, [6] Cardiac Surgery Unit, Hôpital Henri Mondor, Université Paris 12, Créteil, France, [7] Herzzentrum Dresden GmbH Universitätsklinik, Dresden, Germany, [8] Cardiac Surgery Unit, UZ Gasthuisberg Leuven, Leuven, Belgium, [9] Cardiothoracic and Vascular Surgery, Hannover Medical School, Hannover, Germany, [10] Heart, Vascular and Thoracic Institute, Cleveland Clinic, Cleveland, OH, United States, [11] Department of Cardiac Surgery, Medical University of Innsbruck, Innsbruck, Austria, [12] Lens Hospital and Bois Bernard Private Hospital, Lens, France, [13] Poitiers University Hospital, Poitiers, France, [14] Fondazione Poliambulanza Istituto Ospedaliero, Brescia, Italy, [15] Department of Cardiac Surgery, Medical University of Vienna, Vienna, Austria, [16] Department of Cardiac Surgery, University Hospital Angers, Angers, France, [17] University Heart Center Freiburg, Bad Krozingen, Germany, [18] Catharina Ziekenhuis, Eindhoven, Netherlands, [19] Division of Cardiac Surgery, Quebec Heart and Lung Institute, Quebec, QC, Canada, [20] University Heart Center Hamburg, Universitätsklinikum Hamburg Eppendorf (UKE), Hamburg, Germany, [21] University General Hospital Virgen de la Arrixaca, Murcia, Spain, [22] Cliniques Universitaires Saint-Luc (UCL), Bruxelles, Belgium, [23] Cardiac Surgery, Cardiovascular Research Institute Maastricht (CARIM), Maastricht, Netherlands

Objective: Sutureless aortic valves are an effective option for aortic valve replacement (AVR) showing non-inferiority to standard stented aortic valves for major cardiovascular and cerebral events at 1-year. We report the 1-year hemodynamic performance of the sutureless prostheses compared with standard aortic valves, assessed by a dedicated echocardiographic core lab.

Methods: Perceval Sutureless Implant vs. Standard Aortic Valve Replacement (PERSIST-AVR) is a prospective, randomized, adaptive, open-label trial. Patients undergoing AVR, as an isolated or combined procedure, were randomized to receive a sutureless [sutureless aortic valve replacement (Su-AVR)] (n = 407) or a stented sutured [surgical AVR (SAVR)] (n = 412) bioprostheses. Site-reported echocardiographic examinations were collected at 1 year. In addition, a subgroup of the trial population (Su-AVR n = 71, SAVR = 82) had a complete echocardiographic examination

OPEN ACCESS

Edited by:
Elena Aikawa,
Brigham and Women's Hospital and Harvard Medical School, United States

Reviewed by:
Michael Hofmann,
University of Zurich, Switzerland
Maruti Haranal,
National Heart Institute, Malaysia
Mohammed Idhrees,
SIMS Hospital, India

***Correspondence:**
Theodor Fischlein
theodor.fischlein@klinikum-nuernberg.de
Elena Caporali
elena.caporali@eoc.ch

[†]These authors have contributed equally to this work and share first authorship
[‡]PERSIST-AVR Investigators reported in Supplementary Material

Specialty section:
This article was submitted to Heart Valve Disease, a section of the journal Frontiers in Cardiovascular Medicine

Received: 28 December 2021
Accepted: 21 January 2022
Published: 18 February 2022

Citation:
Fischlein T, Caporali E, Asch FM, Vogt F, Pollari F, Folliguet T, Kappert U, Meuris B, Shrestha ML, Roselli EE, Bonaros N, Fabre O, Corbi P, Troise G, Andreas M, Pinaud F, Pfeiffer S, Kueri S, Tan E, Voisine P, Girdauskas E, Rega F, García-Puente J, De Kerchove L, Lorusso R and on behalf of the PERSIST-AVR Investigators (2022) Hemodynamic Performance of Sutureless vs. Conventional Bioprostheses for Aortic Valve Replacement: The 1-Year Core-Lab Results of the Randomized PERSIST-AVR Trial. Front. Cardiovasc. Med. 9:844876. doi: 10.3389/fcvm.2022.844876

independently assessed by a Core Lab (MedStar Health Research Institute, Washington D.C., USA) for the evaluation of the hemodynamic performance.

Results: The site-reported hemodynamic data of stented valves and sutureless valves are stable and comparable during follow-up, showing stable reduction of mean and peak pressure gradients through one-year follow-up (mean: 12.1 ± 6.2 vs. 11.5 ± 4.6 mmHg; peak: 21.3 ± 11.4 vs. 22.0 ± 8.9 mmHg). These results at 1-year are confirmed in the subgroup by the core-lab assessed echocardiogram with an average mean and peak gradient of 12.8 ± 5.7 and 21.5 ± 9.1 mmHg for Su-AVR, and 13.4 ± 7.7 and 23.0 ± 13.0 mmHg for SAVR. The valve effective orifice area was 1.3 ± 0.4 and 1.4 ± 0.4 cm^2 at 1-year for Su-AVR and SAVR. These improvements are observed across all valve sizes. At 1-year evaluation, 91.3% ($n = 42$) of patients in Su-AVR and 82.3% in SAVR ($n = 51$) groups were free from paravalvular leak (PVL). The rate of mild PVL was 4.3% ($n = 2$) in Su-AVR and 12.9% ($n = 8$) in the SAVR group. A similar trend is observed for central leak occurrence in both core-lab assessed echo groups.

Conclusion: At 1-year of follow-up of a PERSIST-AVR patient sub-group, the study showed comparable hemodynamic performance in the sutureless and the stented-valve groups, confirmed by independent echo core lab. Perceval sutureless prosthesis provides optimal sealing at the annulus with equivalent PVL and central regurgitation extent rates compared to sutured valves. Sutureless valves are therefore a reliable and essential technology within the modern therapeutic possibilities to treat aortic valve disease.

Keywords: aortic stenosis, aortic valve replacement, sutureless aortic valves, stented bioprostheses, randomized trial

INTRODUCTION

Aortic valve stenosis is the most common valvular heart disease in adults. The early recognition and management of this pathology are very important because untreated asymptomatic and symptomatic severe diseases result in poor outcomes if managed with conservative treatment. In these patients, therefore, aortic valve replacement (AVR) represents the treatment of choice (1–4). New prostheses have been developed to minimize the surgical risk in patients with multiple comorbidities and to reduce operating times. Sutureless prostheses have shown promising results in terms of mortality, morbidity, and hemodynamic performance (5–7). Several studies have demonstrated that sutureless valves decrease the cardiopulmonary bypass (CPB) and aortic cross-clamping (ACC) times, facilitating minimally and conventional invasive cardiac surgery (5–8), but no randomized controlled trials have directly compared this technology with traditional stented valves (9). Recently, the Perceval Sutureless Implant vs. Standard AVR (PERSIST-AVR) trial has been published with overall 1-year results demonstrating no substantial difference between sutureless vs. conventional tissue valves for isolated or combined surgical AVR (SAVR) (10, 11). The present study addressed the hemodynamic performance at 1 year in the sutureless and the stented-valve groups, in a limited patient subgroup analyzed by the enrollment sites and by an independent echo core lab.

METHODS

Details about the design of the PERSIST-AVR trial have been previously published (10). The PERSIST-AVR trial is a multicenter, prospective, randomized, open-label, noninferiority trial with an adaptive design, conceived to demonstrate the noninferiority of the Perceval sutureless prosthesis compared with standard stented aortic bioprostheses in patients with severe symptomatic aortic valve stenosis. The study was approved by the local Ethical Committees and Institutional Review Boards (IRB: local no. METC151138, national no. NL56524.068), and the participants gave written informed consent before enrolment in the study.

From March 2016 to September 2018, adult patients with severe symptomatic aortic valve stenosis who were candidates for isolated or combined SAVR procedure for native aortic valve disease were prospectively enrolled at 47 international centers and randomized (1:1 blocked randomization) with the Perceval sutureless valve (Perceval, Corcym S.r.l., Saluggia, Italy) or a standard stented aortic bioprosthesis (selected on the basis of surgeon's discretion).

Abbreviations: ACC, aortic cross-clamping; CPB, cardiopulmonary bypass; PERSIST-AVR, PERceval Sutureless Implant vs. Standard Aortic Valve Replacement; SAVR, surgical aortic valve replacement; Su-AVR, sutureless aortic valve replacement; EOA, effective orifice area; EOAi, effective orifice area index.

Clinical and echocardiographic follow-up was performed at hospital discharge, between 1 and 3 months, and at 1 year. Site-reported echocardiographic examinations were collected and, in addition, a subgroup of the trial population had a complete echocardiographic examination independently assessed by a Core Lab (MedStar Health Research Institute, Washington D.C., USA) for the evaluation of the hemodynamic performance. Peak and mean aortic gradients were obtained by using Continuous Wave Doppler (CW) using the simplified Bernoulli equation.

Statistical Analysis

Analyses were conducted on the per-protocol population (excluding patients with Major Deviation) (10, 11) with Core-lab assessed data.

Descriptive statistics have been calculated, using as reference the number of subjects in the relevant analysis population according to the nature of each parameter as follows: categorical variables are reported as absolute and relative frequencies; for quantitative (continuous) parameters, a number of subjects with available and missing data, mean, standard deviation (SD), median, quartiles (Q1-Q3), and extreme values [Minimum; Maximum] are reported. The aortic mean and peak pressure gradients (P2) were also analyzed considering the left ventricular outflow tract (LVOT) gradients (P1) and calculated using the modified Bernoulli equation (P2-P1).

RESULTS

A total of 914 patients were enrolled, and 910 underwent randomization at 47 international centers. The population in the primary outcome analysis (per protocol) involved 819 patients, 407 in the sutureless group and 412 in the stented group (11).

The subgroup of the trial per-protocol population with complete echocardiographic examination independently assessed by a Core Lab comprises 71 patients implanted with Perceval sutureless prosthesis and 82 implanted with a stented valve; patients were selected according to the site capability to follow the echo core lab protocol by the study.

Preoperative patient profiles and operative characteristics demonstrated no differences in pre-operative risk (EUROSCORE II/STS SCORE) and baseline characteristics between patients implanted with the Perceval sutureless prosthesis and the stented valve cohorts (**Tables 1**, **2**). A mini-sternotomy approach was used in 49.3% of the Perceval group and 51.2% of the stented group; the number of concomitant procedures was also well balanced between the two cohorts (**Table 3**).

The site-reported hemodynamic data of the stented valves and sutureless valves were comparable at one-year follow-up (**Table 4**).

These results at 1 year are confirmed in the subgroup of core-lab assessed echo (**Table 5**), with an average mean and peak gradient at 1 year of 12.8 ± 5.7 and 21.5 ± 9.1 mmHg for sutureless AVR (Su-AVR), and 13.4 ± 7.7 and 23.0 ± 13.0 mmHg for SAVR. Valve effective orifice area was 1.3 ± 0.4 and 1.4 ± 0.4 cm^2 at 1 year for Su-AVR and SAVR. These improvements are observed across all valve sizes (more details in the **Supplementary Material**). At 1-year evaluation, 91.3% (n = 42) of the patients in the Su-AVR group and 82.3% in the SAVR group (n = 51) were free from paravalvular leak (PVL), while 87.0% (n = 40) of the patients in the Su-AVR group and 82.3% in the SAVR group (n = 51) were free from a central leak. The rate of mild PVL was 4.3% (n = 2) in the Su-AVR and 12.9% (n = 8) in the SAVR group, respectively.

TABLE 1 | Patients' baseline characteristics.

	PERCEVAL (n = 71)	STENTED (n = 82)	p-value
Age (y)	74.7 ± 5.7	74.7.0 ± 4.5	>0.05
Female sex	32 (45.1%)	35 (42.7%)	>0.05
Hypertension	53 (74.6%)	68 (82.9%)	>0.05
Dyslipidemia	40 (56.3%)	57 (69.5%)	>0.05
Diabetes	20 (28.2%)	23 (28.0%)	>0.05
Tobacco user	12 (16.9%)	28 (34.1%)	<0.05
Chronic lung disease	5 (7.0%)	5 (6.1%)	>0.05
Pulmonary hypertension	1 (1.4%)	2 (2.4%)	>0.05
Neoplasia	7 (9.9%)	4 (4.9%)	>0.05
Peripheral vascular disease	6 (8.5%)	9 (11.0%)	>0.05
Carotid artery disease	3 (4.2%)	9 (11.0%)	>0.05
Angina	7 (9.9%)	6 (7.3%)	>0.05
Coronary artery disease	28 (39.4%)	29 (35.4%)	>0.05
Previous PCI	5 (7.0%)	11 (13.4%)	>0.05
Myocardial infarction	3 (4.2%)	3 (3.7%)	>0.05
Heart failure	1 (1.4%)	2 (2.4%)	>0.05
Transient ischemic attack	1 (1.4%)	0 (0.0%)	>0.05
Stroke	4 (5.6%)	3 (3.7%)	>0.05
Previous CABG	1 (1.4%)	1 (1.2%)	>0.05
Pre-existing pacemaker	1 (1.4%)	1 (1.2%)	>0.05
STS score	2.5 ± 2.2	2.1 ± 1.3	>0.05
EuroSCORE II	1.9 ± 1.1	1.8 ± 1.1	>0.05

Values are mean ± standard deviation, n (%).
PCI, percutaneous coronary intervention. CABG, coronary artery bypass graft. STS, society of thoracic surgeons.

TABLE 2 | Preoperative echocardiographic features.

	PERCEVAL (n = 71)	STENTED (n = 82)	p-value
Mean pressure gradient (mmHg)	52.1 ± 15.2	46.6 ± 11.3	0.0146
Peak pressure gradient (mmHg)	82.7 ± 24.9	75.8 ± 17.5	0.0575
Effective orifice area (cm^2)	0.7 ± 0.2	0.7 ± 0.2	1.0000
Left Ventricular Ejection Fraction (%)	59.9 ± 10.7	60.7 ± 9.6	>0.05

Values are mean ± standard deviation, n (%).

DISCUSSION

This is a sub-analysis of the first randomized, controlled study (PERSIST-AVR trial) comparing sutureless vs. conventional stented bioprostheses for isolated SAVR (10, 11). On-site and core-lab echocardiographic findings, in a limited patient subgroup, were assessed and compared regarding hemodynamic performances and prosthesis-related regurgitation. The primary endpoint of this study demonstrates that the hemodynamic data

TABLE 3 | Intraoperative characteristics.

	PERCEVAL ($n = 71$)	STENTED * ($n = 82$)	*p*-value
Full sternotomy	36 (50.7%)	40 (48.8%)	1.000
Ministernotomy	35 (49.3%)	42 (51.2%)	1.000
Bicuspid aortic valve†	12 (16.9%)	9 (11.0%)	0.4084
Concomitant CABG	20 (28.2%)	24 (29.3%)	1.000
Concomitant Septal myectomy	6 (8.5%)	4 (4.9%)	0.5117
Concomitant Aortic annulus enlargement	0 (0.0%)	1 (1.2%)	1.000
Concomitant AF treatment and PFO closure	5 (7.0%)	6 (7.3%)	1.000
Valve size			
S (21 mm)	7 (9.9%)	NA	
M (23 mm)	21 (29.6%)	NA	
L (25 mm)	30 (42.3%)	NA	
XL (27 mm)	13 (18.3%)	NA	
19 mm	NA	1 (1.2%)	
21 mm	NA	24 (29.3%)	
23 mm	NA	37 (45.1%)	
25 mm	NA	17 (20.7%)	
27 mm	NA	3 (3.7%)	
Total mean valve size	24.4 ± 1.8	22.9 ± 1.7	

Values are mean ± standard deviation, n (%). † *Sievers type 1 only allowed per protocol. NA, not applicable. CABG, coronary artery bypass graft. AF, atrial fibrillation. PFO, patent foramen ovale.* * *Stented valve model described in* ***Supplementary Material***.

TABLE 4 | Hemodynamic data up to 1-year visit (site-reported).

	1 year		*p*-value
	PERCEVAL	STENTED	
Mean Gradient (mmHg)	11.5 ± 4.6	12.1 ± 6.2	0.6092
Peak Gradient (mmHg)	22.0 ± 8.9	21.3 ± 11.4	0.6961
EOA (cm^2) (mean±SD)	1.6 ± 0.5	1.8 ± 0.6	0.0569
EOAi (cm^2/m^2) (mean±SD)	0.9 ± 0.2	0.9 ± 0.3	1.0000
Left ventricular ejection fraction (mean±SD)	62.1 ± 8.1	61.1 ± 8.4	0.4964
Left ventricular mass (g) (mean±SD)	198.8 ± 75.9	202.1 ± 74.8	0.8223
Paravalvular leak	$N = 63$	$N = 74$	1.000
None/Trace	61 (96.8)	71 (95.9)	
Mild	2 (3.2)	2 (2.7)	
Moderate/Severe	0 (0.0)	1 (1.4)	
Central leak	$N = 63$	$N = 74$	0.7101
None/Trace	62 (98.4)	73 (98.6)	
Mild	1 (1.6)	0 (0.0)	
Moderate/Severe	0 (0.0)	1 (1.4)	

Values are mean ± standard deviation, n (%). EOA, effective orifice area index. EOAi, effective orifice area index indexed to body surface area.

of stented valves and sutureless valves were comparable up to 1-year follow-up, showing a stable reduction of mean and peak pressure gradients through 1-year follow-up. Furthermore, as a secondary endpoint, no difference in terms of para-valvular or central valve regurgitation was found between groups.

The use of sutureless bioprostheses has been widely reported to reduce procedure times in aortic valve replacement, both with conventional or minimally invasive approaches (6–8). Despite the extensive experience with Su-AVR (5–8, 12), no randomized, prospective, controlled studies have been performed comparing conventional vs. sutureless-based AVR. Based on this lack, the PERSIST-AVR trial, consisting of a prospective, randomized controlled study in patients undergoing isolated AVR or combined procedure with sutureless or stented bioprostheses, was conducted in 47 centers worldwide (10). The one-year results have shown non-inferiority between Su-AVR and SAVR regarding Major Adverse Cardiac and Cerebrovascular Events (MACCE) at 1-year follow-up (11). However, besides general and main clinical outcomes, several other aspects have been addressed by the PERSIST-AVR trial, including valve hemodynamic assessment at discharge and during the follow-up, with programmed postoperative consultation (10). These investigations included valve-related hemodynamic assessment, also addressing the incidence and extent of implanted bioprosthesis-related regurgitation, already highlighted by the Registry-based analysis (9). Indeed, as well-known, trans-catheter valves, due to the lack of suture-based implantation, may experience the presence of various ranges of valvular regurgitation, mostly para-valvular, but also centrally located. This complication has affected mainly percutaneous trans-catheter valve implantation but has been observed also in the surgical approach with rapid deployment and sutureless prosthesis (9). The reasons for such post-implant regurgitation account for the presence of uneven surface that can lead to PVL or for an incomplete annular sealing due to incorrect valve sizing and also partially retained and unresected calcification (in Su-AVR procedures) (13, 14). As a matter of fact, such a hemodynamic dysfunction has never been shown to be of substantial importance after Su-AVR, but a large Registry analysis has recently shown not-reassuring data about this phenomenon in sutureless valves. The present analysis demonstrated that sutureless valve implantation is associated with a similar rate and extent of either paravalvular or central regurgitation compared to stented bioprostheses. A recent study (6) demonstrated satisfactory hemodynamic performance with the Perceval sutureless bioprosthesis with a stable reduction in gradients in all valve sizes and a stable increase in the valve-effective orifice area, with significant regression in the left ventricular (LV) mass throughout the 5 years of follow-up. Moreover, a low incidence of PVL was reported, showing that the sutureless valve ensures correct sealing at the level of the aortic annulus. Similar results have also been shown (8) in a huge cohort of patients treated with Perceval sutureless prosthesis implanted through a right anterior mini-thoracotomy approach. Mean pressure gradients and LV mass, as well as the diameters, decreased significantly from preoperative values to follow-up. Moderate PVL occurred in one patient only from the sub-group, without hemolysis or symptoms, and therefore not requiring treatments.

Same excellent hemodynamic performances are coming from the largest single-center cohort of patients with the

TABLE 5 | Hemodynamic data up to 1-year visit (core-lab assessed).

	1 year		*p*-value
	PERCEVAL	**STENTED**	
Mean Gradient [mmHg] (P2)	12.8 ± 5.7	13.4 ± 7.7	0.6445
Peak Gradient [mmHg] 4(VAO)2	21.5 ± 9.1	23.0 ± 13.0	0.4854
Mean Gradient [mmHg] (P2 -P1)	10.0 ± 5.3	11.1 ± 6.8	0.3881
Peak Gradient [mmHg] 4(V2A-V2L)	16.7 ± 8.2	19.2 ± 11.8	0.2371
EOA (cm^2) (mean±SD)	1.3 ± 0.4	1.4 ± 0.4	0.3069
EOAi (cm^2/m^2) (mean±SD)	0.7 ± 0.2	0.7 ± 0.2	1.0000
Left ventricular ejection fraction (mean±SD)	63.0 ± 5.5	64.0 ± 5.6	0.5567
Left ventricular mass (g) (mean±SD)	163.8 ± 45.5	175.2 ± 45.1	0.3883
Left ventricular mass index (g/m^2) (mean±SD)	91.0 ± 17.6	91.2 ± 21.4	0.9711
Paravalvular leak	*N* = 46	*N* = 62	0.3148
None/Trace	42 (91.3)	51 (82.3)	
Mild	2 (4.3)	8 (12.9)	
Moderate/Severe	0 (0.0)	0 (0.0)	
Not evaluable	2 (4.3)	3 (4.8)	
Central leak	*N* = 46	*N* = 62	0.8419
None/Trace	40 (87.0)	51 (82.3)	
Mild	4 (8.7)	8 (12.9)	
Moderate/Severe	0 (0.0)	0 (0.0)	
Not evaluable	2 (4.3)	3 (4.8)	

Values are mean ± standard deviation, n (%). EOA, effective orifice area. EOAi, effective orifice area index indexed to body surface area. Peak and mean aortic gradients were obtained by using Continuous Wave Doppler (CW) using the simplified Bernoulli equation.

Perceval sutureless bioprosthesis. The mean pressure gradient, the LV ejection fraction, and mass decreased significantly from the preoperative value to follow-up ($p < 0.001$). Moderate paravalvular leakage occurred in only 3 patients without hemolysis who did not require any treatment; while the other 2 patients with paravalvular leak were reoperated for incomplete expansion of the bioprosthesis (12).

Regarding the overall hemodynamic performance, the PERSIST-AVR findings, at 1-year from the surgical procedure, have shown an effective reduction of transvalvular aortic gradients, with a progressive improvement from hospital discharge to 1-year follow-up, and no significant difference between the sutureless and the sutured groups.

The use of core-lab investigation may play a critical role in such investigations, providing an independent assessment from individual site analysis. The analysis of a subgroup of PERSIST-AVR patients with such an independent assessment showed, notably, no difference, also in terms of prosthesis-related leakage, either paravalvular or central.

Continued investigations are warranted to further and more thoroughly explain these outcomes in the sutureless valve cohort.

Limits of the Study

The findings of this controlled, randomized study were obtained through a multicenter, worldwide study representing a wide clinical experience. The choice of the stented valve was at the discretion of the operating physician, and the surgical techniques or influence of specific tissue valves employed was not considered in this sub-analysis, for which a limited number of patients were enrolled. Furthermore, the original study was not powered for this *ad hoc* analysis, and a limited number of patients were included in the core-lab assessment.

CONCLUSION

This study showed comparable 1-year hemodynamic performances in the sutureless and stented-valve groups, confirmed by an independent echo core lab. Perceval sutureless bioprosthesis provides optimal sealing at the annulus site with equivalent PVL rates of sutured valves. Sutureless valves are a reliable and essential technology in modern therapeutic options for the treatment of aortic valve disease. No difference was found with regards to central or paravalvular regurgitation, although a favorable trend was shown in the sutureless valve, indicating a correct sealing at the aortic annulus.

DATA AVAILABILITY STATEMENT

The raw data supporting the conclusions of this article will be made available by the authors, without undue reservation.

ETHICS STATEMENT

The study was reviewed and approved by the local Ethical Committees and Institutional Review Boards (IRB: Local No. METC151138, National No. NL56524.068) and the participants gave written informed consent before enrolment to participate in the study.

AUTHOR CONTRIBUTIONS

TFi, EC, and RL designed the research and have been accountable for its supervision. TFi, EC, FA, FV, FPo, and TFo analyzed and interpreted the data and wrote the paper. UK, BM, MS, and ER provided assistance on data curation. NB, OF, PC, and GT provided intellectual inputs to the clinical study. MA, FPi, and SP have been accountable for the methodology. SK, ET, PV, and EG generated clinical statistics data. FR, JG-P, and LD provided technical assistance. All authors contributed to the article and approved the submitted version.

FUNDING

The PERSIST-AVR Trial is funded by Corcym S.r.l.

SUPPLEMENTARY MATERIAL

The Supplementary Material for this article can be found online at: https://www.frontiersin.org/articles/10.3389/fcvm.2022.844876/full#supplementary-material

REFERENCES

1. Banovic M, Putnik S, Penicka M, Doros G, Deja MA, Kockova R, et al. Aortic Valve ReplAcemenT versus Conservative Treatment in Asymptomatic SeveRe Aortic Stenosis: The AVATAR Trial. *Circulation*. (2021). doi: 10.1161/CIRCULATIONAHA.121.057639. [Epub ahead of print].
2. Taniguchi T, Morimoto T, Shiomi H, Ando K, Kanamori N, Murata K, et al. Initial surgical versus conservative strategies in patients with asymptomatic severe aortic stenosis. *J Am Coll Cardiol.* (2015) 66:2827–38. doi: 10.1016/j.jacc.2015.10.001
3. Kang DH, Park SJ, Lee SA, Lee S, Kim DH, Kim HK, et al. Early surgery or conservative care for asymptomatic aortic stenosis. *N Engl J Med.* (2020) 382:111–9. doi: 10.1056/NEJMoa1912846
4. Vahanian A, Beyersdorf F, Praz F, Milojevic M, Baldus S, Bauersachs J, et al. 2021 ESC/EACTS Guidelines for the management of valvular heart disease. *Eur J Cardiothorac Surg.* (2021) 60:727–800. doi: 10.1093/ejcts/ezab389
5. Szecel D, Eurlings R, Rega F, Verbrugghe P, Meuris B. Perceval sutureless aortic valve implantation: midterm outcomes. *Ann Thorac Surg.* (2021) 111:1331–7. doi: 10.1016/j.athoracsur.2020.06.064
6. Fischlein T, Meuris B, Folliguet T, Hakim-Meibodi K, Misfeld M, Carrel T, et al. Midterm outcomes with a sutureless aortic bioprosthesis in a prospectivemulticenter cohort study. *J Thorac Cardiovasc Surg*. (2021) S0022-5223(21)00001-5. doi: 10.1016/j.jtcvs.2020.12.109
7. Glauber M, Di Bacco L, Cuenca J, Di Bartolomeo R, Baghai M, Zakova D, et al. Minimally invasive aortic valve replacement with sutureless valves: results from an international prospective registry. *Innovations (Phila).* (2020) 15:120–30. doi: 10.1177/1556984519892585
8. Solinas M, Bianchi G, Chiaramonti F, Margaryan R, Kallushi E, Gasbarri T, et al. Right anterior mini-thoracotomy and sutureless valves: the perfect marriage. *Ann Cardiothorac Surg.* (2020) 9:305–13. doi: 10.21037/acs-2019-surd-172
9. Ensminger S, Fujita B, Bauer T, Möllmann H, Beckmann A, Bekeredjian R, et al. Rapid deployment versus conventional bioprosthetic valve replacement for aortic stenosis. *J Am Coll Cardiol.* (2018) 71:1417–28. doi: 10.1016/j.jacc.2018.01.065
10. Lorusso R, Folliguet T, Shrestha M, Meuris B, Kappetein AP, Roselli E, et al. Sutureless versus Stented Bioprostheses for Aortic Valve Replacement: the randomized PERSIST-AVR study design. *Thorac Cardiovasc Surg.* (2020) 68:114–23. doi: 10.1055/s-0038-1675847
11. Fischlein T, Folliguet T, Meuris B, Shrestha ML, Roselli EE, McGlothlin A, et al. Sutureless versus conventional bioprostheses for aortic valve replacement in severe symptomatic aortic valve stenosis. *J Thorac Cardiovasc Surg.* (2021) 161:920–32. doi: 10.1016/j.jtcvs.2020.11.162
12. Concistrè G, Chiaramonti F, Bianchi G, Cerillo A, Murzi M, Margaryan R, et al. Aortic Valve Replacement With Perceval Bioprosthesis: Single-Center Experience With 617 Implants. *Ann Thorac Surg.* (2018) 105:40–6. doi: 10.1016/j.athoracsur.2017.05.080
13. Ferrari E, Siniscalchi G, Tozzi P, von Segesser L. Aortic annulus stabilization technique for rapid deployment aortic valve replacement. *Innovations (Phila).* (2015) 10:360–2. doi: 10.1097/imi.0000000000000192
14. Hori D, Yamamoto T, Kusadokoro S, Fujimori T, Mieno MN, Kimura N, et al. Evaluation of oversizing in association with conduction disorder after implantation of a rapid deployment valve. *J Artif Organs.* (2021). doi: 10.1007/s10047-021-01301-4. [Epub ahead of print].

Conflict of Interest: UK was employed by Herzzentrum Dresden GmbH Universitätsklinik. This study received funding from Corcym S.r.l. The funder had the following involvement with the study: all trial-related activities and participated in site selection, data monitoring, trial management, and statistical analysis. TFi: consultant CORCYM and BioStable. TFo: consultant CORCYM (Steering Committee). BM and MS: consultant CORCYM Steering Committee and Proctor. ER: consultant CORCYM (Steering Committee and Proctor), speaker for Abbott, consultant, speaker and investigator for Edwards and Medtronic. NB: educational grants: Edwards Lifesciences and CORCYM, Speaker Honoraria: Edwards Lifesciences, CORCYM and Medtronic. OF, GT, SP, SK, JG-P: consultant CORCYM (Proctor). MA: consultant Abbott and Edwards (Proctor), advisor Medtronic. FR: consultant CORCYM and AtriCure (Proctor), Research Support Recipient Medtronic. RL: Consultant Medtronic, LivaNova, CORCYM and Getinge (honoraria paid to the Maastricht University) and Member of the Medical Advisory Board for Eurosets (honoraria paid to the Maastricht University). FA has no personal conflict of interest but directs an academic Core laboratory carrying institutional contracts (MedStar Health) for his work with Corcym/Livanova, Edwards, Medtronic, Boston Scientific, Abbott, Foldax, Biotronik.

The remaining authors declare that the research was conducted in the absence of any commercial or financial relationships that could be construed as a potential conflict of interest.

Publisher's Note: All claims expressed in this article are solely those of the authors and do not necessarily represent those of their affiliated organizations, or those of the publisher, the editors and the reviewers. Any product that may be evaluated in this article, or claim that may be made by its manufacturer, is not guaranteed or endorsed by the publisher.

frontiers in Cardiovascular Medicine

REVIEW
published: 21 February 2022
doi: 10.3389/fcvm.2022.836441

Functional Tricuspid Regurgitation: Behind the Scenes of a Long-Time Neglected Disease

Mattia Vinciguerra[1]*, *Marta Sitges*[2,3,4], *Jose Luis Pomar*[5,6], *Silvia Romiti*[1], *Blanca Domenech-Ximenos*[3,7], *Mizar D'Abramo*[1], *Eleonora Wretschko*[1], *Fabio Miraldi*[1] *and Ernesto Greco*[1]

[1] Department of Clinical, Internal Medicine, Anesthesiology and Cardiovascular Sciences, Sapienza University of Rome, Rome, Italy, [2] Cardiovascular Institute, Hospital Clinic, University of Barcelona, Barcelona, Spain, [3] Institut D'Investigacions Biomèdiques August Pi i Sunyer (IDIBAPS), Barcelona, Spain, [4] Centro de Investigación Biomédica en Red (CIBERCV), Instituto de Salud Carlos III, Madrid, Spain, [5] Department of Cardiac Surgery, Clinic Barcelona Hospital University, Barcelona, Spain, [6] Department of Cardiac Surgery, Barnaclinic, Barcelona, Spain, [7] Department of Radiology, Hospital Clínic, Barcelona, Spain

Severe tricuspid valve regurgitation has been for a long time a neglected valve disease, which has only recently attracted an increasing interest due to the notable negative impact on the prognosis of patients with cardiovascular disease. It is estimated that around 90% of tricuspid regurgitation is diagnosed as "functional" and mostly secondary to a primary left-sided heart disease and, therefore, has been usually interpreted as a benign condition that did not require a surgical management. Nevertheless, the persistence of severe tricuspid regurgitation after left-sided surgical correction of a valve disease, particularly mitral valve surgery, has been associated to adverse outcomes, worsening of the quality of life, and a significant increase in mortality rate. Similar results have been found when the impact of isolated severe tricuspid regurgitation has been studied. Current knowledge is shifting the "functional" categorization toward a more complex and detailed pathophysiological classification, identifying various phenotypes with completely different etiology, natural history and, potentially, an invasive management. The aim of this review is to offer a comprehensive guide for clinicians and surgeons with a systematic description of "functional" tricuspid regurgitation subtypes, an analysis centered on the effectiveness of existing surgical techniques and a focus on the emergent percutaneous procedures. This latter may be an attractive alternative to a standard surgical approach in patients with high-operative risk or isolated tricuspid regurgitation.

Keywords: functional tricuspid regurgitation, right ventricle, annuloplasty, transcatheter approach, prosthetic ring

OPEN ACCESS

Edited by:
Luca Testa,
IRCCS San Donato Polyclinic, Italy

Reviewed by:
Antonio Popolo Rubbio,
IRCCS San Donato Polyclinic, Italy
Alexander Sedaghat,
University Hospital Bonn, Germany

***Correspondence:**
Mattia Vinciguerra
mattia_vinciguerra@libero.it

Specialty section:
This article was submitted to Heart Valve Disease, a section of the journal Frontiers in Cardiovascular Medicine

Received: *15 December 2021*
Accepted: *24 January 2022*
Published: *21 February 2022*

Citation:
Vinciguerra M, Sitges M, Luis Pomar J, Romiti S, Domenech-Ximenos B, D'Abramo M, Wretschko E, Miraldi F and Greco E (2022) Functional Tricuspid Regurgitation: Behind the Scenes of a Long-Time Neglected Disease. Front. Cardiovasc. Med. 9:836441. doi: 10.3389/fcvm.2022.836441

INTRODUCTION

Right ventricle (RV) overload and tricuspid annular (TA) dilatation have been identified from the outset as the main causes in the pathogenesis of tricuspid regurgitation (TR) following left heart valvular disease (LHVD). The absence of primary abnormalities of the valvular apparatus has led TR, from the earliest studies, to be approached as of a "functional" nature mediated by pressure and volume overload that affect the geometry of RV, right atrium (RA), and TA (1, 2).

In a simplistic manner, an inadequate systolic closure in the presence of a structurally normal valvular apparatus may define the functional TR (FTR). The complexity emerges when leaflet coaptation is assessed in the setting of the disease, with different etiological mechanisms, besides LHVD, responsible in triggering annular and/or subvalvular morphological modifications (3). The growing interest for TR and the advances in imaging, three-dimensional (3D) echocardiography and cardiovascular MR (CMR) among others, have allowed FTR to be categorized in more detail. The pathophysiological comprehension of the different TR phenotypes, identified according to the etiological mechanism and the associated natural history, may significantly help clinicians and surgeons in the decision-making.

Indeed, in the setting of LHVD, both the severe mitral regurgitation and aortic stenosis have a high percentage, up to 50 and to 25%, respectively, and the concomitant presence of at least moderate TR, with worsening or late onset of the TR when the solely left heart valvular disease was surgically corrected (4–11).

In the light of these findings, the guidelines, supported by the absence of an increased operative risk, recommend tricuspid valve (TV) surgery during the surgical management of left-sided disease, with an improvement in RV function and functional status, if the disease is not very advanced (12).

In contrast, knowledge about the natural history and the timing of intervention in isolated TR remain poor because its clinical onset usually occurs in an advanced stage of the disease, which may increase periprocedural morbidity and mortality (12). Moreover, there is also scarce evidence on the role and timing of TV surgery and newer transcatheter repair approaches.

PATHOGENESIS OF FTR

In the pathogenesis of FTR, valvular coaptation results impaired due to mainly two mechanisms: TA dilatation with distortion of its morphology and restricted motion of leaflets caused by increased tethering.

Due to the peculiar anatomy of TV, when the functional dilatation of TA occurs, typically, the septal portion is spared, involving the anterior and the posterior leaflet attachment. Thus, the normal "saddle-shaped" structure is altered toward more circular and planar geometry (3).

The magnitude of annular dilatation correlates with greater degrees of TR and, in particular, the threshold beyond which coaptation results significantly inadequate is notably lower than for mitral regurgitation, with 40 rather than 75%, respectively (13, 14).

Therefore, the loss of coaptation is importantly influenced by the dilatation and distortion of TA, often coexisting with leaflets pulled down the annular plane due to increased tethering. In this latter case, anterior and posterior papillary muscles (PMs) are displaced due to RV cavity change in size and shape (15).

An *in-vitro* study that simulated annular dilatation and PMs displacement showed that when considered alone, both the conditions may lead to significant FTR (14). This finding highlights the importance of carefully studying the primary disease processes that cause FTR.

According to the recent literature, FTR may be classified as secondary to:

- Left heart valvular disease.
- Right heart dysfunction (RHD) with or without pulmonary hypertension (PH).
- Right atrium enlargement and dysfunction.

In the majority of FTR cases, the primary triggering condition is LHVD, mainly chronic mitral regurgitation followed by aortic valve stenosis and mitral valve stenosis (16, 17).

The different causes of FTR determine significant anatomic differences in RV, TV, and TA anatomy.

Interestingly, FTR secondary to PH, mainly associated to LHVD or in the setting of primary PH due to pulmonary disease such as chronic pulmonary embolism among others, showed only mild annular dilatation, but excessive valve tenting height with a conical deformation of RV (16).

The progressive RV dilatation, promoted by the relative lack in muscular tissue of RV, due to the increased afterload, is triggered by PH. Different studies have demonstrated the role of PH as a determinant of FTR severity; in a vicious circle, the chronic pressure and volume overload increase leaflets tethering, ultimately worsening TR (18).

Besides the absolute value of pulmonary artery systolic pressure in defining the severity of the PH, the onset of significant FTR is strongly associated with right heart remodeling (19). Indeed, in the absence of PH, RV dysfunction due to ischemic injury or cardiomyopathy may lead to adverse remodeling, PMs displacement, and increased leaflets tethering, causing FTR (20).

On the other side of the spectrum lesions, FTR with a larger basal deformation of the RV and a lower annular/leaflet coverage ratio due to greater annular dilatation, typically occurs due to RA enlargement and dysfunction (16).

Atrial FTR (AFTR) was for long time called idiopathic FTR, so categorized due to the absence of any obvious cause; recently, its accurate study has allowed to revise the pathophysiological classification, awarding to the RA a primary role as its main determinant (17, 21–23).

Indeed, current literature has emphasized the underappreciated issue associated to the atrial failure and its prognostic implication in worsening natural history of heart failure among others (24).

Atrial FTR reflects the TV leaflets malcoaptation because of the imbalance between TA and leaflets area, caused by RA enlargement and dysfunction.

The advanced age and the presence of persistent/permanent atrial fibrillation (AF) are typically associated to the AFTR, reflecting as common denominator of the atrial contractile dysfunction (21, 23). In particular, the onset of AF may modulate myocytes action potential and calcium release from the sarcoplasmic reticulum; regardless by AF, in the elderly, the frequent diastolic dysfunction may lead to an increase in atrial pressure and atrial stretch (25, 26).

In the study of Utsunomyia et al. (27), who compared subjects affected by AFTR and ventricular FTR, the assessment of the RA remodeling has allowed to conclude that RA volume and its ratio

with RV end-systolic volume are independent predictor of TA volume in AFTR.

Interestingly, they stratified AFTR according to severity of regurgitation in severe and massive/torrential TR, showing in this latter more complex lesions with excessive TA dilation associated to different degrees of leaflets tethering (27).

What emerges by the afore discussed categorization is a strong association between RV, RA, and valvular changes and in the light of this complex interaction, FTR may be interpreted as a complex syndrome with multifaceted spectrum of pathogenesis, natural history, and outcome.

Therefore, the qualitative evaluation of FTR based on pathophysiological categorization should be integrated with quantitative measurements and parameters exploited by imaging to improve the decision-making process and offer individualized management for our patients.

DIAGNOSTICS

Echocardiography

The first-line imaging recommended in the assessment of TR is the transthoracic echocardiography, which is useful to provide information regarding to the main determinants of the disease and to estimate its severity.

In the setting of FTR, the assessment of TV anatomy, in order to exclude any structural abnormalities, anticipates the measurement of TA diameter, RV size and function, RA size, and the estimation of pulmonary artery pressures (PAPs) (28).

The measurement of TA diameter has represented the critical component univocally used to guide the procedural planning of TV intervention. The cutoff value of 40 mm or 21 mm/m^2 indexed for the body surface area has been established and still used as threshold in surgical decision-making to approach TV in concomitant procedures. Nevertheless, the two-dimensional (2D) echocardiographic measurements fail to consider the 3D nonplanar structure of TA and in addition the interindividual variability. In comparison, 3D echocardiography, obtained by the transthoracic window rather than the transesophageal one because of the better visualization, is significantly less influenced by TA shape and orientation (28).

The comprehensive study of RV size and function has notably implications in the accurate categorization of FTR and it has an important prognostic value (29). Indeed, the geometrical modification of the right chamber may be influenced by primary abnormalities in the setting of RHD and indirectly due to LHVD, leading to elliptical/spherical shape and increased leaflets tethering.

The evaluation of RV size and function is a key determinant of prognosis and potential intervention in patients with TR. RV evaluation with echocardiography is challenging due to the complex 3D geometry of the RV. Typically, the first approach to the RV includes RV size estimation from the four-chamber view, evaluating its diameter at the basal level (normal up to 42 mm) and also its relative size as compared to the left ventricle (LV) (the normal RV is always smaller than the LV). Qualitative estimation of RV systolic motion from this view also provides a first impression of RV systolic motion. Longitudinal shortening of the basal segments is the main contributor to global RV function; therefore, the assessment of global function can also be provided by measuring the tricuspid annular plane systolic excursion (TAPSE) from M-mode scans through the TA in the four-chamber view (abnormal below 17 mm). Determination of peak systolic annular velocity (S wave from tissue Doppler imaging of the tricuspid annulus) also provides a global index of RV systolic function (values below 11 cm/s indicate systolic dysfunction). However, both the TAPSE and annular S wave values are influenced by loading conditions. Volumetric methods to assess RV ejection fraction are cumbersome by using 2D echocardiography due to the particular geometry of the RV and, therefore, 3D echocardiography, despite limited by visual quality and spatial resolution, is preferred. In the absence of 3D echocardiography, RV fractional area change obtained from the planimetry of the endocardial border of the RV performed in the four-chamber view and its relative change in systole and diastole is typically used to assess RV systolic function. Finally, myocardial deformation imaging determining global longitudinal strain of the RV is another essential tool in the evaluation of RV systolic function that can be successfully obtained with echocardiography. Typically, the free wall RV global strain is obtained from the four-chamber view with normal values above 20% or even higher in the presence of volume overload such as the case of patients with TR. This parameter has shown added prognostic value in several clinical settings such as cardiogenic shock and PH (30, 31).

The extent of leaflet tethering (including the measurement of tethering distance, area, and volume), the mode of leaflet coaptation, and the RA size offer supplementary information regarding the natural history of the FTR, allowing to stage the severity of the disease according to the complexity of lesions (28).

Besides the qualitative description improved by the use of 3D echocardiography (**Figure 1**), the severity of TR needs to be related to quantitative parameters, in order to make reproducible its staging. The measurement of the diameter of the vena contracta of the regurgitant jet and the tricuspid effective regurgitant orifice obtained by the proximal isovelocity surface area (PISA) method are the largely used parameters. The cutoff used to estimate the severity of TR is similar to those identified for mitral valve regurgitation, with 0.70 cm and 0.40 cm^2, respectively, for the vena contracta and for the effective regurgitant orifice area, as threshold to quantify severe TR.

Several issues affect the staging role assigned to these quantitative values; in particular: the anatomical difference existing between TV and its left counterpart, associated to the higher respiratory function and loading variability. The 3D echocardiography allows to partly overcome the anatomical disagreement, even though failing to solve the limitations related to the assessment of a single frame developed on a tomographic plane in the setting of a variable dynamic disease (28, 32).

Cardiac Magnetic Resonance

Patients with TR are a heterogeneous population at different stages of right heart remodeling. CMR is the gold standard imaging technique for the quantitative and qualitative assessment of the heart, particularly the RV morphology and function and,

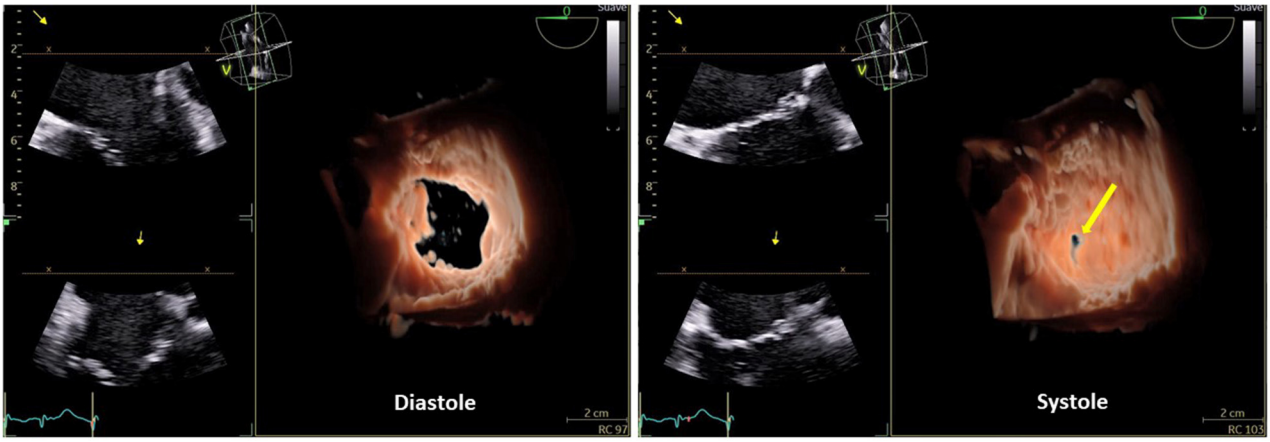

FIGURE 1 | Three-dimensional (3D) echocardiography of the tricuspid valve with front view, from the right atrium in diastole and systole where the central coaptation defect (yellow arrow), due to annular dilation, is seen.

indeed, it has diagnostic value and it can provide valuable information to improve the decision-making process on the management of TR (**Figures 2A,B**) (33).

Cardiac magnetic resonance allows a comprehensive assessment of FTR, starting from the qualitative visualization of valve regurgitation with flow turbulence and acceleration visualized in the cine images as an area of local signal drop. The qualitative grading has shown a moderate correlation with the quantitative assessment, although influenced by different limitations such as the difficult arising from the correct visualization in presence of pacemaker leads and the bias associated to various technical factors.

The more accurate quantitative measurement, although limited by existing validated cutoff and, therefore, the still poor experience, allows to calculate the regurgitant volume (RVol) through TV with both the indirect and direct methods. In the first case, RVol is derived from the right ventricular volumetric stroke volume, demonstrating to be a good prognostic predictor in patients underwent to the surgical management of isolated TR.

In contrast, the direct calculation of RVol depends by the flow assessment through the valve, but it is still challenging due to intrinsic factor associated to the atrioventricular annuli (34).

Moreover, the determination of the RV morphology and RV cavity size assessed by CMR cine-sequence images has been proved to have prognostic value in different clinical settings (35, 36). Recently, Iacuzo et al. (37) have highlighted the fundamental role that TA plays in the surgical decision to perform preventive combined TV annuloplasty in patients with mitral valve prolapse. They found that the best cutoff for the prediction of RV dysfunction in these patients is a TA diameter index value of 19 mm/m^2 measured by CMR, beyond which combined TV annuloplasty should be considered.

Besides heart cavities assessment, CMR can also accurately evaluate the pulmonary vasculature and it has been proposed as an alternative to invasive right heart catheterization and echocardiography in assessing pulmonary circulation hemodynamics and to estimate pulmonary vascular resistance (6). The CMR-derived model was estimated as: pulmonary vascular resistance [in Wood units (WUs)] = 19.38 − [4.62 × Ln pulmonary artery average velocity (in cm/s)] − [0.08 × RV ejection fraction (in %)] (24). This CMR method to noninvasively estimate pulmonary vascular resistance has been used in patients with PH and also in patients with heart failure and reduced LV ejection fraction (EF), in whom pulmonary vascular resistance > 5 WU was associated with an increased risk of adverse events at 9 months follow-up (38, 39). Based on all this, we believe that this CMR method could also be integrated in the global evaluation of the RV in the setting of FTR in order to better understand if the RV contractile reserve is struggling to maintain output against an increased afterload, a finding which, indeed, previous studies have shown that entails a poor prognosis (39).

Additionally, myocardial strain has received growing interest as an alternative measure of myocardial performance since it has proven to better recognize and characterize subclinical biventricular systolic dysfunction as compared with conventional imaging modalities based on EF (40, 41). In fact, it is well known that impairment in the longitudinal deformation precedes the reduction in EF, giving rise to subclinical pump impairment in most heart diseases (42, 43). CMR feature tracking (FT) allows the assessment of strain from routine cine images and besides its diagnostic value, it might also have a prognostic value in patients with TR. Recently, Romano et al. (44) found that RV longitudinal strain assessed by CMR-FT is an independent predictor of mortality in patients with severe FTR, incremental to common clinical and imaging risk factors.

Better identification of high-risk patients that benefit from a closer follow-up together with the implementation of a global RV imaging evaluation that includes the assessment of estimated PVR and the early detection of RV dysfunction by using FT may potentially play a role in determining optimal timing of intervention of patients with FTR.

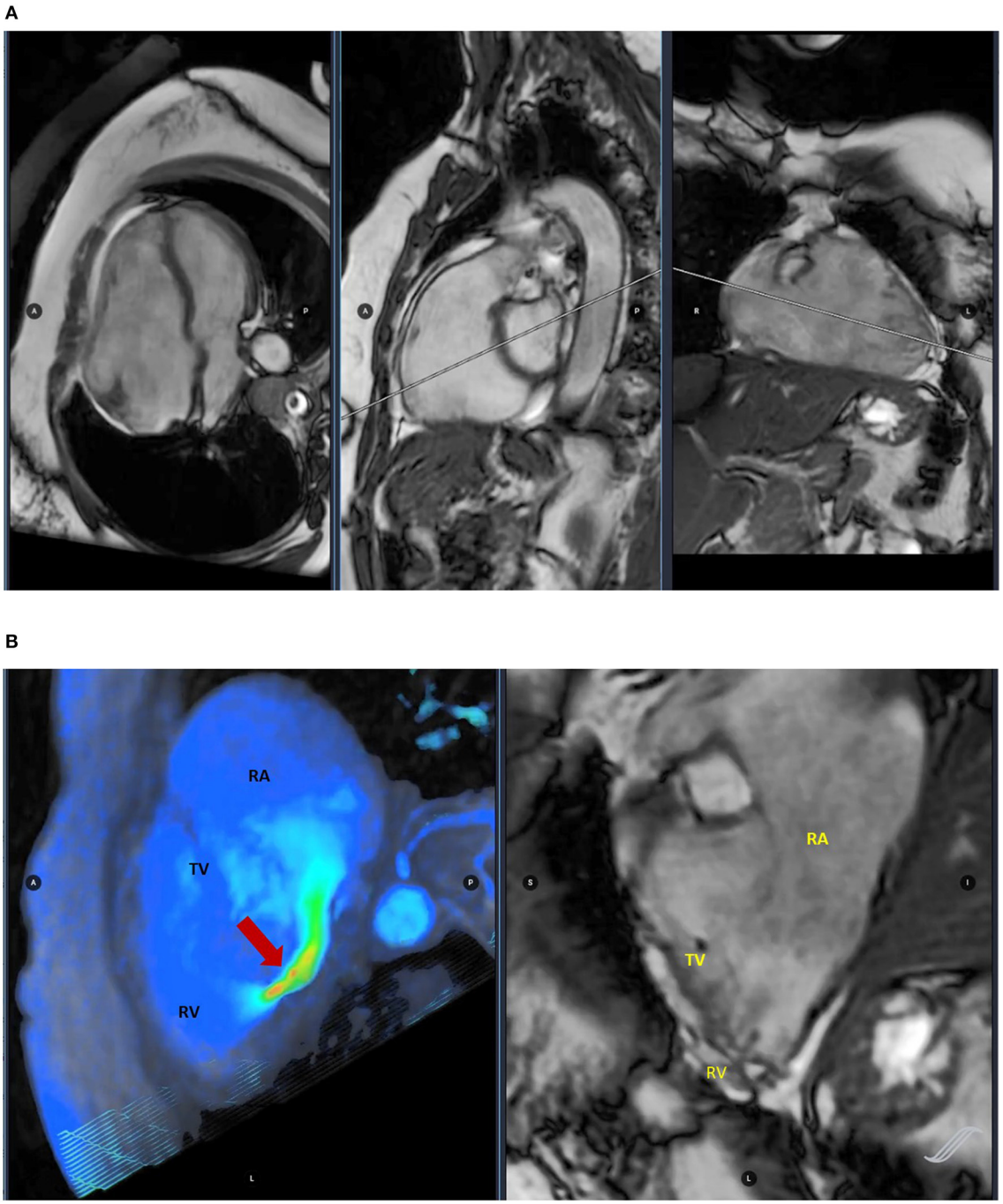

FIGURE 2 | Cardiac magnetic resonance (CMR) imaging assessing ventricular volumes **(A)** and four-dimensional (4D) flow image evaluating tricuspid regurgitation (TR) (red arrow) **(B)**.

THERAPY

A recent growing surgical interest in the management of FTR has reversed course, polarized in the past by the wrong concept of disease regression after properly solving LHVD (1).

The consequence of the less attention received rather than for mitral valve regurgitation has been easily translated in a still lacking surgical experience in offering a targeted approach.

Although, in absence of a clear evidence demonstrating superiority of one surgical approach over others, TV repair, mainly annuloplasty, represents the preferred options in the

management of FTR. A growing interest emerged at the end of 90' in various minimally invasive and video-assisted surgical approaches (45–50). TV replacement may be a viable option when risk for TR recurrence after repair is considered too high.

A great challenge, in the surgical decision-making, is represented by the management of electrical conduction abnormalities in concomitance with TR, which can facilitate the need for pacemaker implantation in the postoperative period. An accurate evaluation of the possibility to implant epicardial leads is necessary in order to reduce the risk of TR recurrence mainly due to prosthesis leaflets damage following the traditional leads implantation.

In this paragraph, we review the most commonly TV repair techniques to offer a focus insight into the future perspectives of surgery in the management of FTR in the era of transcatheter approach. **Tables 1**, **2** summarize, respectively, the main characteristics of the principal FTR surgical techniques and the transcatheter devices.

Tricuspid Valve Annuloplasty Techniques and Outcomes

The cornerstone of the TV repair techniques has found its foundation in counteracting the dilatation of TA, with annuloplasty being the most widely used approach.

First, the way of the annular plication was undertaken following the concept of the suture bicuspidization. The posterior annular portion of TV, being the less unsupported segment of TV ring, dilates achieving up to 80% from its normal dimension in the setting of FTR. This anatomic finding was at the basis of suture bicuspidization technique (51). The technique, initially described by Kay et al. (52) and then modified by Ghanta et al. (53), consists in placing a double pledget-supported mattress suture from the anteroposterior to the posteroseptal commissure, resulting in a posterior suture bicuspidization.

Although highly reproducible, the tension created by the suture lines and the high technical failure associated to severe TA dilatation have limited the use of the suture annuloplasty toward alternative strategies such as the implantation of prosthetic ring or band (54).

De Vega proposed, after understanding the way TA was dilated, a double continuous running suture with the aim to plicate the anterior and the posterior portions of the annulus avoiding the septal due to the lack of distension and to avoid the conduction tissue. Even though this semicircular suture annuloplasty was initially designed for rheumatic TV disease, it reached a great success in the management of FTR, mainly because it was safe, effective, at least in the short term, easily reproducible, and cheap (54, 55). Nevertheless, even if a series of De Vega annuloplasty modifications has been developed in order to avoid suture tear and massive TR, this phenomenon, called "bowstring," was rather frequently reported after suture annuloplasty (54).

The technical aspects of the various De Vega annuloplasty modifications followed the rationale to achieve better coaptation, reduced annular dimensions, and a better distribution of forces along the suture in order to prevent tear in the endocardium (56–60). The absence of constant mid- and long-term follow-up has limited a wider reproducibility of some of these techniques.

Alain Carpentier, emphasizing the criticisms associated to the principles of the suture annuloplasty, proposed the use of suitably sized and shaped prosthetic rings. In the former, the asymmetric placement of the sutures results in localized plication and in variable degrees of functional stenosis. On the contrary, the rationale for

TABLE 1 | Summary table with the description of the principal surgical technique in the correction of the functional tricuspid regurgitation (FTR).

Type of technique/device	Description	Strength	Limitation
Suture bicuspidization	Double pledget-supported mattress suture from the anteroposterior to the posteroseptal commissure	Easily reproducible	frequent technical failures
De Vega annuloplasty	Double continuous running suture along anterior and posterior portions of the annulus	Safe, effective, easily reproducible, cheap	Occasional Suture tear: "Bowstring" phenomenon
Prosthetic annuloplasty: - Duran-Medtronic flexible ring - Carpentier-Edwards semi-rigid ring - Cosgrove-Edwards flexible band - Duran-Medtronic flexible band and others …	Implantation of a prosthetic band or ring	Reduction of recurrent dilatation by a non expandable frame	May Need additional gestures in complex lesions (excessive leaflets tethering)
Papillary muscles septalization	The approximation of the anterior PM, attached to the RV free wall and more prone to displacement, toward the interventricular septum	The technique allows to increase the surface of coaptation of leaflets reducing the rate of TR recurrence	Lack of large series reported
Leaflet augmentation	Leaflet augmentation using a pericardial patch	The technique allows to increase the leaflets surface improving systolic area closure	Lack of large series reported Eventual degeneration of pericardial patch (stiffer and retraction)

TABLE 2 | Summary table with the description of the more used transcatheter technique/device of tricuspid valve intervention.

Type of technique/device	Description	Strength	Limitation	Ongoing trials
Transcatheter tricuspid valve replacement				
Transcatheter tricuspid valve replacement: -Orthotopic implantation -Heterotopic implantation	Implantation of a prosthetic valve in the tricuspid location or in the vena cava	Alternative option to repair techniques, mainly in patients with degeneration of previous tricuspid valve correction	Lack of experience	
Leaflets coaptation device				
TriClip (Abbott, Chicago, Illinois)	Edge-to-edge repair	Satisfactory reduction of tricuspid regurgitation and improvement in the functional class for patients not suitable for surgery	Lack of comprehensive data on eligible patients	
FORMA system (Edwards Lifesciences, Irvine, California)	Implantation of a balloon spacer anchored to right ventricle apex able to reduce regurgitant orifice area	Alternative options to edge-to-edge repair	Invasiveness of the device	
Suture annuloplasty devices				
- Trialign (Mitralign Inc, Tewksbury, MA) - Tricinch (4Tech Cardio Ltd., Galway, Ireland)	System of anchors placed on the anterior and posterior segments of the tricuspid annulus	Reduction of tricuspid annulus diameter in patients not suitable for surgery	Lack of mid-term follow-up data	Safety and Feasibility of the Transcatheter Tricuspid Valve Repair System (Trialign) **Trials Identifier:** NCT04936802
Prosthetic annuloplasty devices				
- Cardioband system (Edwards Lifesciences, Irvine, CA, USA) - Millipede IRIS (Millipede Inc., Santa Rosa, CA, USA)	Transcatheter implantation of a prosthetic annulus	Reduction of tricuspid regurgitation in patients deemed inoperable	Lack of mid-term follow-up data	

the implantation of a prosthetic rigid ring was based on the respect of anatomic and physiologic TA geometry, allowing to avoid recurrent dilatation with a nondeformable frame (61).

The Duran-Medtronic totally flexible tricuspid and the Carpentier-Edwards semi-rigid rings were later followed by the flexible Cosgrove-Edwards and Duran-Medtronic bands.

The flexible band was specifically designed on the basis of the improved knowledge regarding dynamic saddle-shaped structure of TA and about its pathological dilatation that involves particularly anterior and posterior segments (62).

McCarthy et al. (63) compared the durability of tricuspid annuloplasty in the management of FTR by using four techniques: De Vega procedure, Peri-Guard annuloplasty, Carpentier-Edwards semi-rigid ring, and Cosgrove-Edwards flexible band. In the long-term follow-up, a substantial worsening in the recurrence of TR was associated to the two nonring annuloplasties. Indeed, along the follow-up, severity of regurgitation increased more rapidly when these procedures were performed, slower with the flexible band and more stable across time with semi-rigid ring. The authors explained the higher recurrence of severe FTR in the gradual redilatation of the TA due to the persistent PH, in the absence of a nondeformable frame.

The superiority of the prosthetic annuloplasty ring, in ensuring a higher durability of FTR correction, a better long-term survival, and event free-survival, was largely demonstrated (64–68).

Nevertheless, the main finding of the retrospective study published by McCarthy et al. (63) was the failure of the tricuspid valve annuloplasty, regardless by the implantation of a prosthetic ring, to consistently counteract functional regurgitation. Even though stable across time, the prevalence of severe regurgitation 1 month postoperatively was 15% for the semi-rigid ring technique. This latter allowed to achieve higher freedom from moderate-to-severe TR when compared with flexible bands (69).

Over the years, a variety of prosthesis for annuloplasty has been presented, notably ensuring improvement in remodeling TV annulus, respecting the 3D anatomical dynamic characteristics. The development of the 3D-shaped prosthetic rings has allowed to resemble more accurately the healthy human TA, reducing the recurrence of the TR in the long-term follow-up, with an incidence reported in a recent study, which compared the use of the Medtronic 3D Contour and the Edwards MC3 prosthetic rings, of almost 15% of TR > 2+, mainly of moderate nature (70, 71). Newer rings are today commercially available, but their long-term outcomes are still to be reported in the scientific literature.

Current and Future Perspectives

"Prophylactic" Annuloplasty

The late onset of TR after left-sided surgery, regardless by the presence of preoperative TR, highlights the dynamic nature of TR, which, in contrast with what Nina Braunwald believed, does not regress spontaneously (1). Dreyfus et al. (7) used the

annular dimension as target to address TV, including patients only with none or mild trace of TR. The chosen threshold to manage TV, in the setting of left-sided surgery, was a diameter greater than twice the normal size (i.e., > 70 mm) inspected intraoperatively. The cutoff allowed to divided population study in the two groups of treatment: mitral valve repair (MVRe) alone and MVRe plus tricuspid annuloplasty. This latter group showed better outcomes in terms of late recurrence of TR; postoperative TR grade increased significantly in the group underwent isolated MV surgery (7). These results demonstrated the irreversible progression of annular dilatation, being not influenced by the correction of the LVHD, and introduced the concept of the "prophylactic annuloplasty".

The echocardiographic equivalent of the intraoperative threshold has been identified in 40 mm. Tricuspid annuloplasty was performed, in addition to left-sided surgery, in patients with TA dilatation more than 40 mm, independently by the grade of TR, in a cohort of 43 patients in the study published by Van de Veire et al. (6).

The authors analyzed retrospectively two cohorts temporally distinct, with the introduction of the "prophylactic annuloplasty" in the management of FTR in the more recent group of patients. A significant decrease of TR, transtricuspid gradient and a reduction of the RV volumes leading to reverse remodeling were observed (6). These findings have been confirmed by other studies (72, 73). The satisfactory outcomes achieved and the low in-hospital mortality and morbidity associated to the TV annuloplasty, although increasing operation time, promoted this preventive treatment to become recommended, according to the valvular heart disease guidelines, during left-sided surgery (74, 75).

Benedetto et al. (72) observed, at 12 months follow-up with preoperative TR $\leq$ 2+, no cases of moderate-to-severe TR in the group, which underwent tricuspid annuloplasty vs. 28% in the control group (isolated MV surgery).

Interestingly, the subgroup analysis demonstrated an advantage of TV annuloplasty toward TR caused by rheumatic or ischemic injury, failing to show significant benefits in degenerative etiology. The authors explained the ineffectiveness of the additional treatment identifying some predisposing risk factors such as worse functional class and the presence of AF, responsible of long-standing RV pressure overload.

In addition, the high variability correlated to the broad range of degenerative disease raised various questions about the predictivity of TA diameter as a valid cutoff for decision-making (76).

Although tricuspid annuloplasty represents a coherent surgical approach in counteracting TA dilatation in the early stage of disease when LVHD correction is performed, a single threshold in the setting of a multifaceted syndrome is a limitation in achieving excellent results. Studies, tailored on the different etiology and pathophysiology, designed in order to identify targeted parameters, are mandatory.

Valvular and Subvalvular Repair Techniques

The wrong assumption that TA dilation is always the primary cause of leaflet malcoaptation and that TV annuloplasty is able to correct FTR counteracting also leaflet tethering, is generally incorrect; in fact, there is a high early residual rate of TR when tethering is excessive (76). Indeed, Fukuda et al. (77) have demonstrated the role of TV tethering in predicting residual TR early after surgery; in particular, identifying as significant values: tethering height > 0.76 cm and tethering areas > 1.63 cm^2.

Therefore, the geometry of the TV can vary according to the major determinants of its severity, TA dilatation, leaflet tethering (particularly of the septal leaflet), and the grade of PH, designing a complex variety of lesions (78).

In such cases, additional surgical strategies in order to improve results of TV repair are necessary, allowing to reduce early technical failure and TR recurrence.

Surgery at subvalvular level with PMs approximation has demonstrated to be effective in reducing TR independently by the use of tricuspid annuloplasty and it is able to promote changes in the RV geometry leading to reverse remodeling. The technical aspects of this surgical strategy are based on the approximation of the anterior PM, attached to the RV free wall and more prone to displacement, toward the interventricular septum (79).

Excellent outcomes have been achieved by using PMs "septalization" in the management of the massive FTR caused by distorted geometry of the TV and adverse remodeling of the RV (80–83).

In the setting of severe tethering, the restricted mobility leads to the failure of the leaflets in covering the whole orifice; leaflet augmentation using an autologous pericardial patch found its rationale in this concept. Dreyfus et al. (84) promoted to use this technique when annuloplasty ring alone is not adequate to impact significantly on the TR when a tethering height <8 mm has been assessed during preoperative echocardiography. The increase of the surface area of coaptation, combined with TV annuloplasty allows to counteract FTR caused by complex lesions, accomplishing excellent short-term results (85, 86). Stiffness of the pericardial patch and retraction have been mentioned as potential long-term limitations.

Transcatheter Approaches

The great technological improvements and the experience achieved in the field of the transcatheter repair or replacement of the aortic and mitral valves have accelerated the use of the transcatheter tricuspid valve interventions (TTVIs) in high-risk surgical patients. The possibility to recur to a less invasive surgical option of treatment, in particular in selected patients such as who underwent to previous TV surgery, allows to reduce the high incidence of postoperative mortality and morbidity associated to the reintervention. Nevertheless, the lack of a complete understanding of the role and timing of the TV surgery represented a limitation in allowing a standardized management (87).

A broad armamentarium including multiple devices aimed to repair and replacement has been developed in the field of tricuspid disease.

Transcatheter TV replacement includes the orthotopic implantation of a prosthetic valve in the tricuspid location or the heterotopic implantation of prosthetic valves in the vena cava. These approaches are particularly limited to the patients with

degeneration of previous TV correction (repair or replacement) and particularly for those with very advances stages of TR where repair is not going to provide a durable solution (88, 89).

The coaptation and annuloplasty devices represent other available options of the transcatheter TV repair.

The MitraClip system (Abbott Vascular, Santa Clara, California, USA) has found in the TriClip system (Abbott, Chicago, Illinois, USA), the corresponding leaflets coaptation device. In particular, the edge-to-edge repair of the TV with the TriClip system (Abbott, Chicago, Illinois, USA) or the Pascal system (Edwards Lifesciences, Irvine, California, USA) is the most largely performed coaptation technique (**Figure 3**), with retrospective and prospective analysis that demonstrated a reduction in TR and improvement in the functional class (90, 91). The Triluminate Pilot Study (92) prospectively enrolled symptomatic patients with TR $\geq$ 2 not suitable for surgery, to evaluate the safety and performance of the TriClip device at 1-year follow-up. The durability of the TriClip system in the follow-up was sustained with the 87% of patients that experienced a TR reduction of $\geq$ 1 grade, with torrential or massive TR less prone to achieve a satisfactory correction rather than severe TR. Besides TR grade reduction, which remained stable across the follow-up, significant improvements in the clinical status, quality of life, and hospitalization rate have been achieved, further showing reverse RV remodeling (93). Although the results promise well, study limitations such as the small sample size and the exclusion of patients with severe PH or high coaptation gap make necessary large randomized controlled study, which are currently being performed in the currently including phase of the Triluminate Pilot Study where patients are randomized to receive either medical treatment or edge-to-edge repair with the TriClip system.

On a scaled-down, the early feasibility of other TTVR system, conceptualized in order to improve the leaflet coaptation, has been achieved in smaller sample size with the Forma system (Edwards Lifesciences, Irvine, California, USA). The regurgitant orifice area results reduced with a balloon spacer anchored to the RV apex (87, 94). Besides the limited early good results, the invasiveness of the device raised different perplexity mainly in the setting of unsuccessful procedure.

On the other hand, the suture annuloplasty devices, Trialign (Mitralign Incorporation, Tewksbury, Massachusetts, USA) and Tricinch (4Tech Cardio Ltd., Galway, Ireland, UK), provide to counteract TA dilatation, reducing the orifice dimension with a system of anchors placed on the anterior and posterior segments (95, 96).

The release of annuloplasty ring devices was performed by using the Cardioband system (Edwards Lifesciences, Irvine, California, USA) and the Millipede IRIS system (Millipede Incorporation, Santa Rosa, California, USA). At early follow-up, the impact on TR and clinical status was promising in high-risk surgical patients deemed inoperable, including those who underwent prior surgical repair showing residual or recurrent TR.

The analysis of data collected on patients undergoing any type of TTVI (>70% transcatheter edege-to-edge repair) in multiple centers in Europe and North America was performed by Taramasso et al. (83), showing a superiority at 1-year follow-up of transcatheter approach vs. medical management, when procedure results successful. The population study was composed by high-risk surgery patients with FTR in the majority of cases (95.2%). The main outcomes achieved by the study were low mortality, high procedural safety, and significant improvements in the functional class at early- and mid-term follow-up (97–99).

Nevertheless, similar outcomes to those managed medically have been showed in patient with unsuccessful TTVI. Interestingly, a coaptation depth > 1 cm has been identified as predictive of technical failure, suggestive of excessive valve tethering and RV remodeling, expression of the late phase of disease (85). The development of new transcatheter prosthesis will probably address these stages of the disease.

Percutaneous or transthoracic insertion of a bioprosthesis to replace the nonrepairable TV has been attempted in several

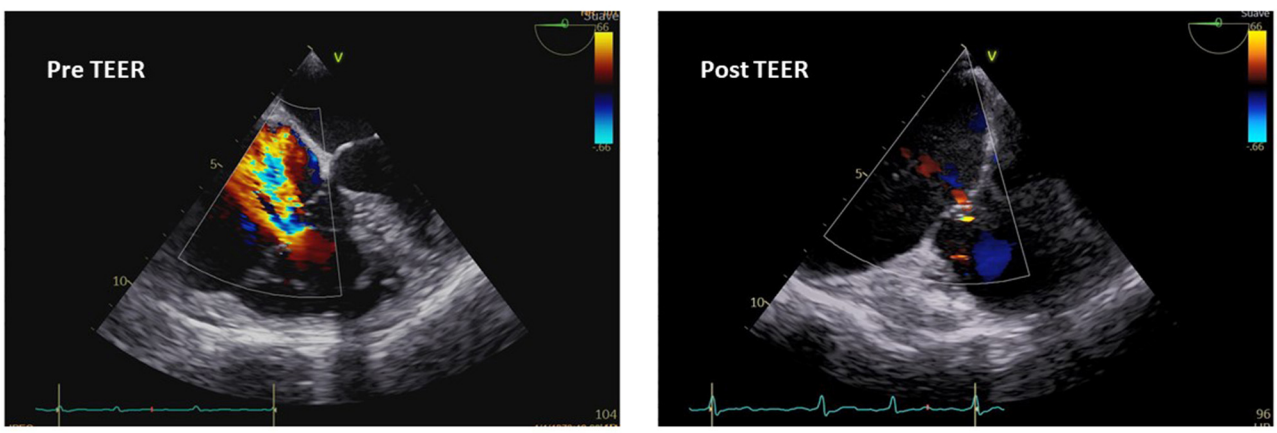

FIGURE 3 | Transesophageal echocardiography imaging and pre- and postoperative assessment of TR after transcatheter edge-to-edge repair (TEER).

patients successfully. Sizes up to 54 F required are indeed a limitation to solve in coming years (100).

These findings emphasize the necessity to improve knowledge regarding FTR pathophysiology, in order to better understand the role of TTVI in the natural history of the disease.

CONCLUSION

The concept of TV as a passive bystander to the LHVD should be abandoned. FTR is a multifaceted disease, including a broad spectrum of lesions. The technological advances in cardiac imaging with the use of 3D echocardiography and CMR have restored notoriety to the study and management of the FTR and may ensure to accurately categorize FTR phenotypes and establish quantitative parameters useful to guide clinicians and surgeons.

Annuloplasty has demonstrated to be limited to address FTR in its early stage with the necessity to integrate the repair technique by using a more targeted approach, which ensures an improved valvular coaptation counteracting excessive leaflet tethering. Nevertheless, the use of annuloplasty with prosthetic ring may successfully treat TA dilatation in the setting of mild-to-moderate FTR when left-sided surgery is performed.

Therefore, the role of surgery in the transcatheter era, with TTVI representing a valid option for high-surgical risk patients, depends mostly by the correct understanding of the natural history of disease, with a growing armamentarium of techniques in the surgeon's hands.

AUTHOR CONTRIBUTIONS

MV and EG: conceptualization. MV, MS, BD-X, and JL: writing—original draft preparation. EG, FM, SR, EW, and MD'A: review and editing. All authors contributed to the article and approved the submitted version.

REFERENCES

1. Braunwald NS, Ross J Jr, Morrow AG. Conservative management of tricuspid regurgitation in patients undergoing mitral valve replacement. *Circulation.* (1967) 35:I63–9. doi: 10.1161/01.CIR.35.4S1.I-63
2. Carpentier A, Deloche A, Hanania G, Forman J, Sellier P, Piwnica A, et al. Surgical management of acquired tricuspid valve disease. *J Thorac Cardiovasc Surg.* (1974) 67:53–65. doi: 10.1016/S0022-5223(19)39760-0
3. Mahmood F, Kim H, Chaudary B, Bergman R, Matyal R, Gerstle J, et al. 3rd, Gorman RC, Khabbaz KR. Tricuspid annular geometry: a three-dimensional transesophageal echocardiographic study. *J Cardiothorac Vasc Anesth.* (2013) 27:639–46. doi: 10.1053/j.jvca.2012.12.014
4. Shiran A, Sagie A. Tricuspid regurgitation in mitral valve disease incidence, prognostic implications, mechanism, and management. *J Am Coll Cardiol.* (2009) 53:401–8. doi: 10.1016/j.jacc.2008.09.048
5. Genereux P, Pibarot P, Redfors B, et al. Staging classification of aortic stenosis based on the extent of cardiac damage. *Eur Heart J.* (2017) 38:3351–8. doi: 10.1093/eurheartj/ehx381
6. Van de Veire NR, Braun J, Delgado V, et al. Tricuspid annuloplasty prevents right ventricular dilatation and progression of tricuspid regurgitation in patients with tricuspid annular dilatation undergoing mitral valve repair. *J Thorac Cardiovasc Surg.* (2011) 141:1431–9. doi: 10.1016/j.jtcvs.2010.05.050
7. Dreyfus GD, Corbi PJ, Chan KM, Bahrami T. Secondary tricuspid regurgitation or dilatation: which should be the criteria for surgical repair? *Ann Thorac Surg.* (2005) 79:127–32. doi: 10.1016/j.athoracsur.2004.06.057
8. Goldstone AB, Howard JL, Cohen JE, et al. Natural history of coexistent tricuspid regurgitation in patients with degenerative mitral valve disease: implications for future guidelines. *J Thorac Cardiovasc Surg.* (2014) 148:2802–9. doi: 10.1016/j.jtcvs.2014.08.001
9. Kalbacher D, Schafer U, von Bardeleben RS, et al. Impact of tricuspid valve regurgitation in surgical high-risk patients undergoing MitraClip implantation: results from the TRAMI registry. *EuroIntervention.* (2017) 12:e1809–16. doi: 10.4244/EIJ-D-16-00850
10. Dumont C, Galli E, Oger E, et al. Pre- and postoperative tricuspid regurgitation in patients with severe symptomatic aortic stenosis: importance of pre-operative tricuspid annulus diameter. *Eur Heart J Cardiovasc Imaging.* (2018) 19:319–28. doi: 10.1093/ehjci/jex031
11. Yajima S, Yoshioka D, Toda K, et al. Definitive determinant of late significant tricuspid regurgitation after aortic valve replacement. *Circ J.* (2018) 82:886–94. doi: 10.1253/circj.CJ-17-0996
12. Vahanian A, Beyersdorf F, Praz F, Milojevic M, Baldus S, Bauersachs J, et al. (2021). ESC/EACTS Guidelines for the management of valvular heart disease: Developed by the Task Force for the management of valvular heart disease of the European Society of Cardiology (ESC) and the European Association for Cardio-Thoracic Surgery (EACTS). *Eur J Cardiothorac Surg.* (2021) 60:727–800. doi: 10.1093/ejcts/ezab389
13. Nemoto N, Lesser JR, Pedersen WR, Sorajja P, Spinner E, Garberich RF, et al. Pathogenic structural heart changes in early tricuspid regurgitation. *J Thorac Cardiovasc Surg.* (2015) 150:323–30. doi: 10.1016/j.jtcvs.2015.05.009
14. Spinner EM, Shannon P, Buice D, Jimenez JH, Veledar E, Del Nido PJ, et al. In vitro characterization of the mechanisms responsible for functional tricuspid regurgitation. *Circulation.* (2011) 124:920–9. doi: 10.1161/CIRCULATIONAHA.110.003897
15. Sanz J, Sanchez-Quintana D, Bossone E, Bogaard HJ, Naeije R. Anatomy function, and dysfunction of the right ventricle: JACC State-of-the-Art Review, J. *Am Coll Cardiol.* (2019) 73:1463–82. doi: 10.1016/j.jacc.2018.12.076
16. Topilsky Y, Khanna A, Le Tourneau T, Park S, Michelena H, Suri R, et al. Clinical context and mechanism of functional tricuspid regurgitation in patients with and without pulmonary hypertension. *Circ Cardiovasc Imaging.* (2012) 5:314–23. doi: 10.1161/CIRCIMAGING.111.967919
17. Mutlak D, Lessick J, Reisner SA, Aronson D, Dabbah S, Agmon Y. Echocardiography-based spectrum of severe tricuspid regurgitation: the frequency of apparently idiopathic tricuspid regurgitation. *J Am Soc Echocardiogr.* (2007) 20:405–8. doi: 10.1016/j.echo.2006.09.013
18. Patel KM, Kumar NS, Neuburger PJ, Desai RG, Krishnan S. Functional Tricuspid Regurgitation in Patients With Chronic Mitral Regurgitation: An Evidence-Based Narrative Review. *J Cardiothorac Vasc Anesth.* (2021) S1053-0770(21)00445-6. doi: 10.1053/j.jvca.2021.05.032
19. Mutlak D, Aronson D, Lessick J, Reisner SA, Dabbah S, Agmon Y. Functional tricuspid regurgitation in patients with pulmonary hypertension: is pulmonary artery pressure the only determinant of regurgitation severity? *Chest.* (2009) 135:115–21. doi: 10.1378/chest.08-0277
20. Prihadi EA, Delgado V, Leon MB, Enriquez-Sarano M, Topilsky Y, Bax JJ. Morphologic types of tricuspid regurgitation: characteristics and prognostic implications. *JACC Cardiovasc Imaging.* (2019) 12:491–9. doi: 10.1016/j.jcmg.2018.09.027
21. Florescu DR, Muraru D, Volpato V, Gavazzoni M, Caravita S, Tomaselli M, et al. Atrial Functional Tricuspid Regurgitation as a Distinct Pathophysiological and Clinical Entity: No Idiopathic Tricuspid Regurgitation Anymore. *J Clin Med.* (2022) 11:382. doi: 10.3390/jcm11020382
22. Kasai A, Nishikawa H, Ono N, Unno M, Kakuta Y, Hamada M, et al. Clinical evaluation of severe idiopathic tricuspid regurgitation. *J Cardiol.* (1990) 20:937–44.

23. Silbiger JJ. Atrial functional tricuspid regurgitation: An underappreciated cause of secondary tricuspid regurgitation. *Echocardiography.* (2019) 36:954–7. doi: 10.1111/echo.14327
24. Bisbal F, Baranchuk A, Braunwald E, Bayés de. Luna A, Bayés-Genís A. Atrial failure as a clinical entity: JACC review topic of the week. *J Am Coll Cardiol.* (2020) 75:222–32. doi: 10.1016/j.jacc.2019.11.013
25. Greiser M, Neuberger HR, Harks E, El-Armouche A, Boknik P, de Haan S, et al. Distinct contractile and molecular differences between two goat models of atrial dysfunction: AV block-induced atrial dilatation and atrial fibrillation. *J Mol Cell Cardiol.* (2009) 46:385–94. doi: 10.1016/j.yjmcc.2008.11.012
26. Tsang TS, Gersh BJ, Appleton CP, Tajik AJ, Barnes ME, Bailey KR, et al. Left ventricular diastolic dysfunction as a predictor of the first diagnosed nonvalvular atrial fibrillation in 840 elderly men and women. *J Am Coll Cardiol.* (2002) 40:1636–44. doi: 10.1016/S0735-1097(02)02373-2
27. Utsunomiya H, Harada Y, Susawa H, Ueda Y, Izumi K, Itakura K, et al. Tricuspid valve geometry and right heart remodelling: insights into the mechanism of atrial functional tricuspid regurgitation. *Eur Heart J Cardiovasc Imaging.* (2020) 21:1068–78. doi: 10.1093/ehjci/jeaa194
28. Badano LP, Hahn R, Rodríguez-Zanella H, Araiza Garaygordobil D, Ochoa-Jimenez RC, Muraru D. Morphological assessment of the tricuspid apparatus and grading regurgitation severity in patients with functional tricuspid regurgitation: thinking outside the box. *JACC Cardiovasc Imaging.* (2019) 12:652–64. doi: 10.1016/j.jcmg.2018.09.029
29. Romero Delgado T, Travieso Gonzalez A, Luque Diaz T, Vivas Balcones D, Casado PM, Vilacosta I. "Analysis of right ventricle echocardiographic function parameters for the prediction of outcomes in significant functional tricuspid regurgitation." *European Heart Journal* 42.Supplement_1 (2021): ehab724-0118. doi: 10.1093/eurheartj/ehab724.0118
30. Rudski LG, Lai WW, Afilalo J, Hua L, Handschumacher MD, Chandrasekaran K, et al. Guidelines for the echocardiographic assessment of the right heart in adults: a report from the American Society of Echocardiography endorsed by the European Association of Echocardiography, a registered branch of the European Society of Cardiology, and the Canadian Society of Echocardiography. *J Am Soc Echocardiogr.* (2010) 23:685–713. doi: 10.1016/j.echo.2010.05.010
31. Badano LP, Addetia K, Pontone G, Torlasco C, Lang RM, Parati G. Guidelines for the echocardiographic assessment of the right heart in adults: a report from the American Society of Echocardiography endorsed by the European Association of Echocardiography, a registered branch of the European Society of Cardiology, and the Canadian Society of Echocardiography Advanced imaging of right ventricular anatomy and function. *Heart.* (2020) 106:1469–76. doi: 10.1136/heartjnl-2019-315178
32. Badano LP, Muraru D, Enriquez-Sarano M. Assessment of functional tricuspid regurgitation. *Eur Heart J.* (2013) 34:1875–85. doi: 10.1093/eurheartj/ehs474
33. Pelliccia A, Caselli S, Sharma S, Basso C, Bax JJ, Corrado D, et al. European Association of Preventive Cardiology (EAPC) and European Association of Cardiovascular Imaging (EACVI) joint position statement: recommendations for the indication and interpretation of cardiovascular imaging in the evaluation of the athlete's heart. *Eur Heart J.* (2018) 39:1949–69. doi: 10.1093/eurheartj/ehx532
34. Hahn RT, Thomas JD, Khalique OK, Cavalcante JL, Praz F, Zoghbi WA. Imaging assessment of tricuspid regurgitation severity. *JACC Cardiovasc Imaging.* (2019) 12:469–90. doi: 10.1016/j.jcmg.2018.07.033
35. Kawut SM, Barr RG, Lima JA, Praestgaard A, Johnson WC, Chahal H, et al. Right ventricular structure is associated with the risk of heart failure and cardiovascular death: the Multi-Ethnic Study of Atherosclerosis (MESA)-right ventricle study. *Circulation.* (2012) 126:1681–8. doi: 10.1161/CIRCULATIONAHA.112.095216
36. Oosterhof T, van Straten A, Vliegen HW, Meijboom FJ, van Dijk APJ, Spijkerboer AM, et al. Preoperative thresholds for pulmonary valve replacement in patients with corrected tetralogy of Fallot using cardiovascular magnetic resonance. *Circulation.* (2007) 116:545–51. doi: 10.1161/CIRCULATIONAHA.106.659664
37. Iacuzio L, Essayagh B, Civaia F, Dan Schouver E, Rusek S, Dommerc C, et al. Right-sided heart structural and functional remodeling in mitral regurgitation secondary to mitral valve prolapse. *Am J Cardiol.* (2018) 122:2095–103. doi: 10.1016/j.amjcard.2018.08.062
38. García-Alvarez A, Fernández-Friera L, Mirelis JG, Sawit S, Nair A, Kallman J, et al. Non-invasive estimation of pulmonary vascular resistance with cardiac magnetic resonance. *Eur Heart J.* (2011) 32:2438–45. doi: 10.1093/eurheartj/ehr173
39. Fabregat-Andrés O, Estornell-Erill J, Ridocci-Soriano F, et al. Prognostic value of pulmonary vascular resistance by magnetic resonance in systolic heart failure. *Arq Bras Cardiol.* (2016) 106:226–35. doi: 10.5935/abc.20160020
40. Bijnens BH, Cikes M, Claus P, Sutherland GR. Velocity and deformation im- aging for the assessment of myocardial dysfunction. *Eur J Echocardiogr.* (2009) 10:216–26. doi: 10.1093/ejechocard/jen323
41. Russo C, Jin Z, Elkind MSV, Rundek T, Homma S, Sacco RL, et al. Prevalence and prognostic value of subclinical left ventricular systolic dysfunction by global longitudinal strain in a community-based cohort. *Eur J Heart Fail.* (2014) 16:1301–9. doi: 10.1002/ejhf.154
42. Cikes M, Sutherland GR, Anderson LJ, Bijnens BH. The role of echocardiographic deformation imaging in hypertrophic myopathies. *Nat Rev Cardiol.* (2010) 7:384–96. doi: 10.1038/nrcardio.2010.56
43. Kraigher-Krainer E, Shah AM, Gupta DK, Santos A, Claggett B, Pieske B, et al. Impaired systolic function by strain imaging in heart failure with preserved ejection fraction. *J Am Coll Cardiol.* (2014) 63:447–56. doi: 10.1016/j.jacc.2013.09.052
44. Romano S, Dell'atti D, Judd RM, Kim RJ, Weinsaft JW, Kim J, et al. Prognostic value of feature-tracking right ventricular longitudinal strain in severe functional tricuspid regurgitation: a multicenter study. *JACC Cardiovasc Imaging.* (2021) 14:1561–8. doi: 10.1016/j.jcmg.2021.02.009
45. Russo M, Di Mauro M, Saitto G, Lio A, Berretta P, Taramasso M, et al. Beating Versus Arrested Heart Isolated Tricuspid Valve Surgery: Long-term Outcomes. Ann Thorac Surg. (2021). Apr 5:S0003-4975(21) 00649-4.
46. Casselman F, Aramendi J, Bentala M, Candolfi P, Coppoolse R, Gersak B, et al. Endoaortic clamping does not increase the risk of stroke in minimal access mitral valve surgery: a multicenter experience. *Ann Thorac Surg.* (2015) 100:1334–9. doi: 10.1016/j.athoracsur.2015.04.003
47. Marullo AGM, Irace FG, Vitulli P, Peruzzi M, Rose D, D'Ascoli R. et al. Recent developments in minimally invasive cardiac surgery: evolution or revolution? *Biomed Res Int.* (2015) 2015:483025. doi: 10.1155/2015/483025
48. Chirichilli I, D'Ascoli R, Rose D, Frati G, Greco E. Port Access (Thru-Port System) video-assisted mitral valve surgery. *J Thorac Dis.* (2013) 5:S680–5.
49. Speziale G, Nasso G, Esposito G, Conte M, Greco E, Fattouch K, et al. Results of mitral valve repair for Barlow disease (bileaflet prolapse) via right minithoracotomy versus conventional median sternotomy: a randomized trial. *J Thorac Cardiovasc Surg.* (2011) 142:77–83. doi: 10.1016/j.jtcvs.2010.08.033
50. Greco E, Zaballos JM, Alvarez L, Urso S, Pulitani I, Sàdaba R, et al. Video-assisted mitral surgery through a micro-access: a safe and reliable reality in the current era. *J Heart Valve Dis.* (2008) 17:48–53.
51. Deloche A, Guerinon J, Fabiani JN, Morillo F, Caramanian M, Carpentier A, et al. Etude anatomique des valvulopathies rhumatismales tricuspidiennes: Application à l'étude des différentes valvuloplasties [Anatomical study of rheumatic tricuspid valve diseases: Application to the study of various valvuloplasties]. *Ann Chir Thorac Cardiovasc.* (1973) 12:343–9.
52. Kay JH Maselli-Campagna G, Tsuji KK. Surgical treatment of tricuspid. Insufficiency. *Ann Surg.* (1965) 162:53–8. doi: 10.1097/00000658-196507000-00009
53. Ghanta RK, Chen R, Narayanasamy N, McGurk S, Lipsitz S, Chen FY, et al. Suture bicuspidization of the tricuspid valve versus ring annuloplasty for repair of functional tricuspid regurgitation: midterm results of 237 consecutive patients. *J Thorac Cardiovasc Surg.* (2007) 133:117–26. doi: 10.1016/j.jtcvs.2006.08.068
54. Raja SG, Dreyfus GD. Surgery for functional tricuspid regurgitation: current techniques, outcomes and emerging concepts. *Expert Rev Cardiovasc Ther.* (2009) 7:73–84. doi: 10.1586/14779072.7.1.73
55. De Vega NG. La anuloplastia selectiva, regulable y permanente. Una técnica original para el tratamiento de la insuficiencia tricúspide [Selective,

adjustable and permanent annuloplasty. An original technic for the treatment of tricuspid insufficiency]. *Rev Esp Cardiol*. (1972) 25:555–6.
56. Antunes MJ, Girdwood RW. Tricuspid annuloplasty: a modified technique. *Ann Thorac Surg*. (1983) 35:676–8. doi: 10.1016/S0003-4975(10)61084-3
57. Revuelta JM, Garcia-Rinaldi R. Segmental tricuspid annuloplasty: a new technique. *J Thorac Cardiovasc Surg*. (1989) 97:799–801. doi: 10.1016/S0022-5223(19)34529-5
58. Shatapathy P, Aggarwal BK, Kamath SG. Tricuspid valve repair: a rational alternative. *J Heart Valve Dis*. (2000) 9:276–82.
59. Goksin I, Yilmaz A, Baltalarli A, Goktogan T, Karahan N, Turk UA, et al. Modified semicircular constricting annuloplasty (Sagban's annuloplasty) in severe functional tricuspid regurgitation: alternative surgical technique and its mid-term results. *J Card Surg*. (2006) 21:172–5. doi: 10.1111/j.1540-8191.2006.00203.x
60. Sarraj A, Duarte J. Adjustable segmental tricuspid annuloplasty: a new modified technique. *Ann Thorac Surg*. (2007) 83:698–9. doi: 10.1016/j.athoracsur.2006.04.026
61. Carpentier A, Deloche A, Dauptain J, Soyer R, Blondeau P, Piwnica A, et al. A new reconstructive operation for correction of mitral and tricuspid insufficiency. *J Thorac Cardiovasc Surg*. (1971) 61:1–13. doi: 10.1016/S0022-5223(19)42269-1
62. McCarthy JF, Cosgrove DM. 3rd. Tricuspid valve repair with the cosgrove-edwards annuloplasty system. *Ann Thorac Surg*. (1997) 64:267–8. doi: 10.1016/S0003-4975(97)00348-2
63. McCarthy PM, Bhudia SK, Rajeswaran J, Hoercher KJ, Lytle BW, Cosgrove DM, et al. Tricuspid valve repair: durability and risk factors for failure. *J Thorac Cardiovasc Surg*. (2004) 127:674–85. doi: 10.1016/j.jtcvs.2003.11.019
64. Matsuyama K, Matsumoto M, Sugita T, Nishizawa J, Tokuda Y, Matsuo T, et al. De Vega annuloplasty and Carpentier-Edwards ring annuloplasty for secondary tricuspid regurgitation. *J Heart Valve Dis*. (2001) 10:520–4.
65. Rivera R, Duran E, Ajuria M. Carpentier's flexible ring versus De Vega's annuloplasty. A prospective randomized study. *J Thorac Cardiovasc Surg*. (1985) 89:196–203. doi: 10.1016/S0022-5223(19)38814-2
66. Filsoufi F, Salzberg SP, Abascal V, Adams DH. Surgical management of functional tricuspid regurgitation with a new remodeling annuloplasty ring. *Mt Sinai J Med*. (2006) 73:874–9.
67. Tang GH, David TE, Singh SK, Maganti MD, Armstrong S, Borger MA. Tricuspid valve repair with an annuloplasty ring results in improved long-term outcomes. *Circulation*. (2006) 114:I577–81. doi: 10.1161/CIRCULATIONAHA.105.001263
68. Parolari A, Barili F, Pilozzi A, Pacini D. Ring or suture annuloplasty for tricuspid regurgitation? A meta-analysis review. *Ann Thorac Surg*. (2014) 98:2255–63. doi: 10.1016/j.athoracsur.2014.06.100
69. Algarni KD, Alfonso J, Pragliola C, Kheirallah H, Adam AI, Arafat AA. Long-term outcomes of tricuspid valve repair: the influence of the annuloplasty prosthesis. *Ann Thorac Surg*. (2021) 112:1493–500. doi: 10.1016/j.athoracsur.2020.09.038
70. Mathur M, Malinowski M, Timek TA, Rausch MK. Tricuspid annuloplasty rings: a quantitative comparison of size, nonplanar shape, and stiffness. *Ann Thorac Surg*. (2020) 110:1605–14. doi: 10.1016/j.athoracsur.2020.02.064
71. Carino D, Zancanaro E, Lapenna E, Ruggeri S, Denti P, Iaci G. et al. Long-term results of tricuspid annuloplasty with 3-dimensional-shaped rings: effective and durable! *Eur J Cardiothorac Surg*. (2021) 60:115–21. doi: 10.1093/ejcts/ezab111
72. Benedetto U, Melina G, Angeloni E, Refice S, Roscitano A, Comito C, et al. Prophylactic tricuspid annuloplasty in patients with dilated tricuspid annulus undergoing mitral valve surgery. *J Thorac Cardiovasc Surg*. (2012) 143:632–8. doi: 10.1016/j.jtcvs.2011.12.006
73. Pettinari M, De Kerchove L, Lazam S, Pasquet A, Gerber B, Vanoverschelde JL, et al. Mid-term results of a randomized trial of tricuspid annuloplasty for less-than-severe functional tricuspid regurgitation at the time of mitral valve surgery. *Eur J Cardiothorac Surg*. (2019) 55:851–8. doi: 10.1093/ejcts/ezy378
74. Otto CM, Nishimura RA, Bonow RO, Carabello BA, Erwin III JP, Gentile F, et al. 2020 ACC/AHA guideline for the management of patients with valvular heart disease: executive summary: a report of the American College of Cardiology/American Heart Association Joint Committee on Clinical Practice Guidelines. *J Am Coll Cardiol*. (2021) *77*:450–500. doi: 10.1016/j.jacc.2020.11.035
75. Baumgartner H, De Backer J, Babu-Narayan SV, Budts W, Chessa M, Diller GP, et al. 2020 ESC Guidelines for the management of adult congenital heart disease: The Task Force for the management of adult congenital heart disease of the European Society of Cardiology (ESC). Endorsed by: Association for European Paediatric and Congenital Cardiology (AEPC), International Society for Adult Congenital Heart Disease (ISACHD). *Eur Heart J*. (2021) *42*:563–645. doi: 10.1093/eurheartj/ehaa554
76. Tourmousoglou C. Is the diameter of tricuspid annulus or functional tricuspid regurgitation the key parameter for performing 'prophylactic annuloplasty'? *Eur J Cardiothorac Surg*. (2020) 57:203. doi: 10.1093/ejcts/ezz066
77. Fukuda S, Song JM, Gillinov AM, McCarthy PM, Daimon M, Kongsaerepong V, et al. Tricuspid valve tethering predicts residual tricuspid regurgitation after tricuspid annuloplasty. *Circulation*. (2005) 111:975–9. doi: 10.1161/01.CIR.0000156449.49998.51
78. Park YH, Song JM, Lee EY, Kim YJ, Kang DH, Song JK. Geometric and hemodynamic determinants of functional tricuspid regurgitation: a real-time three-dimensional echocardiography study. *Int J Cardiol*. (2008) 124:160–5. doi: 10.1016/j.ijcard.2006.12.036
79. Yamauchi H, Vasilyev NV, Marx GR, Loyola H, Padala M, Yoganathan AP, et al. Right ventricular papillary muscle approximation as a novel technique of valve repair for functional tricuspid regurgitation in an ex vivo porcine model. *J Thorac Cardiovasc Surg*. (2012) 144:235–42. doi: 10.1016/j.jtcvs.2012.01.028
80. Matsumiya G, Kohno H, Matsuura K, Sakata T, Tamura Y, Watanabe M, et al. Right ventricular papillary muscle approximation for functional tricuspid regurgitation associated with severe leaflet tethering. *Interact Cardiovasc Thorac Surg*. (2018) 26:700–2. doi: 10.1093/icvts/ivx406
81. Couetil JP, Nappi F, Spadaccio C, Fiore A. Papillary muscle septalization for functional tricuspid regurgitation: Proof of concept and preliminary clinical experience. *JTCVS Techniques*. (2021). doi: 10.1016/j.xjtc.2021.09.027
82. Lohchab SS, Chahal AK, Agrawal N. Papillary muscle approximation to septum for functional tricuspid regurgitation. *Asian Cardiovasc Thorac Ann*. (2015) 23:747–50. doi: 10.1177/0218492315570644
83. Doenst T, Faerber G. A new technique for tricuspid valve repair addressing the subvalvular apparatus in functional tricuspid regurgitation. *Interact Cardiovasc Thorac Surg*. (2021) 33:525–6. doi: 10.1093/icvts/ivab134
84. Dreyfus GD, Raja SG, John Chan KM. Tricuspid leaflet augmentation to address severe tethering in functional tricuspid regurgitation. *Eur J Cardiothorac Surg*. (2008) 34:908–10. doi: 10.1016/j.ejcts.2008.07.006
85. Choi JB, Kim NY, Kim KH, Kim MH, Jo JK. Tricuspid leaflet augmentation to eliminate residual regurgitation in severe functional tricuspid regurgitation. *Ann Thorac Surg*. (2011) 92:e131–3. doi: 10.1016/j.athoracsur.2011.08.019
86. Pettinari M, Bertrand P, Van Kerrebroeck C, Vandervoort P, Gutermann H, Dion R. Mid-term results of leaflet augmentation in severe tricuspid functional tethering. *Eur J Cardiothorac Surg*. (2016) 50:504–8. doi: 10.1093/ejcts/ezw039
87. Alkhouli M, Lopez JJ, Mathew V. Transcatheter therapy for severe tricuspid regurgitation: learning to understand the forgotten valve. *J Am Coll Cardiol*. (2019) 74:3009–12. doi: 10.1016/j.jacc.2019.09.029
88. Aboulhosn J, Cabalka AK, Levi DS, Himbert D, Testa L, Latib A, et al. Transcatheter valve-in-ring implantation for the treatment of residual or recurrent tricuspid valve dysfunction after prior surgical repair. *JACC Cardiovasc Interv*. (2017) 10:53–63. doi: 10.1016/j.jcin.2016.10.036
89. Mehta AR, Sale S, Navia J, Kapadia S, Krishnaswamy A, Alfirevic A. Anesthetic and procedural considerations for patients undergoing tricuspid valve replacement with navigate valved stent. *J Cardiothorac Vasc Anesth*. (2019) 33:1991–4. doi: 10.1053/j.jvca.2018.09.024
90. Lauten A, Figulla HR, Unbehaun A, Fam N, Schofer J, Doenst T, et al. Interventional treatment of severe tricuspid regurgitation: early clinical experience in a multicenter, observational, first-in-man study. *Circ Cardiovasc Interv*. (2018) 11:e006061. doi: 10.1161/CIRCINTERVENTIONS.117.006061
91. Orban M, Rommel K-P, Ho EC, Unterhuber M, Pozzoli A, Connelly KA, et al. Transcatheter edge-to-edge tricuspid repair for severe tricuspid

regurgitation reduces hospitalizations for heart failure. *J Am Coll Cardiol HF.* (2020) 8:265–76. doi: 10.1016/j.jchf.2019.12.006
92. Besler C, Orban M, Rommel K-P, Braun D, Patel M, Hagl C, et al. Predictors of procedural and clinical outcomes in patients with symptomatic tricuspid regurgitation undergoing transcatheter edge-to-edge repair. *J Am Coll Cardiol Intv.* (2018) 11:1119–28. doi: 10.1016/j.jcin.2018.05.0062
93. Lurz P. Stephan von Bardeleben R, Weber M, Sitges M, Sorajja P, Hausleiter J, et al. Transcatheter edge-to-edge repair for treatment of tricuspid regurgitation. *J Am Coll Cardiol.* (2021) 77:229–39. doi: 10.1016/j.jacc.2020.11.038
94. Perlman G, Praz F, Puri R, Ofek H, Ye J, Philippon F, et al. Transcatheter tricuspid valve repair with a new transcatheter coaptation system for the treatment of severe tricuspid regurgitation: 1-year clinical and echocardiographic results. *JACC Cardiovasc Interv*. (2017) 10:1994–2003. doi: 10.1016/j.jcin.2017.06.036
95. Hahn RT, Meduri CU, Davidson CJ, Lim S, Nazif TM, Ricciardi MJ, et al. Early feasibility study of a transcatheter tricuspid valve annuloplasty: SCOUT trial 30-day results. *J Am Coll Cardiol.* (2017) 69:1795–806. doi: 10.1016/j.jacc.2017.01.054
96. Calen C, Taramasso M, Guidotti A, Kuwata S, Nietlispach F, Zuber M, et al. Successful tricinch-in-tricinch transcatheter tricuspid valve repair. *JACC Cardiovasc Interv.* (2017) 10:e75–7. doi: 10.1016/j.jcin.2017.01.032
97. Taramasso M, Benfari G, van der Bijl P, Alessandrini H, Attinger-Toller A, Biasco L, et al. Transcatheter versus medical treatment of patients with symptomatic severe tricuspid regurgitation. *J Am Coll Cardiol.* (2019) 74:2998–3008. doi: 10.1016/j.jacc.2019.09.028
98. Taramasso M, Alessandrini H, Latib A, Asami M, Attinger-Toller A, Biasco L, et al. Outcomes after current transcatheter tricuspid valve intervention: mid-term results from the international trivalve registry. *JACC Cardiovasc Interv.* (2019) 12:155–65. doi: 10.1016/j.jcin.2018.10.022
99. Taramasso M, Gavazzoni M, Pozzoli A, Dreyfus GD, Bolling SF, George I, et al. Tricuspid regurgitation: predicting the need for intervention, procedural success, and recurrence of disease. *JACC Cardiovasc Imaging.* (2019) 12:605–21. doi: 10.1016/j.jcmg.2018.11.034
100. Navia JL, Kapadia S, Elgharably H, Maluenda G, Bartuś K, Baeza C, et al. Transcatheter tricuspid valve implantation of navigate bioprosthesis in a preclinical model. *JACC Basic Transl Sci.* (2018) 3:67–79. doi: 10.1016/j.jacbts.2017.08.003

Conflict of Interest: The authors declare that the research was conducted in the absence of any commercial or financial relationships that could be construed as a potential conflict of interest.

frontiers in Cardiovascular Medicine

ORIGINAL RESEARCH
published: 17 March 2022
doi: 10.3389/fcvm.2022.793666

Atypical Expression of Smooth Muscle Markers and Co-activators and Their Regulation in Rheumatic Aortic and Calcified Bicuspid Valves

Najma Latif[1,2], Padmini Sarathchandra[2], Ann McCormack[1], Magdi H. Yacoub[1,2] and Adrian H. Chester[1,2]*

[1] Heart Science Centre, Magdi Yacoub Institute, Harefield, United Kingdom, [2] National Heart and Lung Institute, Imperial College London, London, United Kingdom

OPEN ACCESS

Edited by:
Hanjoong Jo,
Emory University, United States

Reviewed by:
Katherine Yutzey,
Cincinnati Children's Hospital Medical Center, United States
Maurizio Pesce,
Monzino Cardiology Center (IRCCS), Italy

***Correspondence:**
Najma Latif
n.latif@imperial.ac.uk

Specialty section:
This article was submitted to Heart Valve Disease, a section of the journal Frontiers in Cardiovascular Medicine

Received: *12 October 2021*
Accepted: *22 February 2022*
Published: *17 March 2022*

Citation:
Latif N, Sarathchandra P, McCormack A, Yacoub MH and Chester AH (2022) Atypical Expression of Smooth Muscle Markers and Co-activators and Their Regulation in Rheumatic Aortic and Calcified Bicuspid Valves. Front. Cardiovasc. Med. 9:793666. doi: 10.3389/fcvm.2022.793666

Objective: We have previously reported that human calcified aortic cusps have abundant expression of smooth muscle (SM) markers and co-activators. We hypothesised that cells in bicuspid aortic valve (BAV) cusps and those affected by rheumatic heart valve (RHV) disease may follow a similar phenotypic transition into smooth muscle cells, a process that could be regulated by transforming growth factors (TGFs).

Aims: Cusps from eight patients with BAV and seven patients with RHV were analysed for early and late SM markers and regulators of SM gene expression by immunocytochemistry and compared to healthy aortic valves from 12 unused heart valve donors. The ability of TGFs to induce these markers in valve endothelial cells (VECs) on two substrates was assessed.

Results: In total, 7 out of 8 BAVs and all the RHVs showed an increased and atypical expression of early and late SM markers α-SMA, calponin, SM22 and SM-myosin. The SM marker co-activators were aberrantly expressed in six of the BAV and six of the RHV, in a similar regional pattern to the expression of SM markers. Additionally, regions of VECs, and endothelial cells lining the vessels within the cusps were found to be positive for SM markers and co-activators in three BAV and six RHV. Both BAVs and RHVs were significantly thickened and HIF1α expression was prominent in four BAVs and one RHV. The ability of TGFβs to induce the expression of SM markers and myocardin was greater in VECs cultured on fibronectin than on gelatin. Fibronectin was shown to be upregulated in BAVs and RHVs, within the cusps as well as in the basement membrane.

Conclusion: Bicuspid aortic valves and RHVs expressed increased numbers of SM marker-positive VICs and VECs. Concomittantly, these cells expressed MRTF-A and

myocardin, key regulators of SM gene expression. TGFβ1 was able to preferentially upregulate SM markers and myocardin in VECs on fibronectin, and fibronectin was found to be upregulated in BAVs and RHVs. These findings suggest a role of VEC as a source of cells that express SM cell markers in BAVs and RHVs. The similarity between SM marker expression in BAVs and RHVs with our previous study with cusps from patients with aortic stenosis suggests the existance of a common pathological pathway between these different pathologies.

Keywords: rheumatic, bicuspid, valve, endothelial cells, interstitial cells

HIGHLIGHTS

- Increased and aberrant expression of SM markers and co-activators was observed in all the BAV and RHV cusps.
- The pattern of expression was diffuse in the RHD and localised around calcified areas in BAV.
- RHV showed expression of SM markers and SM co-activators in both VICs, VECs and vessels, BAV showed expression in VICs and a smaller percentage of VECs.
- Strong HIF1α expression was present in 4 of the BAV and 2 RHV and the pattern of expression did not correlate with SM markers.
- TGFβ1 did not significantly influence SM expression by VECs on gelatin.
- Combined fibronectin coating and TGFβ1 treatment resulted in increased expression of SM markers and myocardin by VECs.
- BAV and RHV cusps demonstrated enhanced expression of fibronectin.

INTRODUCTION

Bicuspid aortic valve (BAV) has an estimated prevalence of 0.5–2% (1), a male predominance of about 3:1 and is a developmental aberration (2). The valves usually exhibit normal function at birth, however, the development of valve disease is expedited and typically develops at a much younger age than in people with tricuspid aortic valves. BAV complications include moderate to severe aortic regurgitation (prevalence 13–30%), moderate to severe aortic stenosis (12–37%) and aortic dilatation (20–40%) with lower incidences of endocarditis (3). BAVs experience abnormal flow patterns compared to tricuspid valves resulting in higher mechanical stresses on the cusps and together with inflammation and increased lipid deposition, the process of mineralisation is initiated. It is known that BAV has a heritable nature, however, the genetic causes are still unravelling with mutations in NOTCH1 being implicated (4) and a potential role for GATA5 (5).

Abbreviations: BAV, bicuspid aortic valve; RHV, rheumatic heart valve; SM, smooth muscle; TGF, transforming growth factor; MRTF-A, myocardin related transcription factor A; VIC, valve interstitial cell; VEC, valve endothelial cell; PCNA, proliferating nuclear cell antigen; HIF1α, hypoxia inducible factor 1α.

Rheumatic heart valve (RHV) disease is an autoimmune disease affecting 0.49% of the population in developing countries (6). It is a major problem in sub-Saharan Africa, South Asia and Oceania with an estimated global incidence of 33.4 million cases and 319,400 deaths (7). Heart valve inflammation is thought to be triggered by group A streptococcal pharyngitis and in 3.6% this is followed by acute rheumatic fever (8). Rheumatic fever, if left untreated, can develop into rheumatic heart disease characterised by chronic inflammation, neovascularisation and mild calcification (9). The mitral valve is universally affected, however, concomittant aortic valve disease increases with age (8) and aortic valve pathology is understudied despite its clinical significance. Calcification in rheumatic patients is thought to be actively regulated, not simply dystrophic and warrants investigation.

Despite having different underlying aetiologies, inflammation, remodelling, valvular damage and calcification are common end points in BAV and RHV. The phenotypic changes in the valve interstitial cells (VICs) and valve endothelial cells (VECs) populations in BAV and RHV are poorly defined. Transforming growth factors (TGFs), which exist in three isoforms, TGFβ1, TGFβ2, and TGFβ3, have been implicated to play a role in a number of cardiovascular diseases, including the development of calcific aortic valve disease (10, 11). In BAV, circulating TGFβ1/endoglin has been shown to be upregulated (12, 13), while in RHV, TGFβ1 levels are raised in endothelial cells and SM cells of the vessels, in the perivascular interstitial cells and stroma of the valves as well as α-SMA positive cells in fibrotic areas cusp tissue and in the left atrial appendage of patients in chronic atrial fibrillation (14, 15). One important role for TGFs, together with increased mechanical strain, inflammatory cytokines and activation of Notch1, is to drive the process of endothelial to mesenchymal transformation (EMT) (16–20), which mediates the de-differentiation of endothelial cells into mesenchymal cells. This process has been implicated in the increased number of α-SM actin positive cells in an ovine model of functional mitral valve disease (21).

We and others have previously shown that differentiated cells are present in human calcified valves in the form of myofibroblasts and smooth muscle (SM) cells (22). We hypothesise that the native cell population in BAV and RHV undergo a similar transition process with the expression of SM markers as in aortic valve calcification which can be driven by the effects of TGFs.

MATERIALS AND METHODS

In total, 8 BAV cusps (mean age 26 years, age range 4–31, two females and six males), 7 RHV cusps (mean age 31 years, age range 7–38, one female and six male) and 12 normal aortic valve cusps (mean age 48 years, age range 36–55, eight male, two female) were used for immunocytochemistry and for cell isolation and culture. In total, 7 of the BAVs were calcified, one was fused but not calcified and 4 of the RHVs were calcified.

Cell Isolation and Culture

Healthy human aortic valve cusps were excised and washed in PBS. The valve cusps were incubated in a collagenase solution (Type A, 0.15% w/v; Roche, Life Sciences, South San Francisco, CA, United States) for 10 mins at 37°C under a forceful agitation to remove the VECs. After centrifugation of the solution containing the VECs, the resulting VEC pellets were resuspended in media and plated out in gelatin-coated tissue culture flasks. VECs were grown until confluent in endothelial media, defined as Endothelial Cell Growth Medium 2 (ECGM; PromoCell, Heidelberg, Germany) containing 150 U/ml penicillin/streptomycin (P/S; Sigma Aldrich, Dorset, UK), 2 mM endothelial cell growth supplement, and 20% heat-inactivated fetal calf serum (FCS; Helena Biosciences, Sunderland, United Kingdom). VECs were phenotyped using flow cytometry with antibodies against CD31 and α-SMA (Dako) and cultures with >95% VEC purity were used.

All human studies have been approved by the North London Research Ethics Committee (Ref 10H0724818). These studies have been performed in accordance with the ethical standards

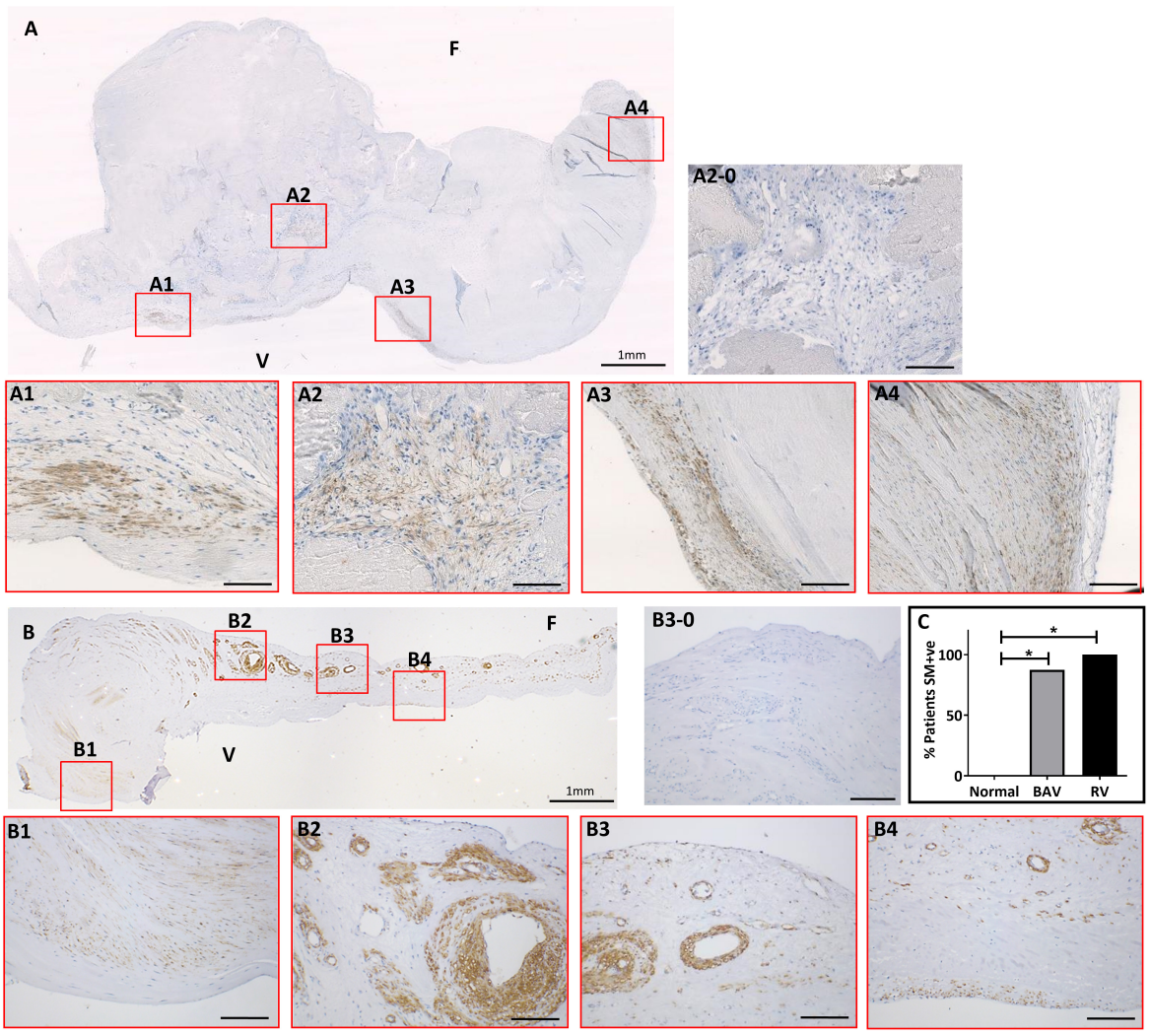

FIGURE 1 | The expression of smooth muscle (SM) markers in a bicuspid aortic valve (BAV) **(A)** and a rheumatic heart valve (RHV) cusps **(B)**. Expanded panels in red boxes show staining patterns from consecutive sections with negative control **(A2-0)**, SM22 **(A1)**, α-SMA **(A2)**, calponin **(A3)**, and SM-myosin **(A4)**. Expanded panels in red boxes show staining patterns from consecutive sections of B with negative control **(B3-0)**, SM22 **(B1)**, α-SMA **(B2)**, calponin **(B3)**, and SM-myosin **(A4)**. Panel **(C)** shows graph showing the incidence of aberrant SM +ve staining in BAV and RHV cusps. F and V represent fibrosal and ventricularis side, respectively. Scale bar in expanded panels represents 200 μm. *$p < 0.005$.

laid down in the 1964 Declaration of Helsinki and its later amendments. All donors gave their written informed consent prior to their inclusion in the study.

Immunochemistry

Valves were washed with PBS, fixed in 10% formal saline for 24 h, washed in distilled water and immersed in EDTA for 2 weeks at 37°C after which processing for paraffin sections was carried out. Five micrometer thick paraffin wax sections of decalcified human bicuspid and rheumatic valve tissue were dewaxed and rehydrated into water, washed in phosphate buffered saline (PBS) for 5 mins. Consecutive (adjacent) sections were used to allow regional staining patterns to be correlated with all the markers. The slides were immersed in 0.1 M citrate buffer (pH 6) and microwaved for 10 mins before blocking for endogenous peroxidases using 0.3% hydrogen peroxide in PBS. Sections were washed twice in PBS and blocked using 3% bovine serum albumin (w/v) (BSA) in PBS containing 1% v/v Tween-20 followed by staining for: α-smooth muscle actin (α-SMA), smooth muscle myosin heavy chain (SM-MHC), calponin, SM22, CD31, vimentin (all Dako), Runx2 (Abcam), myocardin (Covalab), MRTF-A (Santa-Cruz), fibronectin (Actis), PCNA (Biotechnology), HIF1α (Novus), GAPDH (Chemicon), TGFs (R&D), and TGF receptors (Thermofisher, Hemel Hempstead, UK). Negative controls consisted of 3% BSA in PBS containing 1% v/v Tween 20, isotype controls for the monoclonals and rabbit serum for the polyclonals. Primary antibodies were then removed by washing the sections three times in PBS followed by a second layer of biotinylated goat anti-mouse or swine anti-rabbit immunoglobulins (IgG-Vector laboratories) in PBS. Sections were then washed three times in PBS before 1 h incubation with Avidin-Biotin Complex ABC-Vector laboratories). Reactivity was detected using diaminobenzidine tetrahydrochloride (DAB tablets-Sigma) (25 mg/ml) and hydrogen peroxide (0.01% w/v). Sections were then counter stained with Mayers haematoxylin and viewed on Ziess Axioskop microscope. Photomicrographs were taken using Nikon DMX1200 camera.

Immunofluorescence

Valve endothelial cells were seeded onto pre-coated gelatin or fibronectin coverslips and cultured for 10 days with or without TGFs. For immunofluorescent staining, coverslips were washed two times with PBS, fixed in 4% formaldehyde solution (Sigma Aldrich, Dorset, UK) for 10 mins and washed three times with PBS to remove the fixative solution. The coverslips were permeabilised with Triton-X-100 (0.5% v/v) for 3 mins and blocked for 30 min with BSA (3% w/v) and then incubated with primary antibodies at RT for 1 h. After thorough washing in PBS-Tween (PBS-T; Sigma Aldrich, Dorset, UK, 0.1% v/v), coverslips were stained with FITC-conjugated secondary antibodies (Invitrogen, Inchinnan, UK) for 1 h at room temperature and subsequently with DAPI for 10 mins to visualise the cell nuclei. Coverslips were washed with PBS-T, mounted on glass slides in Permafluor aqueous mounting fluid (Beckman Coulter, Fullerton, CA, United States) and analysed with confocal imaging technology.

Transforming Growth Factors-β Treatment of Valve Endothelial Cells

Valve endothelial cells were grown on coverslips coated with 1% gelatin or 10 μg/mL fibronectin, serum-starved in DMEM containing 0.4% FCS for 24 h before being treated with 10 ng/ml of TGFβ1, TGFβ2, and TGFβ3 (R&D) for 10 days. Cells were washed with PBS and fixed in 4% paraformaldehyde for 10 mins. Staining was carried out as above.

Ethics

This study was approved by the Royal Brompton hospital ethics review board and informed consent was obtained from the subjects.

Statistics

All data was tested for normality and appropriate tests were applied. A fisher's exact test was performed on actual numbers for **Figures 1C**, **2G,H**, one way ANOVA and Kruskal-Wallis were used to test for significance using GraphPad Prism 5 and a p value of <0.05 was considered significant.

RESULTS

Bicuspid Aortic Valves and Rheumatic Heart Valves Show Aberrant Expression of Smooth Muscle Markers

The expression of SM cells is localised to the base of the ventricularis in normal human cusps (**Supplementary Figure 1**). Occasionally a few SM cells, by their expression of SM-MHC, can be seen in the region from the base to the central region of the cusps in the ventricularis but hardly any SM cells are detected in the region from the central part of the cusps to the co-apting edge. These SM cells in normal valves express early SM markers such as α-SMA and SM22 and also late SM marker SM-MHC.

The expression of α-SMA, calponin, SM22 and SM-MHC showed mirrored patterns of staining in the same cells and regions of each valve using consecutive sections. This staining was present in clusters of cells of varying numbers predominantly around calcified nodules in BAVs but also distal to calcified zones (**Figure 1A**). The co-apting edges of the BAVs were markedly thickened and calcified and showed this aberrant expression more frequently than other regions of the cusp. The fibrosa and spongiosa also showed small clusters of cells expressing SM-MHC and other SM markers distal to the calcified region without any signs of calcification or thickening. A band of cells staining positive for SM markers was observed in the fibrosa in 5 BAVs. Cells positive for early and late SM markers were increased in number and present in an atypical, spatiotemporal way in 7 out of 8 of the BAVs (those that were calcified, not in the fused BAV) compared to none of the normal controls ($p < 0.005$; **Figure 1C**).

Early and late SM markers showed an extensive increase and atypical expression in all of the RHVs compared to none of the normal controls ($p < 0.005$; **Figure 1C**). This was present in a patchy manner without any specific pattern and present in all the layers and from the base to co-apting edge (**Figure 1B**). A high

percentage VICs in the cusps stained positive for SM-MHC and other SM markers. Five of the 7 RHVs revealed the presence of many of neo-vessels which showed expression of early and late SM markers in their vasculature and endothelial lining. Significantly higher numbers of RHVs showed increased SM staining compared to normal controls ($p < 0.005$). There was no significant difference between the numbers of BAVs and RHVs showing increased SM staining (**Figure 1C**).

Bicuspid Aortic Valves and Rheumatic Heart Valves Show Expression of Smooth Muscle Co-activators

The SM co-activators, myocardin (**Figure 2A**) and MRTF-A (**Figure 2B**) showed no expression in normal cusps except to the base of the ventricularis mirroring the localisation of the SM cells (**Supplementary Figure 1**).

In total, 6 out of 8 BAVs showed an atypical expression of myocardin (**Figures 2C,G**) and MRTF-A (**Figures 2D,G**) which was co-localised to the pattern of the SM markers in their previous sequentially cut sections compared to none of the controls ($p < 0.001$). This staining was predominantly around the calcified zones and the co-apting edges but also present distally. Their expression was also present in all three layers of the valve.

In total, 6 out of 7 RHVs showed an increased atypical pattern of expression of myocardin (**Figures 2E,G**) and MRTF-A (**Figures 2F,G**) compared to the normal controls ($p < 0.001$). This pattern mirrored that of the SM markers in their previous sequentially cut sections with patchy positive staining of VICs in all the layers, from the base to the co-apting edge. The vasculature of all the neo-vessels was positively stained for both markers. There was no significant difference between the numbers of BAVs and RHs showing co-factor staining (**Figure 2G**).

Valve Endothelial Cells From Bicuspid Aortic Valves and Rheumatic Heart Valves Aberrantly Express Smooth Muscle Markers and Co-activators

In total, 3 out of 8 BAVs showed VECs that were positive for SM markers and co-activators (myocardin and MRTF-A) compared

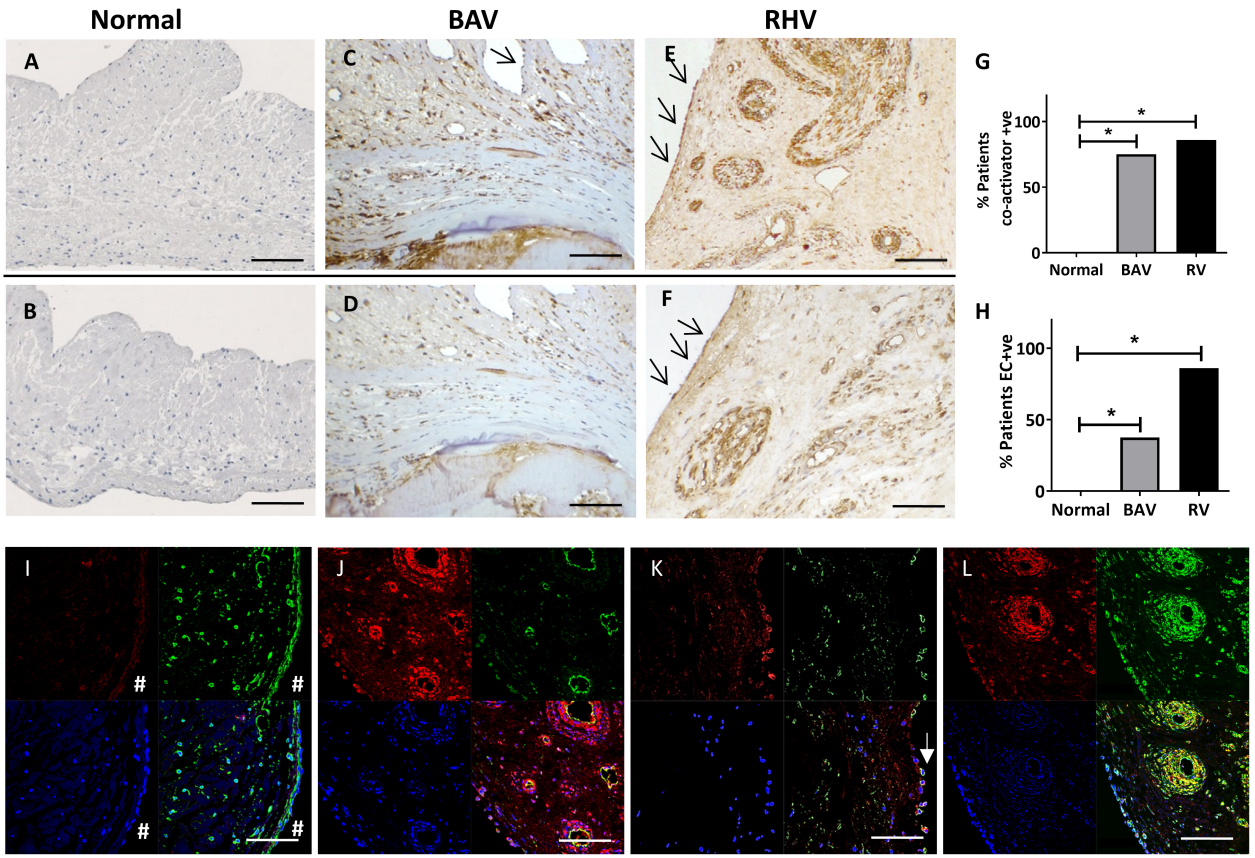

FIGURE 2 | The expression of co-activators myocardin **(A,C,E)** and MRTF-A **(B,D,F)** in normal, BAV and RHV cusps. Graph showing the incidence of BAV and RHD cusps positive for aberrant co-activator expression **(G)** and aberrant expression of co-activators in valve endothelial cells (VECs) **(H)**. Panels **(I–L)** show colocalization of markers in bottom right panels. No expression of myocardin (red) in a normal cusp in VICs or VECs (#), vimentin (green) present in both cell types **(I)**. RHV valve showing myocardin (red) in the endothelial cells and SM cells of their vasculature, (CD31, green) of the vessels and colocalisation in endothelial cells **(J)**. Some surface VECs of a BAV showing co-expression of myocardin (red) with CD31 (green) **(K)**. RHV showing myocardin (red) and SM-MHC (green) in SM of vasculature and some VICs (left side of vessels) **(L)**. Blue is DAPI staining. Scale bar represents 200 μm. *$p < 0.001$.

to none of the normal controls ($p < 0.01$). These positive VECs were partly on the valve surface, but mostly on ECs lining small neovessels (**Figures 2C,D,H**).

All of the RHVs showed some regions of positive VEC staining for SM markers and co-activators compared to none of the normal controls ($p < 0.0001$). Regions of the endothelium on both aortic and ventricular surfaces of the cusps, and ECs lining the small to large neo-vessels were found to be positive for SM markers and co-activators in RHVs (**Figures 2E,F,H**).

There was no significant difference between the numbers of BAVs and RHVs staining positive for SM markers and co-activators. The pattern of staining for myocardin and MRTF-A

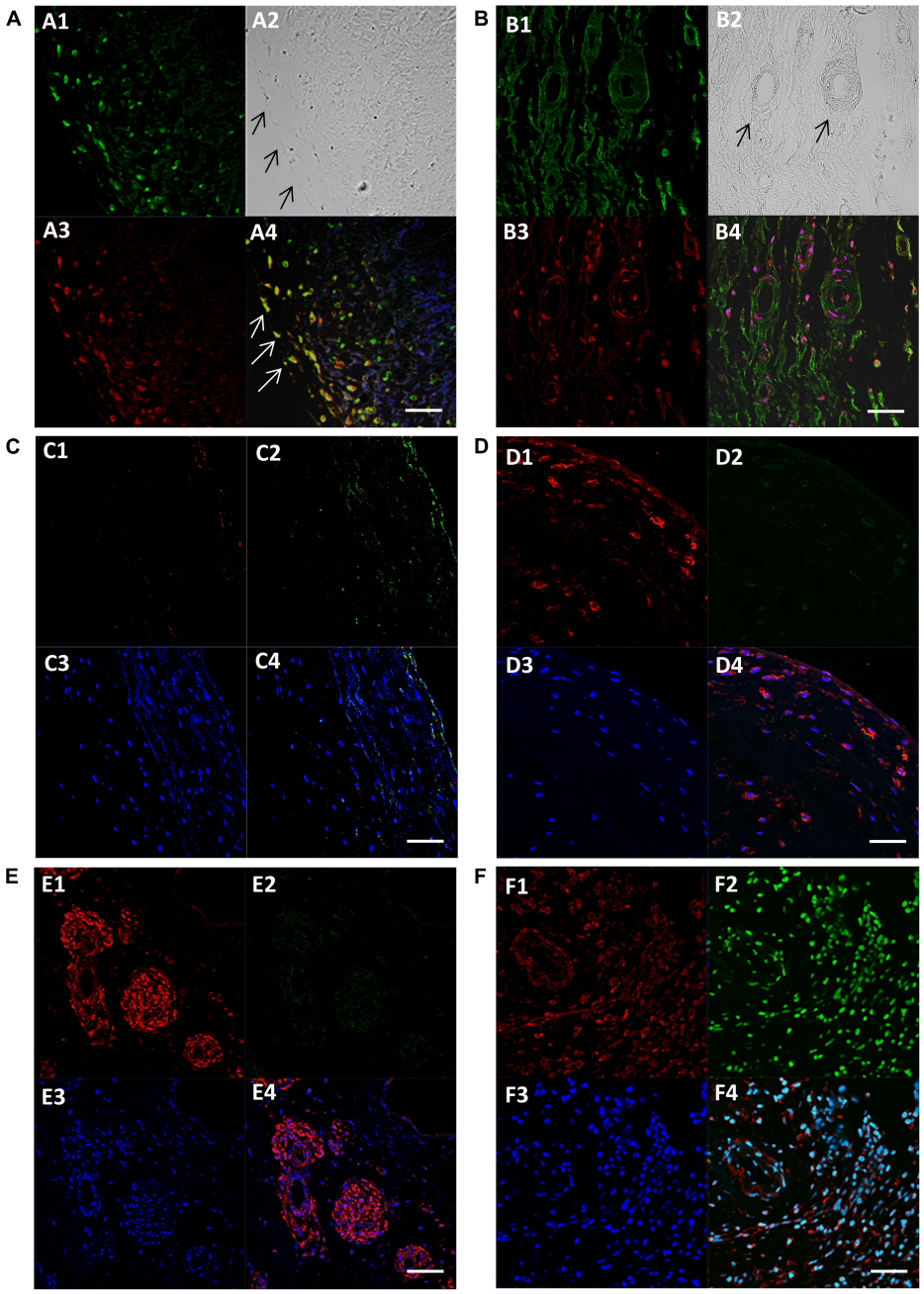

FIGURE 3 | Fluorescent images showing expression of SM-myosin **(A1)**, phase contrast image of the same location showing the edge of the cusp on the left **(A2)**, expression of Runx2 **(A3)**, and co-localisation of SM-myosin and Runx2 **(A4)** in a BAV cusp. Expression of SM-myosin **(B1)**, phase contrast **(B2)**, Runx2 **(B3)**, and co-localisation of SM-myosin and Runx2 **(B4)** in a RHV cusp. Expression of myocardin **(C1–F1)**, PCNA **(C2–F2)**, DAPI **(C3–F3)** and co-localisation of all three respective previous panels **(F1–F4)** in a normal control (**C** panel), BAV cusp (**D** panel), RHV cusp (**E** panel), and tumour tissue (**F** panel) as positive control for PCNA. Scale bar represents 50 μm.

in VECs and VICs mostly overlapped in each valve for BAVs and RHVs as could be seen with staining using consecutive sections (**Figures 2C,D**).

To definitively identify the phenotype of the cells expressing the co-activators, co-localisation staining was performed. Normal valves showed no staining for myocardin in the VICs or VECs (**Figure 2I**). RHVs showed myocardin in the endothelial cells of the vessels (**Figure 2J**) as well as in the SM cells of their vasculature (**Figures 2J,L**) and both BAVs and RHVs showed expression in VICs expressing SM-MHC (**Figure 2L**). Some surface VECs (both ventricular and fibrosal sides) of both BAVs and RHVs showed co-expression of myocardin (**Figure 2K**).

Valve Endothelial Cells Co-express Smooth Muscle Markers and Markers of Calcification

We questioned whether the VECs that expressed SM markers also co-expressed markers of calcification. We observed that some VECs at the surface and just under the surface of 5 BAVs were able to co-express SM markers and Runx2 (**Figures 3A1–4**). Four RHVs showed more co-expression of SM and Runx2 in VECs of the neovessels than the cusp surfaces (**Figures 3B1–4**).

Cells Expressing Smooth Muscle Markers and Co-activators Are Not Proliferative

The presence of cells expressing SM markers within the BAVs and RHVs provoked the question of whether these cells are contractile or synthetic and we assessed this by co-staining for proliferative markers PCNA and Ki67 with myocardin. We did not observe any PCNA or Ki67 (not shown) staining that colocalised with the SM markers (**Figures 3C–F**).

Assessment of Hypoxia Inducible Factor 1α and Correlation With Smooth Muscle Markers

Both BAV and RHV were significantly thickened with BAV having a maximal average thickness of 2.97 ± 1.2 mm and RHV, 2.05 ± 0.56 mm. Cells in such thick BAVs and RHVs may become hypoxic and initiate pathways to induce hypoxia inducible factor 1α (HIF1α). The expression of HIF1α was correlated with SM markers by analysing HIF1α in all groups. Normal cusps showed rare nuclear HIF1α-positive VICs, however, of the seven normal cusps analysed, three showed some ventricular VEC nuclear HIF1α positivity with the occasional nuclear positive VIC (**Figures 4A,B**). There was no HIF1α expression in the BAV that was not calcified despite being thickened. Of the remaining seven calcified, thickened BAVs, four showed many VICs with nuclear HIF1α expression (**Figure 4C**) around and distal to calcified regions, with numbers of positive cells far outnumbering those expressing SM markers and the remaining BAVs showed occasional nuclear positive VICs. There was occasional surface (both sides) nuclear VEC HIF1α expression in 2 BAVs (**Figure 4C**) and the endothelial cells of vessels were marginally positive (**Figure 4D**). Three of the RHVs showed no expression of HIF1α. The other four showed strong nuclear expression of HIF1α on some fibrosal and ventricular VEC (**Figures 4E,F**) and weaker expression in the vasculature of the vessels (**Figure 4F**). Only 1 RHV showed endothelium positivity of the vessels and the same RHV showed some HIF1α in VICs. The pattern of HIF1α did not correspond to the SM marker expression in BAVs and RHVs.

Smooth Muscle Markers and Co-activators Are Modulated by Transforming Growth Factors and Substrate Coating in Valve Endothelial Cells

We have previously shown that TGFβ1 was able to upregulate the expression of SM markers and MRTF-A in VICs so we sought to address whether TGFβs could modulate their expression in VECs as well as assessing the role of surface coating with gelatin and fibronectin. On gelatin coated slides, VECs treated with TGFβ1 only showed a significant expression of SM22 ($p < 0.05$), treated with TGFβ2 showed a significant expression of αSMA ($p < 0.05$) and SM22 ($p < 0.05$) and treated with TGFβ3 showed a significant expression of αSMA ($p < 0.05$), SM22 ($p < 0.05$) and myocardin ($p < 0.01$; **Figure 5A**).

However, when VECs were cultured on fibronectin, TGFβ1 was able to significantly increase calponin ($p < 0.05$), α-SMA ($p < 0.05$) and SM22 ($p < 0.01$); TGFβ2 was able to significantly increase calponin ($p < 0.05$), αSMA ($p < 0.05$), SM22 ($p < 0.01$) and myocardin ($p < 0.05$); TGFβ3 was able to significantly

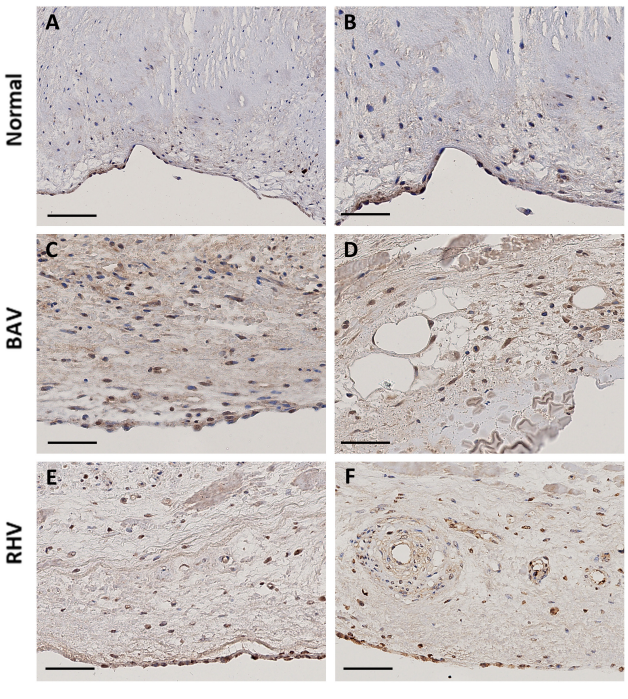

FIGURE 4 | The expression of HIF1α in a normal cusp **(A,B)**, BAV **(C,D)**, and RHV **(E,F)**. Scale bar is 100 μm in panel **(A)** and 50 μm in all other panels.

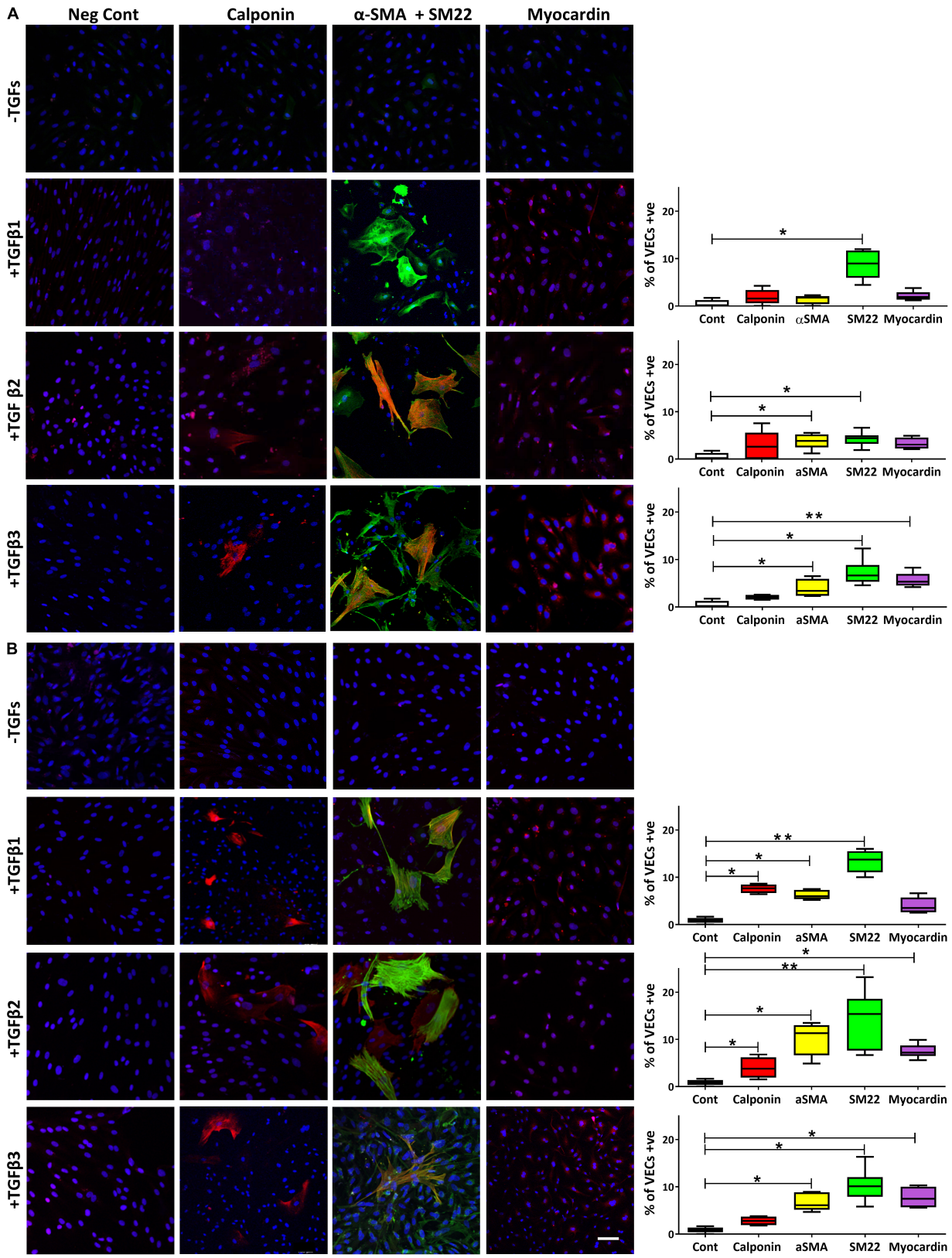

FIGURE 5 | The expression of calponin, α-SMA and SM22 merged, and myocardin in VECs plated on gelatin **(A)** and on fibronectin **(B)** and treated with TGFs. Scale bar represents 50 μm. *p,0.05, **$p < 0.01$.

increase αSMA ($p < 0.05$) and SM22 ($p < 0.05$) and myocardin ($p < 0.05$; **Figure 5B**).

Fibronectin Is Upregulated in Bicuspid Aortic Valves and Rheumatic Heart Valves

As the response of VECs to upregulate SM markers and myocardin was more pronounced when treated with TGFβs cultured on fibronectin, we questioned whether the expression of fibronectin was dysregulated in BAVs and RHVs. Normal cusps showed moderate staining in the fibrosa and ventricularis with reduced and patchy staining in the spongiosa (**Figure 6A**). 6/8 BAVs (**Figure 6B**) and 5/7 RHVs (**Figure 6C**) showed increased intensity of staining for fibronectin in the fibrosa, ventricularis and in the basal lamina with increased patchy staining of the spongiosa. Quantitation showed significantly increased levels of fibronectin in BAVs and RHVs (**Figure 6D**), $p < 0.05$.

Transforming Growth Factor βs Enhance Fibronectin Expression by Valve Endothelial Cells Preferentially Plated on Fibronectin

As fibronectin was increased in BAVs and RHVs, we questioned whether TGFs were able to differentially upregulate fibronectin produced by VECs, whether plated on gelatin or fibronectin.

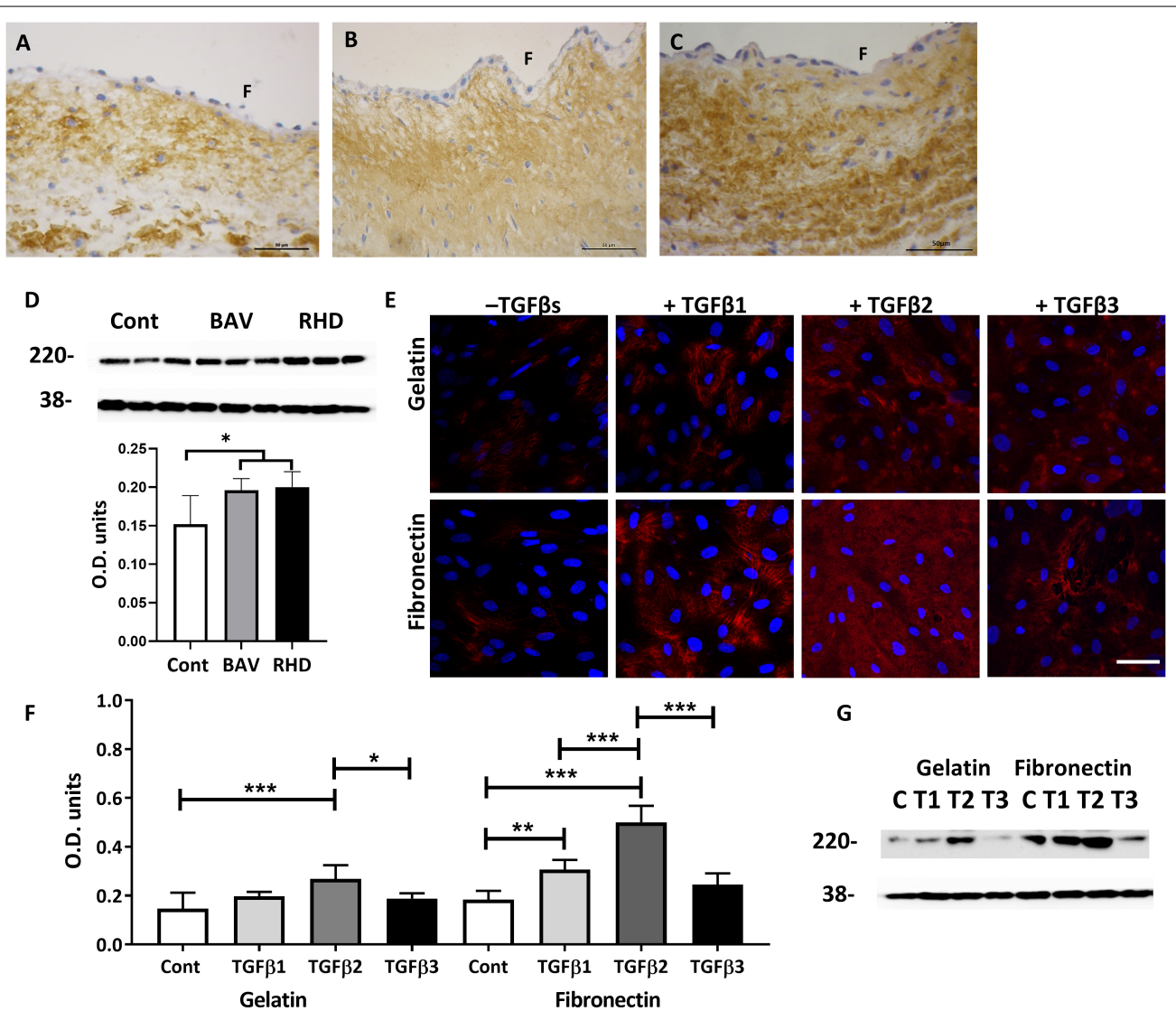

FIGURE 6 | The expression of fibronectin on a normal **(A)** BAV, **(B)** RHV, **(C)** cusp, and quantitative levels **(D)**. The expression of fibronectin by VECs plated on gelatin (top panel) and on fibronectin (bottom panel) and treated with TGFs **(E)**. Graph showing the level of expression of fibronectin by VECs when plated on gelatin or fibronectin and treated with TGFs **(F)** and the corresponding Western blot showing levels of fibronectin at 220 kD and the housekeeping protein GAPDH at 38 kD **(G)**. Panel **(F)** represents the fibrosal side. Scale bar in panel **(A–C)** is 50 μm, in panel **(D)** is 100 μm. *p,0.05, **$p < 0.01$, ***$p < 0.001$.

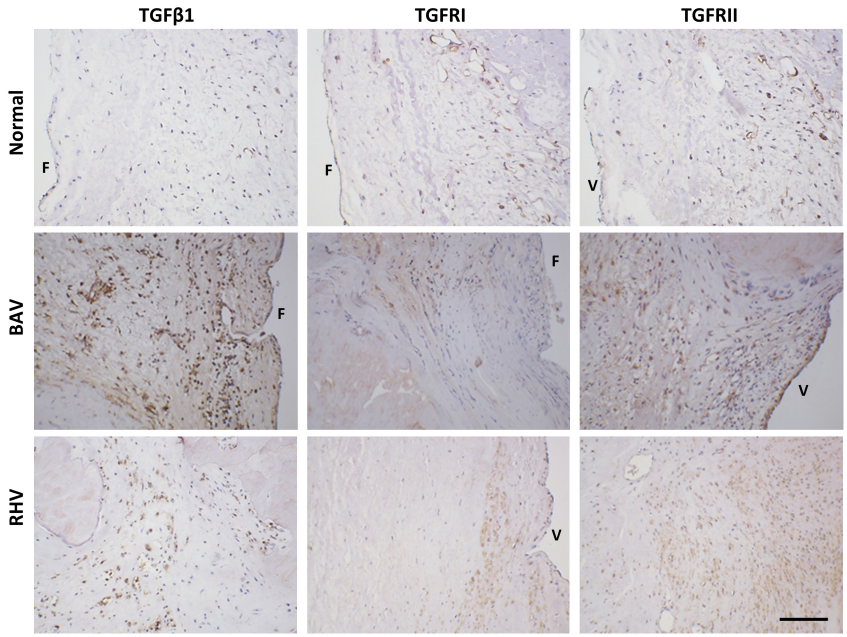

FIGURE 7 | The expression of transforming growth factor β1 (TGFβ1), TGFR1, and TGFRII in normal, BAV and RHV cusps. F and V represent the fibrosal and ventricularis side, respectively. Scale bar is 200 μm.

Untreated VECs plated on gelatin and fibronectin showed a similar low intensity of staining and level for fibronectin (**Figures 6E–G**). TGFβ1 was able to significantly upregulate the expression of fibronectin by VECs but only when plated on fibronectin ($p < 0.01$). TGFβ2 was able to significantly upregulate the expression of fibronectin by VECs plated on gelatin and fibronectin ($p < 0.001$). Increased expression of fibronectin was observed within the VECs and in the extracellular spaces (**Figure 6E**). However, TGFβ3 was unable to upregulate fibronectin by VECs either on gelatin or fibronectin coated plates (**Figures 6F,G**).

Transforming Growth Factor β1, TGFRI, and TGFRII Are Upregulated in Bicuspid Aortic Valves and Rheumatic Heart Valves

There was no to very little expression of TGFβ1 in normal cusps, however, BAVs and RHVs showed greatly increased numbers of VICs staining positive for TGFβ1. The antibodies for TGFβ2 and TGFβ3 were found not be suitable for human valve tissue in paraffin sections. Both TGFRI and TGFRII were found to be expressed in up to 50% of normal VICs, however, some regions in cusps from BAVs and RHVs showed 100% expression of TGFRII (**Figure 7**).

DISCUSSION

Calcification is expedited in BAVs and occasionally present in aortic RHVs and this is partly driven by the native cell population and partly through inflammatory cells, mediators and disturbed flow patterns. We have shown that both the VECs and VICs of BAVs and RHVs exhibit an atypical expression of SM markers and the co-activators myocardin and MRTF-A. The expression of these markers can be induced in VECs by TGFβs, an effect that is enhanced when the cells were cultured on fibronectin. Fibronectin expression in the diseased groups was found to be enhanced within the cusp layers as well as in the basement membrane providing a conducive environment for VEC differentiation. The elevated expression of TGFβ receptors concomittant with enhanced fibronectin expression in BAVs and RHVs would facilitate the signalling by TGFs in BAVs and RHVs.

We have previously shown an upregulated and dysregulated spatial expression of SM markers and co-activators, myocardin and MRTFs, in both the VICs and VECs of calcified tricuspid valves (22). α-SMA has been shown previously in calcified valves and the valvular cells were ascribed a myofibroblastic phenotype, however, when these cells also co-express SM-specific markers such as SM-myosin heavy chain, SM master co-activator myocardin and structural charactersitics of SM cells, these cells are best described as SM cells. A minority of cells expressing α-SMA did not express the SM-MHC in our previous study and in this study and are thus myofibroblasts. It is quite plausible that the VICs expressing the early SM marker SM22 without the late marker SM-MHC are designated myofibroblasts before they go on to expressing the late SM markers and co-activators. Remarkably there is scarce published data on the phenotypic changes occuring in human BAVs. One study reported no difference in the expression of α-SMA between BAV and TAV VICs in culture (23), however, it is known that VICs differentiate

in vitro (24, 25) and this difference would have been nullified by *in vitro* culture under their conditions. Similarly, the expression of SM markers and co-activators have not been previously shown in VICs and VECs in RHV.

The SM marker and co-activator expressing cells were shown not to be proliferative by the absence of PCNA in myocardin positive cells and are most likely to be of the contractile type as they strongly expressed SM-MHC and myocardin. Overexpression of myocardin has been shown to inhibit cell cycle progression (26) and both MRTF-A and -B have anti-proliferative effects (27). The differentiation of valvular cells into a contractile nature, as we have shown previously in tricuspid calcified valves (22) may be a compensatory mechanism to overcome the stiffening entailed during the disease process.

Valve endothelial cell differentiation into SM types has been previously reported by us (22) and endothelial cells have been shown to have transdifferentiation potential into the SM phenotype by inducing the expression of myocardin (28) and cyclic strain (29).

Normal aortic cusps have a mean thickness of 0.60 ± 0.21 mm and this allows diffusion of oxygen without the need for a vascular system (30). Only 4 BAVs and 1 RHV showed an increase in HIF1α in VICs despite being significantly thicker. The abundance of HIF1α in BAVs did not result in significant neoangiogenesis in the central layers though vessels were observed in the outer layers of 3 BAVs. Surprisingly, 4 of the 7 RHVs showed strong HIF1α expression in the surface VECs where hypoxic conditions would not be expected. There is significance in the expression of HIF1α in the SM cells of the vasculature as HIF1α has been shown to play a role in phosphate-induced vascular SM cell calcification (31). We have previously documented a similar pattern of expression of HIF1α in rheumatic mitral VICs, surface VECs and in vessels and the induction of HIF1α by hypoxic conditions (32). HIF1α can also be induced by disturbed flow (33) and TNFα (34) and has been shown in stenotic aortic valves (35). The role of HIF1α warrants further investigation in diseased cusps.

Proinflammatory cytokines play a role in the progression and maintenance of valvular cell differentiation and TGFβ1 has been shown to be present in degenerative calcific aortic stenotic cusps. Contradictingly, TGFβ1 was shown not to be increased in the media from BAV or rheumatic valves (36) but in another study found to be highly present in 70% of rheumatic mitral valves (14). Elevated TGFβ1 can also result from polymorphisms in the TGF1 gene and it was shown that RV patients have a lower frequency of TGFβ1 C?T (509) genotype and a higher frequency of T?C (869) allele with the latter polymorphism resulting in raised TGFβ 1 (37).

Transforming growth factor β1-mediated endothelial to mesenchymal transformation (EMT) has been shown to correlate with enhanced expression of laminin and fibronectin (38). TGF-β1 is extremely important in inducing the differentiation of VICs to myofibroblasts (25, 39). The expression of all three isoforms of TGFβs will play a significant role in the differentiation of adult VECs undergoing EMT and further differentiating to express SM markers. All three isoforms have been shown to induce EMT in human microvascular ECs with the effect of TGFβ2 being most pronounced (40). The presence of SM markers and co-activators in VECs of BAVs and RHVs is indicative of an on-going EMT process in these cells. Cues from specific ECM components can also play a role in the EMT process and fibronectin was shown to be present at early stages of EMT and appeared as a progressively expanding gradient of material with the greatest density nearer the myocardium in the AV canal and outflow tract (41). Fibronectin is abundant in the ECM through which endocardial-mesenchymal cells migrate as they begin formation of the cushion tissue (41) and it is a key component of the basement membrane on which the VECs reside. EMT is a crucial process for valve development but is not restricted to embryonic development as adult ovine mitral VECs have been shown to undergo EMT (42).

We have previously shown the spatial expression of fibronectin in normal aortic valves (43) and now show that BAVs and RHVs demonstrated an enhanced expression of fibronectin within the valves and at regions of the basement membrane. This increased expression of fibronectin is expressed by VICs that have become activated in response to injury (44) and by the VECs. The combination of increased fibronectin and TGFs can synergistically provide the signals for VEC EMT and drive the differentiation process further to express SM markers and co-activators. Alterations in ECM composition are known to affect EMT with collagen IV and fibronectin promoting EMT in ovine mitral VECs (45) and high levels of chondroitin sulphate have been shown to induce the highest rates of EMT in porcine VECs (46).

Inhibiting the pathological differentiation of resident cells of the valve is key in the therapeutic intervention and prevention of calcification. The high propensity of SM cells to calcify and result in atherosclerotic lesions suggests that this SM-type differentiation would be a key step for intervention. However, it remains to be determined what proportion of resident cells differentiate to osteoblastic-type cells through the SM phenotype and whether some cells can bypass this transition.

This report documents the atypical expression of SM markers and co-activators in BAVs and RHVs and shows that the TGFs can preferentially increase these markers dependent on substrate transformation in terms of composition and stiffness. It is likely that the SM-positive cells in the diseased BAV and RHV are derived from endothelial cells, via an EMT process, from differentiation of the VIC population and possibly from infiltrating cells. The significance of the SM cells may be that they have a greater propensity to calcify. The elevated expression of fibronectin and TGF receptors augments this efficacy of the signalling pathways that stimulate the VECs to express SM markers. Further studies are warranted to ascertain the pathological contribution of SM cells in the valves and whether strategies aimed at blocking this transformation would prove beneficial as a therapeutic intervention. This study has provided an insight into the phenotypic changes in the valve cell population that occur in BAVs and RHVs. Understanding the

contribution that specific cell phenotypes make to valve disease represents an important step toward the development of novel strategies to control or prevent the progression of the disease.

DATA AVAILABILITY STATEMENT

The original contributions presented in the study are included in the article/**Supplementary Material**, further inquiries can be directed to the corresponding author.

ETHICS STATEMENT

The studies involving human participants were reviewed and approved by Royal Brompton and Harefield Ethics Committee. The patients/participants provided their written informed consent to participate in this study.

AUTHOR CONTRIBUTIONS

NL designed and executed the work, analysed the data, wrote the manuscript, and proofread. PS and AM performed some of the experiments. MY and AC designed, wrote, and proofread. All authors contributed to the article and approved the submitted version.

FUNDING

We would like to acknowledge the Magdi Yacoub Institute for funding this research.

SUPPLEMENTARY MATERIAL

The Supplementary Material for this article can be found online at: https://www.frontiersin.org/articles/10.3389/fcvm.2022.793666/full#supplementary-material

REFERENCES

1. Tutar E, Ekici F, Atalay S, Nacar N. The prevalence of bicuspid aortic valve in newborns by echocardiographic screening. *Am Heart J.* (2005) 150:513–5. doi: 10.1016/j.ahj.2004.10.036
2. Siu SC, Silversides CK. Bicuspid aortic valve disease. *J Am Coll Cardiol.* (2010) 55:2789–800.
3. Masri A, Svensson LG, Griffin BP, Desai MY. Contemporary natural history of bicuspid aortic valve disease: a systematic review. *Heart.* (2017) 103:1323–30. doi: 10.1136/heartjnl-2016-309916
4. Garg V, Muth AN, Ransom JF, Schluterman MK, Barnes R, King IN, et al. Mutations in NOTCH1 cause aortic valve disease. *Nature.* (2005) 437:270–4. doi: 10.1038/nature03940
5. Laforest B, Andelfinger G, Nemer M. Loss of Gata5 in mice leads to bicuspid aortic valve. *J Clin Invest.* (2011) 121:2876–87. doi: 10.1172/JCI44555
6. Zuhlke LJ, Steer AC. Estimates of the global burden of rheumatic heart disease. *Glob Heart.* (2013) 8:189–95.
7. Watkins DA, Johnson CO, Colquhoun SM, Karthikeyan G, Beaton A, Bukhman G, et al. Global, regional, and national burden of rheumatic heart disease, 1990-2015. *N Engl J Med.* (2017) 377:713–22. doi: 10.1056/NEJMoa1603693
8. Carapetis JR, Beaton A, Cunningham MW, Guilherme L, Karthikeyan G, Mayosi BM, et al. Acute rheumatic fever and rheumatic heart disease. *Nat Rev Dis Primers.* (2016) 2:15084.
9. Xiao F, Zheng R, Yang D, Cao K, Zhang S, Wu B, et al. Sex-dependent aortic valve pathology in patients with rheumatic heart disease. *PLoS One.* (2017) 12:e0180230. doi: 10.1371/journal.pone.0180230
10. Agrotis A, Kalinina N, Bobik A. Transforming growth factor-beta, cell signaling and cardiovascular disorders. *Curr Vasc Pharmacol.* (2005) 3:55–61. doi: 10.2174/1570161052773951
11. Jian B, Narula N, Li QY, Mohler ER III, Levy RJ. Progression of aortic valve stenosis: TGF-beta1 is present in calcified aortic valve cusps and promotes aortic valve interstitial cell calcification via apoptosis. *Ann Thorac Surg.* (2003) 75:457–65; discussion 65–6. doi: 10.1016/s0003-4975(02)04312-6
12. Hillebrand M, Millot N, Sheikhzadeh S, Rybczynski M, Gerth S, Kolbel T, et al. Total serum transforming growth factor-beta1 is elevated in the entire spectrum of genetic aortic syndromes. *Clin Cardiol.* (2014) 37:672–9. doi: 10.1002/clc.22320
13. Rocchiccioli S, Cecchettini A, Panesi P, Farneti PA, Mariani M, Ucciferri N, et al. Hypothesis-free secretome analysis of thoracic aortic aneurysm reinforces the central role of TGF-beta cascade in patients with bicuspid aortic valve. *J Cardiol.* (2017) 69:570–6. doi: 10.1016/j.jjcc.2016.05.007
14. Kim L, Kim DK, Yang WI, Shin DH, Jung IM, Park HK, et al. Overexpression of transforming growth factor-beta 1 in the valvular fibrosis of chronic rheumatic heart disease. *J Korean Med Sci.* (2008) 23:41–8. doi: 10.3346/jkms.2008.23.1.41
15. Zhang D, Liu X, Chen X, Gu J, Li F, Zhang W, et al. Role of the MAPKs/TGF-beta1/TRAF6 signaling pathway in atrial fibrosis of patients with chronic atrial fibrillation and rheumatic mitral valve disease. *Cardiology.* (2014) 129:216–23. doi: 10.1159/000366096
16. Paranya G, Vineberg S, Dvorin E, Kaushal S, Roth SJ, Rabkin E, et al. Aortic valve endothelial cells undergo transforming growth factor-beta-mediated and non-transforming growth factor-beta-mediated transdifferentiation in vitro. *Am J Pathol.* (2001) 159:1335–43. doi: 10.1016/s0002-9440(10)62520-5
17. Balachandran K, Alford PW, Wylie-Sears J, Goss JA, Grosberg A, Bischoff J, et al. Cyclic strain induces dual-mode endothelial-mesenchymal transformation of the cardiac valve. *Proc Natl Acad Sci USA.* (2011) 108:19943–8. doi: 10.1073/pnas.1106954108
18. Farrar EJ, Butcher JT. Heterogeneous susceptibility of valve endothelial cells to mesenchymal transformation in response to TNFalpha. *Ann Biomed Eng.* (2014) 42:149–61. doi: 10.1007/s10439-013-0894-3
19. Mahler GJ, Farrar EJ, Butcher JT. Inflammatory cytokines promote mesenchymal transformation in embryonic and adult valve endothelial cells. *Arterioscler Thromb Vasc Biol.* (2013) 33:121–30. doi: 10.1161/ATVBAHA.112.300504
20. Yang JH, Wylie-Sears J, Bischoff J. Opposing actions of Notch1 and VEGF in post-natal cardiac valve endothelial cells. *Biochem Biophys Res Commun.* (2008) 374:512–6. doi: 10.1016/j.bbrc.2008.07.057
21. Bischoff J, Casanovas G, Wylie-Sears J, Kim DH, Bartko PE, Guerrero JL, et al. CD45 expression in mitral valve endothelial cells after myocardial infarction. *Circ Res.* (2016) 119:1215–25. doi: 10.1161/CIRCRESAHA.116.309598
22. Latif N, Sarathchandra P, Chester AH, Yacoub MH. Expression of smooth muscle cell markers and co-activators in calcified aortic valves. *Eur Heart J.* (2015) 36:1335–45. doi: 10.1093/eurheartj/eht547
23. Aggarwal A, Ferrari G, Joyce E, Daniels MJ, Sainger R, Gorman JH III, et al. Architectural trends in the human normal and bicuspid aortic valve leaflet and its relevance to valve disease. *Ann Biomed Eng.* (2014) 42:986–98. doi: 10.1007/s10439-014-0973-0
24. Latif N, Quillon A, Sarathchandra P, McCormack A, Lozanoski A, Yacoub MH, et al. Modulation of human valve interstitial cell phenotype and function using a fibroblast growth factor 2 formulation. *PLoS One.* (2015) 10:e0127844. doi: 10.1371/journal.pone.0127844
25. Porras AM, van Engeland NC, Marchbanks E, McCormack A, Bouten CV, Yacoub MH, et al. Robust generation of quiescent porcine valvular interstitial

cell cultures. *J Am Heart Assoc.* (2017) 6:e005041. doi: 10.1161/JAHA.116.005041
26. Milyavsky M, Shats I, Cholostoy A, Brosh R, Buganim Y, Weisz L, et al. Inactivation of myocardin and p16 during malignant transformation contributes to a differentiation defect. *Cancer Cell.* (2007) 11:133–46. doi: 10.1016/j.ccr.2006.11.022
27. Shaposhnikov D, Descot A, Schilling J, Posern G. Myocardin-related transcription factor A regulates expression of Bok and Noxa and is involved in apoptotic signalling. *Cell Cycle.* (2012) 11:141–50. doi: 10.4161/cc.11.1.18499
28. Ji H, Atchison L, Chen Z, Chakraborty S, Jung Y, Truskey GA, et al. Transdifferentiation of human endothelial progenitors into smooth muscle cells. *Biomaterials.* (2016) 85:180–94. doi: 10.1016/j.biomaterials.2016.01.066
29. Cevallos M, Riha GM, Wang X, Yang H, Yan S, Li M, et al. Cyclic strain induces expression of specific smooth muscle cell markers in human endothelial cells. *Differentiation.* (2006) 74:552–61. doi: 10.1111/j.1432-0436.2006.00089.x
30. Yacoub MH, Tsang V, Sarathchandra P, Jensen H, Hughes S, Latif N. Long-term adaptive versus maladaptive remodelling of the pulmonary autograft after the Ross operation. *Eur J Cardiothorac Surg.* (2020) 57:977–85. doi: 10.1093/ejcts/ezaa019
31. Mokas S, Lariviere R, Lamalice L, Gobeil S, Cornfield DN, Agharazii M, et al. Hypoxia-inducible factor-1 plays a role in phosphate-induced vascular smooth muscle cell calcification. *Kidney Int.* (2016) 90:598–609. doi: 10.1016/j.kint.2016.05.020
32. Salhiyyah K, Sarathchandra P, Latif N, Yacoub MH, Chester AH. Hypoxia-mediated regulation of the secretory properties of mitral valve interstitial cells. *Am J Physiol Heart Circ Physiol.* (2017) 313:H14–23. doi: 10.1152/ajpheart.00720.2016
33. Fernandez Esmerats J, Villa-Roel N, Kumar S, Gu L, Salim MT, Ohh M, et al. Disturbed flow increases UBE2C (ubiquitin E2 ligase C) via loss of miR-483-3p, inducing aortic valve calcification by the pVHL (von Hippel-Lindau protein) and HIF-1alpha (hypoxia-inducible factor-1alpha) pathway in endothelial cells. *Arterioscler Thromb Vasc Biol.* (2019) 39:467–81. doi: 10.1161/ATVBAHA.118.312233
34. Parra-Izquierdo I, Sanchez-Bayuela T, Lopez J, Gomez C, Perez-Riesgo E, San Roman JA, et al. Interferons are pro-inflammatory cytokines in sheared-stressed human aortic valve endothelial cells. *Int J Mol Sci.* (2021) 22:10605. doi: 10.3390/ijms221910605
35. Perrotta I, Moraca FM, Sciangula A, Aquila S, Mazzulla S. HIF-1alpha and VEGF: immunohistochemical profile and possible function in human aortic valve stenosis. *Ultrastruct Pathol.* (2015) 39:198–206. doi: 10.3109/01913123.2014.991884
36. Kochtebane N, Passefort S, Choqueux C, Ainoun F, Achour L, Michel JB, et al. Release of leukotriene B4, transforming growth factor-beta1 and microparticles in relation to aortic valve calcification. *J Heart Valve Dis.* (2013) 22:782–8.
37. Chou HT, Chen CH, Tsai CH, Tsai FJ. Association between transforming growth factor-beta1 gene C-509T and T869C polymorphisms and rheumatic heart disease. *Am Heart J.* (2004) 148:181–6. doi: 10.1016/j.ahj.2004.03.032
38. Sales VL, Engelmayr GC Jr, Mettler BA, Johnson JA Jr, Sacks MS, Mayer JE Jr. Transforming growth factor-beta1 modulates extracellular matrix production, proliferation, and apoptosis of endothelial progenitor cells in tissue-engineering scaffolds. *Circulation.* (2006) 114(1 Suppl.):I193–9. doi: 10.1161/CIRCULATIONAHA.105.001628
39. Walker GA, Masters KS, Shah DN, Anseth KS, Leinwand LA. Valvular myofibroblast activation by transforming growth factor-beta: implications for pathological extracellular matrix remodeling in heart valve disease. *Circ Res.* (2004) 95:253–60. doi: 10.1161/01.RES.0000136520.07995.aa
40. Sabbineni H, Verma A, Somanath PR. Isoform-specific effects of transforming growth factor beta on endothelial-to-mesenchymal transition. *J Cell Physiol.* (2018) 233:8418–28. doi: 10.1002/jcp.26801
41. Kitten GT, Markwald RR, Bolender DL. Distribution of basement membrane antigens in cryopreserved early embryonic hearts. *Anat Rec.* (1987) 217:379–90. doi: 10.1002/ar.1092170409
42. Wylie-Sears J, Aikawa E, Levine RA, Yang JH, Bischoff J. Mitral valve endothelial cells with osteogenic differentiation potential. *Arterioscler Thromb Vasc Biol.* (2011) 31:598–607. doi: 10.1161/ATVBAHA.110.216184
43. Latif N, Sarathchandra P, Taylor PM, Antoniw J, Yacoub MH. Localization and pattern of expression of extracellular matrix components in human heart valves. *J Heart Valve Dis.* (2005) 14:218–27.
44. Fayet C, Bendeck MP, Gotlieb AI. Cardiac valve interstitial cells secrete fibronectin and form fibrillar adhesions in response to injury. *Cardiovasc Pathol.* (2007) 16:203–11. doi: 10.1016/j.carpath.2007.02.008
45. Wang Z, Calpe B, Zerdani J, Lee Y, Oh J, Bae H, et al. High-throughput investigation of endothelial-to-mesenchymal transformation (EndMT) with combinatorial cellular microarrays. *Biotechnol Bioeng.* (2016) 113:1403–12. doi: 10.1002/bit.25905
46. Dahal S, Huang P, Murray BT, Mahler GJ. Endothelial to mesenchymal transformation is induced by altered extracellular matrix in aortic valve endothelial cells. *J Biomed Mater Res A.* (2017) 105:2729–41. doi: 10.1002/jbm.a.36133

Conflict of Interest: The authors declare that the research was conducted in the absence of any commercial or financial relationships that could be construed as a potential conflict of interest.

Publisher's Note: All claims expressed in this article are solely those of the authors and do not necessarily represent those of their affiliated organizations, or those of the publisher, the editors and the reviewers. Any product that may be evaluated in this article, or claim that may be made by its manufacturer, is not guaranteed or endorsed by the publisher.

frontiers | Frontiers in Cardiovascular Medicine

ORIGINAL RESEARCH
published: 06 April 2022
doi: 10.3389/fcvm.2022.840647

Profiling Genome-Wide DNA Methylation Patterns in Human Aortic and Mitral Valves

Sarah Halawa[1,2], Najma Latif[3,4], Yuan-Tsan Tseng[3,4], Ayman M. Ibrahim[1,5], Adrian H. Chester[3,4], Ahmed Moustafa[2,6], Yasmine Aguib[1,4*†] and Magdi H. Yacoub[1,3,4*†]*

[1] Aswan Heart Centre, Aswan, Egypt, [2] Biotechnology Graduate Program, American University in Cairo, New Cairo, Egypt, [3] Heart Science Centre, Magdi Yacoub Institute, Harefield, United Kingdom, [4] National Heart and Lung Institute (NHLI), Imperial College London, London, United Kingdom, [5] Zoology Department, Faculty of Science, Cairo University, Giza, Egypt, [6] Department of Biology, American University in Cairo, New Cairo, Egypt

OPEN ACCESS

Edited by:
Michel Puceat,
Institut National de la Santé et de la Recherche Médicale (INSERM), France

Reviewed by:
Francesca Bartoli-Leonard,
Brigham and Women's Hospital and Harvard Medical School, United States
Marco Morselli,
University of Parma, Italy

***Correspondence:**
Magdi H. Yacoub
m.yacoub@imperial.ac.uk
Yasmine Aguib
y.aguib@imperial.ac.uk
Sarah Halawa
sarah.halawa@aswanheartcentre.com

†These authors have contributed equally to this work and share senior authorship

Specialty section:
This article was submitted to Heart Valve Disease, a section of the journal Frontiers in Cardiovascular Medicine

Received: 21 December 2021
Accepted: 11 March 2022
Published: 06 April 2022

Citation:
Halawa S, Latif N, Tseng Y-T, Ibrahim AM, Chester AH, Moustafa A, Aguib Y and Yacoub MH (2022) Profiling Genome-Wide DNA Methylation Patterns in Human Aortic and Mitral Valves. Front. Cardiovasc. Med. 9:840647. doi: 10.3389/fcvm.2022.840647

Cardiac valves exhibit highly complex structures and specialized functions that include dynamic interactions between cells, extracellular matrix (ECM) and their hemodynamic environment. Valvular gene expression is tightly regulated by a variety of mechanisms including epigenetic factors such as histone modifications, RNA-based mechanisms and DNA methylation. To date, methylation fingerprints of non-diseased human aortic and mitral valves have not been studied. In this work we analyzed the differential methylation profiles of 12 non-diseased aortic and mitral valve tissue samples (in matched pairs). Analysis of methylation data [reduced representation bisulfite sequencing (RRBS)] of 16,101 promoters genome-wide revealed 584 differentially methylated (DM) promoters, of which 13 were reported in endothelial mesenchymal trans-differentiation (EMT), 37 in aortic and mitral valve disease and 7 in ECM remodeling. Both functional classification as well as network analysis showed that the genes associated with the DM promoters were enriched for WNT-, Cadherin-, Endothelin-, PDGF-, HIF-1 and VEGF- signaling implicated in valvular physiology and pathophysiology. Additional enrichment was detected for TGFB-, NOTCH- and Integrin- signaling involved in EMT as well as ECM remodeling. This data provides the first insight into differential regulation of human aortic and mitral valve tissue and identifies candidate genes linked to DM promoters. Our work will improve the understanding of valve biology, valve tissue engineering approaches and contributes to the identification of relevant drug targets.

Keywords: epigenetics, heart valves, NOTCH signaling, extracellular matrix (ECM), endothelial mesenchymal trans-differentiation (EMT), HIF-1 signaling pathway, regulation of actin cytoskeleton, promoters

INTRODUCTION

Heart valves perform a range of sophisticated functions that ensure unidirectional blood flow during systole, prevent backflow during diastole, enhance coronary blood flow and maintain left ventricular as well as myocardial function (1). These functions are sustained throughout the human's lifetime and require tight regulation of the valve cells and extracellular matrix (ECM), which continuously interact together enabling the valves to actively adapt to their complex hemodynamic and biomechanical environments (1, 2).

The mature valves consist of valve interstitial cells (VICs) populating a central layered ECM (3). The specific functions and hemodynamic environment of the mitral and the aortic valve (4, 5) could require distinct gene regulation by epigenetics including DNA methylation.

Epigenetics refers to heritable phenotype changes that do not involve changes in the DNA sequence itself and includes mechanisms such as histone modifications, RNA-based mechanisms and DNA methylation (6). DNA methylation is a process by which a methyl group is added to the 5th carbon of cytosine, which alters the structure of the DNA molecule thus allowing differential regulation of gene expression either through obstructing transcription factor (TF) binding or through the recruitment of methyl-binding proteins, which bind complexes responsible for chromatin remodeling (7). This process is heritable as well as tissue-specific and plays a major role in various physiological processes linked to cardiogenesis such as cardiomyocyte development, maturation and cardiac regeneration (8, 9). Aberrant changes in methylation profiles are associated with cardiovascular diseases (CVDs) such as ventricular septal defects, tetralogy of Fallot, atherosclerosis as well as other CVDs that lead to end-stage heart failure (10–13).

We here provide an initial insight into differential methylation profiles of non-diseased heart valves.

MATERIALS AND METHODS

Ethics Statement and Study Cohort/Samples

This study was approved by the Royal Brompton hospital ethics review board / Brompton and Harefield trust ethics committee (REC approval 10/H0724/18) and is abiding by all the standards of the Declaration of Helsinki. Written informed consent was obtained from the donors prior to their inclusion in the study. Twelve non-diseased valves free from calcification (6 aortic and 6 mitral valves; 10 males: 2 females; age range 42–64 years, mean age 52.2 years, SD 9.9682) were used in this study. After applying inclusion/exclusion criteria three of the twelve valves were excluded from the downstream analysis (**Table 1**, **Supplementary Figure 1**). The non-diseased valves were obtained from unused valves of healthy donor hearts, who died of non-cardiac diseases (**Table 1**). History, macroscopic, and microscopic evaluation were additionally performed to make sure that the donor hearts chosen are free from cardiovascular and valvular complications. The exclusion criteria of donor hearts were previously described in (14).

TABLE 1 | Cohort demographic and clinical characteristics.

Donor no.	Gender	Age	Cause of death	Aortic sample label	Mitral sample label
1.	Male	62	Intracerebral hemorrhage	G1T*	G2T*
2.	Male	44	Transplant recipient	G3T*	G4T
3.	Male	44	Transplant recipient	G5T	G6T
4.	Male	42	Intracranial thrombosis	G7T	G8T
5.	Male	57	Intracerebral hemorrhage	G9T	G10T
6.	Female	64	Intracerebral hemorrhage	G11T	G12T

Removed from dataset.

Tissue Sampling and DNA Extraction

Aortic and mitral valves from donor hearts were provided by the Royal Brompton Valve biobank. The ischemic time for fresh tissue harvest was set to not exceed 24 h. The aortic and mitral valve leaflets were excised and separately deendothelialized using collagenase II for 10 min at 37°C as the focus of the study was the interstitial cell population. The leaflets were then washed using PBS, snap frozen and stored in −80°C for DNA extraction. DNA was isolated from deendothelialized tissue using the FitAmp^{TM} Blood and Cultured Cell DNA Extraction Kit (Epigentek, NY, USA, catalog #: P-1018) and was subsequently eluted in TE buffer in a total volume of 40 μl. DNA was finally quantified and quality controlled *via* Qubit fluorescence.

Bisulfite Conversion, Library Preparation and Sequencing

For each sample, 300 ng of DNA was digested for 2 h with the MSP1 enzyme (20U/sample at 37°C) followed by 2 h with TaqαI (20U/sample at 65°C). Digested, CGI enriched DNA fragments <300 bps in length, were selected for using MQ Binding Beads and subsequently collected for bisulfite treatment. Bisulfite treatment was performed using the Methylamp DNA Bisulfite Conversion Kit (Epigentek, NY, USA, catalog #: P-1001). Bisulfite conversion efficiency of the bisulfite-treated DNA was determined by RT-PCR using two pairs of primers against bisulfite-converted DNA (b-actin) and against unconverted DNA (GAPDH), for the same bisulfite-treated DNA samples. Conversion was deemed successful, if more than 99% of the DNA were converted (Epigentek, NY, USA).

Post-bisulfite PBAT-mediated library preparation was performed using the P-1056A kit. First, DNA end polishing and adaptor ligation was performed. This was followed by library amplification using indexed primers and library purification. The final purified library was eluted in 12 μl of water. Assessment of library quality was done *via* bioanalyzer and KAPA library quantification (Roche, CA, USA). Finally, 10 nM of sample libraries were subjected to single-end enhanced RRBS on Illumina HiSeq 2500.

Data Quality Control and Processing

A summary of the bioinformatics analysis workflow can be found in (**Figure 1**, **Supplementary Figure 2**). First, raw reads were subjected to Quality Control (QC) using FastQC version 0.10.1 (15). Trim Galore version 0.3.7 was then used

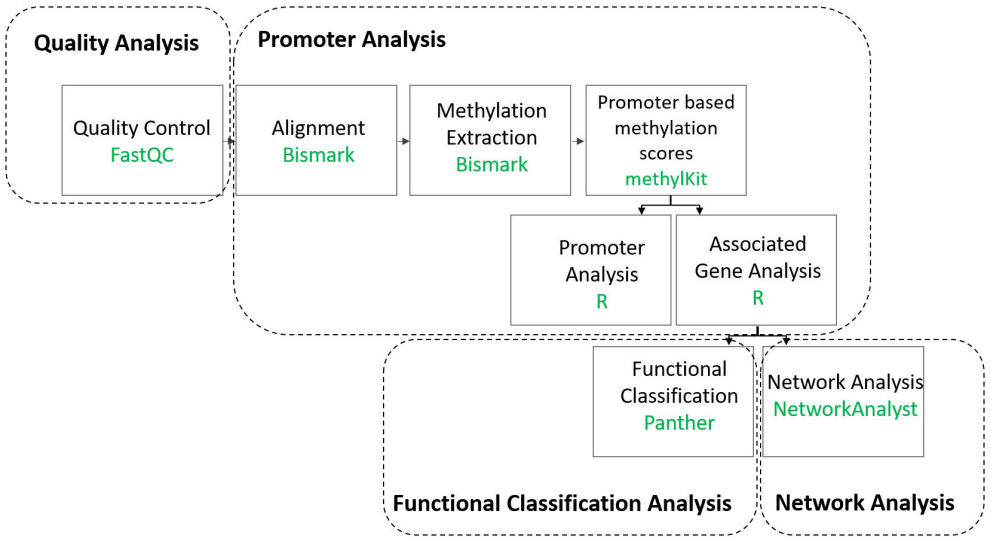

FIGURE 1 | Summary of the data analysis workflow.

to remove low quality reads, adapters as well as RRBS-related residues that are artificially added during the end-repair step (16). Trimmed reads were then mapped to the UCSC Homo sapiens genome sequence (version hg19) using Bismark version 0.13.0 (17). To permit only up to one mismatch per seed region, the option "-n 1" was set for Bowtie version 1.0.0 utilized by Bismark (18). Methylation information was extracted from Bismark's sorted and filtered mapping results at base resolution using Bismark's methylation extraction software (17). The subsequent analysis was performed in the CpG context. The R package methylKit version 0.9.2 was used for further analysis of the Bismark methylation extraction reports (19). Samples that generated a minimum of 60 million reads (**Supplementary Figure 1**) were included in the analysis (**Table 1**) and processed methylKit. Methylation information found in the aforementioned extraction reports was summarized by methylKit over RefSeq promoters, defined as regions located 1 kb before or after a transcription start site (20). Coverage for each promoter was calculated as the sum of the methylated and unmethylated cytosines. The methylation percentage was calculated as a weighted average of cytosine methylation status (21), which corresponds to the overall proportion of methylated cytosines to the sum of all cytosines within the bin (here promoter with the specified coordinates), and which is covered by a minimum number of reads (21). The promoters were subsequently filtered based on coverage (minimal 5 and maximal 99.9 percentile) and merged for comparative analysis with only those promoters that are covered in all replicates being considered. Additional QC steps can be found in the **Supplementary Materials** Online (**Supplementary Figures 3**, **4**). RRBS data was deposited in EMBL-EBI's European Genome-phenome Archive (EGA) and is accessible through EGA's accession number EGAD00001006303.

Differentially Methylated Region Analysis

The difference in the methylation level of a promoter between aortic and mitral tissue was calculated as the difference between the weighted average of the percent methylation values of all mitral tissue samples and the weighted average of the percent methylation values of all aortic tissue samples at this promoter. A positive methylation difference (hypermethylation) indicated increased methylation in the promoter associated with mitral compared to aortic tissue. The significance of this difference was evaluated by methylKit using logistic regression (19). To correct for multiple hypothesis testing, the sliding linear model (SLIM) method was used by methylKit (19). DM promoters were finally filtered with the cut-off chosen as a methylation difference that is larger than 10 % and a q-value that is <0.05. Annotation of DMRs with genic features, primarily promoters, was carried out by methylKit using the genomation package (19).

Enrichment and Functional Classification Analysis

The Protein Analysis Through Evolutionary Relationships (PANTHER) tool was utilized to perform functional enrichment analysis with the background of 16,101 promoters. PANTHER was also used to categorize genes whose promoters were found to be DM according to their molecular functions, biological processes, protein classes, pathways and cellular components (22).

Construction of Protein-Protein Interaction Networks

Genes associated with DM promoters were used as seed genes to construct PPI networks using NetworkAnalyst (23). The International Molecular Exchange (IMEx) Interactome database, which contains literature-curated comprehensive data from

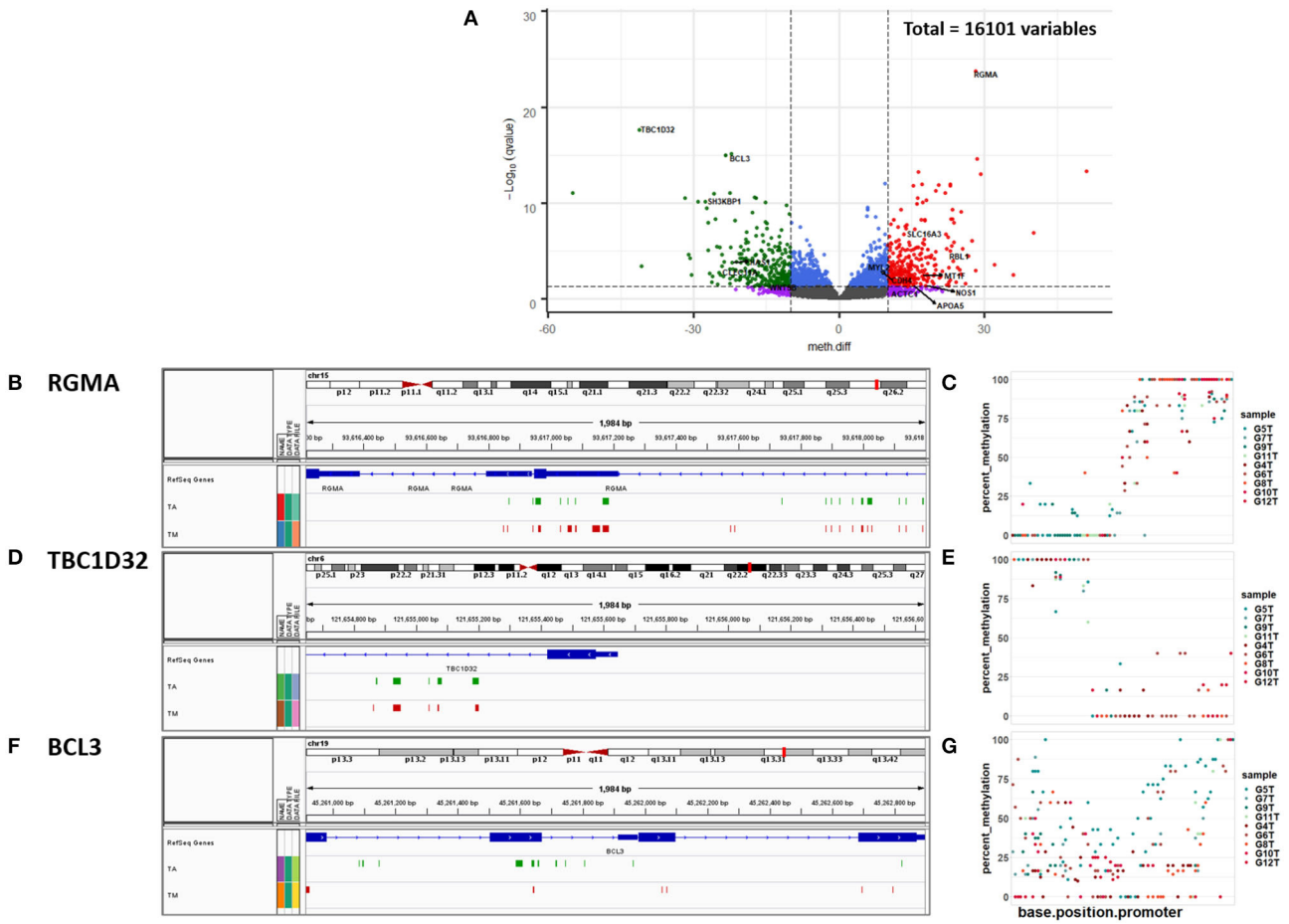

FIGURE 2 | (A) Volcano plot of promoter methylation profiles. The vertical lines x = −10 and x = 10 represent our chosen methylation difference (meth.diff) cut-off value of |10|. meth.diff is calculated as described in the Methods. The horizontal line [y = -$\log_{10}$ (0.05) = 1.3] shows our chosen q-value cut-off of 0.05. The circles represent the 16,101 promoters, of which 584 are differentially methylated (DM). Each circle in the volcano plot represents a promoter with its meth.diff and -$\log_{10}$ (q-value). Gray circles denote promoters that are not DM. Purple circles represent promoters that are biologically, but not statistically significant. Blue circles depict the opposite trend. Red and green circles show promoters that are both statistically and biologically significant. Genes with a meth.diff > 0 (red) show increased methylation in the mitral compared to the aortic valve (↑) and genes with a meth.diff < 0 (green) show decreased methylation in the mitral compared to the aortic valve (↓). Snapshots of the IGV genome browser showing the top 3 most significantly differentially methylated promoters linked to **(B)** RGMA **(C)** TBC1D32 and **(D)** BCL3, respectively (coordinates identified in **Supplementary Table 1**). TM denotes the union of the percent methylation values in all mitral samples that are >70% and which are present in the mitral but not in the aortic samples. TA denotes the union of the percent methylation values in all aortic samples that are >70% and which are present in the aortic but not in the mitral samples. Scatter plots of the percent methylation per base per promoter of the top 3 most significantly differentially methylated promoters linked to **(E)** RGMA **(F)** TBC1D32 and **(G)** BCL3, respectively (coordinates identified in **Supplementary Table 1**). Aortic samples: G5T, G7T, G9T, G11T; mitral samples (G4T, G6T, G8T, G10T, G12T).

InnateDB, was used by NetworkAnalyst for the generation of the generic network (23). For network construction, methylation difference values of alternative promoters of the same seed gene were replaced by their average before proceeding to network construction (23). The resulting network was trimmed to the minimum to encompass only nodes that connect the original seed genes. Functional enrichment analysis of all seed genes was performed using NetworkAnalyst's Function Explorer using GO, KEGG and Reactome databases. Enrichment *p*-values were computed based on the hypergeometric test utilized by the Function Explorer (23). NetworkAnalyst's Module Explorer, was used to identify smaller significantly densely connected subnetworks using the Walktrap algorithm (23). Visualization of PANTHER, KEGG and Reactome pathway terms was performed using the GOplot R package (24).

RESULTS

Aortic and Mitral Valves Show Different Methylation Signatures in 584 Promoters

DMR analysis identified 584 significantly DM promoters, of which 305 showed increased methylation in mitral and 279 in aortic valve tissue (**Figure 2A**, **Supplementary Table 1**).

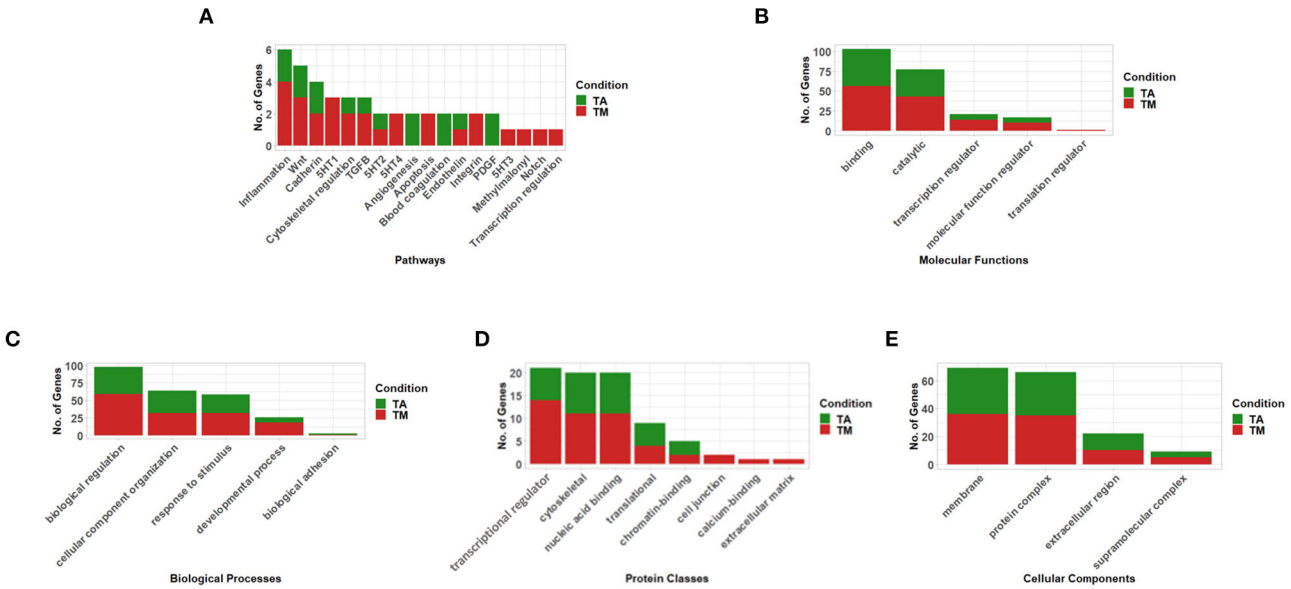

FIGURE 3 | Functional classification of genes associated with differentially methylated promoters (q-value < 0.05 & meth.diff >|10|) between aortic and mitral tissue according to **(A)** Pathways, **(B)** Molecular Functions, **(C)** Biological Processes, **(D)** Protein Classes and **(E)** Cellular Components (selected results, the remaining can be found in **Supplementary Figure 5**– analysis performed using PANTHER). In the stacked bar graphs, TA (green) labels genes with promoters that show increased methylation in the aortic compared to the mitral valves and TM (red) shows genes whose promoters exhibit increased methylation in the mitral compared to the aortic valves.

The gene Repulsive Guidance Molecule A (RGMA) was associated with the most significantly DM promoter (**Figures 2B,C, Supplementary Table 1**) followed by TBC1 Domain Family Member 32 (TBC1D32) (**Figures 2D,E, Supplementary Table 1**), B-Cell Lymphoma 3 (BCL3) (**Figures 2F,G, Supplementary Table 1**) and the long non-coding RNA RP11-1149O23.3 among others (**Figure 2A, Supplementary Table 1**).

When we investigated genes linked to the significant differentially methylated promoters in isolation, no significant enrichment was found. When functional classification analysis was performed, the genes associated with the DM promoters were grouped into key valve-related functions and pathways (**Figures 3A–E, Supplementary Figure 5**) with their methylation direction specified in (**Supplementary Table 1**). Key valve-related pathways such as Wingless/Integrated (WNT)-, Cadherin-, Transforming Growth Factor Beta (TGFB)-, Integrin-, Endothelin-, Platelet-Derived Growth Factor (PDGF)-, NOTCH signaling as well as angiogenesis and general transcription regulation were identified utilizing the PANTHER Pathway database (**Figure 3A**, **Supplementary Table 2**).

When the genes were classified by their molecular function, 69.5% of the genes had a binding and catalytic activity including key genes such as Nitric Oxide Synthase 1 (NOS1) (q-value = 0.04, meth.diff = 17.9 %). Other genes exhibited transcription regulator-, translation regulator- and molecular function regulator activities. The latter category included relevant genes such as Apolipoprotein A5 (APOA5) (q-value = 0.037, meth.diff = 15.3%) and Natriuretic Peptide B (NPPB) (q-value = 0.0027, meth.diff = 15.58%) (**Figure 3B**, **Supplementary Table 3**).

Among the relevant biological processes categorizing the genes were "biological regulation" and "cellular component organization or biogenesis." The former included notable genes such as Metallothionein 1F (MT1F) (q-value = 0.004, meth.diff = 17.07%) and the latter included two pertinent ones namely Hyaluronan Synthase 1 (HAS1) (*q*-value = 0.00015, meth.diff = 22.15%) as well as Actin Alpha Cardiac Muscle 1 (ACTC1) (q-value= 0.049, meth.diff = 11.23%) (**Figure 3C, Supplementary Table 4**).

Genes were also grouped into relevant protein classes such as gene-specific transcriptional regulator proteins, which included SMAD Family Member 3 (SMAD3) (*q*-value = 0.0019, meth.diff = 10.25%), cytoskeletal proteins, which contained Myosin Light Chain 2 (MYL2) (q-value = 0.013, meth.diff = 11.14%) and chromatin-binding protein, which encompassed RB Transcriptional Corepressor Like 1 (RBL1) (q-value = 9.5e-06, meth.diff = 22.98%) (**Figure 3D**, **Supplementary Table 5**).

Finally, the cellular component categories into which the genes could be classified were membrane- and extracellular regions among others. Relevant genes such as C-Type Lectin Domain Containing 11A (CLEC11A) (q-value = 0.002, meth.diff = 24.72%) were included in the latter and Solute Carrier Family 16 Member 3 (SLC16A3) (q-value = 1.78e-07, meth.diff = 13.4%) in the former category (**Figure 3E**, **Supplementary Table 6**).

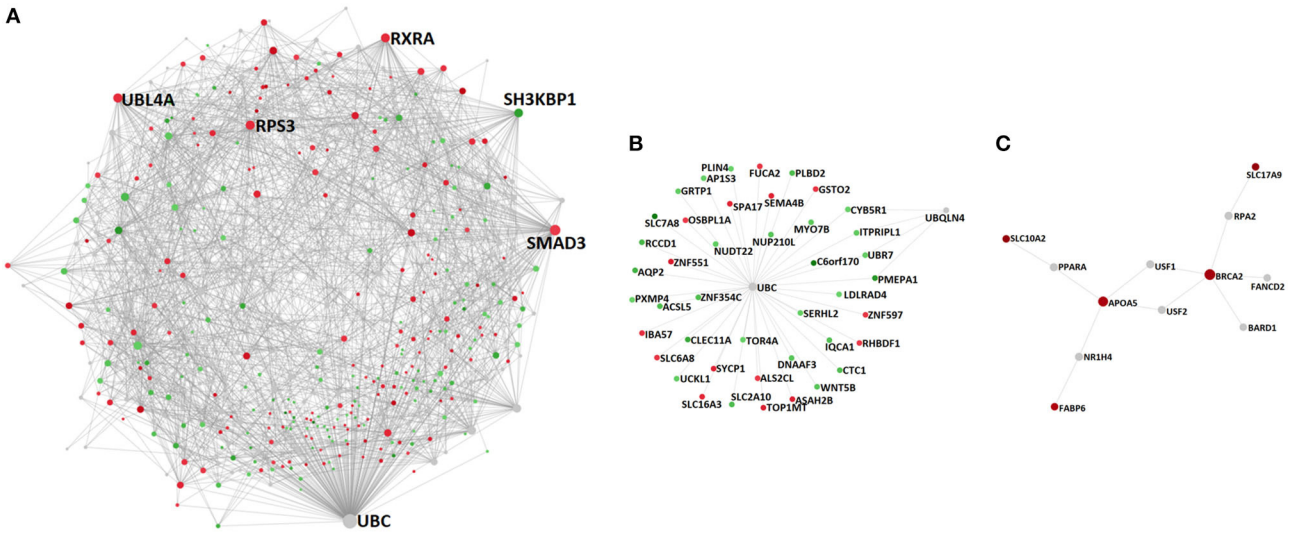

FIGURE 4 | PPI networks constructed upon the genes associated with differentially methylated promoters between non-diseased aortic and mitral valve tissue and the proteins that are necessary to interconnect them: **(A)** complete network, **(B)** subnetwork 1 (*p*-value 3.04e-13) and **(C)** subnetwork 2 (*p*-value 0.047). Depicted nodes are classified according to their methylation direction: nodes representing genes showing increased methylation in mitral compared to aortic tissue (red), nodes depicting increased methylation in aortic vs. mitral tissue (green) and nodes representing genes that are not part of the input dataset (gray). Node sizes are proportional to their betweenness centrality values. Betweenness centrality reflects the number of shortest paths passing through a node, while degree refers to the number of connections/edges/PPIs that a node has to other nodes. Hub nodes **(A)** UBC, SMAD3, UBL4A, RPS3, RXRA, **(B)** UBC and **(C)** BRCA2 and APOA5 can be clearly identified on the respective networks.

Network Analysis Enabled a Systems-Based Assessment and Revealed Additional Valve-Related Pathways Such as Hypoxia-Inducible Factor 1 and Vascular Endothelial Growth Factor Signaling

After functionally categorizing the genes, whose promoters were significantly DM between the aortic and mitral valves on a genome-wide level, we wanted to assess whether we can predict significantly enriched PPIs among those genes as well as the proteins that are necessary to interconnect them to enable a systems-level analysis.

For that purpose, we mapped those DM genes onto a generic PPI database (see Methods) and constructed a PPI network, which ultimately comprised 715 nodes (genes) of which 308 were seed genes and 2,131 edges (PPIs) (**Figure 4A**, **Supplementary Table 7**). Among the network's constituent proteins were several hub nodes, the most connected of which were Ubiquitin C (UBC) (Betweenness centrality = 129,377.98; Degree = 200), SMAD3 (Betweenness centrality = 27,152.04; Degree = 75), Ubiquitin Like 4A (UBL4A) (Betweenness centrality = 13,019.92; Degree = 50), Ribosomal Protein S3 (RPS3) (Betweenness centrality = 9,508.1; Degree = 50), Retinoid X Receptor Alpha (RXRA) (Betweenness centrality = 12,661.72; Degree = 47) and SH3 Domain Containing Kinase Binding Protein 1 (SH3KBP1) (Betweenness centrality = 13,005.65; Degree = 44) (**Figure 4A, Supplementary Table 7**).

In addition to inspecting the topological properties of the constructed network, we performed functional enrichment analysis of both the hyper- and hypomethylated proteins of the subnetwork as well as them connecting these proteins. This analysis showed significant enrichment of pathways and functions.

Many pathways, which are pertinent to valvular mechanisms, were identified *via* KEGG pathway enrichment analysis including apoptosis, Nuclear Factor Kappa-light-chain-enhancer of activated B cells (NF-κB) signaling pathway, fluid shear stress and atherosclerosis, Tumor necrosis factor (TNF) signaling pathway, osteoclast differentiation, Interleukin 17 (IL-17) signaling pathway, HIF-1 signaling pathway, regulation of actin cytoskeleton, VEGF signaling pathway and TGFB signaling pathway (FDR < 0.05, **Table 2**).

To investigate whether relevant significantly enriched pathways are present independent of the choice of the pathway database, we furthermore performed Reactome enrichment analysis, which exclusively highlighted additional key valve-related pathways such as immune response, regulation of lipid metabolism, PDGF, NOTCH1, Fibroblast Growth Factor Receptor (FGFR) and transcription (FDR < 0.05, **Supplementary Table 8**). Similar to KEGG, it showed enrichment for apoptosis-, TFGB-, interleukin- and hypoxia-related pathways (**Table 2**, **Supplementary Table 8**).

After inspecting significant valve-related pathways, we checked whether there are enriched biological processes, molecular functions and cellular components related to the molecular regulation of valve-related processes based on GO databases. Relevant biological processes included transcription, apoptosis, growth factor signaling as well as regulation of cellular component organization (FDR < 0.05, **Supplementary Table 9**).

TABLE 2 | List of pathways resulting from enrichment analysis of the network (**Figure 4A**) constructed upon the genes associated with the differentially methylated hypo- and hypermethylated promoters using the KEGG pathway database.

KEGG Pathways	Tot[a]	Exp[b]	Hits[c]	Pval[d]	FDR[e]	Seed genes[f]	Other genes[g]
Apoptosis	136	7.91	31	2.56E-11	6.8E-10	CASP7, TUBA8, CTSZ	DDIT3, BIRC2, TNFRSF1A, TRADD, IKBKG, RELA, NFKBIA, ACTB, XIAP, TP53, RAF1, CTSB, BIRC3, PIK3R1, FOS, NFKB1, FAS, AKT1, MAPK1, IKBKB, CTSD, TUBA1A, BCL2L11, TRAF2, ITPR3, JUN, FASLG, ACTG1
NF-κB signaling pathway	100	5.82	23	8.40E-09	1.03E-07	ZAP70, TAB1	TRAF6, UBE2I, BIRC2, TNFRSF1A, TRADD, IKBKG, NFKB2, RELA, NFKBIA, XIAP, BTK, IRAK1, MYD88, BIRC3, NFKB1, IKBKB, PLCG1, LCK, TRAF2, CSNK2B, LYN
Fluid shear stress and atherosclerosis	139	8.08	26	8.57E-08	8.01E-07	NQO1, GSTO2	SUMO3, TNFRSF1A, IKBKG, RELA, CAV1, ACTB, TP53, HSP90AA1, SQSTM1, PIK3R1, CTNNB1, FOS, NFKB1, AKT1, SRC, PLAT, IKBKB, RAC1, SUMO1, SUMO2, HSP90AB1, VEGFA, JUN, ACTG1
TNF signaling pathway	110	6.4	22	2.55E-07	2.19E-06	CASP7, TAB1, BCL3, DNM1L	BIRC2, TNFRSF1A, TRADD, IKBKG, RELA, NFKBIA, BIRC3, PIK3R1, FOS, NFKB1, FAS, AKT1, MAPK1, IKBKB, CREB1, TRAF2, CEBPB, JUN
Osteoclast differentiation	128	7.44	23	1.01E-06	7.32E-06	TAB1, LCP2, FHL2	TRAF6, TNFRSF1A, IKBKG, NFKB2, RELA, NFKBIA, BTK, SQSTM1, PIK3R1, FOS, NFKB1, AKT1, GRB2, MAPK1, IKBKB, RAC1, CREB1, LCK, TRAF2, JUN
IL-17 signaling pathway	93	5.41	19	1.20E-06	8.31E-06	CSF3	TRAF6, TRADD, IKBKG, RELA, NFKBIA, HSP90AA1, FOS, NFKB1, MAPK1, IKBKB, MAPK6, GSK3B, ELAVL1, S100A9, HSP90AB1, TRAF2, CEBPB, JUN
HIF-1 signaling pathway	100	5.82	19	3.78E-06	2.36E-05	LDHA	GAPDH, VHL, CREBBP, RELA, STAT3, ERBB2, EGFR, PIK3R1, NFKB1, HIF1A, AKT1, MAPK1, CDKN1A, EP300, CUL2, PLCG1, ENO3, VEGFA
Regulation of actin cytoskeleton	214	12.4	29	1.56E-05	8.69E-05	MYL2, PAK6, LIMK1, F2R, FGD1, FGD3	MYL12A, ACTB, WAS, PPP1CA, RAF1, CRK, EGFR, PIK3R1, SRC, MAPK1, IQGAP1, SOS1, RAC1, CDC42, FN1, WASL, CRKL, PPP1CC, PAK2, GIT1, VAV2, ACTG1, ARHGEF7
VEGF signaling pathway	59	3.43	10	0.00192	0.00671	NA	RAF1, PIK3R1, AKT1, SRC, MAPK1, RAC1, CDC42, PLCG1, PLA2G4A, VEGFA
TGFB signaling pathway	92	5.35	13	0.00241	0.00817	RGMA, RBL1, SMAD3, E2F4, HAMP	CREBBP, MYC, SMAD2, SMAD7, MAPK1, SP1, EP300, CUL1

[a] "Tot" refers to the total number of genes that belong to the particular KEGG pathway as per the chosen reference list of genes, which is hg19 in our case, [b] "Exp" denotes the number of genes to be expected in our gene list for the particular KEGG pathway, [c] "Hits" describes the number of genes in our list that map to the particular KEGG pathway, [d] "Pval" is equivalent to the enrichment p-value computed using the hypergeometric test (see Methods), [e] "FDR" stands for false discovery rate, which is the method used to correct the corresponding p-value for multiple testing, [f] "Seed genes" represent genes associated with significantly differentially hyper- and hypomethylated promoters and [g] "Other genes" denote genes that are part of the minimum non-seed genes that are necessarily required to connect the seed genes to construct the network. The methylation direction of the seed genes can be found in ***Supplementary Table 1****.*

Molecular functions associated with transcription as well as histone acyltransferase activity such as chromatin-, histone deacetylase-, TF-, SMAD- and NF-κB-binding were among the pertinent significantly enriched molecular functions (FDR < 0.05, **Supplementary Table 10**). Finally, the most relevant significantly enriched cellular components were Transcription

TABLE 3 | Genes associated with differentially methylated promoters between aortic and mitral valve tissue and their involvement in valve development and disease.

Gene	Description	Development	Disease
NOS1	Nitric oxide synthase 1 (neuronal)	Heart (25)	BAV[a] (25)
ACTC1	Actin, alpha, cardiac muscle 1	Heart (26)	MMV[b] (27)
MYL2	Myosin, light chain 2, regulatory, cardiac	Heart (28)	
MT1F	Metallothionein 1F		MMV (29)
CLEC11A	C-Type lectin domain containing 11A		MMV (30)
RBL1	Retinoblastoma-like 1 (p107)		BAV (31), AS (32)
SLC16A3	Solute carrier family 16, member 3 (monocarboxylate transporter)		BAV (33), AS[c] (34)
NPPB	Natriuretic peptide B	EMT[d] (35)	MR[e] (36)
CDH4	Cadherin 4, type 1, R-cadherin (retinal)	Valve (37)	
HAS1	Hyaluronan synthase 1		CAVD[f] (38)
WNT5B	Wingless-type MMTV integration site family, member 5B		CAVD (39)
Ubiquitin-related genes		Protein QC[g] in the heart (40)	BAVs (41), atherosclerosis (42)
SMAD3	SMAD family member 3	Cardio-genesis (43)	AD[h] (44)
RXRA	Retinoid X receptor, alpha		Valve malformation (45)
SH3KBP1	SH3-domain kinase binding protein 1		CAVD (46)
APOA5	Apolipoprotein A-V		AS (47–49)

[a]BAV, bicuspid aortic valve; [b]MMV, myxomatous mitral valve; [c]AS, aortic valve stenosis; [d]EMT, endothelial mesenchymal trans-differentiation; [e]MR, mitral valve regurgitation; [f]CAVD, calcific aortic valve disease; [g]QC, quality control; [h]AD, thoracic aortic aneurysm and dissection.

Factor II D (TFIID) complex, spliceosomal complex, chromatin, histone deacetylase complex as well as actin cytoskeleton (FDR < 0.05, **Supplementary Table 11**).

In addition to examining the network structure as a whole, we performed a module analysis (see Methods), to identify subnetworks that show a significantly increased connection density compared to other modules of the parent network. The first identified subnetwork (*p*-value 3.04e-13) comprised 45 nodes, of which 43 were seed genes and contained the following hub nodes: UBC, also identified as a hub protein of the parent network (Betweenness centrality = 43; Degree = 939) and Ubiquilin 4 (UBQLN4), not identified previously (Betweenness centrality = 3; Degree = 4) (**Figure 4B, Supplementary Tables 12**, **13**).

The second subnetwork (*p*-value 0.047) contained 12 nodes, of which 5 were seed genes with Breast And Ovarian Cancer Susceptibility Protein 2 (BRCA2) (Betweenness centrality = 33.5; Degree = 5) as well as APOA5 (Betweenness centrality = 32.5; Degree = 4) being its main hub proteins. Interestingly, all of the module's constituent seed nodes exhibited increased methylation in mitral compared to aortic tissue (**Figure 4C, Supplementary Table 14**). Relevant enriched pathways in this module included homologous recombination (KEGG/Reactome) and Peroxisome Proliferator-Activated Receptor (PPAR) signaling pathway (KEGG) (FDR < 0.05, **Supplementary Table 15**). The module's biological processes contained lipid homeostasis and cellular response to external stimulus (FDR < 0.05, **Supplementary Table 15**). Finally, the most relevant enriched molecular functions encompassed DNA-, enzyme- and TF- binding (FDR < 0.05, **Supplementary Table 15**).

Global Analysis of Detected Pathways and Genes Shows the Role of Methylation in EMT and ECM Remodeling

All the utilized analysis methods of genes and pathways show that DNA methylation plays a crucial role in valve development and disease. Indeed, some of the detected genes and pathways are involved in developmental processes such as cardiogenesis, EMT and protein QC and/or diseases such as myxomatous mitral valve (MMV), BAV and AD (**Tables 3**, **4**).

We further generated a GOChord plot to link the pathways in **Table 4** to their constituent genes, which are associated with DM promoters (**Figure 5A**). The plot revealed several pathways sharing the same genes, such as NF-κB signaling, TNF signaling and osteoclast differentiation, which contain TGFB Activated Kinase 1 Binding Protein 1 (TAB1) and Integrin- and PDGF signaling, which include Collagen Type V Alpha 3 (COL5A3) (**Figure 5A**).

A GOCircle plot visualizes the significance of each pathway in **Table 4** and to show the direction of promoter methylation of their constituent genes (**Figure 5B**). The most significant pathways in **Table 4** were NF-κB, TNF signaling and osteoclast differentiation, which share TAB1 (**Figure 5A**) and are implicated in aortic stenosis (AS) (**Table 4**).

DISCUSSION

This study provides new information regarding the DNA methylation landscape in human non-diseased heart valves. Heart valves have a complex structure and function that are sensitive to their environment and exhibit characteristic

TABLE 4 | Pathways involving the genes associated with the differentially methylated promoters between aortic and mitral valve tissue and their implication in valve development and disease.

Pathway	Description	Development	Disease
TGFB signaling	Transforming growth factor beta signaling	EMT[a] (50)	ECM[b] remodeling (51), MVP[c] (52), AS[d] (53, 54)
NOTCH signaling		EMT (50), (55)	BAV[e] (55, 56), AS (55) and fetal cardiac defects (57)
FGF signaling	Fibroblast growth factor signaling	EMT (58)	Valve malformation (58)
WNT signaling		heart, EMT (39, 50)	
Cadherin signaling		EMT (59)	
PDGF signaling	Platelet-derived growth factor	heart (60)	
VEGF signaling		EMT (50)	
Integrin signaling		EMT (50), cell-ECM (61, 62)	
HIF-1 signaling			RMV[f], MMV[g] (63)
Angiogenesis			RMV (64)
IL-17 signaling			IE[h] (65)
NF-κB signaling			AS (66)
TNF signaling			AS (67)
Osteoclast differentiation pathways			AS (68)
Endothelin signaling		VICs[i] regulation by VECs[j] (69)	AS (70)
Apoptotic pathways			AS (71)
PPAR signaling		lipid metabolism (72)	

[a]EMT, endothelial mesenchymal trans-differentiation; [b]ECM, extracellular matrix; [c]MVP, mitral valve prolapse; [d]AS, aortic valve stenosis; [e]BAV, bicuspid aortic valve; [f]RMV, rheumatic mitral valve; [g]MMV, myxomatous mitral valve; [h]IE, infective endocarditis; [i]VICs, valve interstitial cells; [j]VECs, valve endothelial cells.

phenotypic and functional differences. Valve-type specific differences begin to appear during valve formation and development and are expressed in the valve's distinct anatomical structures, environmental milieus and susceptibility to disease. In this work we focus on two of the four valves, the mitral and aortic valves and their epigenetic profiles.

While there are several studies exploring the epigenetics of abnormal valves in the literature (57, 73, 74), they are not standardized and do not include methylation of normal valves. Previous studies have addressed how DNA methylation affects valvular disease processes. These studies investigated DNA methylation mechanisms that can transform VICs of stenotic aortic valves into leukotriene-producing immune-like cells *via* targeted promoter methylation measurement of 5-lipoxygenase (5-LO) (75), and those that lead to the disruption of both the organization of the ECM and the communication between the cells and the ECM in bicuspid aortic valve (BAV) by investigating miR-29 expression level utilizing qRT-PCR (76). Other studies focused on uncovering associations between methylation changes and the development of rheumatic heart valve disease using ELISA (77), and on detecting the genome-wide DNA methylation landscape underpinning BAV and aortic dissection (AD) *via* methylation array (78).

We used RRBS to measure DNA methylation as it targets CpG-rich islands and promoters genome-wide (79). It is crucial to couple this sequencing method with suited bioinformatics workflows, that rely on rigorous QC of RRBS-characteristic issues as well as of bisulfite sequencing-specific parameters such as the efficiency of bisulfite conversion (80). RRBS thus can allow for a comprehensive view not limited by predefined sets of CpG loci probes (81).

In this study, 584 of 16,101 promoters were found to be DM between aortic and mitral tissue and their associated genes associated were found to be implicated in valvular health and disease mechanisms. RGMA was associated with the most significantly DM promoter. It is a member the RGM protein family, the first known BMP selective co-receptor family able to induce BMP signaling that is dysregulated in CAVD (82, 83). TBC1D32, the gene associated with the second most DM promoter, is implicated in the pathogenesis of ciliopathies in humans (84), which are caused by defects in the human primary cilium known to play a role in establishing left-right asymmetry during heart development (85), to restrain ECM production during physiological aortic valve development and to play a role in the etiology of BAV in humans (86). Finally, BCL3, the gene associated with the third most DM promoter, is known to play a role in atherosclerosis (87), with atherosclerosis-like lesions potentially leading to AS (88).

Further genes, that were associated with DM promoters (summarized in **Table 3**) include NOS1, ACTC1 and MYL2, which play key roles in heart development (25, 26, 28), with ACTC1 additionally being implicated in MMV and NOS1 in BAV (25, 27). MT1F and CLEC11 further contribute to MMV (29, 30), while RBL1 and SLC16A3 to BAV (31, 33). NPPB is involved in EMT by exhibiting excessive synthesis of the cardiac jelly, a precursor of the cushions, in zebrafish and is overexpressed in

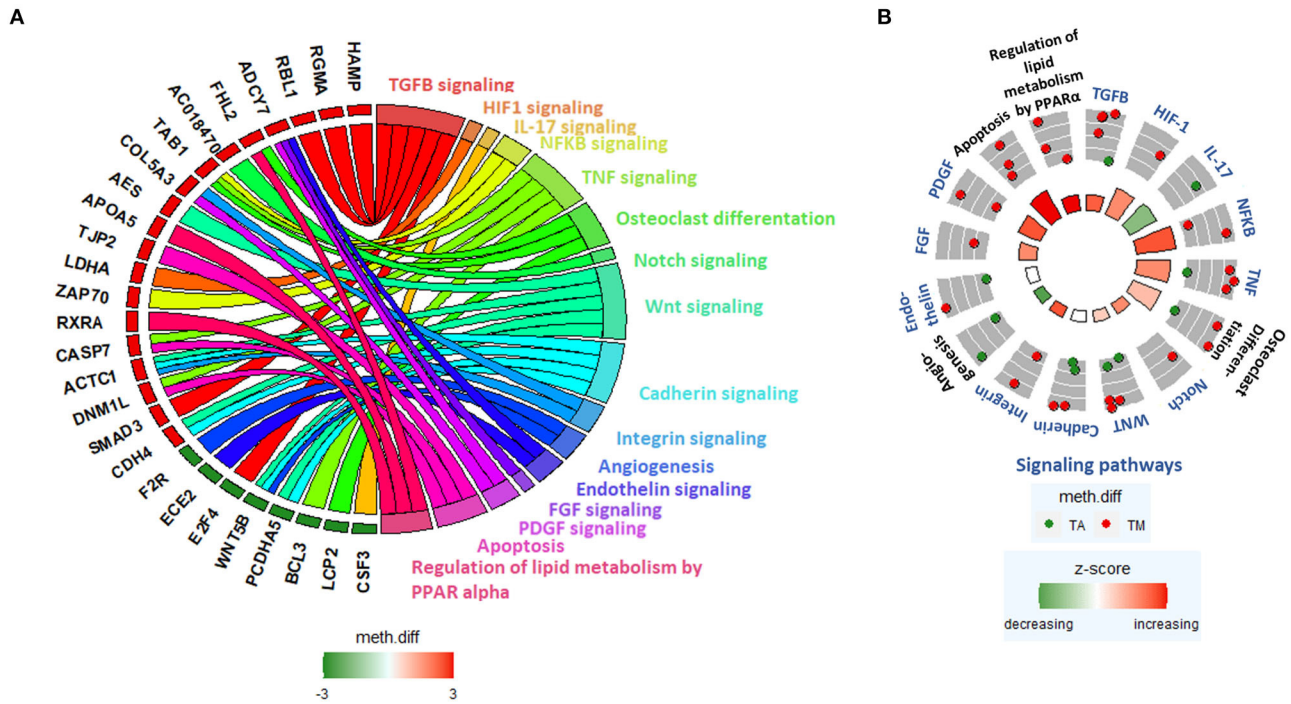

FIGURE 5 | (A) GOChord plot linking selected pathways to their constituent genes, which are associated with DM promoters. Green-to-red colors next to the selected genes reflect their meth.diff values. **(B)** GOCircle plot representing the relevant pathways and their constituent genes that are associated with DM promoters. The inner circle consists of bar plots, whose heights reflect the significance of the pathway and whose color reflect the z-score, which approximates the overall direction of change in methylation for each pathway. The outer circle shows scatterplots of the meth.diff values of each of the pathway's constituent genes.

the ventricles of patients with chronic volume overload caused by regurgitant mitral valve lesions (35, 36). Cadherin-4 (CDH4) is both significantly DM and expressed during the development of embryonic mice (37). Finally, HAS1 and Wingless/Integrated 5B (WNT5B) contribute to CAVD (38, 39), and SLC16A3 to AS (34).

The network constructed upon the genes linked to DM promoters identified hub proteins known to be involved in different aortic and mitral valve mechanisms. UBC and UBL4A, the two most connected hub genes of the network, belong to the ubiquitin family, whose members play a role in BAVs as well as in atherosclerosis (41, 42). The network's first submodule was additionally entirely centered around UBC further highlighting the importance of the ubiquitin system, which is key to performing protein QC in the heart (40). SMAD3, the second most connected hub node, plays an important role in cardiogenesis (43), and is linked to thoracic aortic aneurysm and dissection (44). RXRA, a member of the RA signaling pathway and the network's third hub node, is linked to OFT and AV canal malformations, which influence proper aortic and mitral valve development (45). Finally, the hub node SH3KBP1 is implicated in CAVD (46). The second submodule of the network contained only two hub nodes APOA5 and BRCA2. Dyslipidemia linked to Lipoprotein a (LPA)-associated APOA5 has been detected in AS (74), with the reduction of LPA levels *via* PSCK9 inhibitors constituting promising therapeutic avenues for AS treatment (47–49). BRCA2, has not been associated with valvular mechanisms in the literature and thus should be further investigated.

Detected pathways were relevant to valvular development and disease (**Table 4**). For example, TGFB- and NOTCH signaling pathways activate EMT by downregulating VE-Cadherin (50, 55), which decreases cell adhesion of the transforming endocardial cells enabling them to break away from the endocardium and to migrate into the cardiac jelly, where they can transform into mesenchyme cells creating cushions that expand and fuse to ultimately form cardiac valves (50). TGFB signaling is also implicated in pathological ECM remodeling (51), MVP (52), AS (53), and NOTCH pathways in BAV and AS (55). FGF signaling further promotes OFT myocardial cell invasion to the cardiac cushion during EMT, with its disruption leading to malformed OFT valves in mice (58). Canonical WNT- and Cadherin signaling add to cushion development and remodeling during EMT (50, 59), with WNT pathways being additionally implicated in valve stratification and well as in the patterning of the heart forming field (50). Similar to WNT- and Cadherin-, the PDGF signaling pathway is also involved in cardiogenesis, particularly in the formation of the primordial heart tube (60). Both the VEGF- and Integrin signaling pathways contribute to post-EMT

maturation, in that the former establishes an equilibrium between proliferation and differentiation of cells in the cushion (50), and the latter enables ECM remodeling through the generation of a mechano-transducing network that connects the cells to the ECM providing a link that relays external metabolic and hemodynamic factors (61, 62). HIF-1 signaling is involved in pathological ECM remodeling associated with RMV and MMV disease (63). Aberrant angiogenesis and IL-17 signaling are also implicated in RMV and infective endocarditis (IE), respectively (64, 65). NF-κB-, TNF-, Osteoclast differentiation-, Endothelin and Apoptotic pathways are involved in AS (66–68, 70, 71), with the Endothelin pathway additionally being implicated in the regulation of VICs by VECs (69). Finally, the detected PPAR signaling pathway is linked to lipid metabolism and is enriched among other lipid-related genes in the second mitral valve-specific subnetwork (72). The enrichment of PPAR signaling, the uniform increased methylation of the subnetwork's constituent genes in mitral compared to aortic valves and APOA5 being a hub node, indicate that this subnetwork exhibits major methylation alterations related to the metabolism of lipids. The regulation and expression of lipid-related genes need to be further dissected as it has been reported in a previous study that increased fatty infiltration of valves is observed in MVP (89).

One very interesting aspect of this dataset is having 4 matched pairs (**Table 1**). Comparisons within individuals that have both aortic and mitral samples (**Supplementary Figures 6A–F**) revealed that promoters identified by our original non-matched analysis have been re-captured in the matched analysis with additional promoters identified by the matched analysis (**Supplementary Figures 6A–F**). Matched analysis can provide additional insight particularly when powered by sufficient replicates as it eliminates inherent genetic differences between samples which needs to be integrated in the design of the future large-scale study.

Our analysis provided a comprehensive catalog of genes and pathways that are differentially regulated between aortic and mitral valves, establishing the basis for upcoming whole-genome bisulfite sequencing (WGBS) studies to additionally interrogate methylation of gene-bodies and other non-promoter regions. Additional insights can be obtained from histone-modification and RNA-based experiments as well as the interaction of such epigenetic mechanisms with DNA methylation. Functional validation of genes and pathways of interest on the transcriptomic and proteomic level will confirm candidate DM biomarkers, which can serve as potential drug targets. Additionally, the same analysis on the VIC level will be done to confirm cell-type specific signals that might have been affected by the tissue's intrinsic cell heterogeneity. Such analysis will provide novel mechanistic insights into the distinct roles of the individual components.

Limitations-In this study, due to the scarcity of human non-diseased donor heart valves, a relatively small number of valves was examined ($n = 12$) and two of the four heart valves were studied. Further validation is required to evaluate the clinical significance of the methylation markers identified. An enhancement of the methodology used in this manuscript will be utilized in future studies for example by performing WGBS.

CONCLUSION

To conclude, this is the first study that explores the genome-wide DNA methylation landscape characterizing human non-diseased aortic and mitral valves. By investigating genes that are linked to DM promoters and their associated pathways, we discovered that the cells as well as the ECM of the aortic and mitral valve have different methylation signatures. The detected pathways included TGFB-, NOTCH-, FGF-, WNT-, Cadherin- and VEGF signaling pathways associated with EMT, Integrin- and HIF-1 signaling linked to ECM remodeling and NF-κB-, TNF-, osteoclast differentiation, Endothelin- and IL-17 signaling observed in aortic and mitral valve disease. Especially with the increasing incidence and prevalence of valve disease worldwide due to the world's increasing population age in developed and the failure to address RHVD in low and middle-income countries (LMICs) (5), it is very important to acquire a better understanding of the genetic and epigenetic make-up of cardiac valves and how they are influenced by local conditions, environmental factors and ethnicities as this will affect the development of preventative and therapeutic strategies.

DATA AVAILABILITY STATEMENT

The datasets presented in this study can be found in online repositories. The names of the repository/repositories and accession number(s) can be found below: https://ega-archive.org/datasets/EGAD00001006303, EGAD00001006303; https://ega-archive.org/studies/EGAS00001004559, EGAS00001004559.

ETHICS STATEMENT

The studies involving human participants were reviewed and approved by Royal Brompton Hospital Ethics Review Board / Brompton and Harefield trust Ethics Committee (REC approval 10/H0724/18). The patients/participants provided their written informed consent to participate in this study.

AUTHOR CONTRIBUTIONS

NL, YA, and MY: conceptualization. SH: data curation, formal analysis, validation, writing–original draft, and software. YA and MY: funding acquisition. SH, NL, Y-TT, and AHC: investigation. SH, NL, AM, YA, and MY: methodology. NL and YA: project administration. NL, AMI, AHC, and YA: resources. AM, YA, and MY: supervision. SH, AM, and YA: visualization. NL, AM, YA, and MY: writing–review and editing. All authors contributed to the article and approved the submitted version.

FUNDING

This research was funded by Magdi Yacoub Institute (MYI) and Magdi Yacoub Foundation (MYF). SH was partially supported by Al Alfi Foundation (Al Alfi PhD Fellowship in Applied Sciences and Engineering).

ACKNOWLEDGMENTS

We thank Professor John Chambers, Marie Loh, Zhou Li and all the team for hosting SH's research visit at Lee Kong Chian School of Medicine.

SUPPLEMENTARY MATERIAL

The Supplementary Material for this article can be found online at: https://www.frontiersin.org/articles/10.3389/fcvm.2022.840647/full#supplementary-material

REFERENCES

1. Chester AH, El-Hamamsy I, Butcher JT, Latif N, Bertazzo S, Yacoub MH. The living aortic valve: from molecules to function. *Glob Cardiol Sci Pract.* (2014) 2014:52–77. doi: 10.5339/gcsp.2014.11
2. Yacoub MH. In search of living valve substitutes. *J Am Coll Cardiol.* (2015) 66:889–91. doi: 10.1016/j.jacc.2015.07.007
3. Yacoub MH, Cohn LH. Novel approaches to cardiac valve repair. from structure to function: part I. *Circulation.* (2004) 109:1064–72. doi: 10.1161/01.CIR.0000115634.66549.4D
4. Roy A, Brand NJ, Yacoub MH. Molecular characterization of interstitial cells isolated from human heart valves. *J Heart Valve Dis.* (2000) 9:459–464.
5. Yacoub MH, Takkenberg JJM. Will heart valve tissue engineering change the world? *Nat Clin Pract Cardiovasc Med.* (2005) 2:60–1. doi: 10.1038/ncpcardio0112
6. Kalozoumi G, Tzimas C, Sanoudou D. The expanding role of epigenetics. *Glob Cardiol Sci Pract.* (2012) 2012:7. doi: 10.5339/gcsp.2012.7
7. Miller JL, Grant PA. The role of DNA methylation and histone modifications in transcriptional regulation in humans. *Subcell Biochem.* (2013) 61:289–317. doi: 10.1007/978-94-007-4525-4_13
8. Gilsbach R, Preissl S, Grüning BA, Schnick T, Burger L, Benes V, et al. Dynamic DNA methylation orchestrates cardiomyocyte development, maturation and disease. *Nat Commun.* (2014) 5:5288. doi: 10.1038/ncomms6288
9. Chaturvedi P, Tyagi SC. Epigenetic mechanisms underlying cardiac degeneration and regeneration. *Int J Cardiol.* (2014) 173:1–11. doi: 10.1016/j.ijcard.2014.02.008
10. Zhu C, Bin YZ, Chen XH, Pan Y, Dong XY, Qian LM, et al. Screening for differential methylation status in fetal myocardial tissue samples with ventricular septal defects by promoter methylation microarrays. *Mol Med Rep.* (2011) 4:137–43. doi: 10.3892/mmr.2010.407
11. Sheng W, Qian Y, Zhang P, Wu Y, Wang H, Ma X, et al. Association of promoter methylation statuses of congenital heart defect candidate genes with tetralogy of fallot. *J Transl Med.* (2014) 12:31. doi: 10.1186/1479-5876-12-31
12. Tabaei S, Tabaee SS. DNA methylation abnormalities in atherosclerosis. *Artif Cells Nanomed Biotechnol.* (2019) 47:2031–41. doi: 10.1080/21691401.2019.1617724
13. Movassagh M, Choy MK, Knowles DA, Cordeddu L, Haider S, Down T, et al. Distinct epigenomic features in end-stage failing human hearts. *Circulation.* (2011) 124:2411–22. doi: 10.1161/CIRCULATIONAHA.111.040071
14. Latif N, Sarathchandra P, Chester AH, Yacoub MH. Expression of smooth muscle cell markers and co-activators in calcified aortic valves. *Eur Heart J.* (2015) 36:1335–45. doi: 10.1093/eurheartj/eht547
15. Andrews S. *FastQC A Quality Control tool for High Throughput Sequence Data*. (2010). Available online at: https://www.bioinformatics.babraham.ac.uk/projects/fastqc/.
16. Krueger F. Trim Galore. *A wrapper tool around Cutadapt and FastQC to consistently apply quality and adapter trimming to FastQ files*. (2015). Available online at: https://www.bioinformatics.babraham.ac.uk/projects/trim_galore/.
17. Krueger F, Andrews S. Bismark: a flexible aligner and methylation caller for Bisulfite-seq applications. *Bioinformatics.* (2011) 27:1571–2. doi: 10.1093/bioinformatics/btr167
18. Langmead B, Trapnell C, Pop M, Salzberg SL. Ultrafast and memory-efficient alignment of short DNA sequences to the human genome. *Genome Biol.* (2009) 10:R25. doi: 10.1186/gb-2009-10-3-r25
19. Akalin A, Kormaksson M, Li S, Garrett-Bakelman FE, Figueroa ME, Melnick A, et al. methylKit: a comprehensive R package for the analysis of genome-wide DNA methylation profiles. *Genome Biol.* (2012) 13:R87. doi: 10.1186/gb-2012-13-10-r87
20. Karolchik D, Hinrichs A, Furey T, Roskin K, Sugnet C, Haussler D, et al. The UCSC table browser data retrieval tool. *Nucleic Acids Res.* (2004) 32:D493–6. doi: 10.1093/nar/gkh103
21. Adusumalli S, Omar M, Soong R, Benoukraf T. Methodological aspects of whole-genome bisulfite sequencing analysis. *Brief Bioinform.* (2016) 17:243–8. doi: 10.1093/bib/bbu016
22. Mi H, Muruganujan A, Casagrande JT, Thomas PD. Large-scale gene function analysis with the panther classification system. *Nat Protoc.* (2013) 8:1551–66. doi: 10.1038/nprot.2013.092
23. Xia J, Benner M, Hancock R. NetworkAnalyst - integrative approaches for protein–protein interaction network analysis and visual exploration. *Nucleic Acids Res.* (2014) 42:W167–74. doi: 10.1093/nar/gku443
24. Walter W, Sánchez-Cabo F, Ricote M. GOplot: an R package for visually combining expression data with functional analysis. *Bioinformatics.* (2015) 31:2912–4. doi: 10.1093/bioinformatics/btv300
25. Liu Y. *Role Of Nitric Oxide In Embryonic Heart Development And Adult Aortic Valve Disease*. (2014). Available online at: https://ir.lib.uwo.ca/etd/2108 (accessed June 26, 2020).
26. Matsson H, Eason J, Bookwalter CS, Klar J, Gustavsson P, Sunnegårdh J, et al. Alpha-cardiac actin mutations produce atrial septal defects. *Hum Mol Genet.* (2008) 17:256–65. doi: 10.1093/hmg/ddm302
27. Hulin A, Deroanne C, Lambert C, Defraigne JO, Nusgens B, Radermecker M, et al. Emerging pathogenic mechanisms in human myxomatous mitral valve: lessons from past and novel data. *Cardiovasc Pathol.* (2013) 22:245–50. doi: 10.1016/j.carpath.2012.11.001
28. England J, Loughna S. Heavy and light roles: myosin in the morphogenesis of the heart. *Cell Mol Life Sci.* (2013) 70:1221–39. doi: 10.1007/s00018-012-1131-1
29. Hulin A, Deroanne CF, Lambert CA, Dumont B, Castronovo V, Defraigne J-O, et al. Metallothionein-dependent up-regulation of TGF-β2 participates in the remodelling of the myxomatous mitral valve. *Cardiovasc Res.* (2012) 93:480–9. doi: 10.1093/cvr/cvr337
30. Thalji NM, Hagler MA, Zhang H, Casaclang-Verzosa G, Nair AA, Suri RM, et al. Nonbiased molecular screening identifies novel molecular regulators of fibrogenic and proliferative signaling in myxomatous mitral valve disease. *Circ Cardiovasc Genet.* (2015) 8:516–28. doi: 10.1161/CIRCGENETICS.114.000921
31. Blunder S, Messner B, Scharinger B, Doppler C, Zeller I, Zierer A, et al. Targeted gene expression analyses and immunohistology suggest a pro-proliferative state in tricuspid aortic valve-, and senescence and viral infections in bicuspid aortic valve-associated thoracic aortic aneurysms. *Atherosclerosis.* (2018) 271:111–9. doi: 10.1016/j.atherosclerosis.2018.02.007
32. Gošev I, Zeljko M, Durić Ž, Nikolić I, Gošev M, Ivčević S, et al. Epigenome alterations in aortic valve stenosis and its related left ventricular hypertrophy. *Clin Epigenetics.* (2017) 9:106. doi: 10.1186/s13148-017-0406-7
33. Padang R, Bagnall RD, Tsoutsman T, Bannon PG, Semsarian C. Comparative transcriptome profiling in human bicuspid aortic valve disease using RNA sequencing. *Physiol Genomics.* (2015) 47:75–87. doi: 10.1152/physiolgenomics.00115.2014
34. Bossé Y, Miqdad A, Fournier D, Pépin A, Pibarot P, Mathieu P. Refining molecular pathways leading to calcific aortic valve stenosis by studying gene expression profile of normal and calcified stenotic human aortic valves. *Circ Cardiovasc Genet.* (2009) 2:489–98. doi: 10.1161/CIRCGENETICS.108.820795
35. Grassini DR, Lagendijk AK, De Angelis JE, Da Silva J, Jeanes A, Zettler N, et al. Nppa and nppb act redundantly during zebrafish cardiac development to

confine AVC marker expression and reduce cardiac jelly volume. *Dev.* (2018) 145:dev160739. doi: 10.1242/dev.160739
36. Sergeeva IA, Christoffels VM. Regulation of expression of atrial and brain natriuretic peptide, biomarkers for heart development and disease. *Biochim Biophys Acta Mol Basis Dis.* (2013) 1832:2403–13. doi: 10.1016/j.bbadis.2013.07.003
37. Chamberlain AA, Lin M, Lister RL, Maslov AA, Wang Y, Suzuki M, et al. methylation is developmentally regulated for genes essential for cardiogenesis. *J Am Heart Assoc.* (2014) 3:e000976. doi: 10.1161/JAHA.114.000976
38. Grande-Allen KJ, Osman N, Ballinger ML, Dadlani H, Marasco S, Little PJ. Glycosaminoglycan synthesis and structure as targets for the prevention of calcific aortic valve disease. *Cardiovasc Res.* (2007) 76:19–28. doi: 10.1016/j.cardiores.2007.05.014
39. Albanese I, Yu B, Al-Kindi H, Barratt B, Ott L, Al-Refai M, et al. Role of noncanonical wnt signaling pathway in human aortic valve calcification. *Arterioscler Thromb Vasc Biol.* (2017) 37:543–52. doi: 10.1161/ATVBAHA.116.308394
40. Day SM. The ubiquitin proteasome system in human cardiomyopathies and heart failure. *Am J Physiol Hear Circ Physiol.* (2013) 304:H1283–93. doi: 10.1152/ajpheart.00249.2012
41. Mohamed SA, Hanke T, Schlueter C, Bullerdiek J, Sievers HH. Ubiquitin fusion degradation 1-like gene dysregulation in bicuspid aortic valve. *J Thorac Cardiovasc Surg.* (2005) 130:1531–6. doi: 10.1016/j.jtcvs.2005.08.017
42. Yamada T, Satoh S, Sueyoshi S, Mitsumata M, Matsumoto T, Ueno T, et al. Ubiquitin-positive foam cells are identified in the aortic and mitral valves with atherosclerotic involvement. *J Atheroscler Thromb.* (2009) 16:472–9. doi: 10.5551/jat.No1248
43. Li F-F, Zhou J, Zhao D-D, Yan P, Li X, Han Y, et al. Characterization of SMAD3 gene variants for possible roles in ventricular septal defects and other congenital heart diseases. *PLoS ONE.* (2015) 10:e0131542. doi: 10.1371/journal.pone.0131542
44. Regalado ES, Guo DC, Villamizar C, Avidan N, Gilchrist D, McGillivray B, et al. Exome sequencing identifies SMAD3 mutations as a cause of familial thoracic aortic aneurysm and dissection with intracranial and other arterial aneurysms. *Circ Res.* (2011) 109:680–6. doi: 10.1161/CIRCRESAHA.111.248161
45. Kubalak SW, Hutson DR, Scott KK, Shannon RA. Elevated transforming growth factor beta2 enhances apoptosis and contributes to abnormal outflow tract and aortic sac development in retinoic X receptor alpha knockout embryos. *Development.* (2002) 129:733–46. doi: 10.1242/dev.129.3.733
46. Zhang Y, Ma L. Identification of key genes and pathways in calcific aortic valve disease by bioinformatics analysis. *J Thorac Dis.* (2019) 11:5417–26. doi: 10.21037/jtd.2019.11.57
47. Radhakrishna U, Albayrak S, Alpay-Savasan Z, Zeb A, Turkoglu O, Sobolewski P, et al. Genome-wide DNA methylation analysis and epigenetic variations associated with congenital aortic valve stenosis (AVS). *PLoS ONE.* (2016) 11:e0154010. doi: 10.1371/journal.pone.0154010
48. Thanassoulis G. Preventing aortic stenosis by changing the way we think about an old disease. *JAMA Cardiol.* (2020) 5:627–9. doi: 10.1001/jamacardio.2020.0722
49. Bergmark BA, O'Donoghue ML, Murphy SA, Kuder JF, Ezhov M V, Ceška R, et al. An exploratory analysis of proprotein convertase subtilisin/kexin type 9 inhibition and aortic stenosis in the FOURIER trial. *JAMA Cardiol.* (2020) 5:709–13. doi: 10.1001/jamacardio.2020.0728
50. Armstrong EJ, Bischoff J. Heart valve development: endothelial cell signaling and differentiation. *Circ Res.* (2004) 95:459–70. doi: 10.1161/01.RES.0000141146.95728.da
51. Walker GA, Masters KS, Shah DN, Anseth KS, Leinwand LA. Valvular myofibroblast activation by transforming growth factor-β: Implications for pathological extracellular matrix remodeling in heart valve disease. *Circ Res.* (2004) 95:253–60. doi: 10.1161/01.RES.0000136520.07995.aa
52. Ng CM, Cheng A, Myers LA, Martinez-Murillo F, Jie C, Bedja D, et al. TGF-β-dependent pathogenesis of mitral valve prolapse in a mouse model of Marfan syndrome. *J Clin Invest.* (2004) 114:1586–92. doi: 10.1172/JCI200422715
53. Clark-Greuel JN, Connolly JM, Sorichillo E, Narula NR, Rapoport HS, Mohler Iii ER, et al. Transforming growth factor-1 mechanisms in aortic valve calcification: increased alkaline phosphatase and related events. *Ann.* (2007) 83:946–53. doi: 10.1016/j.athoracsur.2006.10.026
54. Ferrari S, Pesce M. The complex interplay of inflammation, metabolism, epigenetics, and sex in calcific disease of the aortic valve. *Front Cardiovasc Med.* (2022) 8:1971. doi: 10.3389/fcvm.2021.791646
55. Macgrogan D, Luna-Zurita L, de la Pompa JL. Notch signaling in cardiac valve development and disease. *Birth Defects Res Part A Clin Mol Teratol.* (2011) 91:449–59. doi: 10.1002/bdra.20815
56. Gutierrez J. *DNA Methylation Analysis of Bicuspid Aortic Valve in Turner Syndrome*. (2021). Available online at: https://books.google.com.eg/books/about/DNA_Methylation_Analysis_of_Bicuspid_Aor.html?id=AAOFzgEACAAJ&redir_esc=y.~
57. Zhou J, Xiong Y, Dong X, Wang H, Qian Y, Ma D, et al. Genome-wide methylation analysis reveals differentially methylated CpG sites and altered expression of heart development-associated genes in fetuses with cardiac defects. *Exp Ther Med.* (2021) 22:1–11. doi: 10.3892/etm.2021.10464
58. Zhang J, Chang JYF, Huang Y, Lin X, Luo Y, Schwartz RJ, et al. The FGF-BMP signaling axis regulates outflow tract valve primordium formation by promoting cushion neural crest cell differentiation. *Circ Res.* (2010) 107:1209–19. doi: 10.1161/CIRCRESAHA.110.225318
59. Zhou J, Bowen C, Lu G, Knapp C, Recknagel A, Norris RA, et al. Cadherin-11 expression patterns in heart valves associate with key functions during embryonic cushion formation, valve maturation and calcification. *Cells Tissues Organs.* (2013) 198:300–10. doi: 10.1159/000356762
60. Bloomekatz J, Singh R, Prall OWJ, Dunn AC, Vaughan M, Loo CS, et al. Platelet-derived growth factor (PDGF) signaling directs cardiomyocyte movement toward the midline during heart tube assembly. *Elife.* (2017) 6:e21172. doi: 10.7554/eLife.21172
61. Li R, Wu Y, Manso AM, Gu Y, Liao P, Israeli S, et al. β1 integrin gene excision in the adult murine cardiac myocyte causes defective mechanical and signaling responses. *Am J Pathol.* (2012) 180:952–62. doi: 10.1016/j.ajpath.2011.12.007
62. Kamel PI, Qu X, Geiszler AM, Nagrath D, Harmancey R, Taegtmeyer H, et al. Metabolic regulation of collagen gel contraction by porcine aortic valvular interstitial cells. *J R Soc Interface.* (2014) 11:20140852. doi: 10.1098/rsif.2014.0852
63. Salhiyyah K, Sarathchandra P, Latif N, Yacoub MH, Chester AH. Hypoxia-mediated regulation of the secretory properties of mitral valve interstitial cells. *Am J Physiol Circ Physiol.* (2017) 313:H14–23. doi: 10.1152/ajpheart.00720.2016
64. Yoshioka M, Yuasa S, Matsumura K, Kimura K, Shiomi T, Kimura N, et al. Chondromodulin-I maintains cardiac valvular function by preventing angiogenesis. *Nat Med.* (2006) 12:1151–9. doi: 10.1038/nm1476
65. Yeh CY, Shun CT, Kuo YM, Jung CJ, Hsieh SC, Chiu YL, et al. Bin, Yang CJ, Chia JS. Activated human valvular interstitial cells sustain interleukin-17 production to recruit neutrophils in infective endocarditis. *Infect Immun.* (2015) 83:2202–12. doi: 10.1128/IAI.02965-14
66. Akahori H, Tsujino T, Naito Y, Sawada H, Sugahara M, Fukui M, et al. Nuclear factor-κB-hypoxia-inducible factor-2 pathway in aortic valve stenosis. *J Heart Valve Dis.* (2014) 23:558–66.
67. Yu Z, Seya K, Daitoku K, Motomura S, Fukuda I, Furukawa KI. Tumor necrosis factor-α accelerates the calcification of human aortic valve interstitial cells obtained from patients with calcific aortic valve stenosis via the BMP2-Dlx5 pathway. *J Pharmacol Exp Ther.* (2011) 337:16–23. doi: 10.1124/jpet.110.177915
68. Nagy E, Eriksson P, Yousry M, Caidahl K, Ingelsson E, Hansson GK, et al. Valvular osteoclasts in calcification and aortic valve stenosis severity. *Int J Cardiol.* (2013) 168:2264–71. doi: 10.1016/j.ijcard.2013.01.207
69. Mebazaa A, Mayoux E, Maeda K, Martin LD, Lakatta EG, Robotham JL, et al. Paracrine effects of endocardial endothelial cells on myocyte contraction mediated via endothelin. *Am J Physiol - Hear Circ Physiol.* (1993) 265:H1841–6. doi: 10.1152/ajpheart.1993.265.5.H1841
70. Peltonen T, Taskinen P, Näpänkangas J, Leskinen H, Ohtonen P, Soini Y, et al. Increase in tissue endothelin-1 and ETA receptor levels in human aortic valve stenosis. *Eur Heart J.* (2009) 30:242–9. https://doi-org.eres.qnl.qa/10.1093/eurheartj/ehn482 doi: 10.1093/eurheartj/ehn482
71. Jian B, Narula N, Li QY, Mohler ER, Levy RJ. Progression of aortic valve stenosis: TGF-β1 is present in calcified aortic valve cusps and promotes aortic valve interstitial cell calcification via apoptosis. *Ann Thorac Surg.* (2003) 75:457–65. doi: 10.1016/S0003-4975(02)04312-6

72. Lee W-S, Kim J. Peroxisome proliferator-activated receptors and the heart: lessons from the past and future directions. *PPAR Res.* (2015) 2015:18. doi: 10.1155/2015/271983
73. Maredia A, Guzzardi D, Aleinati M, Iqbal F, Khaira A, Madhu A, et al. Aorta-specific DNA methylation patterns in cell-free DNA from patients with bicuspid aortic valve-associated aortopathy. *Clin Epigenetics.* (2021) 13:1–10. doi: 10.1186/s13148-021-01137-y
74. Blaser MC, Kraler S, Luscher TF, Aikawa E. Multi-omics approaches to define calcific aortic valve disease pathogenesis. *Circ Res.* (2021) 128:1371–97. doi: 10.1161/CIRCRESAHA.120.317979
75. Nagy E, Bäck M. Epigenetic regulation of 5-lipoxygenase in the phenotypic plasticity of valvular interstitial cells associated with aortic valve stenosis. *FEBS Lett.* (2012) 586:1325–9. doi: 10.1016/j.febslet.2012.03.039
76. Haunschild J, Schellinger I, Barnard S, von Aspern K, Davierwala P, Misfeld M, et al. Bicuspid aortic valve patients show specific epigenetic tissue signature increasing extracellular matrix destruction. *Interact Cardiovasc Thorac Surg.* (2019) 29:937–43. doi: 10.1093/icvts/ivz210
77. Shen K, Liu H, Jing R, Yi J, Zhou X, DNA. methylation dysregulations in rheumatic heart valve disease. *BMC Cardiovasc Disord.* (2017) 17:159. doi: 10.1186/s12872-017-0585-3
78. Pan S, Lai H, Shen Y, Breeze C, Beck S, Hong T, et al. methylome analysis reveals distinct epigenetic patterns of ascending aortic dissection and bicuspid aortic valve. *Cardiovasc Res.* (2017) 113:692–704. doi: 10.1093/cvr/cvx050
79. Lee YK, Jin S, Duan S, Lim YC, Ng DP, Lin XM, et al. Improved reduced representation bisulfite sequencing for epigenomic profiling of clinical samples. *Biol Proced Online.* (2014) 16:1. doi: 10.1186/1480-9222-16-1
80. Gu H, Smith ZD, Bock C, Boyle P, Gnirke A, Meissner A. Preparation of reduced representation bisulfite sequencing libraries for genome-scale DNA methylation profiling. *Nat Protoc.* (2011) 6:468–81. doi: 10.1038/nprot.2010.190
81. Carmona JJ, Accomando WP, Binder AM, Hutchinson JN, Pantano L, Izzi B, et al. Empirical comparison of reduced representation bisulfite sequencing and Infinium BeadChip reproducibility and coverage of DNA methylation in humans. *NPJ Genomic Med.* (2017) 2:13. doi: 10.1038/s41525-017-0012-9
82. Shi ST, De Gorter DJJ, Hoogaars WMH, Hoen PAC, Ten Dijke P. Overactive bone morphogenetic protein signaling in heterotopic ossification and duchenne muscular dystrophy. *Cell Mol Life Sci.* (2013) 70:407–23. doi: 10.1007/s00018-012-1054-x
83. Gomez-Stallons MV, Wirrig-Schwendeman EE, Hassel KR, Conway SJ, Yutzey KE. Bone morphogenetic protein signaling is required for aortic valve calcification. *Arterioscler Thromb Vasc Biol.* (2016) 36:1398–405. doi: 10.1161/ATVBAHA.116.307526
84. Adly N, Alhashem A, Ammari A, Alkuraya FS. Ciliary genes TBC1D32/C6orf170 and SCLT1 are mutated in patients with OFD Type IX. *Hum Mutat.* (2014) 35:36–40. doi: 10.1002/humu.22477
85. Pierpont ME, Brueckner M, Chung WK, Garg V, Lacro R V, McGuire AL, et al. Genetic basis for congenital heart disease: revisited: a scientific statement from the American heart association. *Circulation.* (2018) 138:e653–711. doi: 10.1161/CIR.0000000000000606
86. Toomer KA, Fulmer D, Guo L, Drohan A, Peterson N, Swanson P, et al. A role for primary cilia in aortic valve development and disease. *Dev Dyn.* (2017) 246:625–34. doi: 10.1002/dvdy.24524
87. Marchetti G, Girelli D, Zerbinati C, Lunghi B, Friso S, Meneghetti S, et al. An integrated genomic-transcriptomic approach supports a role for the proto-oncogene BCL3 in atherosclerosis. *Thromb Haemost.* (2015) 113:655–63. doi: 10.1160/TH14-05-0466
88. Kuusisto J, Räsänen K, Särkioja T, Alarakkola E, Kosma VM. Atherosclerosis-like lesions of the aortic valve are common in adults of all ages: a necropsy study. *Heart.* (2005) 91:576–82. doi: 10.1136/hrt.2004.036848
89. Goyal G, Abbas SH, Diamond MA, Pulinthanathu R. Fatty infiltration of mitral valve: a rare case report and review of literature. *Cureus.* (2019) 11:e6144. doi: 10.7759/cureus.6144

Conflict of Interest: The authors declare that the research was conducted in the absence of any commercial or financial relationships that could be construed as a potential conflict of interest.

Publisher's Note: All claims expressed in this article are solely those of the authors and do not necessarily represent those of their affiliated organizations, or those of the publisher, the editors and the reviewers. Any product that may be evaluated in this article, or claim that may be made by its manufacturer, is not guaranteed or endorsed by the publisher.

frontiers | Frontiers in Cardiovascular Medicine

SYSTEMATIC REVIEW
published: 17 May 2022
doi: 10.3389/fcvm.2022.872288

The Role of Transforming Growth Factor-β Signaling in Myxomatous Mitral Valve Degeneration

*Qiyu Tang[1], Andrew J. McNair[1], Kanchan Phadwal[1], Vicky E. Macrae[1] and Brendan M. Corcoran[1,2]**

[1] The Roslin Institute, The University of Edinburgh, Edinburgh, United Kingdom, [2] Royal (Dick) School of Veterinary Studies, The University of Edinburgh, Edinburgh, United Kingdom

Mitral valve prolapse (MVP) due to myxomatous degeneration is one of the most important chronic degenerative cardiovascular diseases in people and dogs. It is a common cause of heart failure leading to significant morbidity and mortality in both species. Human MVP is usually classified into primary or non-syndromic, including Barlow's Disease (BD), fibro-elastic deficiency (FED) and Filamin-A mutation, and secondary or syndromic forms (typically familial), such as Marfan syndrome (MFS), Ehlers-Danlos syndrome, and Loeys–Dietz syndrome. Despite different etiologies the diseased valves share pathological features consistent with myxomatous degeneration. To reflect this common pathology the condition is often called myxomatous mitral valve degeneration (disease) (MMVD) and this term is universally used to describe the analogous condition in the dog. MMVD in both species is characterized by leaflet thickening and deformity, disorganized extracellular matrix, increased transformation of the quiescent valve interstitial cell (qVICs) to an activated state (aVICs), also known as activated myofibroblasts. Significant alterations in these cellular activities contribute to the initiation and progression of MMVD due to the increased expression of transforming growth factor-β (TGF-β) superfamily cytokines and the dysregulation of the TGF-β signaling pathways. Further understanding the molecular mechanisms of MMVD is needed to identify pharmacological manipulation strategies of the signaling pathway that might regulate VIC differentiation and so control the disease onset and development. This review briefly summarizes current understanding of the histopathology, cellular activities, molecular mechanisms and pathogenesis of MMVD in dogs and humans, and in more detail reviews the evidence for the role of TGF-β .

Keywords: MVP, MMVD, valve interstitial cell, valve endothelial cell, TGF-β, BMP

OPEN ACCESS

Edited by:
Elena Aikawa, Brigham and Women's Hospital and Harvard Medical School, United States

Reviewed by:
Katherine Yutzey, Cincinnati Children's Hospital Medical Center, United States
Anna Malashicheva, Institute of Cytology, Russia

***Correspondence:**
Brendan M. Corcoran
Brendan.Corcoran@ed.ac.uk

Specialty section:
This article was submitted to Heart Valve Disease, a section of the journal Frontiers in Cardiovascular Medicine

Received: *09 February 2022*
Accepted: *12 April 2022*
Published: *17 May 2022*

Citation:
Tang Q, McNair AJ, Phadwal K, Macrae VE and Corcoran BM (2022) The Role of Transforming Growth Factor-β Signaling in Myxomatous Mitral Valve Degeneration. Front. Cardiovasc. Med. 9:872288. doi: 10.3389/fcvm.2022.872288

INTRODUCTION

Mitral valve prolapse (MVP) is one of the most common cardiac valvular abnormality in dogs and humans, and is a major source of morbidity and mortality and a common cause of heart failure, ventricular dysfunction, arrhythmias and sudden cardiac death (1–6). In the dog the condition is more commonly called myxomatous mitral valve disease (MMVD). Since this mitral valvulopathy in both species has various synonyms and myxomatous changes is the predominant pathological finding, in this review the terms MVP and MMVD will be used interchangeably and when needed

for human and dog, respectively. MVP affects to 2–3% of the human population, and more than 10% of individuals over the age of 65 years have mitral valve insufficiency (7, 8). It accounts for 7% of deaths in dogs before 10 years of age and its prevalence is very high, estimated between 30 and 70% of all elderly dogs, with the greater prevalence in small breed dogs and in certain predisposed breeds such as the cavalier King Charles spaniel (CKCS) (9–11). Some forms of MVP will have a congenital or genetic basis, meaning MVP can be further characterized into primary non-syndromic, and secondary syndromic forms (4). Syndromic MVP is commonly associated with global genetic connective tissue disorders, such as Marfan syndrome (MFS), Loeys-Dietz syndrome and Ehlers-Danlos syndrome (12–14). It can also appear as isolated non-syndromic MVP, typically in a familial setting. The first confirmed non-syndromic genetic mutation was for the X-linked FLNA (Filamin-A) gene mutation, which causes valvular defects and progressive myxomatous degeneration and MVP in mice and humans (15–17). For the non-syndromic variants two disease types are reported including Barlow's Disease (BD), where there is myxomatous degeneration and end-stage fibrosis, and fibroelastic deficiency (FED) where there is only myxomatous degeneration with valve thinning rather than thickening (18). FED is typically only seen in the very elderly, while Barlow's Disease (BD) has more commonality with canine MMVD in terms of its slowly acquired development and progression, despite the lack of fibrosis in the dog. Lastly, MMVD has also been described in mice and pigs, induced by gene interference or surgical intervention, but the extent of MMVD in other species as a consequence of aging is unknown (19–21). Details of MMVD in both species are summarized in **Table 1**.

For both syndromic and non-syndromic forms in both species the diseased valves appear histologically similar and exhibit features of myxomatous (myxoid) degeneration. Progressive deterioration of the mitral valves is typically characterized by increased valvular nodularity, leaflet thickening and deformity, excessive accumulation of proteoglycans (GAGs), collagen and elastin fragmentation, increased expression of proteolytic enzymes, disorganized extracellular matrix (ECM) and increased numbers of activated valve interstitial cells (aVICs; activated myofibroblasts) and with more obvious macrophage infiltration in human valves (3, 5, 22–25). Furthermore, in human valves there can be additional fibrosis in end-stage disease (BD) characterized by fibrotic layers on the valve surface, a change not seen in the dog (26–29).

Although, the histopathological changes of myxomatous degeneration are well characterized, some aspects of the underlying molecular changes and its contribution to pathogenesis are still to be identified (22, 30, 31). Most MMVD seen in human and veterinary clinical practice are sporadic and of unknown etiology, although a genetic or inherited basis suspected. However, there is increasing evidence for a primary role for members of the transforming growth factor (TGF)-β superfamily in the pathogenesis and progression of various MMVD forms (5, 32–37). This is not surprising as the TGF-β superfamily are important in the regulation of most cellular events, such as proliferation, differentiation, migration, autophagy, apoptosis and senescence in a variety of cardiovascular diseases (38, 39). While much is known about the cellular and molecular events of the disease in both species, the exact molecular and regulatory mechanisms are not yet elaborated, especially with regard to early disease onset and progression (3–5, 37). In human MVP most studies of non-syndromic forms have been restricted to examining end-stage valves obtained at surgery (29, 34, 35, 40). Information on earlier onset is restricted mainly to inherited connective tissue disorders, such as MFS, osteogenesis imperfecta, and Ehlers-Danlos syndrome, although myxomatous degeneration in those patients can appear with advanced age (17).

$CD45^+$ hematopoietic cells have been detected in human, sheep, and murine MMVD valves related to non-infective causes, although MMVD in the absence of infective endocarditis has traditionally been regarded as a non-inflammatory disease (34, 41–44). The majority of these cells are characterized as macrophages implicating macrophage infiltration as a potential secondary driver of MMVD progression. CD45 expression of mitral VECs can be induced by TGF-β signaling in sheep MMVD (25, 43, 45). TGF-β signaling is enhanced in MMVD in mouse, humans and dogs and has been associated with ECM dysregulation and increased macrophage numbers in diseased valves (4, 32, 34, 46, 47). These data suggest that TGF-β signaling might be associated with the emergence of an inflammatory micro-environment comprised of increased recruitment of pro-inflammatory macrophages from the circulation and immunogenic ECM remodeling, somewhat analogous to features of calcific aortic valve disease (CAVD) (6, 25). In CAVD TGF-β signaling is involved in the pathogenesis, as for MMVD a promoter role in the early VIC activation as shown by up-regulation of α-smooth muscle actin (α-SMA). In dogs with advanced disease there is evidence of a marginal increase in the number of mast cells in affected valves (24), but no involvement of the resident macrophage population or recruitment of inflammatory cells are found in severe MMVD (elderly dogs) (48, 49). Whether there is a macrophage population present in dogs or only during early stage of the disease has yet to be elucidated.

VALVE STRUCTURE, PATHOLOGY, AND CELL AND MOLECULAR CHANGES

The cross-sectional structure of the normal mitral leaflets is similar to the aortic valve, with at least three layers, atrialis, spongiosa, and fibrosa identified, a fourth ventricularis proposed by some, and each with different thickness and cell and ECM composition, and both sides lined with valve endothelial cells (VECs). The thin atrialis contains a large amount of elastin with a mixed amount of scattered collagen fibers and valve interstitial cells (VICs) (50, 51). The spongiosa contains loosely arranged collagen fibers and is rich in glycosaminoglycans (GAGs), such as hyaluronan, and various proteoglycans (52). This layer, consisting mainly of collagen I and III and small numbers of thin elastin fibers. The majority of cells in the spongiosa, and throughout the whole valve, are quiescent VICs (qVICs) along with few mast cells (24, 53–55). The dense fibrosa

TABLE 1 | Characteristics of various forms of MMVD in the human and dogs.

Classification			Histopathological features	Abnormal signaling	Cellular changes
Human MVP	Primary (Non-syndromic)	Barlow's Disease (BD)	1.Typical lesions of myxomatous degeneration 2.End-stage fibrosis 3.Leaflet thickening	1.TGF-β signaling 2.5-HT (serotonin) signaling 3.BMP signaling 4.Wnt/β-catenin	1.Increased aVICs from qVICs 2. Increased macrophage infiltration 3. EndoMT
		Fibroelastic deficiency (FED)	1.Typical lesions of myxomatous degeneration 2.Deficiency in collagen 3.Valve thinning	TGF-β signaling	Increased aVICs from qVICs
		Filamin-A mutation	Typical lesions of myxomatous degeneration	1.TGF-β signaling, 2.Ras/Mek/Erk signaling 3.5-HT (serotonin) signaling	1.Increased aVICs from qVICs
	Secondary (Syndromic forms)	Marfan syndrome (MFS)	Typical lesions of myxomatous degeneration	1.TGF-β signaling 2. BMP signaling 3. Wnt/β-catenin	1. Increased aVICs from qVICs 2. Increased macrophage infiltration 3. EndoMT
		Ehlers-Danlos syndrome	Typical lesions of myxomatous degeneration		
		Loeys–Dietz syndrome	Typical lesions of myxomatous degeneration	TGF-β signaling	
Canine MMVD			1.Typical lesions of myxomatous degeneration 2.Lack of any fibrotic changes	1.TGF-β signaling 2.5-HT (serotonin) signaling 3.BMP signaling	1.Increased aVICs from qVICs 2. EndoMT 3. Lack of inflammatory infiltration

layer is composed of tightly packed collagen bundles arranged parallel to the leaflet free edge and within which are scattered VICs (**Figure 1**).

The gross and histopathological changes in both species are reasonably well characterized, and will be only briefly describe here, but to give contextual background to the role of TGF-β in the disease process (5, 22, 37, 56–58). Changes the endothelium include endothelial loss, cellular pleomorphism, endothelial-to-mesenchymal transition (EndoMT), disruption of the basement membrane and accumulation of aVICs in the sub-endothelium (23, 46, 55). The myxomatous degeneration itself is characterized by expansion of the spongiosa and separation as well as fragmentation of the dense collagen bundles in the fibrosa (5, 59). There is a reduction in connective tissue density, accumulation of a myxoid extracellular matrix rich in GAGs, loss of mature collagen and replacement with immature fibrillar collagen lacking cross-links structural, in all the layers of leaflet as well as the chordae tendineae (60). The main cellular event is the phenotypic differentiation of the VICs from a quiescent phenotype (qVICs) to an activated myofibroblast (aVICs) in the spongiosa and fibrosa, with accumulation of aVICs in the sub-endothelium (46, 61). Furthermore, there is evidence of aVIC persistence with dysregulation of apoptosis, and transcriptomic evidence of altered gene expression associated with cellular senescence (37, 62). Rather than aVICs being cleared for the tissue as would normally happen, their persistence might contribute to the aberrant matric remodeling typical of the disease. The aVICs are presumed responsible for valve matrix degrading, and at a rate exceeding that of production of new collagen and elastin (63). This matrix degeneration is presumed to be due to increased production of various proteolytic enzymes including matrix metalloproteinases (MMP-1, MMP-2, MMP-9, and MMP-13). It should be noted that human valvulopathies heighten the risk of developing endocarditis which is not the case in the dog. The reason for this species difference is unknown. Overall, these pathological changes account for the reduced tensile strength, distorted valve shape and mechanics typical of the disease resulting in the mitral regurgitation and heart failure.

In addition to the naturally occurring forms of MMVD there are various rodent models available, and comment will be made on how they inform thinking on the role of TGF-β (**Table 2**). Many of these models are transgenic and questions can be raised to their validity as models of what is a chronic degenerative disease, but that discussion is beyond the scope of this review.

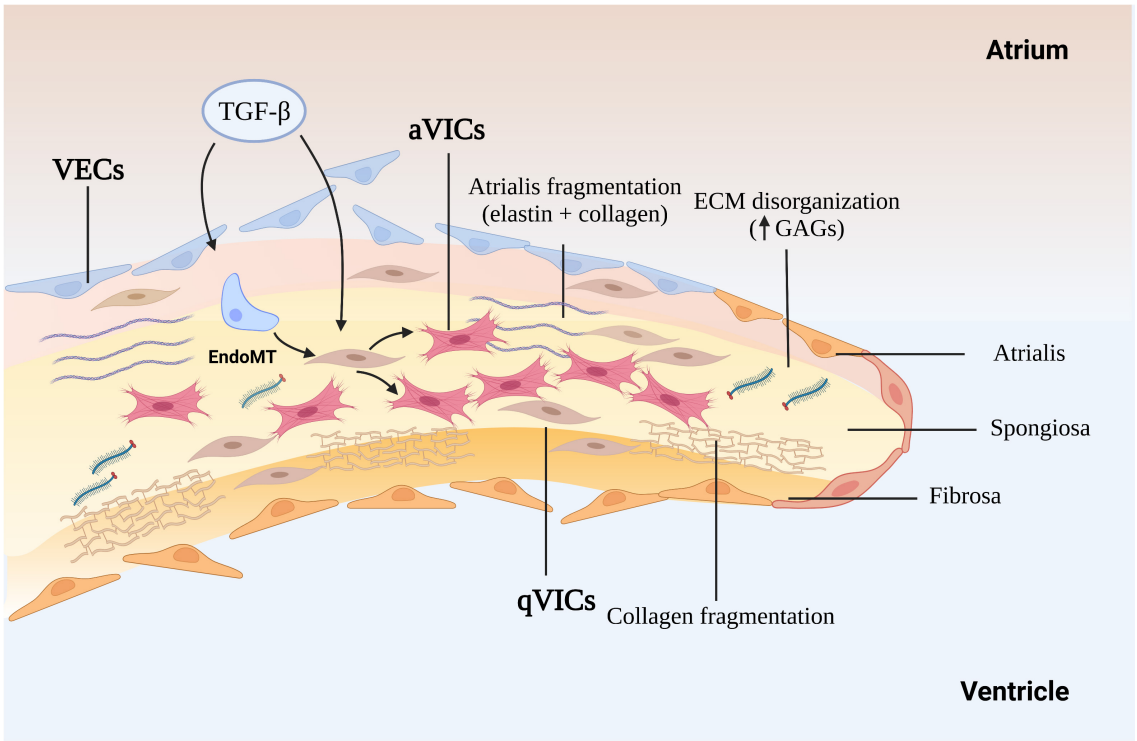

FIGURE 1 | The mechanism of myxomatous degeneration. The schematic shows the endothelial to mesenchymal transition (EndoMT) process and the activation of quiescent valve interstitial cells to myofibroblasts that affect matrix production and remodeling, driving collagen and elastin fragmentation and loss. ECM, extracellular matrix; GAGs, glycosaminoglycans; MMP, matrix metalloprotease; TGF-β, transforming growth factor-β; qVICs, quiescent valvular interstitial cells; aVICs, activated valvular interstitial cells.

THE ROLE OF TRANSFORMING GROWTH FACTOR-β IN MYXOMATOUS MITRAL VALVE DEGENERATION

Effects of Transforming Growth Factor-β on Valvular Interstitial Cells

As mentioned previously, VICs exist in all layers as two distinct phenotypes, qVICs and aVICs, and predominantly in healthy and diseased valves, respectively (64). During development endothelial cells invade the endocardial cushion and are transformed into embryonic progenitor mesenchymal cells to induce ECM remodeling under the regulation of the TGF-β family and bone morphogenetic proteins (BMPs) (65). Once the valve is formed qVICs predominate and maintain valve structure and function (24, 48, 54). VICs in normal valves have a quiescent vimentin^{+}/alpha-smooth muscle actin (αSMA)- phenotype and are presumed to operate in a homeostatic role controlling ECM remodeling and repair (66). TGF-β up-regulation appears to have an important role among various biological pathways in the pathogenesis of the multiple forms of MMVD. Specifically, TGF-β is known to activate qVICs toward a pathologic synthetic phenotype, as shown both in animal models and in human and canine *in vitro* studies (32, 36, 48). Similarly, antagonism of the TGF-βR II receptor by SB431542 transitions aVICs to the qVIC phenotype in a canine low serum culture system, where VICs were isolated from diseased canine mitral valves and maintained in 2% (v/v) FBS media (36). Members of the TGF-β superfamily are overexpressed in surgically excised human diseased valves where aVICs predominate and this is associated with increased expression of MMPs, presumably driving degeneration of collagen and elastin structures (22, 34, 35, 67, 68). Finally, examining transcriptomic data from human valves, upregulation of BMP 4 has been shown to mediate the activation of VICs from healthy quiescent cells to a pathologic synthetic phenotype (67).

Transforming Growth Factor-β Control of EndoMT in Myxomatous Mitral Valve Degeneration

One of the important, but less documented, changes to the endothelium in MMVD is induction of EndoMT, accompanied by activation of transcriptional regulatory mechanisms important in heart valve development, and is seen in both human and canine MMVD (46, 69–71). This is associated with co-expression of hyaluronic acid synthase (HAS)-2 and α-SMA in endothelial cells and increased expression of Sox9, and increased expression of HAS-2 in stromal interstitial cells (46, 52, 72). There are other lines of evidence suggesting a role for EndoMT in MMVD, with a role for TGF-β. Cultured endocardial cells derived from mature ovine valves have been shown to transdifferentiate *via*

TABLE 2 | *In vivo* and *in vitro* models for MMVD.

Classification	*In vivo* animal models	*In vitro* culture models
Myxomatous mitral valve degeneration (MMVD)	1.Mouse treated with AngII (84) 2.Mouse treated with nordexfenfluramine (NDF) (133, 134) 3. FVB mouse (135)	1.Porcine 3D mitral VIC culture system (136) 2.Porcine mitral VIC culture system (100) 3.Human mitral valve tissue culture system (34) 4.Human mitral VIC culture system (34, 114)
Barlow's Disease (BD)	Dogs with spontaneous MMVD (5, 37)	1.Canine 2D mitral VIC and VEC co-culture system (36) 2.Canine 3D tissue-engineered fibrin-based cell culture system (137)
Filamin-A mutation	Filamin-A KO mouse (89)	
Marfan syndrome (MFS) (32, 107)	$Fbn1^{C1039G/+}$ mouse $Fbn1^{C1039G/C1039G}$ mouse	
Ehlers-Danlos syndrome (138)	$Col3a1^{\pm}$ mouse $Col5a1^{\pm}$ mouse	
Loeys–Dietz syndrome (117)	TGF-βR1$^{\pm}$ mouse TGF-βR2$^{\pm}$ mouse TGF-βR1$^{M318R/+}$ mouse TGF-βR2$^{G357W/+}$ mouse	

TGF-β signaling into mesenchymal cells that express α-SMA, and human valve endothelial cells adopt a mesenchymal phenotype after exposure to TGF-β (73, 74). Clonal expansion has shown endothelial-like cells have a strong response to TGF-β, which can then be inhibited by vascular endothelial growth factor (VEGF) (74). *In vitro* mitral valve endothelial cells have been shown to be important for maintaining the quiescence of valve interstitial cells and thereby reciprocally preventing TGF-β-driven EndoMT of endothelial cells (75). Lastly, inhibition of TGF-β by the angiotensin two receptor antagonist losartan can reduce EndoMT of mitral valve endothelial cells *in vitro* in a sheep model and can decrease leaflet thickness and block TGF-β signaling and downstream targets (43). Nevertheless, evidence for EndoMT is restricted to valve transcriptomic data in the dog and human, and found in valve tissue in the dog using IHC, but to what extent this might contribute to the valve VIC population and to disease pathogenesis *in vivo* is unknown (**Figure 2**).

TRANSFORMING GROWTH FACTOR-β INITIATED SIGNALING PATHWAYS IN MYXOMATOUS MITRAL VALVE DEGENERATION

The TGF-β family consists of a large variety of pleiotropic multifunctional proteins that play significant roles in embryonic development, autoimmunity, cancer, fibrotic disorders, and cardiovascular diseases (34, 76–79). TGF-βs and BMPs are considered as the most important initiators of the signaling pathway (80–83). Although the effect of TGF-βs and BMPs on the initiation and progression of MMVD has been shown, the molecular and regulatory events involved are highly complex resulting from a large number of signaling interactions promoted by diverse molecular mechanisms. Many of these interaction still need to be elucidated.

TGF-β-mediated valvular fibrosis is only observed in end-stage human MMVD and seen as fibrotic over-lays developing on the atrial and ventricular sides of leaflets. However the myxomatous degeneration found in both species is believed to be highly TGF-β-dependent (5, 37). Various studies have suggested the important roles for the members of TGF-β family in the initiation and development of MMVD in humans, mouse and dog (32–37, 47, 48, 67). Pathway analysis by transcriptomic profiling in human and canine valve tissue has identified TGF-β signaling as the dominant pathway in both the development and progression of MMVD (37, 84). Increased expression of multiple TGF-β isoforms in parallel with the accumulation of ECM components and transformation of VICs into myofibroblasts is observed in the surgically excised samples of myxomatous valves from human and dog (34, 37, 47, 85, 86). In a transgenic fibrillin (Fbn)-1-deficient mouse Marfan Disease model, where TGF-β signaling was potentiated, VICs are phenotypical altered with associated myxomatous ECM remodeling (32, 87). Transformation of qVICs to the diseased activated myofibroblast phenotype can be blocked with TGF-β-neutralizing antibodies (NeuAb), antagonism of the TGF-β RII receptor, antagonizing TGF-β signaling and blocking Smad phosphorylation (32, 34–36). In an *in vitro* Marfan Disease model an exon encoded Fbn-1 sequence triggers release of endogenous TGF-β1 and stimulates TGF-β receptor-mediated Smad2 signaling in the presence of cell layer ECM (88). However, it has been shown that non-Smad (non-canonical) signaling pathways are also implicated in MMVD progression, including regulation by several molecular mediators such as filamin A (FLN-A) and scleraxis (Scx) (86, 89).

Canonical Transforming Growth Factor-β-Mediated Signaling Pathways in Myxomatous Mitral Valve Degeneration

Substitution of an epidermal growth factor-like domain in the fibrillin-1 (Fbn-1) gene with a cysteine (C1039G) in transgenic mice will result in increased release of activated TGF-βs to initiate the aberrant signaling that contributes to myxomatous degeneration (32). Significant increased expression of TGF-βs, latency-associated peptides (LAPs), latent TGF-β activator integrins and phosphorylated SMAD2/3 has been reported in MMVD valve tissues using transcriptomic analysis and on histopathology, indicating the key contribution of canonical TGF-β-mediated signaling to MMVD (34, 37, 90, 91). Understanding how TGF-β signaling can control MMVD pathogenesis requires some explanation of the complex pathways involved. Briefly, the TGF-β signaling pathway is initiated by binding of activated TGF-β ligands with TGF-β receptor complexes in the cell membrane. Subsequent to intracellular biosynthesis TGF-β homodimers are secreted extracellularly as

inactive protein complexes, which maintain latency through the non-covalent binding with the pro-peptide latency-associated peptide (LAP). To exert its diverse biological functions TGF-β requires to be liberated from the latent complex and activated extracellularly before binding to its receptors. For example, Fbn-1, as a structural component of the ECM microfibrils, can release (activate) latent TGF-βs from the microfibrils by means of the substitution of Fbn-1 fragments for latent TGF-β-binding proteins (LTBPs) and by its complex interactions with various activators such as integrins (37, 88, 92–95). TGF-β release can also be controlled by torqueing mechanics where the bound protein complex is linked to cells (in this case VICs) by various integrins. Following the activation/release of TGF-βs these homodimers bind to their corresponding transmembrane receptor complexes (TGF-βR I and TGF-βR II) and initiate a complicated intracellular signaling cascade of molecular and regulatory events (96–98). The active receptor complex recruits and activates the downstream signaling effector proteins Smad2 and Smad3 (the canonical pathway) and they form an intracellular complex with co-Smad (Smad4, the mediator Smad) enabling its translocation from the cytoplasm into the nucleus. In the nucleus the Smad complex interacts with the Smad binding elements (SBE) to invoke transcription of various TGF-β-responsive genes, including those involved in ECM remodeling, VIC differentiation and EndoMT (99) (**Figure 3**).

The Role of Mediators in Canonical Transforming Growth Factor-β Initiated Myxomatous Mitral Valve Degeneration

While Smad2/3-mediated signaling probably is a major contributor to the initiating of MMVD, other molecular mediators related to canonical signaling pathways have been shown to play a significant role in the modulation of MMVD progression in animal models *in vivo* and *in vitro* in VICs. These regulatory mechanisms include molecules exerting their effects on MMVD by means of canonical TGF-β signaling pathways or through activation by TGF-β itself. Examples include fibrillin-1 (Fbn-1), filamin A (FLN-A), follistatin-like 1 (Fstl1), fibroblast growth factor (FGF)-2 and angiotensin (Ang) II (32, 84, 89, 100, 101).

Fbn-1 beyond being a structural component of ECM microfibrils has an important role in regulating TGF-β activity and signaling through interaction with LTBP in the myxomatous mitral valve of MFS patients (32). Ng and colleagues showed that the intense immunohistochemical signal of both active TGF-β and its intracellular responder pSmad2 were significantly increased in mitral valves in a MFS mouse model. These observations were further validated by TGF-β antagonism by neutralizing antibodies *in vivo* with rescuing of the myxomatous mitral valve phenotype. Additionally, the expression of the downstream TGF-β-related effectors, which are either members of the TGF-β superfamily or directly mediated by TGF-βs, such as βIGH3, endothelin-1 (EDN1) and BMPs, are upregulated in the mitral valves of MFS mice. This suggests a promoter role of the mutation in Fbn-1 in initiation of canonical TGF-β signaling in MFS, and perhaps more commonly non-syndromic variants of human MMVD (32). Evidence for the extracellular control by Fbn-1 of TGF-β signaling activation in other MFS-induced systemic disorders has been shown in other studies (102–108). Recent work on the age-dependent cardiac remodeling in a mouse model of MFS revealed a comparable expression pattern of the myofibroblast marker α-smooth muscle actin (α-SMA) in cardiac tissues of Fbn-1 transgenic mice and their wild-type littermates.

FLN-A is highly expressed in the mitral valve during development and is significantly diminished after birth, suggesting an important role for FLN-A during valve development (109). Mutations in the FLNA gene had been identified as a cause to a rare X-linked myxomatous valvular disease (17). FLN-A might act as a contributor to the initiation and development of myxomatous cardiac valves by its interaction with activated Smads to regulate TGF-β signaling (110, 111). In contrast, a recent study showed that FLN-A might not be involved in the pathogenesis of non-syndromic MVP, since the mRNA expression level of FLN-A in diseased valves is comparable to control leaflets, despite upregulation of TGF-β1 and pSmad2 signaling in diseased mitral valves (86). Another study also suggested that there were interactions between FLN-A and TGF-β since FLN-A acted as a promoter of TGF-β induced ECM remodeling in Fstl1-deficient mice (101). In a FLN-A knockout mouse the expression of the canonical TGF-β-dependent effector pSmad3 and its downstream target molecule collagen IαI are markedly increased in mitral valves suggesting deficiency in FLN-A positively influences Smad activation and correlates with increased collagen expression (89).

In Fstl1-knockout mice there is a sustained increase in TGF-β signaling after birth, while deletion of Fstl1 from the endocardial lineage results in myxomatous mitral valves with cell proliferation and endocardial-to-mesenchymal transition. Fstl1-deficient mitral valves show significantly upregulated expression of TGF-β in mitral valve VICs. Immunofluorescent analysis has shown that the positive signal for pSmad2/3 is mainly detected in the nuclei of VECs and VICs in diseased mitral leaflets, indicating active TGF-β signaling during postnatal development (101). Additional evidence that Fstl1 could regulate MMVD is shown by increased upregulation of a series of unique makers of ECM remodeling and EndoMT mediated by TGF-β signaling in Fst1-KO mice, including Fbn-1, FLN-A, vimentin and α-SMA. These data suggest important roles of Fstl1 in promoting homeostasis of the mitral valve undergoing embryonic development, postnatal maturation, and even into adulthood (101).

Several studies have shown that fibroblast growth factor (FGF)-2 is able to potentiate canonical pSmad2/3-dependent TGF-β signaling by binding to TGF-β type III receptor beta-glycan, which both possess the binding site of endogenous TGF-β and FGF-2, and thereby result in increased TGF-β availability for the activation of the canonical pathway. A significant role for FGF-2/AKT-1 signaling in mitral VICs in response to experimental wounding and remodeling, independent of the TGF-β/Smad signaling, has been identified (100). Ang II has also been shown to play a significant role in canonical TGF-β-dependent ECM remodeling causing myxomatous degeneration in murine mitral valves. Infusion of Ang II into mice triggers

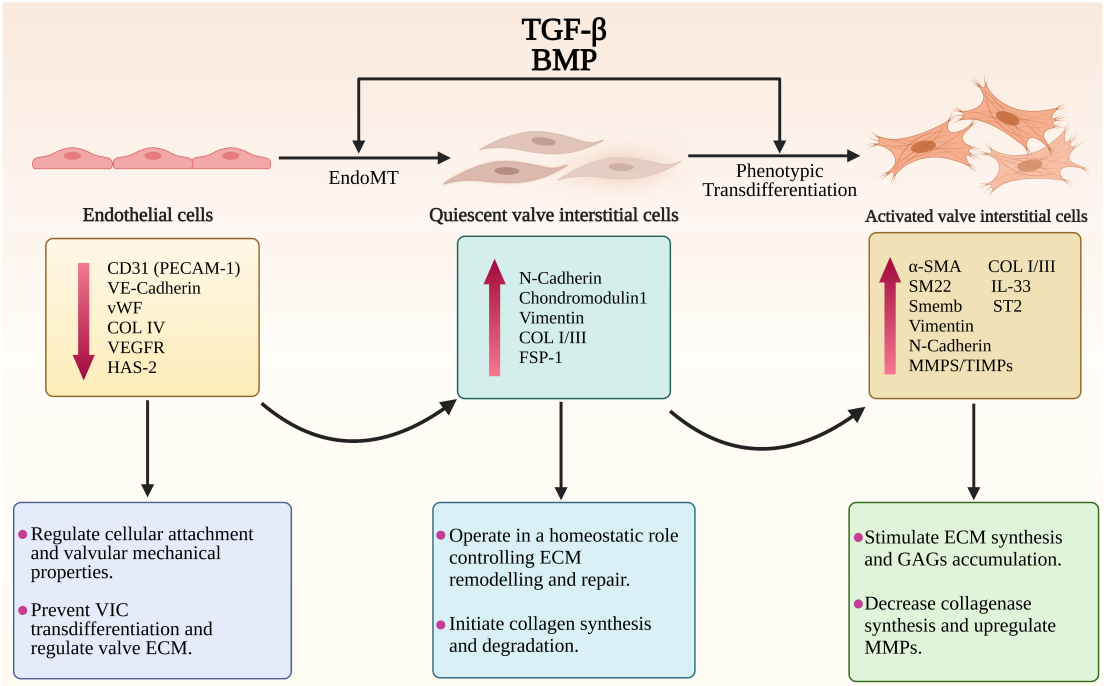

FIGURE 2 | The endothelial to mesenchymal transition (EndoMT) and phenotypic trans-differentiation from quiescent valve interstitial cells (qVICs) to activated valve interstitial cells (aVICs) in the progression of MMVD. The diagram illustrates the phenotypic, gene expression changes and cellular functional changes occurring during MMVD. The phenotypic conversion of endothelial cells into qVICs includes increased production of N-cadherin, vimentin and fibroblast-specific protein-1 (FSP-1). These events are accompanied by downregulation of the markers of endothelial cells such as CD31/platelet-endothelial cell adhesion molecule-1 (CD31/PECAM-1), vascular-endothelial cadherin (VE-cadherin), COL4, vascular epidermal growth factor receptor (VEGFR), and von Willebrand factor (vWF). Furthermore, the TGF-β-activated VICs show a significant increase in unique markers including α-smooth muscle actin (α-SMA), SM22 and Smemb (embryonic smooth muscle myosin) as well as the secretory proteins regulating the ECM disorganization including MMPs/TIMPs, IL-1β, IL-11, and IL-33.

activation of a canonical Smad-mediated TGF-β2 cascade and transcriptional activity of TGF-β-responsive genes (84). There is increased mRNA levels of TGF-β1 and TGF-β2 as well as downstream pSmad2, detected by both qRT-PCR and IHC, alongside an increase in MMP2 and CTGF expression, respectively (84). As previously mentioned canonical TGF-β-induced SMAD2/3-dependent ECM production in cultured human VICs can be effectively inhibited by the Ang II receptor blocker losartan (34).

Non-canonical Transforming Growth Factor-β Signaling in Myxomatous Mitral Valve Degeneration

In addition to the canonical signaling, TGF-β family members contribute to MMVD progression by *via* several non-Smad/non-canonical pathways. Similar to the Smad-dependent signaling, the non-canonical cascades are initially amplified by the phosphorylation of TGF-βRI/II through binding with activated TGF-β ligands regulating downstream cellular activities. These pathways comprise the kinases members from the mitogen-activated protein kinase (MAPK) family and other kinases such as phosphatidylinositol 3-kinase (PI3K). TGF-β can activate all three known MAPK pathways, and these are also known as TGF-β activated kinase 1 (TAK1)-mediated p38 activation, c-Jun amino-terminal kinase (JNK) MAPK, and extracellular signal-regulated kinase (ERK). Signal transduction through these pathways modulates non-Smad-mediated TGF-β-responsive cellular activities. However, these pathways can also modify canonical pathways with complex interactions between non-Smad- or Smad-mediated components occurring in most TGF-β-mediated biological effects. This can result in up- or down-regulation of TGF-β signaling and complex regulation of biological responses (112).

Although Smad-independent TGF-β signaling is implicated in a wide spectrum of intracellular transduction cascades and diverse cellular responses only a few studies have examined its involvement in MMVD (34, 41, 89, 113, 114). Nevertheless, these studies show that non-Smad signaling, including ERK, p38 MAPK, and PI3K, can contribute to MMVD pathogenesis affecting the function of both VICs and VECs by interacting with canonical TGF-β signaling or directly. Recent transcriptomic profiling of canine valve tissues has shown that positively regulated gene expression of the ERK1/2 cascade is most noticeably in end-stage valves (37). In FLNA conditional knockout mice, as found in the human FLNA mutation X-linked MMVD, progression can be attributed to a balance between the opposing regulatory effect of the non-canonical Ras/Mek/Erk and canonical TGF-β-dependent effector pSmad3 (89). In human mitral VICs exposed to cyclic mechanical strain, expression of

TGF-β2 and α-SMA are significantly increased, which is partly dependent on the activation of RhoC/ROCK in tandem with the non-canonical MEK/ERK1/2 pathway (114). The expression of α-SMA induced by activation of the TGF-β-dependent PI3K/AKT signaling is also observed in bone marrow-derived mesenchymal stem cells (MSCs) modified to generate VICs for tissue-engineered heart valves (113). In human mitral VECs EndoMT can be induced *via* TGF-β-mediated activation of Ras/Mek/Erk rather than the canonical pSmad3 signaling with increased expression of the EndoMT markers Slug, Snai1 and MMP-2 (41). TGF-β-mediated ECM production has also been shown to be dependent on non-Smad p38 MAPK pathways, working in combination with the canonical Smad2/3 signaling in diseased VICs in sporadic non-syndromic mitral valve prolapse (34).

The potential interaction between Ang II and TGF-β in the pathogenesis of MMVD should also be considered as this is well recognized in fibrosis and ECM deposition, involving both canonical and non-canonical parts of the TGF-β signaling pathway, and these effects can be inhibited by angiotensin II receptor blockers (ARBs) (34). One consideration, as previously mentioned, is the disparity in the level of fibrosis comparing end-stage canine and human MMVD (BD), and to what extent signaling pathways more important in fibrosis might actually contribute to the ECM remodeling seen with myxomatous degeneration. Nevertheless, activation of Smad-mediated signaling and TGF-β2-responsive gene expression has been observed in the mitral valves of mice treated with Ang II, with a relatively moderate change in the activity of BMP and Wnt-β-catenin signaling, both of which are suggested to contribute to human MMVD (84). The ARB antagonist losartan competitively antagonizes binding of Ang II to the AT1 receptor, but also inhibits progression of aortic root aneurysms in Fbn-1 mutant mice and Marfan disease patients through anti-TGF-β effects (104, 115). It has been proposed that losartan shunts Ang II signaling toward the Type II receptor involving both SMAD and ERK (116). In human mitral VICs treated with losartan, phosphorylation of SMAD2/3 and p38 is inhibited, but not ERK, suggesting SMAD2/3-dependent canonical TGF-β and ERK-independent signaling contribute to MMVD progression. Furthermore, in a mouse model of Loeys-Dietz syndrome (LDS), which exhibits phenotypic features overlap with MMVD and is a consequence of dysregulated TGF-β signaling, losartan normalizes growth of aortic roots and protects the aortic wall from the damage associated with decreased expression of pSmad2, pERK and TGF-β1 ligands (117). Losartan antagonism of TGF-β-dependent pSmad and ERK signaling also prevents EndoMT in ovine VECs and reduces expression of TGF-β and pERK in sheep mitral valve tissues (43, 118). In transgenic Runx2$^{\pm}$ mice treated with AngII there is increased expression levels for the COL3A1 gene and immunostaining for pAKT proteins despite the lack of expression of TGF-β3 and pSMAD2/3 in mitral valve tissues. Conversely, there is increased expression of TGF-β3, COL3A1, p-SMAD2/3 and p-AKT in Runx2$^{+/+}$ mice, suggesting that Runx2 may contribute to trigger tissue ECM responses and cellular proliferation, similar to that seen in MMVD (84). However, a large-scale clinical trial for children and young adults with MFS showed that there were no significant difference in the rate of aortic-root dilatation between the two groups treated with losartan and atenolol, the current standard therapy in most hospitals (119).

Bone Morphogenetic Proteins Signaling in Myxomatous Mitral Valve Degeneration

BMPs are important members of the TGF-β superfamily and may also be involved in MMVD progression. While they were originally discovered because of their capacity to mediate bone and cartilage formation, there is an increasing awareness of their role in non-osteogenic processes, such as heart development, circulation homeostasis and several cardiovascular diseases (120). Similar to TGF-βs BMPs ligands can bind to the heterotetrameric transmembrane receptor complexes comprised of two serine-threonine kinase type I and type II receptors, resulting in initiation of canonical or non-canonical signaling cascades, including the downstream phosphorylation of R-SMAD effector proteins and the three well-characterized ERK, JNK and p38 MAPK pathways (121–123). Following activation of R-SMADs, also known as SMADs 1, 5, and 8, BMPs form heteromeric complexes by binding with the co-Smad mediator, Smad4, and translocate into the nucleus to mediate transcription of BMP-responsive genes (**Figure 3**) (124).

The potential role of BMP signaling was first recognized in MMVD degeneration in a Fbn-1 mutant murine model of MFS. Several studies have shown that BMP 2, 4, and 6 can contribute to cardiac valve development and EndoMT involving a key contribution of Smad1/4/5-dependent BMP signaling (125–129). Although the molecular mechanisms in which the BMPs might impact MMVD pathogenesis have not been clarified some studies suggest that non-canonical BMP4/SOX9 signaling regulates the phenotypic change in VICs and ECM remodeling in human myxomatous mitral valve tissue, with increased gene and protein expression of BMP4, Sox9, CRTAC1, CTGF, α-SMA, vimentin and desmin (67). BMP4 treatment itself results in increased expression of Sox9 and other markers of ECM reorganization and VIC activation in human MMVD valves (67). BMP2 signaling in the human endocardial lineage is essential for remodeling of atrioventricular valves since BMP2 knockout mice show reduced Sox9 expression and mitral valve malformation deficiencies (130). BMP2 and TGF-β1 synergistically stimulate the expression of the transcriptional factors SOX9, Twist1, and Snail1/2 and initiate EndoMT *via* canonical Smad1/5- and Smad2/3-dependent pathways (101). TGF-β induces quiescent VIC activation by BMP2 stimulation in deformed mitral valves in Fstl1-deficient transgenic mouse model indicating a potential molecular target for myxomatous mitral valve disease (101). Comparable activity of canonical TGF-β and BMP signaling has been detected in surgically excised human MMVD tissue (84).

Other Important Pathways in Myxomatous Mitral Valve Degeneration

Several important regulatory pathways besides TGF-β signaling have also been shown to participate in the development of heart valves and progression of MMVD under certain specific cellular

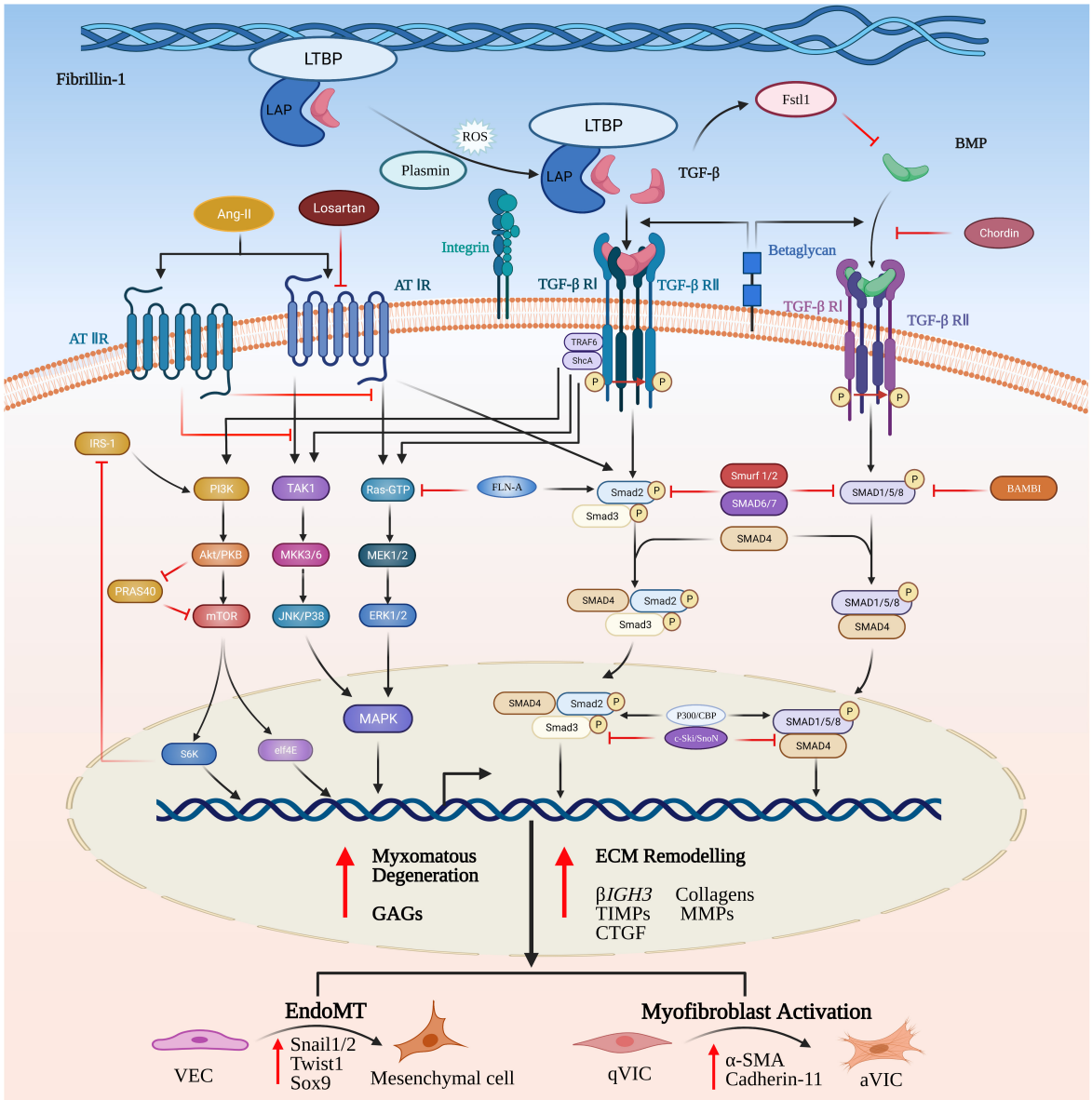

FIGURE 3 | Canonical and non-canonical TGF-β and BMP signaling pathways in MMVD. TGF-β homodimers are secreted extracellularly as inactive protein complexes, maintaining latency through binding with the latency-associated peptide (LAP). Latent TGF-β-binding proteins (LTBPs) form a bridge between fibrillin-1 (Fbn-1) and LAP and serve to sequester the complex into the extracellular matrix (ECM). The complex can be released from the microfibrils by its complex interactions with activators such as reactive oxygen species (ROS), plasmin and integrins. Activation of the latent complex mechanically triggers the complex deformation (torqueing) and the release of active TGF-β. The Smad-mediated TGF-β cascade is initiated by the binding of activated TGF-β homodimers to their corresponding transmembrane heterodimeric TGF-β I/II receptor complex. The active receptor complex recruits and phosphorylates the downstream signaling effector proteins, Smad2 and Smad3. Upon phosphorylation, Smad2/3 is released and forms an intracellular complex with Smad4 that translocates from the cytoplasm into the nucleus, where it interacts with Smad binding elements of TGF-β target genes involved in induction of ECM remodeling, VIC differentiation, EndoMT and myxomatous alterations. The non-canonical pathways are comprised of phosphatidylinositol 3-kinase (PI3K) and the kinases members from mitogen-activated protein kinase (MAPK) family. TGF-β can activate all three known MAPK pathways, referred to as TGF-β activated kinase 1 (TAK1)-mediated p38 activation, c-Jun amino-terminal kinase (JNK) MAPK, and extracellular signal-regulated kinase (ERK). Signal transduction through these pathways modulates non-Smad-mediated TGF-β-responsive cellular activities dependent on a specific cellular type or context. In a similar manner, BMPs bind to their transmembrane complexes to initiate its phosphorylation, but with higher affinity with type I receptor, assisted by type III co-receptors, endoglin and betaglycan. Upon activation the complex results in initiation of canonical or non-canonical signaling cascades.

contexts. These molecular pathways include Wnt/β-catenin and Notch pathways (42, 84, 131). A microarray pathway analyses showed that the expression level of Wnt ligand (Wnt9A) and its receptor (frizzled 8), accompanied by upregulation of the extracellular positive modulator R-Spondin 2 and the target gene runt-related transcription factor 2 (Runx2), were increased

in human MMVD tissues. These observations were further supported by the increased expression of Wnt9A, β-catenin and Wnt-target gene WISP1 in TGF-β2-treated human mitral VICs and Ang II-induced myxomatous degeneration in murine mitral valves (84). The Notch pathway also plays an important role in the development of outflow tract of the heart which starts with EndoMT in the endocardial cells leading to the formation of cardiac valves (132). However, there lacks enough evidence that Notch signaling is directly involved in the onset and progression of MMVD in human and dogs. To what extent TGF-β signaling might interact with these pathways is beyond the scope of this review.

CONCLUSION

MMVD is the most important acquired mitral valve disease in both dogs and humans and its natural history, pathogenesis and progression, pathology, cell and molecular changes are reasonably well characterized. Current areas of investigation are focused on genetic analysis, small and large animal models, the role of TGF-β dysregulation, abnormal EndoMT, and the impact of biomechanical strain in the pathogenesis of MMVD. There is also parallel interest in monocyte infiltration, particularly macrophages, as potential contributors to MMVD pathogenesis, at least in human mitral valvulopathies. While transgenic rodent models and surgically resected human valve tissues give insight into many molecular aspects of MMVD they are limited in modeling the chronicity of this disease and the extensive secondary fibrosis in patient-derived human valve tissues hampers examination of molecular events controlling myxomatous initiation and progression. Interestingly, much more is known about the earlier stages of the disease in the dog, and the naturally occurring disease in the dog might be the best large animal model to study human MMVD considering the shared cellular and molecular events in the two species. The important role of TGF-β signaling in the onset and progression of MMVD has been emphasized by studies using mouse models, valve samples of human and canine myxomatous mitral valves and in *in vitro* canine aVIC cell culture models. Phenotypic transition of qVICs to aVICs induced by dysregulated TGF-β signaling appears to be a key contributor to valve myxomatous degeneration though aberrant matrix remodeling, exerting control through complex canonical and non-canonical signaling pathways interactions and effects, which can conceivably affect the disease phenotype alone or in combinations. To what extent one of these might be a dominant pathway for the diseased is still unknown. Furthermore, what abnormal signaling contributes to the survival and persistence of aVICs in diseased valves remains unanswered. Understanding the mechanisms that control cell persistence in this disease likely will give clues to the pathogenesis and identify potential therapeutic targets in both the dog and human.

DATA AVAILABILITY STATEMENT

The original contributions presented in the study are included in the article/supplementary material, further inquiries can be directed to the corresponding author/s.

AUTHOR CONTRIBUTIONS

QT: major contribution to writing and preparation. AM, KP, and VEM: additional writing and editing. BMC: initiator of review, major contribution to writing and final editing. All authors contributed to the article and approved the submitted version.

FUNDING

QT was funded by the China Scholarship Council (Ph.D.). KP and VEM were supported by funding from the Biotechnology and Biological Sciences Research Council (BBSRC) in the form of an Institute Strategic Programme Grant (BB/J004316/1). For the purpose of open access, the author has applied a Creative Commons Attribution (CC BY) license to any Author Accepted Manuscript version arising from this submission.

REFERENCES

1. Barlow JB, Pocock WA. The significance of late systolic murmurs and mid-late systolic clicks. *Md State Med J.* (1963) 12:76–7.
2. Pensinger RR. Comparative aspects of mitral valve disease in dogs. *Ann N Y Acad Sci.* (1965) 118:525–34. doi: 10.1111/j.1749-6632.1965.tb33974.x
3. Delling FN, Vasan RS. Epidemiology and pathophysiology of mitral valve prolapse new insights into disease progression, genetics, and molecular basis. *Circulation.* (2014) 129:2158–70. doi: 10.1161/CIRCULATIONAHA.113.006702
4. Levine RA, Hagége AA, Judge DP, Padala M, Dal-Bianco JP, Aikawa E, et al. Mitral valve disease–morphology and mechanisms. *Nat Rev Cardiol.* (2015) 12:689–710. doi: 10.1038/nrcardio.2015.161
5. Markby GR, Summers KM, MacRae VE, Corcoran BM. Comparative transcriptomic profiling and gene expression for myxomatous mitral valve disease in the dog and human. *Vet Sci.* (2017) 4:34. doi: 10.3390/vetsci4030034
6. Kim AJ, Xu N, Yutzey KE. Macrophage lineages in heart valve development and disease. *Cardiovasc Res.* (2021) 117:663–73. doi: 10.1093/cvr/cvaa062
7. Freed LA, Levy D, Levine RA, Larson MG, Evans JC, Fuller DL, et al. Prevalence and clinical outcome of mitral-valve prolapse. *N Engl J Med.* (1999) 341:1–7.
8. Devereux RB, Jones EC, Roman MJ, Howard BV, Fabsitz RR, Liu JE, et al. Prevalence and correlates of mitral valve prolapse in a population-based sample of American Indians: the strong heart study. *Am J Med.* (2001) 111:679–85. doi: 10.1016/s0002-9343(01)00981-0
9. Detweiler DK, Patterson DF. The prevalence and types of cardiovascular disease in dogs. *Ann N Y Acad Sci.* (1965) 127:481–516. doi: 10.1111/j.1749-6632.1965.tb49421.x
10. Bonnett B, Egenvall A, Olson P, Hedhammar A. Mortality in insured Swedish dogs: rates and causes of death in various breeds. *Vet Rec.* (1997) 141:40–4. doi: 10.1136/vr.141.2.40
11. Parker HG, Kilroy-Glynn P. Myxomatous mitral valve disease in dogs: does size matter? *J Vet Cardiol.* (2012) 14:19–29. doi: 10.1016/j.jvc.2012.01.006

12. Maron BJ, Epstein SE. Hypertrophic cardiomyopathy. Recent observations regarding the specificity of three hallmarks of the disease: asymmetric septal hypertrophy, septal disorganization and systolic anterior motion of the anterior mitral leaflet. *Am J Cardiol.* (1980) 45:141–54. doi: 10.1016/0002-9149(80)90232-5
13. Judge DP, Rouf R, Habashi J, Dietz HC. Mitral valve disease in Marfan syndrome and related disorders. *J Cardiovasc Transl Res.* (2011) 4:741–7. doi: 10.1007/s12265-011-9314-y
14. Atzinger CL, Meyer RA, Khoury PR, Gao Z, Tinkle BT. Cross-sectional and longitudinal assessment of aortic root dilation and valvular anomalies in hypermobile and classic ehlers-danlos syndrome. *J Pediatr.* (2011) 158: 826–830.e1. doi: 10.1016/j.jpeds.2010.11.023
15. Lardeux A, Kyndt F, Lecointe S, Marec HL, Merot J, Schott JJ, et al. Filamin-a-related myxomatous mitral valve dystrophy: genetic, echocardiographic and functional aspects. *J Cardiovasc Transl Res.* (2011) 4:748–56. doi: 10.1007/s12265-011-9308-9
16. Sauls K, de Vlaming A, Harris BS, Williams K, Wessels A, Levine RA, et al. Developmental basis for filamin-A-associated myxomatous mitral valve disease. *Cardiovasc Res.* (2012) 96:109–19. doi: 10.1093/cvr/cvs238
17. Le Tourneau T, Le Scouarnec S, Cueff C, Bernstein D, Aalberts J, Lecointe S, et al. New insights into mitral valve dystrophy: a filamin-A genotype-phenotype and outcome study. *Eur Heart J.* (2018) 39:1269–77. doi: 10.1093/eurheartj/ehx505
18. Fornes P, Heudes D, Fuzellier JF, Tixier D, Bruneval P, Carpentier A. Correlation between clinical and histologic patterns of degenerative mitral valve insufficiency: a histomorphometric study of 130 excised segments. *Cardiovasc Pathol.* (1999) 8:81–92. doi: 10.1016/s1054-8807(98)00021-0
19. Pedersen HD, Häggström J. Mitral valve prolapse in the dog: a model of mitral valve prolapse in man. *Cardiovasc Res.* (2000) 47:234–43. doi: 10.1016/s0008-6363(00)00113-9
20. Rausch MK, Bothe W, Kvitting JP, Göktepe S, Miller DC, Kuhl E. In vivo dynamic strains of the ovine anterior mitral valve leaflet. *J Biomech.* (2011) 44:1149–57. doi: 10.1016/j.jbiomech.2011.01.020
21. Cui YC, Li K, Tian Y, Yuan WM, Peng P, Yang JZ, et al. A pig model of ischemic mitral regurgitation induced by mitral chordae tendinae rupture and implantation of an ameroid constrictor. *PLoS One.* (2014) 9:e111689. doi: 10.1371/journal.pone.0111689
22. Rabkin E, Aikawa M, Stone JR, Fukumoto Y, Libby P, Schoen FJ. Activated interstitial myofibroblasts express catabolic enzymes and mediate matrix remodeling in myxomatous heart valves. *Circulation.* (2001) 104:2525–32. doi: 10.1161/hc4601.099489
23. Corcoran BM, Black A, Anderson H, McEwan JD, French A, Smith P, et al. Identification of surface morphologic changes in the mitral valve leaflets and chordae tendineae of dogs with myxomatous degeneration. *Am J Vet Res.* (2004) 65:198–206. doi: 10.2460/ajvr.2004.65.198
24. Han RI, Black A, Culshaw GJ, French AT, Else RW, Corcoran BM. Distribution of myofibroblasts, smooth muscle like cells, macrophages, and mast cells in mitral valve leaflets of dogs with myxomatous mitral valve disease. *Am J Vet Res.* (2008) 69:763–9. doi: 10.2460/ajvr.69.6.763
25. Kim AJ, Xu N, Umeyama K, Hulin A, Ponny SR, Vagnozzi RJ, et al. Deficiency of circulating monocytes ameliorates the progression of myxomatous valve degeneration in Marfan syndrome. *Circulation.* (2020) 141:132–46. doi: 10.1161/CIRCULATIONAHA.119.042391
26. McDonald PC, Wilson JE, McNeill S, Gao M, Spinelli JJ, Rosenberg F, et al. The challenge of defining normality for human mitral and aortic valves: geometrical and compositional analysis. *Cardiovasc Pathol.* (2002) 11:193–209. doi: 10.1016/s1054-8807(01)00102-8
27. Roberts WC, Vowels TJ, Ko JM, Hebeler RF Jr. Gross and histological features of excised portions of posterior mitral leaflet in patients having operative repair of mitral valve prolapse and comments on the concept of missing (= ruptured) chordae tendineae. *J Am Coll Cardiol.* (2014) 63:1667–74. doi: 10.1016/j.jacc.2013.11.017
28. Saini N, Saikia UN, Sahni D, Singh RS. A comparative analysis of mitral valve changes in different age groups by histochemical, immunohistochemical and ultrastructural study. *J Anat Soc India.* (2014) 63:103–9. doi: 10.1016/j.jasi.2014.11.012
29. Kruithof BP, Paardekooper L, Hiemstra YL, Goumans MJ, Palmen M, Delgado V, et al. Stress-induced remodelling of the mitral valve: a model for leaflet thickening and superimposed tissue formation in mitral valve disease. *Cardiovasc Res.* (2020) 116:931–43. doi: 10.1093/cvr/cvz204
30. Gupta V, Barzilla JE, Mendez JS, Stephens EH, Lee EL, Collard CD, et al. Abundance and location of proteoglycans and hyaluronan within normal and myxomatous mitral valves. *Cardiovasc Pathol.* (2009) 18:191–7. doi: 10.1016/j.carpath.2008.05.001
31. King BD, Clark MA, Baba N, Kilman JW, Wooley CF. 'Myxomatous' mitral valves: collagen dissolution as the primary defect. *Circulation.* (1982) 66:288–96. doi: 10.1161/01.cir.66.2.288
32. Ng CM, Cheng A, Myers LA, Martinez-Murillo F, Jie C, Bedja D, et al. TGF-beta-dependent pathogenesis of mitral valve prolapse in a mouse model of Marfan syndrome. *J Clin Invest.* (2004) 114:1586–92. doi: 10.1172/JCI22715
33. Obayashi K, Miyagawa-Tomita S, Matsumoto H, Koyama H, Nakanishi T, Hirose H. Effects of transforming growth factor-β3 and matrix metalloproteinase-3 on the pathogenesis of chronic mitral valvular disease in dogs. *Am J Vet Res.* (2011) 72:194–202. doi: 10.2460/ajvr.72.2.194
34. Geirsson A, Singh M, Ali R, Abbas H, Li W, Sanchez JA, et al. Modulation of transforming growth factor-β signaling and extracellular matrix production in myxomatous mitral valves by angiotensin II receptor blockers. *Circulation.* (2012) 126:S189–97. doi: 10.1161/CIRCULATIONAHA.111.082610
35. Hagler MA, Hadley TM, Zhang H, Mehra K, Roos CM, Schaff HV, et al. TGF-β signalling and reactive oxygen species drive fibrosis and matrix remodelling in myxomatous mitral valves. *Cardiovasc Res.* (2013) 99:175–84. doi: 10.1093/cvr/cvt083
36. Tan K, Markby G, Muirhead R, Blake R, Bergeron L, Fici G, et al. Evaluation of canine 2D cell cultures as models of myxomatous mitral valve degeneration. *PLoS One.* (2019) 14:e0221126. doi: 10.1371/journal.pone.0221126
37. Markby GR, Macrae VE, Summers KM, Corcoran BM. Disease severity-associated gene expression in canine myxomatous mitral valve disease is dominated by TGFβ signaling. *Front Genet.* (2020) 11:372. doi: 10.3389/fgene.2020.00372
38. Goumans MJ, van Zonneveld AJ, Ten Dijke P. Transforming growth factor beta-induced endothelial-to-mesenchymal transition: a switch to cardiac fibrosis? *Trends Cardiovasc Med.* (2008) 18:293–8. doi: 10.1016/j.tcm.2009.01.001
39. Goumans MJ, Ten Dijke P. TGF-β signaling in control of cardiovascular function. *Cold Spring Harb Perspect Biol.* (2018) 10:a022210. doi: 10.1101/cshperspect.a022210
40. Garcia-Pena A, Ibarrola J, Navarro A, Sadaba A, Tiraplegui C, Garaikoetxea M, et al. Activation of the interleukin-33/ST2 pathway exerts deleterious effects in myxomatous mitral valve disease. *Int J Mol Sci.* (2021) 22:2310. doi: 10.3390/ijms22052310
41. Sauls K, Toomer K, Williams K, Johnson AJ, Markwald RR, Hajdu Z, et al. Increased infiltration of extra-cardiac cells in myxomatous valve disease. *J Cardiovasc Dev Dis.* (2015) 2:200–13. doi: 10.3390/jcdd2030200
42. Hulin A, Moore V, James JM, Yutzey KE. Loss of axin2 results in impaired heart valve maturation and subsequent myxomatous valve disease. *Cardiovasc Res.* (2017) 113:40–51. doi: 10.1093/cvr/cvw229
43. Bartko PE, Dal-Bianco JP, Guerrero JL, Beaudoin J, Szymanski C, Kim DH, et al. Effect of losartan on mitral valve changes after myocardial infarction. *J Am Coll Cardiol.* (2017) 70:1232–44. doi: 10.1016/j.jacc.2017.07.734
44. Kim AJ, Alfieri CM, Yutzey KE. Endothelial cell lineage analysis does not provide evidence for EMT in adult valve homeostasis and disease. *Anat Rec (Hoboken).* (2019) 302:125–35. doi: 10.1002/ar.23916
45. Bischoff J, Casanovas G, Wylie-Sears J, Kim DH, Bartko PE, Guerrero JL, et al. CD45 expression in mitral valve endothelial cells after myocardial infarction. *Circ Res.* (2016) 119:1215–25.
46. Lu CC, Liu MM, Clinton M, Culshaw G, Argyle DJ, Corcoran BM. Developmental pathways and endothelial to mesenchymal transition in canine myxomatous mitral valve disease. *Vet J.* (2015) 206:377–84. doi: 10.1016/j.tvjl.2015.08.011
47. Hulin A, Deroanne CF, Lambert CA, Dumont B, Castronovo V, Defraigne JO, et al. Metallothionein-dependent up-regulation of TGF-beta2 participates in the remodelling of the myxomatous mitral valve. *Cardiovasc Res.* (2012) 93:480–9. doi: 10.1093/cvr/cvr337

48. Disatian S, Ehrhart EJ III, Zimmerman S, Orton EC. Interstitial cells from dogs with naturally occurring myxomatous mitral valve disease undergo phenotype transformation. *J Heart Valve Dis.* (2008) 17:402–11.
49. Disatian S, Orton EC. Autocrine serotonin and transforming growth factor-b1 signaling mediates spontaneous myxomatous mitral valve disease. *J Heart Valve Dis.* (2009) 18:44–51.
50. von Gise A, Pu WT. Endocardial and epicardial epithelial to mesenchymal transitions in heart development and disease. *Circ Res.* (2012) 110:1628–45. doi: 10.1161/CIRCRESAHA.111.259960
51. Tao G, Kotick JD, Lincoln J. Heart valve development, maintenance, and disease: the role of endothelial cells. *Curr Top Dev Biol.* (2012) 100:203–32. doi: 10.1016/B978-0-12-387786-4.00006-3
52. Hinton RB, Yutzey KE. Heart valve structure and function in development and disease. *Annu Rev Physiol.* (2011) 73:29–46. doi: 10.1146/annurev-physiol-012110-142145
53. Guthrie RB, Edwards JE. Pathology of the myxomatous mitral value. Nature, secondary changes and complications. *Minn Med.* (1976) 59:637–47.
54. Culshaw GJ, French AT, Han RI, Black A, Pearson GT, Corcoran BM. Evaluation of innervation of the mitral valves and the effects of myxomatous degeneration in dogs. *Am J Vet Res.* (2010) 71:194–202. doi: 10.2460/ajvr.71.2.194
55. Han RI, Clark CH, Black A, French A, Culshaw GJ, Kempson SA, et al. Morphological changes to endothelial and interstitial cells and to the extracellular matrix in canine myxomatous mitral valve disease (endocardiosis). *Vet J.* (2013) 197:388–94. doi: 10.1016/j.tvjl.2013.01.027
56. Tamura K, Fukuda Y, Ishizaki M, Masuda Y, Yamanaka N, Ferrans VJ. Abnormalities in elastic fibers and other connective-tissue components of floppy mitral valve. *Am Heart J.* (1995) 129:1149–58. doi: 10.1016/0002-8703(95)90397-6
57. Rabkin-Aikawa E, Farber M, Aikawa M, Schoen FJ. Dynamic and reversible changes of interstitial cell phenotype during remodeling of cardiac valves. *J Heart Valve Dis.* (2004) 13:841–7.
58. Bischoff J, Aikawa E. Progenitor cells confer plasticity to cardiac valve endothelium. *J Cardiovasc Transl Res.* (2011) 4:710–9. doi: 10.1007/s12265-011-9312-0
59. Han RI, Black A, Culshaw G, French AT, Corcoran BM. Structural and cellular changes in canine myxomatous mitral valve disease: an image analysis study. *J Heart Valve Dis.* (2010) 19:60–70.
60. Hadian M, Corcoran BM, Bradshaw JP. Molecular changes in fibrillar collagen in myxomatous mitral valve disease. *Cardiovasc Pathol.* (2010) 19:e141–8. doi: 10.1016/j.carpath.2009.05.001
61. Liu MM, Flanagan TC, Lu CC, French AT, Argyle DJ, Corcoran BM. Culture and characterisation of canine mitral valve interstitial and endothelial cells. *Vet J.* (2015) 204:32–9.
62. Blake RR, Markby GR, Culshaw GJ, Martinez-Pereira Y, Lu CC, Corcoran BM. Survival of activated myofibroblasts in canine myxomatous mitral valve disease and the role of apoptosis. *Res Vet Sci.* (2020) 128:99–106. doi: 10.1016/j.rvsc.2019.11.004
63. Salhiyyah K, Yacoub MH, Chester AH. Cellular mechanisms in mitral valve disease. *J Cardiovasc Transl Res.* (2011) 4:702–9. doi: 10.1007/s12265-011-9318-7
64. Liu AC, Joag VR, Gotlieb AI. The emerging role of valve interstitial cell phenotypes in regulating heart valve pathobiology. *Am J Pathol.* (2007) 171:1407–18. doi: 10.2353/ajpath.2007.070251
65. Armstrong EJ, Bischoff J. Heart valve development: endothelial cell signaling and differentiation. *Circ Res.* (2004) 95:459–70. doi: 10.1161/01.RES.0000141146.95728.da
66. Hakuno D, Kimura N, Yoshioka M, Mukai M, Kimura T, Okada Y, et al. Periostin advances atherosclerotic and rheumatic cardiac valve degeneration by inducing angiogenesis and MMP production in humans and rodents. *J Clin Invest.* (2010) 120:2292–306. doi: 10.1172/JCI40973
67. Sainger R, Grau JB, Branchetti E, Poggio P, Seefried WF, Field BC, et al. Human myxomatous mitral valve prolapse: role of bone morphogenetic protein 4 in valvular interstitial cell activation. *J Cell Physiol.* (2012) 227:2595–604. doi: 10.1002/jcp.22999
68. Hulin A, Deroanne C, Lambert C, Defraigne JO, Nusgens B, Radermecker M, et al. Emerging pathogenic mechanisms in human myxomatous mitral valve: lessons from past and novel data. *Cardiovasc Pathol.* (2013) 22:245–50.
69. Butcher JT, Markwald RR. Valvulogenesis: the moving target. *Philos Trans R Soc Lond B Biol Sci.* (2007) 362:1489–503. doi: 10.1098/rstb.2007.2130
70. Combs MD, Yutzey KE. Heart valve development: regulatory networks in development and disease. *Circ Res.* (2009) 105:408–21. doi: 10.1161/CIRCRESAHA.109.201566
71. Chakraborty S, Combs MD, Yutzey KE. Transcriptional regulation of heart valve progenitor cells. *Pediatr Cardiol.* (2010) 31:414–21. doi: 10.1007/s00246-009-9616-x
72. Akiyama H, Chaboissier MC, Behringer RR, Rowitch DH, Schedl A, Epstein JA, et al. Essential role of Sox9 in the pathway that controls formation of cardiac valves and septa. *Proc Natl Acad Sci USA.* (2004) 101:6502–7. doi: 10.1073/pnas.0401711101
73. Paranya G, Vineberg S, Dvorin E, Kaushal S, Roth SJ, Rabkin E, et al. Aortic valve endothelial cells undergo transforming growth factor-beta-mediated and non-transforming growth factor-beta-mediated transdifferentiation in vitro. *Am J Pathol.* (2001) 159:1335–43. doi: 10.1016/s0002-9440(10)62520-5
74. Paruchuri S, Yang JH, Aikawa E, Melero-Martin JM, Khan ZA, Loukogeorgakis S, et al. Human pulmonary valve progenitor cells exhibit endothelial/mesenchymal plasticity in response to vascular endothelial growth factor-A and transforming growth factor-beta2. *Circ Res.* (2006) 99:861–9. doi: 10.1161/01.RES.0000245188.41002.2c
75. Shapero K, Wylie-Sears J, Levine RA, Mayer JE Jr, Bischoff J. Reciprocal interactions between mitral valve endothelial and interstitial cells reduce endothelialto-mesenchymal transition and myofibroblastic activation. *J Mol Cell Cardiol.* (2015) 80:175–85. doi: 10.1016/j.yjmcc.2015.01.006
76. Border WA, Noble NA. Transforming growth factor beta in tissue fibrosis. *N Engl J Med.* (1994) 331:1286–92.
77. Roberts AB, Sporn MB, Assoian RK, Smith JM, Roche NS, Wakefield LM, et al. Transforming growth factor type beta: rapid induction of fibrosis and angiogenesis in vivo and stimulation of collagen formation in vitro. *Proc Natl Acad Sci USA.* (1986) 83:4167–71. doi: 10.1073/pnas.83.12.4167
78. Varga J, Jimenez SA. Stimulation of normal human fibroblast collagen production and processing by transforming growth factor-beta. *Biochem Biophys Res Commun.* (1986) 138:974–80. doi: 10.1016/s0006-291x(86)80591-5
79. Kyndt F, Gueffet JP, Probst V, Jaafar P, Legendre A, Bouffant FL, et al. Mutations in the gene encoding filamin a as a cause for familial cardiac valvular dystrophy. *Circulation.* (2007) 115:40–9. doi: 10.1161/CIRCULATIONAHA.106.622621
80. Medici D, Potenta S, Kalluri R. Transforming growth factor-β2 promotes snail-mediated endothelial-mesenchymal transition through convergence of SMAD-dependent and SMAD-independent signalling. *Biochem J.* (2011) 437:515–20. doi: 10.1042/BJ20101500
81. Mihira H, Suzuki HI, Akatsu Y, Yoshimatsu Y, Igarashi T, Miyazono K, et al. TGF-β-induced mesenchymal transition of MS-1 endothelial cells requires SMAD-dependent cooperative activation of Rho signals and MRTF-A. *J Biochem.* (2012) 151:145–56. doi: 10.1093/jb/mvr121
82. Pardali E, Sanchez-Duffhues G, Gomez-Puerto MC, Ten Dijke P. TGF-β-induced endothelial-mesenchymal transition in fibrotic diseases. *Int J Mol Sci.* (2017) 18:2157. doi: 10.3390/ijms18102157
83. Van Meeteren LA, Ten Dijke P. Regulation of endothelial cell plasticity by TGF-β. *Cell Tissue Res.* (2012) 347:177–86. doi: 10.1007/s00441-011-1222-6
84. Thalji NM, Hagler MA, Zhang B, Casaclang-Verzosa G, Nair AA, Suri RM, et al. Nonbiased molecular screening identifies novel molecular regulators of fibrogenic and proliferative signaling in myxomatous mitral valve disease. *Circ Cardiovasc Genet.* (2015) 8:516–28. doi: 10.1161/CIRCGENETICS.114.000921
85. Aupperle H, März I, Thielebein J, Schoon HA. Expression of transforming growth factor-beta1, -beta2 and -beta3 in normal and diseased canine mitral valves. *J Comp Pathol.* (2008) 139:97–107. doi: 10.1016/j.jcpa.2008.05.007
86. Rizzo S, Basso C, Lazzarini E, Celeghin R, Paolin A, Gerosa G, et al. TGF-beta1 pathway activation and adherens junction molecular pattern in nonsyndromic mitral valve prolapse. *Cardiovasc Pathol.* (2015) 24:359–67. doi: 10.1016/j.carpath.2015.07.009
87. Dietz HC, Loeys B, Carta L, Ramirez F. Recent progress towards a molecular understanding of Marfan syndrome. *Am J Med Genet C Semin Med Genet.* (2005) 139:4–9. doi: 10.1002/ajmg.c.30068

88. Chaudhry SS, Cain SA, Morgan A, Dallas SL, Shuttleworth CA, Kielty CM. Fibrillin-1 regulates the bioavailability of TGFbeta1. *J Cell Biol.* (2007) 176:355–67. doi: 10.1083/jcb.200608167
89. Toomer K, Sauls K, Fulmer D, Guo L, Moore K, Glover J, et al. Filamin-A as a balance BETWEEN Erk/Smad activities during cardiac valve development. *Anat Rec.* (2019) 302:117–24. doi: 10.1002/ar.23911
90. Surachetpong S, Jiranantasak T, Rungsipipat A, Orton EC. Apoptosis and abundance of Bcl-2 family and transforming growth factor beta1 signaling proteins in canine myxomatous mitral valves. *J Vet Cardiol.* (2013) 15:171–80. doi: 10.1016/j.jvc.2013.02.005
91. Moesgaard SG, Aupperle H, Rajamaki MM, Falk T, Rasmussen CE, Zois NE, et al. Matrix metalloproteinases (MMPs), tissue inhibitors of metalloproteinases (TIMPs) and transforming growth factor-beta (TGF-beta) in advanced canine myxomatous mitral valve disease. *Res Vet Sci.* (2014) 97:560–7. doi: 10.1016/j.rvsc.2014.10.003
92. Annes JP, Chen Y, Munger JS, Rifkin DB. Integrin alphaVbeta6-mediated activation of latent TGF-β requires the latent TGF-β binding protein-1. *J Cell Biol.* (2004) 165:723–34. doi: 10.1083/jcb.200312172
93. Arciniegas E, Frid MG, Douglas IS, Stenmark KR. Perspectives on endothelial-tomesenchymal transition: potential contribution to vascular remodeling in chronic pulmonary hypertension. *Am J Physiol Lung Cell Mol Physiol.* (2007) 293:L1–8. doi: 10.1152/ajplung.00378.2006
94. Arciniegas E, Carrillo LM, De Sanctis JB, Candelle D. Possible role of NFkappaB in the embryonic vascular remodeling and the endothelial mesenchymal transition process. *Cell Adhes Migr.* (2008) 2:17–29. doi: 10.4161/cam.2.1.5789
95. Robertson IB, Horiguchi M, Zilberberg L, Dabovic B, Hadjiolova K, Rifkin DB. Latent TGF-β-binding proteins. *Matrix Biol.* (2015) 47:44–53.
96. Wrana JL, Attisano L, Wieser R, Ventura F, Massagué J. Mechanism of activation of the TGF-β receptor. *Nature.* (1994) 370:341–7. doi: 10.1038/370341a0
97. Hata A, Chen YG. TGF-β signaling from receptors to smads. *Cold Spring Harb Perspect Biol.* (2016) 8:a022061. doi: 10.1101/cshperspect.a022061
98. Heldin CH, Moustakas A. Signaling receptors for TGF-β family members. *Cold Spring Harb Perspect Biol.* (2016) 8:a022053. doi: 10.1101/cshperspect.a022053
99. Euler-Taimor G, Heger J. The complex pattern of SMAD signaling in the cardiovascular system. *Cardiovasc Res.* (2006) 69:15–25. doi: 10.1016/j.cardiores.2005.07.007
100. Han L, Gotlieb AI. Fibroblast growth factor-2 promotes in vitro heart valve interstitial cell repair through the Akt1 pathway. *Cardiovasc Pathol.* (2012) 21:382–9. doi: 10.1016/j.carpath.2011.12.001
101. Prakash S, Borreguero L, Sylva M, Flores Ruiz L, Rezai F, Gunst QD, et al. Deletion of Fstl1 (follistatin-like 1) from the endocardial/endothelial lineage causes mitral valve disease. *Arterioscler Thromb Vasc Biol.* (2017) 37:e116–30. doi: 10.1161/ATVBAHA.117.309089
102. Boileau C, Guo DC, Hanna N, Regalado ES, Detaint D, Gong L, et al. TGF2 mutations cause familial thoracic aortic aneurysms and dissections associated with mild systemic features of Marfan syndrome. *Nat Genet.* (2012) 44:916–21. doi: 10.1038/ng.2348
103. Cañadas V, Vilacosta I, Bruna I, Fuster V. Marfan syndrome. Part 2: treatment and management of patients. *Nat Rev Cardiol.* (2010) 7:266–76. doi: 10.1038/nrcardio.2010.31
104. Habashi JP, Judge DP, Holm TM, Cohn RD, Loeys BL, Cooper TK, et al. Losartan, an AT1 antagonist, prevents aortic aneurism in a mouse model of Marfan syndrome. *Science.* (2006) 312:117–21. doi: 10.1126/science.1124287
105. Isogai Z, Ono RN, Ushiro S, Keene DR, Chen Y, Mazzieri R, et al. Latent transforming growth factor-beta binding protein 1 interacts with fibrillin and is micro-fibril-associated protein. *J Biol Chem.* (2003) 278:2750–7. doi: 10.1074/jbc.m209256200
106. Judge DP, Dietz HC. Marfan syndrome. *Lancet.* (2005) 366:1965–76.
107. Lindsay ME, Schepers D, Bolar NA, Doyle JJ, Gallo E, Fert-Bober J, et al. Loss-of-function mutations in TGF-2 cause a syndromic presentation of thoracic aortic aneurism. *Nat Genet.* (2012) 44:922–7. doi: 10.1038/ng.2349
108. Neptune ER, Frischmeyer PA, Arking DE, Myers L, Bunton TE, Gayraud B, et al. Dysregulation of TGFbeta activation contributes to pathogenesis in Marfan syndrome. *Nat Genet.* (2003) 33:407–11. doi: 10.1038/ng1116
109. Norris RA, Moreno-Rodriguez R, Wessels A, Merot J, Bruneval P, Chester AH, et al. Expression of the familial cardiac valvular dystrophy gene, filamin-A, during heart morphogenesis. *Dev Dyn.* (2010) 239:2118–27. doi: 10.1002/dvdy.22346
110. Sasaki A, Masuda Y, Ohta Y, Ikeda K, Watanabe K. Filamin associates with SMADS and regulates transforming growth factor-β signaling. *J Biol Chem.* (2001) 276:17871–7. doi: 10.1074/jbc.M008422200
111. Derynck R, Zhang YE. Smad-dependent and smad-independent pathways in TGF-beta family signalling. *Nature.* (2003) 425:577–84. doi: 10.1038/nature02006
112. Zhang YE. Non-SMAD signaling pathways of the TGF-β family. *Cold Spring Harb Perspect Biol.* (2017) 9:a022129. doi: 10.1101/cshperspect.a022129
113. Huang W, Xiao DZ, Wang Y, Shan ZX, Liu XY, Lin QX, et al. Fn14 promotes differentiation of human mesenchymal stem cells into heart valvular interstitial cells by phenotypic characterization. *J Cell Physiol.* (2014) 229:580–7. doi: 10.1002/jcp.24480
114. Blomme B, Deroanne C, Hulin A, Lambert C, Defraigne JO, Nusgens B, et al. Mechanical strain induces a pro-fibrotic phenotype in human mitral valvular interstitial cells through RhoC/ROCK/MRTF-A and Erk1/2 signaling pathways. *J Mol Cell Cardiol.* (2019) 135:149–59. doi: 10.1016/j.yjmcc.2019.08.008
115. Brooke BS, Habashi JP, Judge DP, Patel N, Loeys B, Dietz HC. Angiotensin II blockade and aortic-root dilatation in marfan's syndrome. *N Engl J Med.* (2008) 358:2787–95.
116. Habashi JP, Doyle JJ, Holm TM, Aziz H, Schoenhoff F, Bedja D, et al. Angiotensin II type 2 receptor signaling attenuates aortic aneurysm in mice through ERK antagonism. *Science.* (2011) 332:361–5. doi: 10.1126/science.1192152
117. Gallo EM, Loch DC, Habashi JP, Calderon JF, Chen Y, Bedja D, et al. Angiotensin II-dependent TGF-β signaling contributes to loeys-dietz syndrome vascular pathogenesis. *J Clin Invest.* (2014) 124:448–60. doi: 10.1172/JCI69666
118. Wylie-Sears J, Levine RA, Bischoff J. Losartan inhibits endothelial-to-mesenchymal transformation in mitral valve endothelial cells by blocking transforming growth factor-β-induced phosphorylation of ERK. *Biochem Biophys Res Commun.* (2014) 446:870–5. doi: 10.1016/j.bbrc.2014.03.014
119. Lacro RV, Dietz HC, Sleeper LA, Yetman AT, Bradley TJ, Colan SD, et al. Atenolol versus losartan in children and young adults with Marfan's syndrome. *N Engl J Med.* (2014) 371:2061–71. doi: 10.1056/NEJMoa1404731
120. Morrell NW, Bloch DB, ten Dijke P, Goumans MJ, Hata A, Smith J, et al. Targeting BMP signalling in cardiovascular disease and anaemi. *Nat Rev Cardiol.* (2016) 13:106–20. doi: 10.1038/nrcardio.2015.156
121. Scharpfenecker M, van Dinther M, Liu Z, van Bezooijen RL, Zhao Q, Pukac L, et al. BMP-9 signals via ALK1 and inhibits bFGF-induced endothelial cell proliferation and VEGF-stimulated angiogenesis. *J Cell Sci.* (2007) 120:964–72. doi: 10.1242/jcs.002949
122. Kirkbride KC, Townsend TA, Bruinsma MW, Barnett JV, Blobe GC. Bone morphogenetic proteins signal through the transforming growth factor-beta type III receptor. *J Biol Chem.* (2008) 283:7628–37. doi: 10.1074/jbc.M704883200
123. Corradini E,tt JL, Lin HY. The RGM/DRAGON family of BMP co-receptors. *Cytokine Growth Factor Rev.* (2009) 20:389–98. doi: 10.1016/j.cytogfr.2009.10.008
124. Luo JY, Zhang Y, Wang L, Huang Y. Regulators and effectors of bone morphogenetic protein signalling in the cardiovascular system. *J Physiol.* (2015) 593:2995–3011. doi: 10.1113/JP270207
125. Sugi Y, Yamamura H, Okagawa H, Markwald RR. Bone morphogenetic protein-2 can mediate myocardial regulation of atriventricular cushion mesenchymal cell formation in mice. *Dev Biol.* (2004) 269:505–18. doi: 10.1016/j.ydbio.2004.01.045
126. Nakajima Y, Yamagishi T, Hokari S, Nakamura H. Mechanisms involved in valvuloseptal endocardial cushion formation in early cardiogenesis: roles of transforming growth factor (TGF)-β and bone morphogenetic protein (BMP). *Anat Rec.* (2000) 258:119–27. doi: 10.1002/(SICI)1097-0185(20000201)258:2<119::AID-AR1>3.0.CO;2-U

127. Jiao K, Kulessa H, Tompkins K, Zhou Y, Batts L, Baldwin HS, et al. An essential role of Bmp4 in the atrioventricular septation of the mouse heart. *Genes Dev.* (2003) 17:2362–7. doi: 10.1101/gad.1124803
128. Kim RY, Robertson EJ, Solloway MJ. Bmp6 and Bmp7 are required for cushion formation and septation in the developing mouse heart. *Dev Biol.* (2001) 235:449–66. doi: 10.1006/dbio.2001.0284
129. Jackson LF, Qiu TH, Sunnarborg SW, Chang A, Zhang C, Patterson C, et al. Defective valvulogenesis in HB-EGF and TACE-null mice is associated with aberrant BMP signaling. *EMBO J.* (2003) 2:2704–16. doi: 10.1093/emboj/cdg264
130. Saxon JG, Baer DR, Barton JA, Hawkins T, Wu B, Trusk TC, et al. BMP2 expression in the endocardial lineage is required for AV endocardial cushion maturation and remodeling. *Dev Biol.* (2017) 430:113–28. doi: 10.1016/j.ydbio.2017.08.008
131. Aquila G, Kostina A, Vieceli Dalla Sega F, Shlyakhto E, Kostareva A, Marracino L, et al. The notch pathway: a novel therapeutic target for cardiovascular diseases? *Expert Opin Ther Targets.* (2019) 23:695–710. doi: 10.1080/14728222.2019.1641198
132. Del Monte G, Grego-Bessa J, González-Rajal A, Bolós V, De La Pompa JL. Monitoring notch1 activity in development: evidence for a feedback regulatory loop. *Dev Dyn.* (2007) 236:2594–614. doi: 10.1002/dvdy.21246
133. Ayme-Dietrich E, Lawson R, Cˆoté F, de Tapia C, Da Silva S, Ebel C, et al. The role of 5-HT2B receptors in mitral valvulopathy: bone marrow mobilization of endothelial progenitors. *Br J Pharmacol.* (2017) 174:4123–39. doi: 10.1111/bph.13981
134. Ibarrola J, Garaikoetxea M, Garcia-Peña A, Matilla L, Jover E, Bonnard B, et al. Beneficial effects of mineralocorticoid receptor antagonism on myocardial fibrosis in an experimental model of the myxomatous degeneration of the mitral valve. *Int J Mol Sci.* (2020) 21:5372. doi: 10.3390/ijms21155372
135. Ayme-Dietrich E, Da Silva S, Bouabout GA, Arnoux A, Guyonnet J, Becker G, et al. Characterization of the spontaneous degenerative mitral valve disease in FVB mice. *PLoS One.* (2021) 16:e0257022. doi: 10.1371/journal.pone.0257022
136. Zhu AS, Mustafa T, Connell JP, Grande-Allen KJ. Tumor necrosis factor alpha and interleukin 1 beta suppress myofibroblast activation via nuclear factor kappa B signaling in 3D-cultured mitral valve interstitial cells. *Acta Biomater.* (2021) 127:159–68. doi: 10.1016/j.actbio.2021.03.075
137. Liu MM, Flanagan TC, Jockenhovel S, Black A, Lu CC, French AT, et al. Development and evaluation of a tissue-engineered fibrin-based canine mitral valve three-dimensional cell culture system. *J Comp Pathol.* (2018) 160:23–33. doi: 10.1016/j.jcpa.2018.02.001
138. Syx D, Miller RE, Obeidat AM, Tran PB, Vroman R, Malfait Z, et al. Pain-related behaviors and abnormal cutaneous innervation in a murine model of classical Ehlers-Danlos syndrome. *Pain.* (2020) 161:2274–83. doi: 10.1097/j.pain.0000000000001935

Conflict of Interest: The authors declare that the research was conducted in the absence of any commercial or financial relationships that could be construed as a potential conflict of interest.

Publisher's Note: All claims expressed in this article are solely those of the authors and do not necessarily represent those of their affiliated organizations, or those of the publisher, the editors and the reviewers. Any product that may be evaluated in this article, or claim that may be made by its manufacturer, is not guaranteed or endorsed by the publisher.

Advantages of publishing in Frontiers

OPEN ACCESS
Articles are free to read for greatest visibility and readership

FAST PUBLICATION
Around 90 days from submission to decision

HIGH QUALITY PEER-REVIEW
Rigorous, collaborative, and constructive peer-review

TRANSPARENT PEER-REVIEW
Editors and reviewers acknowledged by name on published articles

Frontiers
Avenue du Tribunal-Fédéral 34
1005 Lausanne | Switzerland

Visit us: www.frontiersin.org
Contact us: frontiersin.org/about/contact

REPRODUCIBILITY OF RESEARCH
Support open data and methods to enhance research reproducibility

DIGITAL PUBLISHING
Articles designed for optimal readership across devices

FOLLOW US
@frontiersin

IMPACT METRICS
Advanced article metrics track visibility across digital media

EXTENSIVE PROMOTION
Marketing and promotion of impactful research

LOOP RESEARCH NETWORK
Our network increases your article's readership